T.C.
DOKUZ EYLÜL UNIVERSITY

IZMIR INTERNATIONAL
BIOMEDICINE AND GENOME
INSTITUTE

INVESTIGATION OF FUNCTIONAL CONTRIBUTION OF H1E IN EMT AND MET

GKAMZE IMPRAIMOGLOU KAFAZ

DEPARTMENT OF GENOMICS AND MOLECULAR BIOTECHNOLOGY

Molecular Biology and Genetics

MASTER OF SCIENCE THESIS

IZMIR-2024

THESIS CODE: DEU.IBG.MSc -2021850005

T.C.
DOKUZ EYLÜL UNIVERSITY

IZMIR INTERNATIONAL
BIOMEDICINE AND GENOME
INSTITUTE

INVESTIGATION OF FUNCTIONAL CONTRIBUTION OF H1E IN EMT AND MET

GKAMZE IMPRAIMOGLOU KAFAZ

DEPARTMENT OF GENOMICS AND MOLECULAR BIOTECHNOLOGY

Molecular Biology and Genetics

MASTER OF SCIENCE THESIS

Supervisor: Assoc. Prof. Hani Alotaibi

This work was supported by
TÜBİTAK grant 122N046

IZMIR-2024

THESIS CODE: DEU.IBG.MSc -2021850005

Dokuz Eylül University Izmir International Biomedicine and Genome Institute Department of Genomics and Molecular Biotechnology, Molecular Biology and Genetics graduate program Master of Science student Gkamze Impraimoglou Kafaz has successfully completed her Master of Science thesis titled “**INVESTIGATION OF FUNCTIONAL CONTRIBUTION OF H1E IN EMT AND MET**” on 28/08/2024.

Assoc. Prof. Hani Alotaibi

Dokuz Eylül University

CHAIR

Assoc. Prof. Muhammed Kasim Diril

Dokuz Eylül University

MEMBER

Assist. Prof. Seyit Kale

Katip Celebi University

MEMBER

Dokuz Eylül Üniversitesi İzmir Uluslararası Biyotıp ve Genom Enstitüsü Genom Bilimleri ve Moleküler Biyoteknoloji Anabilim Dalı, Moleküler Biyoloji ve Genetik Yüksek Lisans programı öğrencisi, Gkamze Impraimoglou Kafaz **“EMT ve MET’de H1E’nin Fonksiyonel Katkısının İncelenmesi**” konulu Yüksek Lisans tezini 19/01/2024 tarihinde başarılı olarak tamamlamıştır.

Doç. Dr. Hani Alotaibi
Dokuz Eylül Üniversitesi
BAŞKAN

Doç. Dr. Muhammed Kasim Diril
Dokuz Eylül Üniversitesi
ÜYE

Dr. Öğr. Üyesi Seyit Kale
Katip Çelebi Üniversitesi
ÜYE

TABLE OF CONTENTS

TABLE OF CONTENTS V
LIST OF TABLES IX
LIST OF FIGURES X
LIST OF ABBREVIATIONS XIV
ACKNOWLEDGMENTS XVI
ABSTRACT XVIII
ÖZET XIX
1. INTRODUCTION 1
1.1. Statement and Importance of the Problem 1
1.2. Aim of Study 1
1.3. Hypothesis of Study 2
2. GENERAL INFORMATION 3
2.1. Cellular Plasticity 3
2.2. Epithelial-Mesenchymal Transition (EMT) 7
2.2.1. Developmental EMT 9
2.2.2. EMT In Wound Healing And Fibrosis 11
2.2.3. EMT In Cancer 12
2.2.4 Regulation of EMT 13
2.2.4.1. Transcription Factors 13
2.2.4.2. Signaling Pathways 14
2.2.4.3. Alternative splicing and Non-coding RNA's 15
2.2.4.4. Post-translational Modifications 16
2.2.4.5. Epigenetics 16
2.3. Mesenchymal to Epithelial Transition 18
2.3.1. Regulation of MET 20
2.4. Chromatin Organization 22
2.4.1. Histone Proteins 23
2.4.2. Linker Histones 24
2.4.2.1. Linker Histones Isoforms 26
2.4.2.1.1. Replication Independent Linker Histones 27
2.4.2.1.2. Replication Dependent Linker Histones 28
2.4.2.2.2. Post-translational Modifications of Linker Histones 30

2.5. Rahman Syndrome 32
2.6. Crossroads Of Linker Histones And EMT-MET 35
3. MATERIALS AND METHODS 39
3.1. Type of Study 39
3.2. Time and Place of Study 39
3.3. Materials of Study 39
3.3.1. Cell Lines & Cell Culture Reagents 39
3.3.2. cDNA and qPCR Reagents 40
3.3.3. Plasmid List 40
3.3.4. siRNA Sequence Information 40
3.3.5. Immunofluorescence Labelling Reagents 41
3.3.6. SDS PAGE and Western Blot Reagents 41
3.3.7. Other Chemicals, Consumables, and Commercial Kits 42
3.3.8. Hardware & Machines 42
3.3.9. Chemical Recipes 43
3.3.9.1.Agarose Gel Electrophoresis Solutions 43
3.3.9.2. Western Solution 43
3.3.9.3. Senescence Associated β galactosidase Assay 44
3.4. Variables of Study 45
3.5. Tools For Data Collection 45
3.6. Study Plan and Calendar 45
3.7. Data Evaluation 46
3.7.1. Cell Culture Maintaining and Handling 46
3.7.2. siRNA Transfections 46
3.7.3. CRISPR/Cas9 Genome Editing 46
3.7.3.1. Targeting Vectors and sgRNAs 46
3.7.3.2. Transformation, plasmid conformation and isolation 46
3.7.3.3. Transfection targeting vector and sgRNA, FACS, Selection and Single Cell Sorting 47
3.7.3.4. DNA Extraction and Genotyping 48
3.7.4. Adeno Associated Virus Infection and Cre recombination and Conformation 49
3.7.5. RNA extraction and Gel electrophoresis and Cdna Generation 49
3.7.6. RT-PCR and qPCR 49

3.7.7. Protein extraction and Western Blots 50
3.7.8. H1 extraction and SDS page 51
3.7.9. Growth Curve Analysis 51
3.7.10. Cell Cyle Analysis 52
3.7.11. Fluorescent, ubiquitination-based cell-cycle indicators (Fucci) Transfection and Cell cycle Analysis 52
3.7.12. EMT MET experiments 53
3.7.13. Immunostaining 53
3.7.14. SA-β-Galactosidase Assay 53
3.7.15. Xenograft on Zebrafish larva 54
3.8. Limitation of the Study 55
3.9. Ethics Committee Approval 55
4. RESULTS 56
4.1. siRNA Mediated Silencing of linker histones on MCF10A 56
4.2. Silencing of H1E linker histone in Normal Murine Mammary Gland 59
4.2.1. Selection of siRNA for subsequent experiments 59
4.2.2. Depletion of H1E in NMuMG Cells Results in EMT-like Phenotype 61
4.2.3. Generation of FUCCI Clones and Assessment of Cell Cycle in Knockdown 64
4.2.4. Depletion of H1E in NMuMG Cells Obstracts MET and Results in Mesenchymal-like Phenotype 65
4.2.5. Assessment of Senescence in Knockdown 68
4.3. Development of linker histone H1E knockout NMuMG cell lines 69
4.3.1. CRISPR/Cas9 strategy and Vector Design 70
4.3.2. CRISPR/Cas9 Editing of NMuMG cell, Single Cell Cloning and Genotyping 71
4.4. Proliferation Rate and Cell Cycle Analysis Of BC Clones 74
4.5. EMT-MET Experiments Of BC Clones 75
4.5.1. Epithelial to Mesenchymal Transition of BC Clones 76
4.5.2. Mesenchymal to Epithelial Transition of BC Clones 79
4.6. Generation And Validation of Clones With RAHMAN H1E mutation expression 84
4.6.1. Adeno-Associated Cre Virus Infection 84
4.6.2. Validation of Cre Recombination and Expression of Mutant Protein 84

4.7. Proliferation Rate And Cell Cycle Analysis 87
4.8. EMT-MET Experiments of AC Clones 88
4.8.1. Epithelial to Mesenchymal Transition of AC Clones 88
4.8.2. Mesenchymal to Epithelial Transition of AC Clones 91
4.9. Genotyping of Linker Histone Isoforms 94
4.10. Pathogenic H1E Variant Impaired Cell Plasticity And Accelerated Senescence 96
4.11. Pathogenic H1E Variant Caused Migration and Invasion in Zebrafish 100
4.12. Linker histone compensation in 10AC 101
5. DISCUSSION 103
6. CONCLUSION AND SUGGESTIONS 110
7. REFERENCES 111
8. APPENDIX 135
8.1. Appendix I. 135
8.2. Ethics Approval 137
8.3. Thesis Output 138

LIST OF TABLES

Table 1. PTMs of linker histones and their specific functions. Table adapted from (Hergeth & Schneider, 2015) 31
Table 2. Cell lines 39
Table 3. Cell culture reagents 39
Table 4. cDNA and qPCR Reagents 40
Table 5. Plasmids and viral vectors used in this study. 40
Table 6. siRNA Sequence 40
Table 7. Immunostaining Antibodies 41
Table 8. Immunofluorescence Labelling Reagents 41
Table 9. Antibodie 41
Table 10. Other chemicals and Reagents 41
Table 11. Other Chemicals, Consumables, and Commercial kits 42
Table 12. Hardware and machines used in this study 42
Table 13. List of clones for further experiments 74
Table 14. qPCR Primers and Probe Informations 135
Table 15. PCR Primers for gDNA and cDNA. 136

LIST OF FIGURES

Figure 1. Summary of cell plasticity models 4
Figure 2. Classifications of EMT. 8
Figure 3. EMT in Development and Organogenesis. 10
Figure 4. Signaling pathways regulating EMT(Anushka Dongre & Robert A. Weinberg, 2019). 15
Figure 5. Epigenetic Regulation Mechanisms (Smigielski et al., 2020). 17
Figure 6. Chromatin Compaction and Gene Expression. 23
Figure 7. Tripartite Structure of linker histone 24
Figure 8. H1 bound nucleosome 26
Figure 9. H1 Isoforms and structural differences in chromatosomes 27
Figure 10. PTMs Of Linker Histone H1E. 30
Figure 11. Mutation hotspots in H1E 33
Figure 12. Images of individuals with Rahman Syndrome. 34
Figure 13. Differential expression of linker histones throughout the EMT-MET stages. 37
Figure 14. Illustration of the principle of action of the Fucci system. 52
Figure 15. Xenograft Workflow 54
Figure 16. H1C Depletion Does Not Promote EMT. A. 56
Figure 17. H1D Depletion Does Not Promote EMT 57
Figure 18. H1E depletion promoted an EMT-like phenotype. 58
Figure 19. H1E depletion influenced cell viability. Silencing of H1E affected cell viability. 58
Figure 20. H1E depletion influences the cell cycle 59
Figure 21. Knockdown with different siRNAs resulted in different phenotypic responses. 60
Figure 22. Knockdown efficiencies and targeting sequences of siRNA2 aligned with linker isoforms. 61
Figure 23. Depletion of H1E in NMuMG cells resulted in an EMT-like phenotype. 62
Figure 24. Immunofluorescence Imaging confirmed an EMT-like phenotype. 63
Figure 25. H1E depletion in NMuMG cells resulted in G1 arrest. 65
Figure 26. Illustration of H1E silencing on the onset of MET. 65

Figure 27. H1E knockdown arrested cells in the mesenchymal-like state by obstructing the Mesenchymal-Epithelial Transition..... 66
Figure 28. H1E knockdown arrested cells in the mesenchymal-like state by obstructing the Mesenchymal-Epithelial Transition..... 67
Figure 29. In the absence of H1E, E-cadherin failed to localize to the cell membrane. 68
Figure 30. Cells arrested in the mesenchymal state after silencing of H1E showed a senescence tendency. H1E depleted cells showed a slight affinity for x-gal. 69
Figure 31. H1E levels change throughout of EMT-MET..... 69
Figure 32. Illustration of HDR directed Crispr/Cas9 genome editing of H1E locus. 70
Figure 33. Workflow of CRISPR/Cas9 edited clone generation. 71
Figure 34. Schematic representation of genotyping and genotyping analysis of approved single-cell clones. 72
Figure 35. Final Genotyping Of Selected Clones. 72
Figure 36. Amino Acid Sequence of clones and charge differences of CTD tails. 73
Figure 37. Half-dose depletion of H1E or its Truncation did not affect the growth rate, but deletion of the CTD resulted in retarded growth 74
Figure 38. Half-dose depletion of H1E or its Truncation did not affect the Cell Cycle. 75
Figure 39. 10BC successfully completed epithelial-to-mesenchymal transition. 76
Figure 40. 10BC successfully completed epithelial-to-mesenchymal transition. 77
Figure 41. 11BC Successfully Completed Epithelial-To-Mesenchymal Transition. 78
Figure 42. 24BC Successfully Completed Epithelial-To-Mesenchymal Transition. 79
Figure 43. BC Clones Successfully Completed The Mesenchymal To Epithelial Transition. 80
Figure 44. 10BC Successfully Completed The Mesenchymal-To-Epithelial Transition. 81
Figure 45. 11BC Successfully Completed The Mesenchymal To Epithelial Transition..... 82
Figure 46. 24BC Successfully Completed The Mesenchymal To Epithelial Transition. 83

Figure 47. Schematic illustration of AAV-Cre infection, Cre-recombination, and initiation of Pathogenic Rahman Variant expression. 84
Figure 48. Verification Of Cre Efficiency At The Genomic And RNA Levels By RT-PCR And Assessment Of Morphological Changes In Cells In Response To Rahman Protein. 85
Figure 49. Verification Of Cre Efficiency At The Protein Level. 86
Figure 50. Verification Of Proper Pathogenic Variant Localization. 87
Figure 51. Clone 10 Showed Dramatic Growth Arrest In Response To Pathogenic Protein Expression. 88
Figure 52. Clone 10 Showed Dramatic Cell Cycle Arrest In Response To Pathogenic Protein Expression. 88
Figure 53. Rahman Clones Were Able To Undergo EMT. 89
Figure 54. 10AC Cells Were Able To Undergo EMT 90
Figure 55. 11AC Cells Were Able To Undergo EMT. 90
Figure 56. Phase-Contrast Microscopy Images Showing Different Responses Of Rahman Clones To TGF-β3 Withdrawal. 91
Figure 57. 11AC Successfully Completed The Mesenchymal-To-Epithelial Transition. 92
Figure 58. 10AC Was Not Able To Complete Mesenchymal To Epithelial Transition Successfully. 92
Figure 59. Immunofluorescence staining of clones in each state of the transition anti-E-cadherin and anti-phalloidin. 93
Figure 60. Genomic Examination Of Different Linker Histone Isoforms By Genomic PCR Showed Dosage Depletion Of H1D In Clone 11. 94
Figure 61. H1D was downregulated in clone 11BC, which was consistent with a decrease in genomic screening. 95
Figure 62. Clone 11 showed disruptions in 5’ regulatory region of H1f0 but no difference was detected in overall protein levels of linker histones. 96
Figure 63. 10 AC Retained Mesenchymal Gene Pattern. 96
Figure 64. 10 AC Failed to Gain Epithelial Gene Expression Patter. 97
Figure 65. Inability of 10 AC to complete MET was also apparent at the protein level. 98
Figure 66. IF staining results of clone 10 AC showing halted MET. 99
Figure 67. 10AC Showed β-Galactosidase Activity, Indicating Senescence. 100
Figure 68. 10AC Exhibited Enhanced Motility And Metastatic Features In Zebrafish. 101

Figure 69. 10AC showed differential expression of isoforms during EMT and MET. 102

LIST OF ABBREVIATIONS

EMT: Epithelial-Mesenchymal Transition

MET: Mesenchymal-Epithelial Transition

TGFβ: Transforming Growth Factor Beta

TFs: Transcription Factors

ECM: Extracellular Matrix

miRNA: Micro RNA

circRNA: Circular RNA

LncRNA: Long Non-coding RNA

NMuMG: Normal Murine Mammary Gland Cell Line

MEF: Mouse Embryonic Fibroblast

MMPs: Matrix Metalloproteinases

ESRP1: Epithelial-specific regulatory protein 1

ESRP2: Epithelial-specific regulatory protein 2

HDAC1: Histone deacetylase 1

HDAC2: Histone deacetylase 2

BF: Bright Field

gDNA: Genomic DNA

BSA: Bovine Serum Albumin

Cdh1: E-Cadherin

Cdh2: N-Cadherin

Cebpα: CCAAT Enhancer Binding Protein Alpha

Fn1: Fibronectin

FBS: Fetal bovine serum

Grhl3: Grainyhead like transcription factor 3

Hnf4α: Hepatocyte nuclear factor-4 alpha

Ovol2: Ovo Like Zinc Finger 2

Klf4: Krüppel-like factor 4

Elf3: E74-like factor 3

Snai1: Snail Family Transcriptional Repressor 1

Snai2: Snail Family Transcriptional Repressor 2

Vim: Vimentin

Zeb1: Zinc Finger E-Box Binding Homeobox 1

Zeb2: Zinc Finger E-Box Binding Homeobox 2

Dnmt1: DNA (cytosine-5)-methyltransferase 1

Dnmt3a: DNA (cytosine-5)-methyltransferase 3a

Dnmt3b: DNA-methyltransferase 3 beta

Dnmt3l: DNA (cytosine-5)-methyltransferase 3-like

Uhrf1: Ubiquitin Like With PHD And Ring Finger Domains 1

siRNA: Small interfering RNA

PBS: Phosphate Buffer Saline

RT: Reverse Transcriptase

qPCR: quantitative polymerase chain reaction

BC: Before Cre Recombination

AC: After Cre Recombination

NTD: N-Terminal Domain

CTD: C-Terminal Domain

GD Globular Domain

ACKNOWLEDGMENTS

The successful completion of this work would not have been possible without the invaluable support and guidance of numerous individuals. I am deeply grateful to my advisors, Associate Professor Hani Alotaibi and Dr. Imtiaz Nisar Lone, whose insightful advice and mentorship were instrumental in shaping this study. Their expertise and encouragement were crucial for navigating the challenges encountered throughout this academic journey.

I also extend my heartfelt appreciation to Associate Professor Kasım Diril, Professor Dimitar Angelov, and Professor Stefan Dimitrov for their kind guidance during particularly difficult moments, which helped me overcome obstacles and maintain progress.

I also want to express my gratitude to my precious BSc Supervisor Prof.Dr. Semra Hasançebi, without her I would not be here. Her unwavering support and guidance throughout my undergraduate studies were instrumental in shaping my academic journey. Prof. Hasançebi's mentorship not only helped me develop a strong foundation in my field but also inspired me to pursue further research. Her dedication to her students and passion for science continue to motivate me in my current endeavors.

I would like to thank TÜBİTAK for supporting the project by grant no:122N046

The camaraderie and support of my laboratory colleagues have been indispensable. I would like to express my heartfelt gratitude to Esin Ozkuru Sekeroglu for her invaluable support, both professional and personal. Her encouragement, feedback, and positive influence have been instrumental in shaping my research and maintaining my mental wellbeing throughout this journey. Esin's friendship has made my time in Izmir truly memorable, and I am deeply appreciative of the profound impact she has had on my life. Her unwavering support and guidance have been a constant source of motivation, and I am sincerely thankful for her presence and contribution to my academic and personal growth.

I owe a tremendous debt of gratitude to Tuğçe Batur, whose steadfast moral support was crucial not only for the completion of this work but also for preserving my mental well-being throughout the process. Tuğçe's unwavering belief in my abilities and her constant words of encouragement provided me with the strength to persevere through the most challenging phases of my research. Her keen intellect and willingness to offer constructive criticism have significantly contributed to the refinement of my ideas and overall quality of my work.

I would like to express my sincere gratitude and offer a heartfelt apology to Sule Ece Zangur, a recent addition to our lab, for the rush start with me the

crazy girl who continued experiments with one arm in the cast, dragging her around from one experiment to another. Thank you for your help during my hard times. From new to former I also extend my thanks to Abed Alkarem for his friendship and reassuring conversations. Your calming presence was a source of comfort during moments of anxiety.

Thank you to Inci Yaprak and Helin Sagir for their unwavering support and cherished friendship. Their companionship was invaluable during challenging times of experimental setbacks and moments of discouragement, as well as in celebrating triumphant achievements. Their presence has been a constant source of comfort and joy throughout this journey.

The friendly faces and positive energy of the Alotaibi lab members, both current and former, including Ayça, Büşra, Seray, and Şeyma, provided constant encouragement.

Lastly, I am profoundly thankful for the unwavering support of my dear family and housemate, whose presence and understanding have been a source of strength and comfort throughout this challenging but rewarding academic endeavor.

Finally, I wish to eternalize my gratitude to my dear grandparents, Hasan Impraimoglou Kafaz and Nermin Sali, whom I unexpectedly lost during this journey. They nurtured a stubborn, curious, and dreaming child, who grew into a dedicated woman pursuing her aspirations. May they rest in peace and light.

INVESTIGATION OF
FUNCTIONAL CONTRIBUTION OF H1E IN EMT AND MET

Gkamze Impraimoglou Kafaz, İzmir International Biomedicine and Genome Institute, Dokuz Eylul University Health Campus, Balcova 35340 - Izmir / TURKEY

ABSTRACT

The Epithelial-mesenchymal transition (EMT) and mesenchymal-epithelial transition (MET) are cellular reprogramming events, interrelated but not directly antagonistic. These biological processes are crucial for numerous physiological and pathological mechanisms, including development, wound healing, and tumorigenesis. These processes significantly alter cellular identity without any changes at the genomic level. Various factors, including transcription factors and epigenetic mechanisms, control these transitions. Chromatin conformation, a primary epigenetic regulation, is modulated by the dynamics of histones, the positively charged proteins that fold DNA into chromatin in eukaryotic cells. The fundamental units of chromatin, nucleosomes, are comprised of a DNA fragment, a linker histone, and an octameric core histone complex. These structures play a crucial role in regulating gene expression through their conformational state. H1E linker histone is a member of the H1 family and replication-dependent histones. In the absence of this protein, cell proliferation is negatively affected. Furthermore, mutations in this gene cause dose reduction or truncated protein production, resulting in developmental and functional disorders in specific organs, particularly the brain, and haploinsufficiency of this protein has been associated with autism spectrum disorder. Additionally, patients with a specific C-terminal mutation in H1E and similar clinical outcomes have been identified as having Rahman Syndrome. Although the adverse effects of H1E dysregulation have been established, its effects and mechanism of action on EMT and MET remain unclear. This study aimed to investigate the functional roles of H1E in EMT and MET, with a focus on the absence and presence of the pathogenic H1E variant observed Rahman Syndrome.

Keywords: MET, Chromatin structure, HIST1H1E, EMT, Linker histone, Rahman Syndrome, Crispr/Cas9 genome editing, HDR

EMT ve MET'de H1E'nin Fonksiyonel Katkısının İncelenmesi

Gkamze Impraimoglou Kafaz, İzmir Uluslararası Biyotıp ve Genom Enstitüsü, Dokuz Eylül
Üniversitesi Sağlık Yerleşkesi, Balçova 35340 - İzmir / TÜRKİYE

ÖZET

Epitelyal mezenkimal dönüşüm (EMT) ve mezenkimal epitelyal dönüşüm (MET) süreçleri normal gelişim, yara iyileşmesi ve tümorigenez gibi birçok önemli fizyolojik ve patolojik süreç açısından önem taşıyan farklı iki biyolojik olaydır. Bu süreçler genomik düzeyde bir değişikliğe neden olmaksızın, hücre kimliğini bütünsel olarak değiştirmektedir. Bu değişim epigenetik mekanizmalar ile düzenlenmektedir. Başlıca epigenetik düzenlemelerden biri olan kromatin konformasyonu; ökaryotik hücrelerde DNA'nın kromatine katlanmasını sağlayan, pozitif yüklü proteinler olan histon etkileşimleriyle modüle edilir. Kromatin, küçük bir DNA parçası, bağlayıcı histon ve kor histon oktamer kompleksinden oluşan nükleozom adlı yapının tekrarlarından oluşup konformasyonel statüsüne bağlı olarak gen ifadesini regüle etmektedir. H1E bağlayıcı histon H1 ailesinin bir üyesi ve replikasyon bağımlı histonları alt grubunun bir üyesi olup, yokluğunda hücre proliferasyonun negatif etkilendiği tespit edilmiştir. Bunun yanı sıra bu gendeki protein doz düşümüne veya hatalı protein üretimine sebebiyet veren mutasyonların beyin başta olmak üzere bazı organların gelişim ve fonksiyon bozukluklarına neden olduğu tespit edilmiş ve otizm spektrum bozukluğu ile ilişkilendirilmiş, spesifik bir C-terminal mutasyonu bireylerde gösterdiği ortak fenotip ve klinik tablo ile Rahman sendromu olarak tanımlanmıştır. H1E proteininin disregülasyonunun gelişimsel süreçler üzerindeki negatif etkisi tespit edilmiş olmasına rağmen, EMT ve MET üzerinde ki etkileri ve etki mekanizması karanlıkta bırakılmıştır. Bu çalışma, Rahman Sendromunda gözlemlenen patojenik H1E varyantının varlığı ve H1E yokluğuna odaklanarak EMT ve MET'teki fonksiyonel rollerini araştırmayı amaçladı.

Anahtar kelimeler: MET, Kromatin Yapısı, EMT, Bağlayıcı Histon, HIST1H1E, Rahman Sendromu, Crispr/Cas9, HDR

1. INTRODUCTION

1.1. Statement and Importance of the Problem

Epithelial to mesenchymal transition (EMT) and mesenchymal to epithelial transition (MET) are two distinct biological processes that play crucial roles in numerous significant physiological and pathological mechanisms, including development, wound healing, and tumorigenesis. EMT and MET are events that fundamentally alter cell identity without modifying the cell genome. These processes are regulated by epigenetic mechanisms and exhibit distinctive epigenomic signatures. Chromatin conformation, a key component of the epigenomic signature, is regulated by histone proteins. Chromatin comprises iterative components called nucleosomes, comprised of a DNA fragment of approximately 165 bp or 245 bp, a linker histone, and a core histone octamer complex. Linker histones bind to DNA in the start and exit regions of nucleosomal particles, thereby ensuring nucleosome completion, determining nucleosomal repeat lengths, and stabilizing higher-order chromatin structures. H1.E, a linker histone isoform, specifically histone gene cluster 1 Member E (HIST1H1E), is a constituent of the epigenetic regulator gene family that codes a linker histone that directs the structural organization of chromatin. It belongs to a subgroup of replication histones, and its absence has been observed to negatively impact cell proliferation. Furthermore, mutations in this gene, resulting in reduced or truncated protein production, have been associated with impaired brain development and function, as well as autism spectrum disorder. Additionally, a recently identified mutation affecting the C-terminal tail of the H1E protein has been found to generate a clinical presentation comprising a recognizable facial appearance, intellectual disability, hypothyroidism, abnormal dentition, behavioral problems, cryptorchidism, skeletal and cardiac anomalies, referred to as Rahman syndrome in the nomenclature.

While the significance of the H1E protein in cellular processes has been extensively studied and elucidated from various perspectives, its effects and mechanism of action on EMT and MET remain unexplored. This research aims to investigate the functional roles of H1E in EMT and MET processes utilizing the NMuMG cell line, which is the established EMT and MET model in the literature.

1.2. Aim of Study

The aim of this thesis was to investigate the functional role and importance of H1E linker histones in the EMT and MET processes. Unraveling the effects of pathogenic H1E variant in EMT and MET for possible indications of abnormal organogenesis networks and disruptions in tissue homeostasis.

Aim:

To study whether the absence of linker histone H1E or its pathogenic mutation can affect EMT or MET through disruption of chromatin.

Objectives:

1. To define whether H1E is a crucial particle of EMT or MET network.
2. To determine the effect of nucleosomal and concurrent chromatin level disruption on EMT and MET.
3. To study the impact of a pathogenic linker variant on EMT and MET.

1.3. Hypothesis of Study

During TGF-β treatment, RNA-seq data of NMuMG cells showed significant downregulation of all linker histones as a possible indicator of more relaxed chromatin in the mesenchymal state. However, this downregulation showed distinct turnover upon TGF-β withdrawal. Evidence of favored compact chromatin order in epithelial cells with a determined fate until another stimulus. This study investigated whether disruption of linker histones could affect the tightly regulated chromatin order between transitions. In addition, we focused on linker histones with the ability to generate disease. Here, we hypothesized that depletion of H1E linker histone or the presence of its pathogenic variant would cause arrest in EMT level, disrupting the high cellular plasticity of NMuMG cells and obstructing MET through chromatin-wide dysregulation. Creating the first evidence of chromatin level regulation of the mesenchymal-to-epithelial transition network.

2. GENERAL INFORMATION

2.1. Cellular Plasticity

Multicellular organisms are defined by tissues with dramatically different cellular composition and architecture, keeping the homeostasis owing their own cell plasticity which is strictly controlled by numerous mechanisms (Figure 1). Different cell types within the same tissue are organized in a hierarchical manner according to their potency levels, where cells with higher potency are positioned at the top of the hierarchy and by lowering the level of the potency potential, dropping the hierarchical class until the fully fated mature cells that compose the bottom of the hierarchy (Clevers & Watt, 2018; Hogan et al., 2014; Kume et al., 2000; Scadden, 2014; Wicker & Wagner, 2023). Since time immemorial, it was believed that this hierarchical order was irreversible as the fate of the cells was not DE differentiable. Although recent studies showed that for some cell types, the final fate was not irreversible, and cells of the same lineage can play back and forth in their hierarchical order to retain homeostasis of the tissue in response to endogenous or exogenous stimuli. This ability of cells to change their identity and function in response to physiological or pathological stimuli is referred to as cellular plasticity. (Wicker & Wagner, 2023). Cell plasticity is observed in two types: intra-lineage plasticity, where cells stick to the lineage they originate from and change their identity and function within the lineage, and trans-lineage plasticity, where cells lose the characteristics of their origin and differentiate across different cell lineages, named trans-differentiation. Plasticity is a highly important biological phenomenon that is observed in various tissues and cell types. Intra-lineage plasticity give rise to more limited differentiation, (Lee et al., 2017). To illustrate, neural stem cells exhibit intra-lineage plasticity by differentiating into diverse neuron and glial cell types within the nervous system. In a comparable manner, hematopoietic stem cells maintain their capacity to produce various blood cell types while remaining within the hematopoietic lineage (Hogan et al., 2014). Conversely, mesenchymal stem cells (MSCs) that exhibit trans-lineage plasticity possess the capacity to differentiate into osteogenic, chondrogenic, and adipogenic lineages (Alexanian, 2015; Pfefferle et al., 2019).

Furthermore, specific epithelial cells can undergo EMT, thereby obtaining mesenchymal characteristics and facilitating their migration to diverse tissues (Akhmetkaliyev et al., 2023). These forms of plasticity are crucial for development, tissue repair, and regeneration, enabling cells to adapt to various physiological needs and environmental changes, but can also be destructive when hijacked by cancer cells, which are associated with metastasis and recurrence (Paksa & Rajagopal, 2017). Cell plasticity is crucial during development, where it enables cells to dynamically change their identity and function to form various tissues and organs. Embryonic developmental processes require programming of cellular differentiation systems, which are intimately linked with dynamic cell interactions (Keller, 2005).

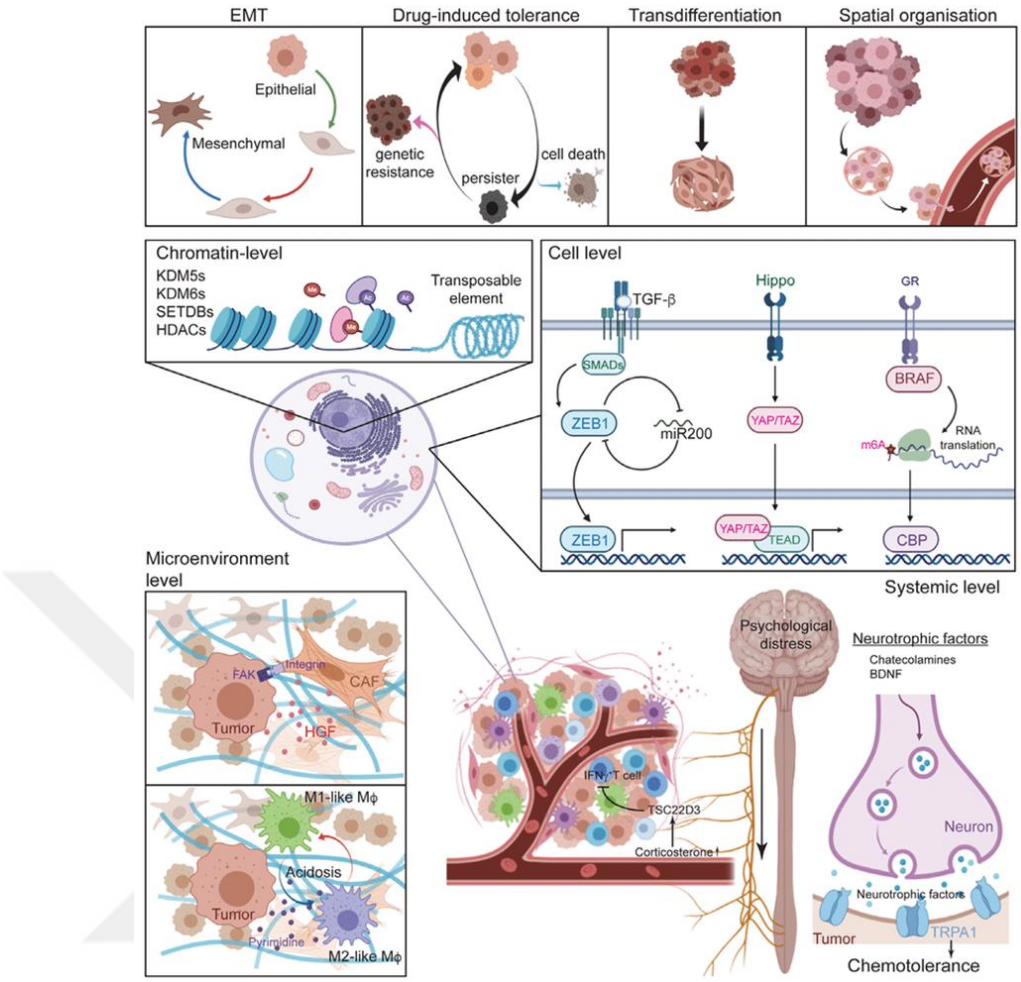

Figure 1. Summary of cell plasticity models. Figure adapted from (Shen & Clairambault, 2020).

In the context of developmental processes, cellular plasticity describes the ability of cells to alter their destiny and assume new functional roles. Cell plasticity during development is a dynamic and complex process that allows cells to acclimate to various internal and external stimuli. A wide array of factors controls this process, including genetic expression, changes in chromatin structure, cellular metabolic conditions, and external environmental stimuli (Buttitta, 2016; Folmes & Terzic, 2014; Hochberg, 2011; Vicente-Duenas et al., 2009). First line of regulation consists of various signaling pathways; Wnt, Notch, Hedgehog and BMP are essential for cell communication through helping cells interpret external and internal signals and coordinate proper proliferation, differentiation and migration (Artavanis-Tsakonas et al., 1999; Clevers, 2006; Ingham & McMahon, 2001; Zhang & Li, 2005). As per external stimuli, microenvironmental cues also create another line of control over cell plasticity through the extracellular matrix, a network of proteins and polysaccharides that provides structural support and biochemical signals to cells (Hynes, 2009). Biochemical stimuli of growth factors and cytokines bind to cell-surface receptors stimulate intracellular signaling

cascades influencing cell fate decisions (Massagué, 2012). Besides the integrins the receptors that mediate cell-ECM interactions as well as cadherins that provide cell-cell adhesion can influence cell architecture through migration, proliferation and survival therefore regulate cell plasticity (Hynes, 2002; Takeichi, 1991). In response to epigenetic mechanisms, environmental stimuli modulate transcription through DNA methylation and histone modifications (Jaenisch & Bird, 2003). This also alters chromatin confirmation, providing access to appropriate transcription factors to further enhance the control of gene expression levels (Kouzarides, 2007). As an illustration, these elements play a crucial role in both triggering and sustaining the process of cellular differentiation. Examples include Sox, Oct, and Nanog, which are involved in maintaining pluripotency and guiding differentiation (Avilion et al., 2003; Chambers et al., 2003). Neural crest cell behavior stands out as a prime illustration of cellular plasticity. Neural crest cells, under stimuli of the above mechanisms, migrate extensively throughout the embryo, giving rise to diverse cell types, such as neurons, glial cells, melanocytes, and cartilage, in response to various signals in their environment (Sauka-Spengler & Bronner-Fraser, 2008).

Cell plasticity not only enables proper organ and tissue development but also orchestrates wound and tissue healing after injury through the regeneration process. In adults, certain cells can revert to a more primitive state or transform into different cell types to aid in tissue repair. This process is known as dedifferentiation or trans-differentiation (Spatz et al., 2021). Following injury, changes in the microenvironment of the cells, especially the changes in composition and stiffness of the extracellular matrix, give rise to external and internal signaling cascades and promote regeneration and repair (Hynes, 2009). In response to these tissues, high plasticity can generate a pool of progenitor cells, with the help of TFs activating the expression of potency-related genes and altering their epigenetic state, reverting to a more primitive state with high plasticity and proliferation properties, and can differentiate into the required somatic cell types for tissue replacement. One of the best examples of regenerative plasticity is held by Schwann cells. These actors of the peripheral nervous system exhibit a remarkable plasticity. Following injury, regulated by Notch and endothelin, they dedifferentiate, downregulate myelin proteins, and upregulate neurotrophic factors and cytokines (Nocera & Jacob, 2020). This transformation promotes axonal regeneration and attracts macrophages to aid in wound healing trough cleaning of cell debris and secretion of factors that promote healing and regeneration (Emilia et al., 2020; Nocera & Jacob, 2020).

Immune cells exhibit a crucial characteristic known as cell plasticity, which allows them to adjust to various functional states when confronted with infections and other challenges (Chen et al., 2023). A prime example is the ability of macrophages to transition between the pro-inflammatory (M1) and anti-inflammatory (M2) states based on environmental cues (Mills, 2012; Sica & Mantovani, 2012). This adaptability is essential for sustaining the immune homeostasis and coordinating effective immune responses. M1 macrophages,

triggered by signals like interferon gamma (IFN-γ), generate immunostimulatory cytokines such as TNF-α, IL-6, and IL-1β, which are vital for countering infections and activating inflammation. In contrast, M2 macrophages, induced by cytokines, including interleukin 4, 10, and 13 (IL-4, IL-10, IL-13), represent the subsequent phase of the immune response (Mills, 2012; Mills, 2015). These cells participate in tissue repair, wound healing, and inflammation resolution by producing anti-inflammatory cytokines and growth factors that support tissue regeneration (Chen et al., 2023). Nevertheless, disruption of immune cell plasticity can result in persistent inflammation and autoimmune disorders (Viola et al., 2019). An illustration of this phenomenon is observed in neutrophils, which undergo a trans-lineage shift in response to the microenvironment's composition (Torres et al., 2019). Terminally differentiated and fully committed neutrophils can attain phenotypic and functional features related with antigen-presenting cells (APCs)(Hampton & Chtanova, 2016; Matsushima et al., 2013) in the inflammatory and pro-type 2 environment of a lesion (Takashima & Yao, 2015). This kind of trans-differentiation is present in rheumatoid arthritis, resulting in sustained inflammation, thereby preventing normal repair (Iking-Konert et al., 2005). Understanding the factors that control immune cell plasticity could lead to new therapeutic approaches.

This plasticity is biologically significant, as it contributes to the normal development of tissues and has implications for the emergence of diseases, such as cancer, when aberrant reprogramming occurs (Vicente-Dueñas et al., 2010). Cancer cells hijack developmental plasticity mechanisms to evade therapeutic interventions and use the acquired properties to migrate and invade various microenvironments (Fatma et al., 2023). Also, cellular plasticity in cancer contributes into acquisition of stem cell-like properties ensuring cells high level ability of self-renewal and proliferation creating the cancer stem cells, CSCs (Mathur et al., 2024). CSCs not only facilitate immune evasion but thanks to their potential to differentiate into numerous varieties they contribute to tumor heterogeneity and resilience against treatments (Fatma et al., 2023). Cancer cells hijack cellular plasticity in various ways. For example, aberrant methylation in the promoter of proto-oncogenes, such as MLH1, BRCA1, and VHL, can silence this gene, causing increased proliferation and unstable fate decisions (Mathur et al., 2024). Furthermore, uncontrollable activation of Wnt signaling, in most cancers triggered by mutations of APC gene and dysregulation of Notch pathway attributable mutations in NOTCH1 gene can result in uncontrolled cell growth and proliferation. The aberrant expression of pluripotency-related TFs such as Sox2 and Myc can result in the gain of stem cell-like properties, including self-renewal and pluripotency. Also, overpopulation of cancer cells in the tissues causes hypoxic conditions leading to expression and secretion of HIFs which promote angiogenesis and metabolic adaptation; therefore, migration of cancer cells due to their newly gained abilities. In all cases, the most favored processes by which cells jump into different characteristics are EMT and MET, where they lose their epithelial stable properties and gain mesenchymal characteristics and unstable potency,

which can be reversed according to appropriate stimuli. (A. Dongre & R. A. Weinberg, 2019; Fatma et al., 2023; Mathur et al., 2024)

It is universally recognized that the epigenome can be altered by environmental fluctuations, allowing cells to control the expression of genes through cellular plasticity programs in which cells change their phenotypes without modifying their genotypes (Duncan et al., 2014; Tulsyan et al., 2022). Cellular plasticity and dynamic gene expression patterns rely on complex and conserved (Tiwari et al., 2020). One of the most well-known processes that determines cellular morphology and dynamic cell interactions is intercellular adhesion, which is tightly regulated by the E-cadherin molecule and considered a functional unit of adhesion (Erami et al., 2016; van Roy & Berx, 2008). Dynamic changes and plasticity required for several biological processes necessitate that Cdh1 be regulated in a controlled manner (Bedi et al., 2014; Erami et al., 2016). In biological processes, such as EMT and MET, are usually associated with switching the expression states of E-cadherin among changes in other molecular signatures. Oscillations during the course of EMT-MET are utilized to stabilize cellular homeostasis (A. Dongre & R. A. Weinberg, 2019; Sedzinski et al., 2016)In conclusion, cellular plasticity enables cells to adjust to various conditions and is essential for normal bodily functions but also responsible for development of diseases. Studying the mechanisms underlying this phenomenon can help us to understand and modify it to improve regenerative medicine and create new cancer treatments.

2.2. Epithelial-Mesenchymal Transition (EMT)

Epithelial-to-mesenchymal transition (EMT) is one of the main features of cell plasticity. Onset of EMT is characterized by loss of apico-basal polarity and cellular adhesion properties, loss of final fate decision, transdifferentiating into mesenchymal cells with gain of invasive and migratory abilities. In molecular basis cells undergoing EMT are defined by downregulation of epithelial markers like CDH1 which is followed by vanishment of its cell adhesion molecule product E-cadherin or its delocalization into cytoplasm (Kalluri & Weinberg, 2009). In response to the loss of E-cadherin on the cell surface and increase in the mesenchymal gene expression, such as vimentin, fibronectin, and especially CDH2, cells lose their tightly connected polarized cobblestone morphology. With the vanishment of E-cadherin from the cell membrane and replacement of it with N-Cadherin, product of CDH2 gene a strong mesenchymal marker, a phenomenon called “cadherin-switch” takes place (Gravdal et al., 2007). Cadherin switch is considered as number one hallmark of EMT and is associated with not only loss of cobblestone morphology but also gain of spindle-shaped morphology caused by loss of tight junction and enables cells migratory and invasive abilities (Yang et al., 2020). Numerous distinct events are engaged in to trigger an EMT and act through intermediate phenotypes till the reach of completion (Kalluri & Weinberg, 2009; S. Lamouille et al., 2014). This includes activation of transcription factors like ZEB and SNAI family and Twist, change of epigenetic signature followed by chromatin conformation changes differential expression

of particular membrane proteins like cadherin-switch, reorganization and expression of cytoskeletal proteins which enable the change of morphology, production of ECM-degrading enzymes and transcriptomic changed including specific non-coding RNA's in state dependent manner (Dave et al., 2011; Gregory et al., 2008; S. Lamouille et al., 2014; Lin & Wu, 2020; Saitoh, 2023).

EMT occurs in three different biological settings that carry out distinct functional roles and are accordingly categorized. Type 1 EMT is present in implantation and development of embryos during gastrulation and organogenesis. (Kalluri & Weinberg, 2009; Nakaya & Sheng, 2008) While type 2 EMT is observed during wound healing, tissue regeneration, and organ fibrosis following an injury(Kalluri & Weinberg, 2009). This kind of EMT is closely associated with inflammation, although the EMT program starts as part of repair process of the injured tissue it would not cease till the inflammation is attenuated. Hence, persistent inflammation of the injured tissue could cause an ongoing EMT process, leading to fibrosis and organ destruction (Barriere et al., 2015). In contrast, type 3 EMT is found in cancer cells with possible mutations in regulatory genes and/or continuous stimuli of the microenvironment. Type 3 EMT is closely associated with metastasis as it gives rise to migratory and invasive abilities of cancer cells enabling metastasis to distant tissues and resistance to therapeutics due to gained mesenchymal properties (Brabletz et al., 2018). Although the functional outcomes of these three distinct EMT's differ dramatically, the regulatory mechanisms underlying these processes are yet to be understood (Figure 2).

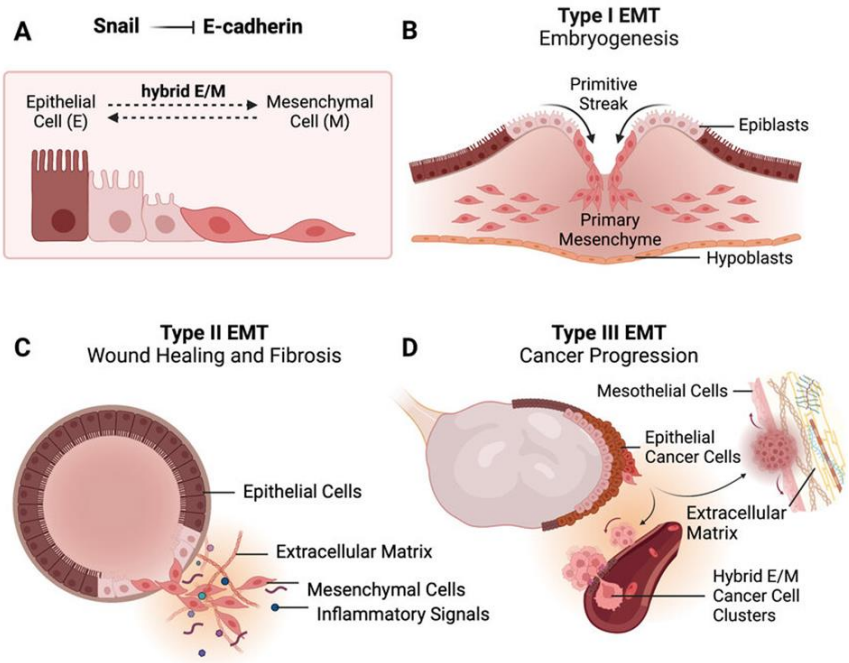

Figure 2. Classifications of EMT. Adapted from (Suzuki et al., 2023).

2.2.1. Developmental EMT

The first event of EMT takes place during the implementation of embryo in the uterus when cells of the extraembryonic region like extra villous trophectodermal cells undergo EMT to pass through the endometrium and anchor in the placenta (Kalluri & Weinberg, 2009). In addition to anchoring in the uterus of the blastocyst, one layer of epithelial cells undergoes EMT during the formation of three germ layers and gastrulation. As the first sign of gastrulation, primitive streak is generated from epithelial cells with robust E-cadherin expression and apica-basal polarity the epiblast layer (Kalluri & Weinberg, 2009; Nakaya & Sheng, 2008). The primitive streak emerges from the grooved invagination along the midsagittal plane of the epiblast, initially forming at the caudal extremity of embryo and progressing towards the future cephalic region, forming the primitive pit with the collected mass of the cells and then the primary tissue organizer region of the primitive node. Epiblast cells undergo programmed modifications regulated by differential protein expressions related to cellular migration and differentiation in this region (Kalluri & Weinberg, 2009; Nakaya & Sheng, 2008, 2013). This phenomenon was found to be strictly controlled by the Wnt signaling pathway (Skromne & Stern, 2001). During formation, primitive streak dysregulation of Wnt8c expression resulted in aberrant formation of primitive streaks, whereas the absence of Wnt3 aborted primitive streak formation (Liu et al., 1999; Pöpperl et al., 1997). Following the generation of a primitive streak, ingression starts with the epithelial- mesenchymal transition of the epiblast cell population. Following the primitive tube, the mesenchymal cells of the epiblast layer migrate and integrate into the hypoblast layer to form the endoderm. The second wave of migrating cells fills the space between the endoderm and epiblast layers to form the mesoderm. Multiple migration and repolarization of cells will next form the three layers of mesoderm the axial, intermediate and lateral mesoderm while the remaining cell of epiblast will form the third germ layer, ectoderm that will give rise to specific organs (Figure 3) (Acloque et al., 2009).

The observed EMT is not only controlled by Wnt signaling but also orchestrated by TFs like Snail, Eomes, and Mesps induced by FGF signaling (Arnold et al., 2008; Chea et al., 2005; Lindsley et al., 2008; Rossant et al., 1997; Shah et al., 1997; Varlet et al., 1997). Snail especially represses E-cadherin and promotes EMT, which takes place by increment of other inducers. Subsequently, the formed mesoderm gives rise to the primary mesenchyme precursors of the paraxial, axial, lateral, and intermediate mesoderm. For instance, in the absence of FGF signaling since the Snai1 expression cannot be enhanced mesenchyme accumulation in the mesoderm was shown to be failed because of the inefficacy of the cells to downregulate CDH1 levels (Ciruna & Rossant, 2001).

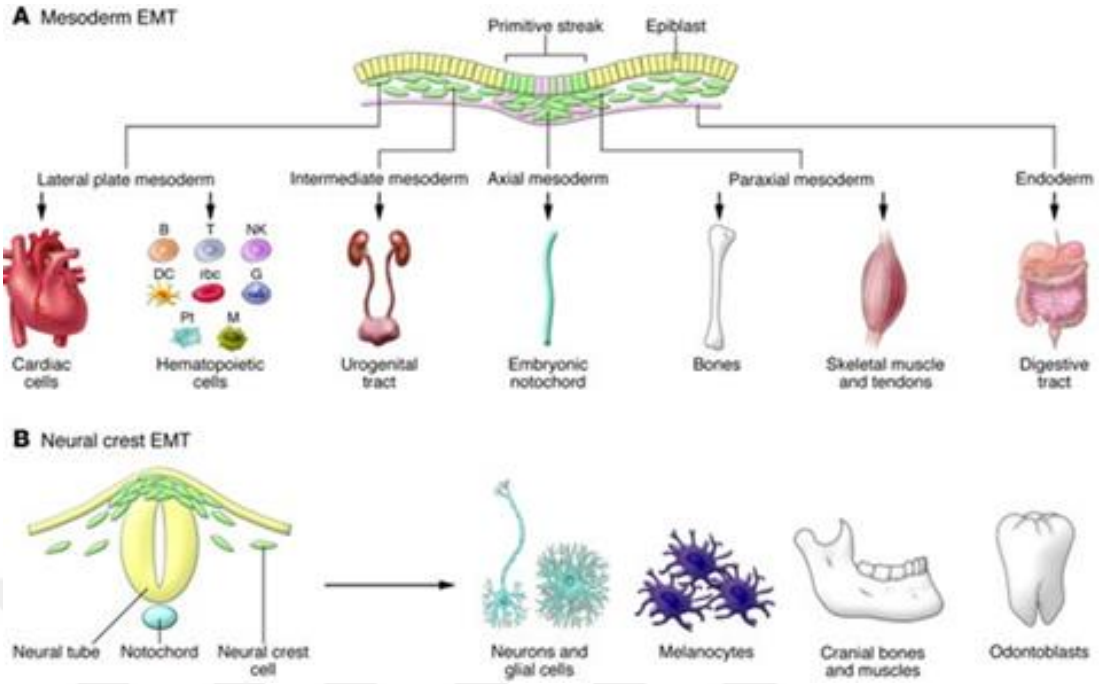

Figure 3. EMT in Development and Organogenesis. (Adapted from Nieto, 2013).

Same wise Snai1 deficient embryos showed accumulation of epithelial cells that were unable to migrate, but mesoderm specification was not altered, indicating possible take-over of yet discovered pathways (Lomelí et al., 2009). It is worth mentioning that Snai1 does not only repress CDH1 expression but also regulates expression of cell adhesion molecules, such as occludins, claudins and polarization genes like Dlg and Crb3 (Arnold et al., 2008; Ikenouchi et al., 2008; Whiteman et al., 2008). EMT observed in gastrulation is associated with canonical Wnt signaling, as studies have shown that Wnt3 deficient embryos are unable to undergo EMT during gastrulation (Lindsley et al., 2006). In addition to the absence of Nodal and Vg1, proteins of the TGF-β superfamily were shown to be involved in gastrulation-associated EMT as their absence aborted the process (Shah et al., 1997; Varlet et al., 1997).

EMT also plays a crucial role in neural crest formation in the neuroectoderm. The upregulation of Sox, Snail, Slug and FoxD3 genes initiate EMT in neuroectodermal cells giving migratory abilities (Kasai et al., 1992; Liem Jr et al., 1995; Nieto et al., 1994). Besides those genes actors of Wnt, FGF, and BMP signaling pathways, together with c-Myp and Msx-1, work together to induce EMT. Upon acquiring mesenchymal characteristics, neural crest cells become mobile, traveling to various locations within the embryo. These cells then undergo differentiation, transforming into diverse cell types such as neurons, glial cells, and melanocytes (Kalluri & Weinberg, 2009; Karafiat et al., 2007; Liem Jr et al., 2000; Villanueva et al., 2002). Strangely compared to typical EMT properties, the induced EMT in early migratory cells is followed by synchronous downregulation of E-cadherin and N-cadherin. Which does not exhibit any mRNA level changes but the protein level diminishment, indicating a post-transcriptional or translational modification.

The expression levels of N-cadherin only return in specific lineages as they localize and differentiate (Thiery, 2003).

Developmental EMT is also a crucial part of organogenesis. In development of heart, endocardial cells undergo EMT or EndMT due to the endothelial origin of the cells and facilitate the formation of valves and septa, contributing to cardiac cushions that develop mature heart structures (von Gise & Pu, 2012). Besides in kidney development EMT give rise to formation of metanephric mesenchyme, that migrate and differentiate into nephrons, fundamental components of the kidney (Herzlinger et al., 1992). Also, the formation of mammary gland from ectoderm takes place by partial EMT – MET processes in the mammary bud, that has previously been formed by local epithelial cell movement in the ectoderm. Cells accumulate in the mammary gland but undergo EMT to migrate and then get through MET to form rudimentary mammary glands (van Genderen et al., 1994). Similarly, during liver generation, hepatoblasts are located in the ventral diverticulum of the foregut, surrounded by a basement membrane undergoing EMT, delaminating from the liver bud, passing through the basal membrane aggregate around the portal vein, and giving rise to primary liver tissue with the induction of MET (Bort et al., 2006). Same wise cells of the pancreatic bud in the endoderm break free from the surrounding basement membrane by a partial EMT prosses and different precursor cell localize to the appropriate regions and go through special MET processes to give rise their fated tissues (Bort et al., 2006). Also, recent studies showed that EMT, in crosstalk with apoptosis, plays a crucial role in facial morphogenesis. Where loss of Pbx1 in murine embryos abolished the EMT induction of cells in λ phase and resulted in cleft lip and primary palate (Losa et al., 2018).

2.2.2. EMT In Wound Healing And Fibrosis

Type 2 EMT is present in wound healing and gives rise to myofibroblasts for the repair process of the wound. Later, EMT is involved in the regeneration of injured tissue (Kalluri & Weinberg, 2009). The primary start signal of type 2 EMT is the occurrence of inflammation in the injured tissue, gives rise to appropriate signaling for the generation of myofibroblasts and the attraction of mandatory immune cells. But if the inflammation is overset in the site of the injury and turns into a chronic event the aberrant induction of EMT process and following excessive ECM deposition provoke fibrosis first in the site of injury and later on in the respective organ (Marconi et al., 2021).

As a first response to injury, hemostatic signaling and transition to the inflammatory state occur with the production and secretion of inflammatory cytokines, such as TGF-β1 and PDGF, mostly by resident fibroblasts and accumulated macrophages (Marconi et al., 2021). This production initiates increased fibroblast proliferation and migration to the site of injury. Fibroblasts at the injury site secrete Matrix Metalloproteinases (MMPs), such as collagenases MMP-1, gelatinases such as MMP-2 and MMP-9, which degrade the gelatin substrates, and stromelysin-like MMP-3, the presence

of whom together with TGF-β1 facilitates myofibroblast production through EMT of neighboring epithelial cells, resident fibroblasts adipocytes, endothelial cells, and fibrocytes (Cui et al., 2017; Marconi et al., 2021). Myofibroblast are fibroblasts with smooth-muscle cell-like characteristics with stellate or spindle morphology with weak eosinophilic but conspicuous cytoplasm with high expression of vimentin, α-SMA and fibronectin. They secrete ECM components and MMPs together with tissue inhibitors of metalloproteinases that facilitate matrix remodeling enables entrance of tissue regenerative stimulator, removal of necrotic cells and wound contraction (Gabbiani, 2003; Kohan et al., 2010; Powell et al., 1999).

In physiological process, as the wound healing progresses myofibroblasts are either removed by apoptosis or dedifferentiate into fibroblasts. But when the inflammation signal persists in the relevant tissue or myofibroblasts remain in the region after formation of the scar tissue, hypervascularization and aberrant deposition of ECM molecules are observed, forming a hypertrophic scar (Ko et al., 2019). Hypertrophic scars create a positive feedback loop by increasing excessive keratinocyte differentiation, which releases VEGF, EGF, CTGF, and TGF-β, stimulating fibroblasts, myofibroblasts, and chronic inflammation that can lead to tissue and organ fibrosis (Wang et al., 2018). Significance of EMT in fibrosis was shown in a mouse model of kidney fibrosis using an endogenous TGF-β inhibitor BMP-7. In these studies administration of BMP-7 resulted in restoration of E-cadherin levels in fibrosis-positive kidney epithelia via its cognate receptors, ALK-2/3/6 and Smad 4/5, concomitantly with halt of EMT and repair and restoration of damaged epithelial structure, possibly through MET (Zeisberg et al., 2003). Another study investigating patients with kidney fibrosis found tissues positive for cytokeratin, vimentin, α-SMA, and ZO-1 aka typical type 2 EMT markers (Kriz et al., 2011). Another study demonstrated that patients with Crohn's disease with fibrotic colon tissues were positive for EMT markers (Bataille et al., 2008).

2.2.3. EMT In Cancer

As mentioned before EMT is also present in cancer cells with destructive outcomes. Cancer cells are influenced by multiple factors, such as inflammatory or hypoxic conditions of overcrowded tumor sites, secretion of growth and migratory cytokines from neighboring cells, accumulation of mutations in EMT regulatory genes, and subsequent aberrant expression of inducer transcription factors, non-coding mRNA's or other molecules that gain mesenchymal features and migratory abilities that lead to the dissemination of cells from the basement membrane and invasion of distant sites, leading to metastasis (Brabletz et al., 2018).

Many studies utilizing mice and cell culture studies demonstrated that activation of the EMT is an essential step for the emergence of cancerous properties. The tumor stroma was found to emanate couple of EMT inducers like HGF, EGF, PDGF, and TGF-β, which result in loop activation of EMT-

triggering TFs such as SNAI family, ZEB1, Twist, FOXC2 and many more (Atiya et al., 2023; Medici et al., 2008; Wang et al., 2015). Exogenous factors together with expression transcription factors, act pleiotropically to enhance cellular signaling networks like Erk/Mapk, PI3K/AKT, mTOR, TCF/LEF and etc (Huang et al., 2024; Shetty et al., 2020; Wang et al., 2015). Most of the time, these changes are followed by feedback loops at the transcriptional level and an altered epigenome, which enhances the acquisition of mesenchymal traits. Mesenchymal cancer cells facilitate resistance to many therapeutic reagents and, with their gained mobility, escape from the present tumor sites entering the blood flow by intravasation and exit trough extravasation and invade distant tissues and organs via MET (Akhmetkaliyev et al., 2023; Debaugnies et al., 2023).

Furthermore to the gain of complete mesenchymal traits, cancer cells may display partial induction of EMT, creating cells harboring both mesenchymal and epithelial characteristics. This intermediate state is called the hybrid E/M state or quasi-mesenchymal state, and is closely related to immune evasion and suppression (Lambert & Weinberg, 2021). This state of cells prevents their recognition by immune cells. Also expression of specific EMT transcription factors mediates resistance to natural killer cells (Rajabi & Kufe, 2017). In addition, some studies have shown that this hybrid state is responsible for the enhanced expression of immunosuppressive proteins such as PD-L1, CD73, and CD276. Also secretion of TGFβ, IL-8, CSF1 and CCL8 from intermediate cells recruit immunosuppressive cells, enhance polarization of tumor associated macrophages (Rajabi & Kufe, 2017).

2.2.4 Regulation of EMT

2.2.4.1. Transcription Factors

Key regulators of the EMT process are transcription factors that comprise multiple families orchestrating together. The first group consists of two proteins of the SNAIL zinc finger family, Snai and Slug. These proteins bind to the E-box sequences in the promoter of the CDH1 gene, leading to transcriptional repression. The increased expression levels of Snai in certain cancer lines resulted in the loss of cell adhesion and gain of a spindle-like phenotype, followed by increased mobility due to the loss of E-cadherin on the cell membrane (Cano et al., 2000). Slug protein also represses the expression of CDH1 by recruiting chromatin-modifying enzymes to its promoter and subsequently promotes the expression of mesenchymal genes such as CDH2 and VIM. Also, nuclear localization of both gene products is associated with resistance against apoptosis (Losa et al., 2018). TGF-β acts as a crucial activation pathway for both proteins, but is not the only activator, as both Wnt and Notch signaling pathway members are associated with protein activation. Snai also promotes the expression of Bcl-xL and Akt, which act as apoptosis inhibitors that can be initiated by TGF-β signaling (Grille et al., 2003).

Another group of regulators consists of the zinc finger E-box binding (ZEB) family proteins ZEB1 and ZEB2 (Marconi et al., 2021). ZEB proteins also regulate CDH1 expression negatively by binding to E-box sequences in promoter region by recruitment of co-repressor protein such as CtBP and histone deacetylases. This action leads to remodeling of chromatin and gain of heterochromatin-like structure and transcriptional repression. ZEB proteins also interact with SNAI protein expression and vice versa. These proteins not only regulate each other, but also regulate the expression of the mir-200 family, which normally targets the transcripts of these proteins and inhibits EMT (Park et al., 2008). ZEB transcription factors are controlled by TGF-β, Wnt, and Ras-MAPK signaling pathways (Samy Lamouille et al., 2014).

A typical helix-loop-helix TF family, TWIST1 and TWIST2, create a third group of regulatory TFs. These proteins act as inhibitors of differentiation proteins and E12/E47, and act on the CDH1 promoter in the same way and activate mesenchymal genes. In some cancerous cell lines, it was found that TWIST1 can decrease the expression of CDH1 and increase the one of CDH2 independently from SNAIL (Cheng et al., 2008). Another study demonstrated that TWIST1 can activate matrix degradation and subsequent degradation of the basement membrane, thereby enhancing EMT (S. W. Harshman et al., 2013). TWIST expression was shown to be induced by NF-κB signaling pathway and Stat3 protein (C. W. Li et al., 2012). Also hypoxia marker HIF-α, that is known to induce EMT in hypoxic conditions of tumor niche, is proposed to induce expression of TWIST by binding to the hypoxia-response element in the promoter of TWIST (Yang et al., 2008).

2.2.4.2. Signaling Pathways

EMT is regulated by various signaling pathways (Figure 4). Major inducer of EMT is accepted as TGF-β pathway. This pathway induces the EMT by promoting regulatory transcription factors (Katsuno et al., 2013). This pathway is activated by binding of TGF-β1, TGF-β2, or TGF-β3 to the TGF-β receptor. Signal transduction can follow two different pathways according to type of the ligand, receptor or stimuli: canonical pathway and noncanonical pathway. The canonical signaling cascade consists of subsequent SMAD phosphorylation and complex formation, which, together with distinct transcription factors, bind to DNA and facilitate the transcription of target genes. This activation is antagonized by a different SMAD protein Smad7, which prevents excessive activation (Zavadil & Böttinger, 2005). While the noncanonical pathway can stimulate a number of signaling cascades, such as AKT/mTOR, Rho, Par6/SMURF Ras/Raf or Mek/Erk, Traf4/6, and subsequently, the NF-κB signaling cascade. Even though the target genes differ according to activated cascade most of them functionally contribute either in induction and maintenance of EMT or apoptosis or in some cases senescence (Wang et al., 2023).

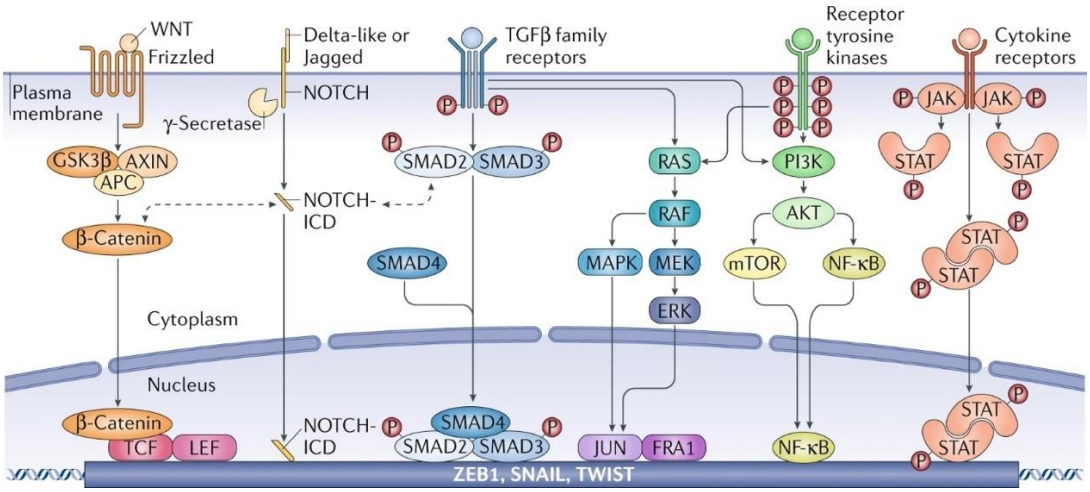

Figure 4. Signaling pathways regulating EMT(Anushka Dongre & Robert A. Weinberg, 2019).

In most of the cases TGF-β signaling, synergistically with upregulated EMT TF's promotes reorganization of cytoskeleton, loss of cell adhesion and subsequent gene expression to facilitate EMT (Tie et al., 2022). Another important regulatory signaling pathway is Wnt/ β-catenin pathway. Upon activation of this pathway by binding Wnt to a cell-surface receptor of the Frizzled family, β-catenin dissociates from the E-cadherin complex in the cell membrane and migrates to the nucleus. β-catenin in the nucleus activates the TCF/LEF complex and promotes the expression of proliferation-, migration-, and growth-related genes (Liu et al., 2022). Simultaneously E-cadherin in the absence of β-catenin on the cell membrane complex gets unstable and translocates to cytoplasm facilating the first hallmark EMT loss of E-cadherin on the cell surface and initiates EMT (Kim et al., 2019). Other signaling pathways like Notch and Hedgehog contribute to EMT by promoting cell survival and growth and by activating EMT inducer transcription factors like Snail and Slug (Gonzalez & Medici, 2014).

2.2.4.3. Alternative splicing and Non-coding RNA's

EMT is also widely regulated in RNA level. Transcripts of proteins involved in cell-cell or cell-matrix adhesion and motility, such as FGFR2, ENAH, CD44, and CTNND1, are regulated by epithelial-specific regulatory proteins 1 and 2 (ESRP1 and ESRP2) (Warzecha et al., 2009) to ensure the maintenance of epithelial properties.

Another post-transcriptional regulatory mechanism involves non-coding RNA's are highly associated with EMT regulation. Micro-RNAs or miRNAs, a class of 20bp non-coding RNA family with regulatory roles in gene expression at the RNA level by targeting the 3' UTR or 5' UTR of mRNA transcripts or, in some cases, the promoter regions also play a vital role in EMT (Setlai et al., 2022). For example, the miR-200 family inhibits EMT by targeting the 3' UTR of ZEB family mRNA's whereas miR-34 suppresses EMT by targeting Snail

and other EMT factors (Dong et al., 2016; Title et al., 2018). Also long non-coding RNAs, lncRNA, single strand of ~200bp long RNA with pleiotropic effects on transcription, translation even in chromatin conformation also exhibit EMT regulatory roles (Pavlič et al., 2022). For example, MALAT1 promotes EMT by interacting with EMT TFs and modifies chromatin structure, while HOTAIR facilitates EMT by recruiting chromatin-modifying complexes to EMT-related gene promoters (Dragonetti et al., 2024; Song et al., 2018).

Another class of non-coding RNAs, circular RNAs, circRNAs, and circular RNA molecules act the same as miRNAs, but targeting miRNAs can facilitate EMT by sponging EMT-inhibiting miRNAs, such as circRNA_100290, which promotes EMT by sponging miR-29b (Khanbabaei et al., 2022; Wang et al., 2021).

2.2.4.4. Post-translational Modifications

Biological processes can be influenced by post-translational modifications of the acting proteins. Such regulation is present for EMT with different modifications. One of such modifications is phosphorylation. Phosphorylation of SNAIL and TWIST affects transcription factor stability and nuclear localization, thereby affecting the EMT. Also, phosphorylation of β-catenin via the activation of Wnt signaling facilitates its translocation to the nucleus and EMT initiation. Glycosylation is another modification. Snail glycosylation under hypoglycemia stabilizes the protein (Freire-de-Lima et al., 2011). Another type of post-translational modification is SUMOylation, which involves the reversible attachment of Small Ubiquitin-like MOdifier (SUMO) to a target protein. SUMO shares a similar three-dimensional structure with ubiquitin (Bogachek et al., 2015). Such modification important in EMT manner is sumoylation of FoxM1. This transcription factor can regulate EMT through Slug distribution. Synchronously FoxM1 is responsible for for repression of miR200b/c in breast cancer. This function is only possible after lysine 463 SUMOylation. This modification enables FoxM1 to repress the tumor supprasive miRNA and maintain the EMT phenotype (Bogachek et al., 2015; Yang et al., 2013).

In contrast, the acetylation of histones can lead to a more open structure and promote EMT. But all these modifications regulate the EMT in a context dependent manner like ubiquitylation of SNAIL facilitates its degradation and halt of EMT while the same modification on the E-cadherin targets it for proteasomal degradation and promotes EMT (Xu et al., 2019).

2.2.4.5. Epigenetics

Epigenetic modifications, in which the expression of genes is drastically altered without any alterations at the genomic level, play a vital role from development to pathogenesis, including EMT (Figure 5). One such mechanism is DNA methylation, which involves the addition of methyl groups from DNMT proteins, typically at CpG islands in promoter regions, and regulates gene

expression negatively (Serrano-Gomez et al., 2016). Such modifications are mostly observed in the E-cadherin promoter during EMT, which facilitates gene silencing via hypermethylation. In breast cancer cells, it was found that ZEB1, through interaction with DNMT1, facilitates hypermethylation of E-cadherin in the promoter and ensures mesenchymal characteristics in cells (Fukagawa et al., 2015).

Another epigenetic mechanism is histone modifications which encompasses various processes such as methylation, acetylation, phosphorylation, and ubiquitination of histone proteins. These modifications can function as either gene expression suppressors or enhancers, or promote the formation of heterochromatin or euchromatin, depending on the specific location of the modification (Chen et al., 2021). For instance, gene silencing-associated methylation of H3K27m2/3 is aberrantly found in metastatic carcinoma cells (Hübner & Spector, 2010). Studies using TGF-β induced EMT, demonstrated that upon induction of EMT TGF-β activates KDM6B, a demethylase, which demethylases H3K27m3 at SNAI promoter activating its expression (Ramadoss et al., 2012).

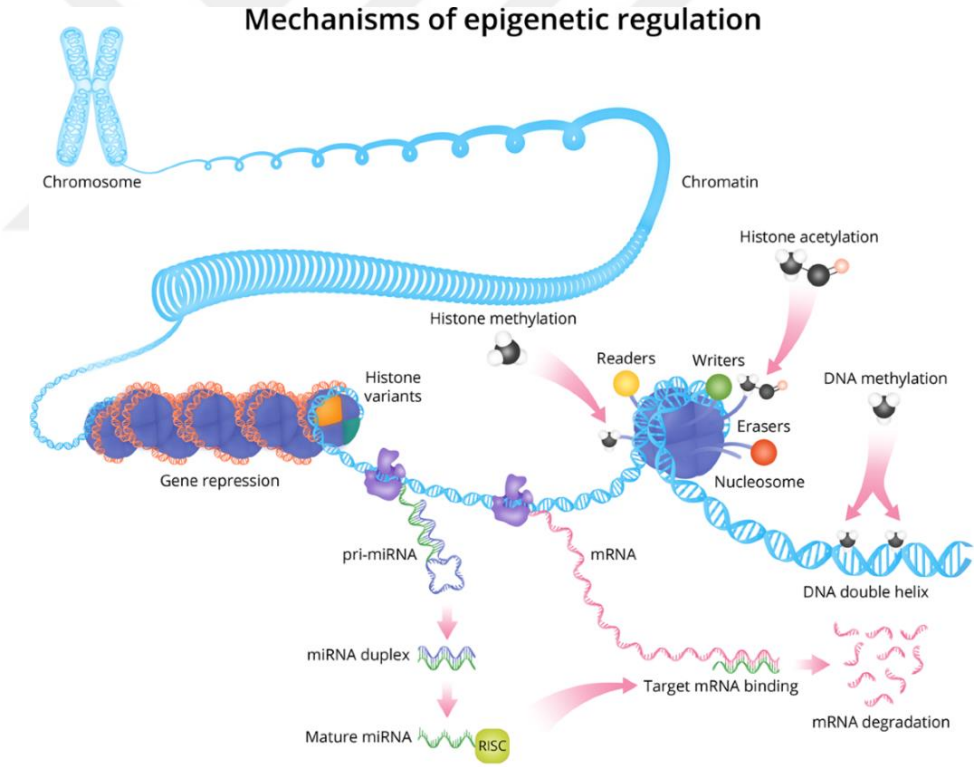

Figure 5. Epigenetic Regulation Mechanisms (Smigielski et al., 2020).

HATs, Histone acetyl transferase, and HDACs (Histone Deacetylazes) are the main actors of Histone acetylation mediated gene regulation. Acetylation of lysine residues in histone proteins results in the neutralization of amino acids, making acetylation status associated with active transcription (Dai & Faller, 2008). In EMT considering manner HDAC is tightly connected

invasive properties of cells. For example, deacetylation of certain histones can lead to the formation of heterochromatin-like structures in regions including CDH1 and reduce access to the transcription machinery restricting its expression. HDAC1 was shown to repress CDH1 and ZO-1 (Lei et al., 2010), while HDAC1 in complex with SMAR1, another CDH1 regulator, can bind to the SLUG promoter, inhibiting its expression and restoring CDH1 expression (Adhikary et al., 2014). Another mechanism is chromatin remodeling by repositioning or restructuring of nucleosomes that can alter the accessibility rate of transcription machinery to DNA. For example loss of ARID1A a subunit of chromatin remodeling complex SWI/SNF can induce EMT while the loss BRG1 subunit of the same complex can repress EMT due to different conformational changes of chromatin (Reske et al., 2020).

2.3. Mesenchymal to Epithelial Transition

The mesenchymal-to-epithelial transition is a process in which mesenchymal cells lose their unstable and migratory characteristics and gain epithelial features. During MET, mesenchymal markers, such as N-cadherin, vimentin, and fibronectin show downregulation, followed by morphological changes, gained of cobblestone morphology with gain of apicobasal polarity with concomitant upregulation of epithelial markers. MET as mentioned above is present in different stages of development, wound healing and tissue regeneration but also in cancer (Chaffer et al., 2007). For many years MET was considered as a inverse process of EMT, and believed to be under control of EMT regulators. However, different studies have shown that downregulation of key EMT inductors and their delocalization from the Cdh1 promoter failed the rapid recovery of Cdh1 and epithelial characteristics of the cells, indicating a more complex and dynamic network of MET regulation. On the other hand, Cdh1 promoter included with all regulatory E-box elements, without the presence of intron 2 is not sufficient to provide a stable cell characteristic. Although determination and regulation of EMT solely depends on these regions this is not true for the MET process (Alotaibi et al., 2015).

MET is a fundamental process of early embryonic development, as described for EMT in the Development section. MET's initial occurrence of MET is observed during implantation, leading to the formation of the trophectoderm and subsequent generation of cells that develop into the embryo's first epithelial layer (Larue & Bellacosa, 2005). In the formation of the three germ layers, migratory cells of the epiblast layer that undergo EMT migrate to distant regions of the embryo and establish not only the other layers but also the body axes through MET by forming organized epithelial layers. Also, during the formation of notochord, anchor structure that regulates the formation of surrounding tissues, mesenchymal cells under MET to form a rod-like structure. Furthermore, later in somitogenesis, formation of axial bone and skeletal muscle precursors, a portion of mesenchyme in presoitic mesoderm undergo MET creating mesenchyme engulfed epithelial capsules called somite (Jarov et al., 2003). It was found that the heterogenic nature of somites was controlled by Cdc42 inhibition, which resulted in aberrant epithelization,

whereas overactivation of the protein prevented the MET process (Nakaya et al., 2004). In the same study, Rac1 was also investigated, showing a culprit role as both silencing and overexpression of the gene disrupted epithelization, indicating a highly controlled level of expression in both states. Later studies have shown that Rac1 acts as a downstream effector of the paraxis gene in the epithelization process of somites. Absence of paraxis gene, which encodes a basic helix-loop-helix transcription factor belonging to Twist family, murine embryos showed disrupted somite formation (Burgess et al., 1996). Since the paraxis is downstream effector of Wnt signaling pathway, another study inhibited the signaling cascade by a soluble inhibitor or removal of Wnt6 and demonstrated the failure of epithelization and decrease in paraxis expression (Schmidt et al., 2004). More loss and gain of function studies showed that Wnt6/Fzd7 signaling cascade plays a crucial role in maintaining somitic epithelial organization by rescuing paraxis expression through the canonical Wnt/-catenin pathway (Linker et al., 2005). Independent from paraxis, investigation of a Wnt ligand co-receptor LRP6 mutant mice failed epithelialization of early mouse somites and delayed ossification, leading to low bone mass similar with Wnt mutants showed role of Wnt pathway (Pinson et al., 2000; Semënov et al., 2001). Another study also showed that signals mediated via paraxial protocadherin (PAPC) and ephrin/Eph are critical for somitic MET in mice and zebrafish (Barrios et al., 2003; Rhee et al., 2003). Ephrin-B2 interacts with EphA4, which regulates MET through modulating cell shape. In addition to these it was found that Mesp2 which is under strict regulation of Notch delta signaling in a feedback loop manner regulates MET in somite formation. Presenilin-1 induces the expression of Dll1, which promotes the expression of Mesp2 which independent presenilin-1 downregulates Dll1 expression. Notably mutant mice for Notch 1, Dll1, Dll3 and RBPJK members of Notch signaling cascade showed disruption in somitogenesis confirming their importance in somitogenesis and MET (Takahashi et al., 2005; Takahashi et al., 2000). Another important TF for MET in somitigenesis is Foxc1 is a critical transcription factor in somitogenesis, playing essential roles in anterior/posterior patterning and epithelial somite formation. The consequences of Foxc1 inhibition include impairment of somitogenesis, reduction in paraxis expression, and the potential for rescue through murine Foxc1 introduction. The absence of Foxc1 expression was associated with the loss of Ephrin-B2 and impaired somite border formation. Foxc1/Foxc2 null mice demonstrated the absence of epithelial somites and lack of paraxis expression, which were restored by ectopic expression of Foxc1/Foxc2 (Kume et al., 2000; Topczewska et al., 2001).

Another well-studied MET occurrence is nephrogenesis during development. First findings, interestingly showed that targeting of classical cadherins R-, and cadherin-6, but not E-cadherin disrupted MET during kidney organogenesis (Hogan et al., 2014; Scadden, 2014). Pax2 plays a crucial role in the initial phases of mesenchymal-to-epithelial transition (MET) in the metanephric mesenchyme, and its downregulation results in unsuccessful MET. Both Pax2 and Pax8 regulate signaling pathways during kidney development, thereby influencing cellular fate and viability. Pax3 triggers

mesenchymal-epithelial transition (MET) in mesenchymal cells, enhancing cell adhesion and epithelial conversion. This process is facilitated by the dynamic redistribution of Rho GTPases Rac1 and PAK2, as well as PIX, to focal adhesions. Additionally, Pax3 regulates cortical actin bundling and determines the shape of epithelial cells (Bouchard et al., 2002; Wiggan et al., 2006). Foxc1 and Foxc2 play crucial roles as transcription factors in kidney development, with their expression also observed in the cardiovascular system, somites, and stromal mesenchymal cells of the kidney. These Fox proteins are integral to mesenchymal-epithelial transition (MET), a vital process in kidney formation. Abnormalities in Fox gene regulation can result in kidney abnormalities, potentially affecting important factors like GDNF and BMP4 (Hatini et al., 1996). BMP7 plays a significant role in inducing mesenchymal-to-epithelial transition (MET) in both developmental and adult tissues. Its ability to induce MET in renal fibroblasts to form functional renal epithelial cells suggests its potential role in cancer progression (Dudley & Robertson, 1997; Zeisberg et al., 2005). This is particularly relevant given BMP7's fundamental role in developmental MET.

2.3.1. Regulation of MET

Similar to EMT, MET, a complex event with the same level of importance, is strictly regulated by various regulators. However, for many years, transcriptomic and epigenetic surveys of MET have been considered to be the same as those of EMT, and very little is known about the MET network. Mesenchymal-epithelial transition (MET) is regulated by intricate networks involving diverse cytokines, transcription factors, and microRNAs.

FGFR2 (Fibroblast growth factor receptor 2) signaling serves a pivotal role in MET, with FGFR2b expression inducing the transition (Oltean et al., 2008; Oltean et al., 2006). Epidermal growth factor receptor (EGFR) inhibition can also promote MET by enhancing E-cadherin expression (Yates et al., 2005; Yates et al., 2007). Bone morphogenetic proteins (BMPs), particularly BMP7, have been demonstrated to induce MET in various cancer types, whereas BMP4 has shown similar results in development (Buijs, Henriquez, et al., 2007; Buijs, Rentsch, et al., 2007; Chaffer et al., 2007; Na et al., 2009). The Wnt signaling pathway, especially involving β-catenin, is implicated in MET regulation (Hlubek et al., 2007; Vincan et al., 2007). In addition, the Notch signaling pathway has also been found to regulate developmental MET.

Transcription factors, such as ZEB1, ZEB2, Snail, and Twist, are typically downregulated during MET (Hong et al., 2009; Na et al., 2009; Yee et al., 2010). Besides those as mentioned above somitogenesis and nephrogenesis studies also identified different transcription factors such as Mesp2, Pax3, Paraxin and Foxc1/2 and etc. In addition to the grainy head transcription factors, Grhl1, Grhl2, and Grhl3, which are conserved across species, play a crucial role in regulating epidermal barrier formation (Yu et al., 2009). Among these, GRHL3 is particularly important for epidermal differentiation and barrier formation during mouse embryogenesis. GRHL proteins protect epidermal

integrity by modifying the chromatin structure and are involved in epidermal differentiation, epigenetic regulation, and chromatin remodeling. The significance of GRHL3 is evident from studies showing that Grhl3 knockout in mice leads to spina bifida and an inability to form a proper skin barrier, resulting in death from dehydration shortly after birth (Chalmers et al., 2006). Grhl3 interacts with Hnf4α and inhibits mesenchymal processes (Alotaibi et al., 2015). The transcription factor Hnf4α, a member of the transcriptional nuclear receptor superfamily, functions as a hepatic differentiation factor and is predominantly expressed in specific tissues, like the hepatic and renal tissue, and gastrointestinal tract (Qu et al., 2023). This factor plays crucial roles in sustaining cellular homeostasis, managing inflammation, and controlling the epithelial phenotype as well as lipid and glucose metabolism (Darsigny et al., 2009). Furthermore another regulatory group is, The Ets family of transcription factors is among the largest, with members exhibiting both widespread and specific tissue expression patterns. These factors are distinguished by their conserved ETS domains, which are DNA-binding regions that recognize a specific 5'-GGA (A/T)-3 DNA sequence (Cooper et al., 2015). As trans-acting phosphoproteins, members of this family can function as both upstream and downstream effectors in various signaling cascades, including MAP kinases, Erk1/2, p38, and JNK (Otero et al., 2012). ELF3 plays a role in regulating MET by altering the expected distribution of E-cadherin in the plasma membrane and can be affected by Grhl3. When Elf3 expression is lost, the initiation of MET is disrupted, causing cells to maintain a mesenchymal state (Sengez et al., 2019). Taking all of the evidence into account, it is possible to propose a positive feedback loop involving Grhl3 and Elf3. Cebpα, a component of the bZIP (basic leucine zipper) transcription factor family, is classified as a CCAAT/enhancer-binding protein (Bertolino et al., 2016). This intronless gene, comprises three transactivation domains, a regulatory region, and a bZIP region (Xu & Tata, 1992). The CEBPα protein exists in two forms, p42 and p30 (Reckzeh & Cammenga, 2010), and serves vital roles in numerous biological events, such as control of hepatogenesis, adipogenesis, and hematopoiesis across multiple cell types. C/EBP proteins interact with p300 (Dhawan et al., 2005). In certain cell types, CEBPα has been associated with the chromatin regulatory proteins p300 and HDAC1 (Dengler et al., 2014).

Krüppel-like factor 4 (KLF4), a transcription factor of the zinc finger family, was initially discovered in a search for TFs involved in regulation of growth (Shields et al., 1996). It plays a essential part in the terminal differentiation and homeostasis of various epithelial tissues, including the maintenance of adherent junction stability and establishment of the skin's barrier function (Cowan et al., 2010). KLF4 regulates transcription in processes such as proliferation, differentiation, apoptosis, and somatic cell reprogramming across various physiological and pathological conditions (Clevers & Watt, 2018; Hogan et al., 2014; Scadden, 2014). Given its ability to promote stem cell activity and regulate growth and differentiation during development, it also plays diverse roles in tumorigenesis. The function of KLF4 varies in different cancers, depending on the cellular context. At the molecular level, studies have shown that KLF4 can both inhibit and be inhibited by SNAIL, which are

members of the SNAI superfamily capable of inducing EMT to varying degrees (Zhou et al., 2020). There is growing evidence in literature regarding KLF4's role in inhibiting EMT and driving MET in various biological contexts. Additionally, E-cadherin is directly regulated by KLF4 at the transcriptional level, a process believed to be crucial for maintaining the epithelial phenotype in mammary epithelial cells (Yu et al., 2011).

MicroRNAs, particularly the miR-200 family, have been found to promote MET by targeting transcriptional repressors of E-cadherin (Gregory et al., 2008; Spender et al., 2009). These regulatory networks function in concert to orchestrate the complex processes of MET in cancer metastasis. The epigenetic regulation of MET remains in the dark. The high susceptibility of the E-cadherin promoter to changes in methylation status, as well as the presence of regulatory TF associated with chromatin modifiers, suggests a strong possibility of distinct epigenomic signatures to be discovered.

2.4. Chromatin Organization

In eukaryotic cells, a nucleus 6μm wide can hold a 2-meter-long genetic material. This phenomenon can be attributed to the folding of DNA on special proteins and their compaction into coils and loops, creating chromatin (Luger et al., 1997). Nucleosomes form the fundamental unit of chromatin structure, comprising 147 base pairs of DNA wrapped around a core histone octamer. This octamer consists of two copies each of histones H2A, H2B, H3, and H4. Nucleosomes are connected to each other through 10–80 bp of linker histones and create a structure that resembles and is named after beads on a string (Hiragami-Hamada & Nakayama, 2019). Secondary structure is formed by linker histone H1 which through its globular domain shows on dyad binding of nucleosome and interacts with linker DNAs through its C-terminal tail creating the chromatosomes and by pulling further together the chromatosomes in a zig-zag pattern facilitating the chromatin fiber. The chromatin fiber further condenses, creating higher-order organization consisting of numerous structures, but specially creating the topologically associated domains by neighboring genes with relevant function or expression time, enabling synchronous accessibility of transcriptional machinery and concomitant expression of relevant genes. These structures are found to be highly flexible throughout the life cycle of a cell, suggesting a “need and want” regulation. This pattern is not equal in every region of the chromatin. Meaning some regions in terminally differentiated cells create a 30nm, compact chromatic structure could possibly be potency related genes creating heterochromatin and further compact structure to prohibit accession of transcription factors (Figure 6) (Quina et al., 2006).

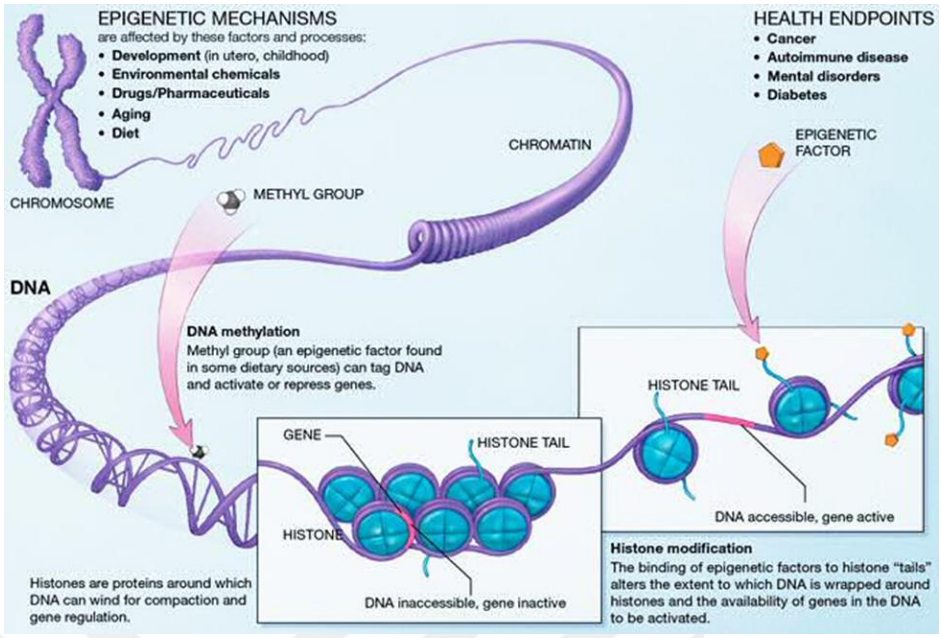

Figure 6. Chromatin Compaction and Gene Expression. NIH

2.4.1. Histone Proteins

The primary DNA holder proteins in eukaryotes are known as histone proteins. In general approach histone proteins are consistent of two big families, the core histone family and the linker histone family. Core histones consist of four different main proteins; H2A, H2B, H3 and H4 and together with different isoforms of each they are encoded by multiple genes, and the mRNA structure of each is characterized by the absence of introns and the presence of 3' stem-loop structures instead of a polyadenylated tail. Histone proteins have a dual-domain structure: a structured histone fold domain and an unstructured N-terminal domain, and are highly conserved structures (Mariño-Ramírez et al., 2005). These histones wrap around the DNA, forming an octameric structure with the main function of the N-terminal tail, to form and maintain the compacted state of chromatin. While the fold domain containing three α-helices separated by two loops show specific pairing of H3 with H4 and H2A with H2B upon distinct heterodimerization. This configuration can form connections through four-helix bundles, resulting in a central H3-H4 tetramer surrounded by two H2A-H2B dimers, with the assistance of chaperone proteins. Chaperones are acidic proteins that interact with highly basic histone proteins, and are responsible for preventing non-specific interactions and their proper transport, storage, and incorporation into the nucleus (Bobde et al., 2021).

The second family of histone H1 linker histones, which will be discussed further in later sections, comprises an exceptionally diverse unit of proteins with a high number of members. These proteins have a tripartite structure with a short N-terminal tail that is believed to guide proteins in specific nucleosomes, a structured globular domain that interacts with the nucleosome

dyad, and a long lysine-rich and positively charged C-terminal tail that interacts with the linker DNA. With the acquisition of linker histones to the nucleosome, the open linker DNA connecting the nucleosomes on the string was brought together to create chromatosomes. Chromatosomes on string are further compacted into chromatin by charge directed interactions of chromatosomes and form a firm but flexible chromatin structure (Bednar et al., 2017).

2.4.2. Linker Histones

The H1 family of linker histones stands out for its exceptional diversity, encompassing the greatest number of subtypes among histone groups (Happel & Doenecke, 2009). These H1 histones are characterized by their high lysine content, making them some of the most positively charged proteins found in cells (Ma et al., 2020). Linker histone H1s are characterized by a tripartite structure comprising three distinct regions. The first is a short, less conserved N-terminal domain (NTD) encompassing approximately 20-35 amino acids (Figure 7). The second is a highly conserved, well-folded central globular domain (GD) of about 80 amino acids. The third domain is an extended, less conserved C-terminal domain (CTD) of approximately 100 amino acids, which exhibits a high degree of intrinsic disorder (Abu Alhaija et al., 2024; Hartman et al., 1977; Noll, 1976). X-ray crystallography has revealed that the GD exhibits a mixed α/β fold structure. The GD's core consists of β-strands and three α-helices. The α1- and α2-helices are separated by β-strands, followed by α3, and two antiparallel β-strands. Extension of these β-strands results in loop formation (Ramakrishnan et al., 1993). In contrast, the NTD exhibits less conservation when compared to the GD and is composed of two distinct subdomains. One of these subdomains is rich in hydrophobic residues, whereas the other, situated closer to the GD, is characterized by a high content of basic amino acids and includes an ARKS sequence. ARKS sequence is consisting of Alanine-Arginine-Lysine-Serine and is a highly conserved regulatory amino acid motive mostly found in histones. This motive plays a significant role in epigenetic regulation as it serves as recognition site for chromodomain proteins like Polycomb and HP1 according to the modifications of the site and regulate the chromatin confirmation influencing gene expression (Fischle et al., 2003).

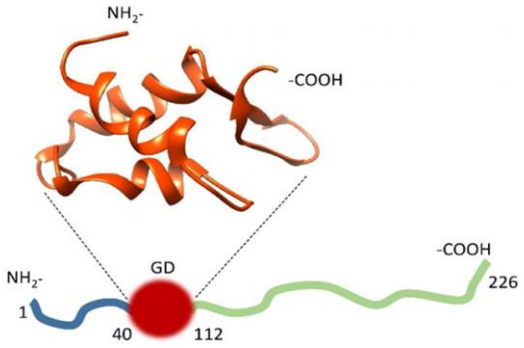

Figure 7. Tripartite Structure of linker histone. N-terminal tail (NTD), structured globular domain (GBD) and unstructured C-terminal Tail (CTD) (Bednar et al., 2017).

In aqueous solution, the NTD of H1s remains unstructured, and upon interaction with DNA, it adopts an α-helical structure (Vila et al., 2001). Across various species and subtypes, the CTD of H1s exhibits consistent amino acid composition, with lysine being the predominant component, resulting in a net positive charge between 30 and 50 (Mariño-Ramírez et al., 2005). The mammalian H1 CTD typically features repetitive (S/T)-P-X-(K/R) consensus sequences (Hao et al., 2021). In aqueous environments, the H1 histone CTD forms a random coil structure, but it can fold when interacting with DNA or exposed to secondary structure-stabilizing compounds (Roque et al., 2005). Both the NTD and CTD undergo a shift from a disordered to an ordered state when binding to the nucleosome (Fang et al., 2012).

The basic amino acid-rich nature of the CTD enables it to neutralize the negative charges on DNA and facilitate chromatin condensation. Although a study has demonstrated that removing the majority of the CTD region does not significantly impact H1-induced chromatin condensation, as this process is primarily influenced by the initial 25 amino acids adjacent to the GD (Lu et al., 2009).Nonetheless, the CTD plays a crucial role in facilitating high-affinity nucleosome binding and chromatin condensation (Caterino & Hayes, 2011; Hendzel et al., 2004; Lu et al., 2009). Notably, binding affinity seems to correlate with CTD length (Hao et al., 2021). For instance, H1.5 and H1.4, which possess the longest CTDs, display the strongest nucleosome binding affinity (Hendzel et al., 2004). In comparison, H1.0's intermediate binding affinity can be attributed to the concentration of positive charges within its CTD (Hao et al., 2021).

Histone H1 plays a crucial role in altering the nucleosome conformational landscape by reducing the distance between two linkers, thereby limiting their mobility. The C-terminal domain (CTD) of H1 primarily engages with one linker, whereas the globular domain (GD) interacts with both the nucleosome dyad and the linkers, forming a stronger bond with the linker opposite to the CTD (Figure 8). These findings highlight H1's asymmetric effect on nucleosome structure, which has important implications for the formation and organization of higher-order chromatin structures. Notably, latest advancements in X-ray crystallography and cryo-electron microscopy has enabled researchers to obtain high-resolution structures of complete H1 histones bound to nucleosomes with linker DNA (Bednar et al., 2017; Caterino & Hayes, 2011).

Linker histones besides their role in the compaction of chromatin into compact fiber and formation of higher-order chromatin structure they also interfere or influence various biological events in the cell. Linker histone can regulate gene expression, DNA repair and replication through dynamic nature of chromatin. Linker histones with a high affinity for linker DNA or other chromatin-associated proteins or their enhanced/inhibited affinity through PTMs can make occasional regions accessible. This phenomenon regulates transcriptomic patterns, cell cycle, apoptosis, DNA protection, and even development and differentiation. Besides a recent study showed that linker

histones can also act as non-coding RNA and regulate expression of genes in transcriptional level (Ivanyi-Nagy et al., 2018).

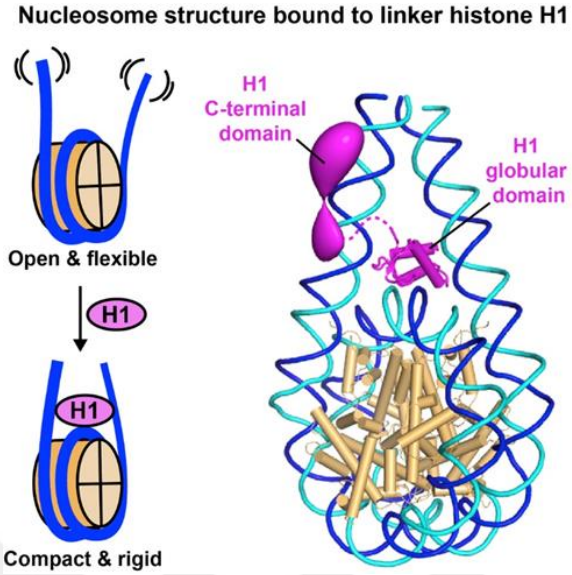

Figure 8. H1 bound nucleosome. Open and relax conformation of nucleosome gains a more rigid and compact conformation with binding of linker histones (Bednar et al., 2017)

2.4.2.1. Linker Histones Isoforms

Linker histone family is diverse unit of proteins with multiple members with same main function and different outcome or specifications. Although the tripartite structure of linker histones, the length and amino acid distribution of each region can differ among isoforms changing their affinity to chromosome and assigning them specific roles (Figure 9) (Sokolova et al., 2022). H1 isoforms are categorized into three distinct groups according to their expression patterns across time and space, resulting in three distinct categories: H1.1–H1.5, whose expression levels are highly linked to cell cycle progression; H1.0 and H1.x, which have a variant mode of expression in somatic cells; and H1t, H1T2, H1LS1, and H1oo, which are exclusively expressed in germ cells (Schuettengruber & Cavalli, 2009). Linker histones can also be categorized as replication-dependent (H1.1–H1.5) or replication-independent (H1.0–H1X). Notably, H1.1–H1.5 and H1x are widely expressed, whereas H1.0 accumulates in terminally differentiated cells and is considered a gatekeeper of fate decisions. The diversity of linker histones comes from the fact that linker histones of the same class show higher similarity to their orthologs across species rather than their intra-species paralogs. Linker histones appear to be evolutionarily conserved in a type-specific manner (S. W. Harshman et al., 2013).

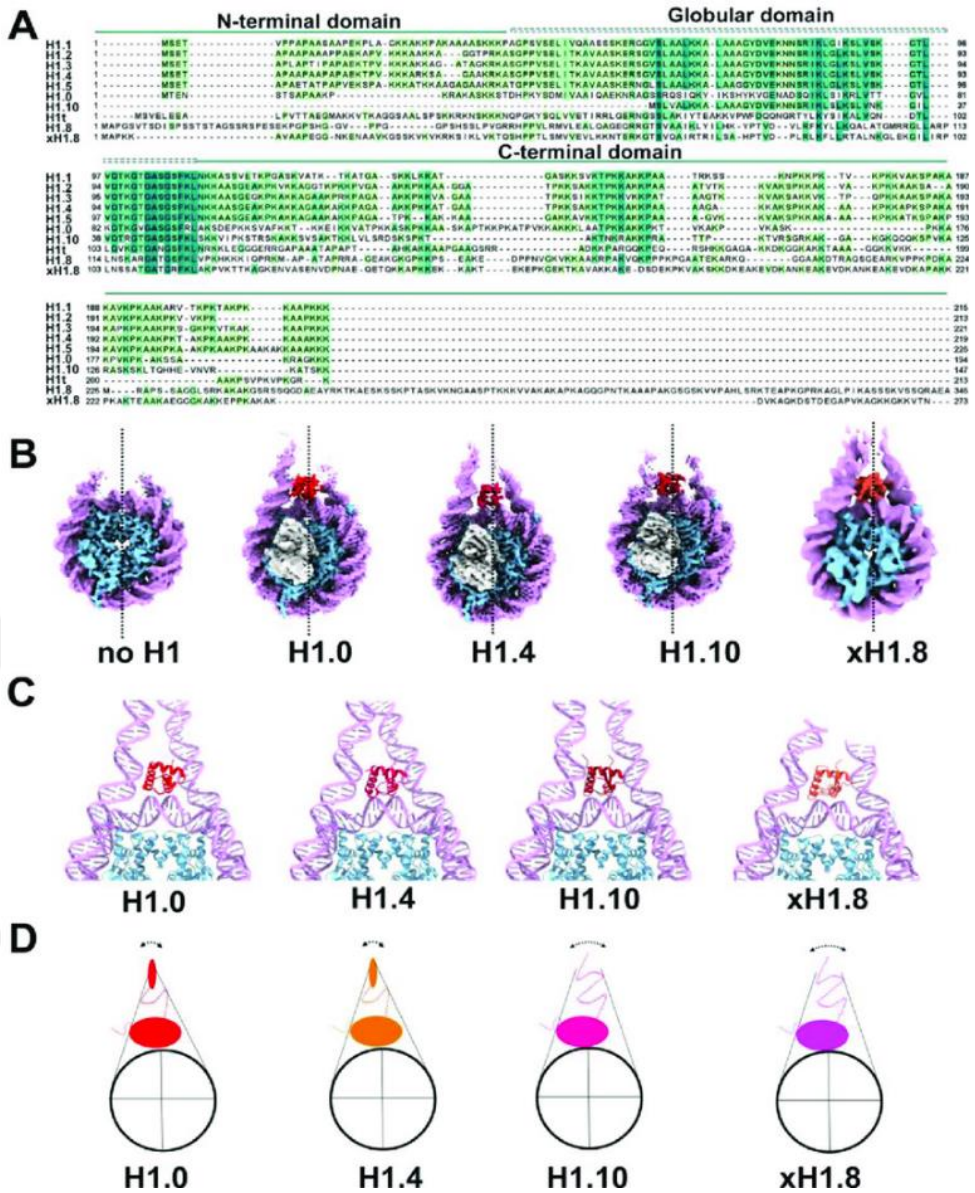

Figure 9. H1 Isoforms and structural differences in chromatosomes. A) Human H1 histone variants and Xenopus H1.8 sequence comparison. (B) Cryo-EM density maps of nucleosomes and chromatosomes containing H1f0(0), H1.E(4), H1.X(10), and xH1.8. (C) Detailed view of nucleosome and chromatosome atomic coordinates with H1.0, H1.4, and H1.10 linker histones, illustrating the interactions between H1's globular domain and linker DNA. (D) Chromatosomes exhibit varying linker DNA angles (in relation to the dyad) and conformations (Sokolova et al., 2022).

2.4.2.1.1. Replication Independent Linker Histones

The expression levels of replication-independent linker histones are not affected by cell cycle events or cell growth but are continuous in the cell. Linker histones in this category can be divided into two subgroups: germ-specific and somatic linker histones.

Germline-specific H1 variants have dissimilar amino acid compositions and unique biochemical functions (Pan & Fan, 2016). For example, H1t demonstrates reduced chromatin-binding affinity and a decreased ability to condense chromatin (Mahadevan et al., 2020). These characteristics are beneficial for promoting recombination during meiosis (Oko et al., 1996). The lower affinity of H1t can be explained by the lack of SPKK/TPKK motifs in its CTD, which is crucial for DNA binding and phosphorylation (Madapura & Rao, 2007). In comparison, H1T2 is notable for its unique composition, featuring a high concentration of arginine and the presence of SPKK/TPKK motifs in its CTD (Tanaka et al., 2005). H1LS, a spermatid-specific linker histone, shows an expression pattern suggesting the replacement of H1t during spermatid elongation, assisting in chromatin reorganization (Yan et al., 2003). H1oo, found in oocytes, has distinctive characteristics, including the longest CTD among the H1 subtypes, which are abundant in acidic amino acids and contain numerous phosphorylation sites. These features indicate a specialized function in chromatin regulation (Tanaka et al., 2001).

Other groups of replication-independent histones consisted of somatic histones H1.0 and H1.X with consistent expression pattern throughout of the cell cycle. H1x, the least conserved isoform of the linker histone family, exhibits ubiquitous expression at higher levels in differentiated cells. Despite having the weakest chromatin-binding affinity, H1x is found at higher concentrations in active genes (Mayor et al., 2015) and DNase hypersensitive sites (Millán-Ariño et al., 2014). It also undergoes ubiquitination in response to DNA double-strand breaks, indicating its involvement in DNA repair signaling (Thorslund et al., 2015). On the other hand, H1.0, known as a replacement linker histone, is expressed solely in fully differentiated cells (Terme et al., 2011). H1.0 shows superior abilities among linker histones in forming highly compact chromatin structures (Clausell et al., 2009), and when overexpressed in dividing cells, it impedes DNA replication (Brown et al., 1996). From a functional standpoint, H1.0 inhibits transcription due to its ability to extensively compact chromatin. Furthermore, H1.0 is concentrated in transcriptionally suppressed DNA regions, such as satellite and telomeric areas, and is one of the most prevalent H1 histones found in the nucleolus.

2.4.2.1.2. Replication Dependent Linker Histones

Various subtypes of linker histone H1 have distinct properties and roles. Common traits of cell-cycle-regulated H1 genes include a single-exon structure without introns, brief non-coding sequences at both ends, and an mRNA terminal hairpin loop that regulates gene expression.

H1.1, among these subtypes, demonstrates the least conservation between mice and humans (Pan & Fan, 2016; Terme et al., 2011). Interestingly, H1.1 has a unique chromatin binding pattern, indicating a specific function, potentially boosting transcription due to its high presence in promoter regions and CpG islands (Izzo et al., 2013). Its expression levels are elevated in less differentiated cells, predominantly found in the thymus, spleen, and

(Terme et al., 2011). H1.1 possesses the lowest chromatin compaction ability among H1 subtypes, favoring a more relaxed chromatin structure (Clausell et al., 2009), and it demonstrates high chromatin mobility owing to its short CTD (Lever et al., 2000).

Conversely, H1.2 is primarily found in differentiated cells (Lennox & Cohen, 1983). It demonstrates a moderate affinity for chromatin binding and limited ability to compact chromatin (Clausell et al., 2009). H1.2 functions as both a transcriptional suppressor and enhancer, though its exact role remains ambiguous (Mayor et al., 2015), (Izzo et al., 2013). Its involvement in both gene activation and deactivation indicates dynamic functionality, as shown by depletion, which leads to cell cycle arrest at the G1 phase (Sancho et al., 2008), potentially influenced by protein interactions or post-translational modifications (Terme et al., 2011). During DNA damage, H1.2 plays a role in conveying apoptotic signals from the nucleus to the cytoplasm in a p53-dependent manner, highlighting its importance in the DNA damage response (Giné et al., 2008; Konishi et al., 2003). When DNA damage occurs, H1.2 undergoes ubiquitination, facilitating the recruitment of DNA damage repair proteins to the affected area (Thorslund et al., 2015), (Mandemaker et al., 2017). FRAP analysis has shown that H1.1 and H1.2, which have short C-terminal domains (CTDs), display greater mobility on chromatin compared to H1 subtypes with longer CTDs, such as H1.4 and H1.5 (Izzo et al., 2013).

H1.3 displays elevated expression in human embryonic stem cells (hESCs) relative to differentiated cells, suggesting a role in pluripotency and self-renewal maintenance (Terme et al., 2011). Interestingly, mice lacking H1.3 show no observable impact on their growth and development (Fan et al., 2001), and reducing H1.3 levels in human embryonic stem cells does not significantly affect their ability to self-renew (Terme et al., 2011). Although, H1.3 is abundant in regions of suppressed transcription, it demonstrates a moderate ability to bind to chromatin and compact it (Clausell et al., 2009). Expression levels of H1.3 shows a 14-fold increase across the S-phase of the cell cycle (Parseghian & Hamkalo, 2001).

The human H1.4 protein exhibits a remarkable 93.5% sequence similarity to its mouse counterpart (Izzo et al., 2013). In mice, the expression of the H1.4 gene increases after birth, indicating its significance in the differentiation processes (Lennox & Cohen, 1983). H1.4 possesses a strong ability to bind and condense chromatin, and it can both inhibit and promote transcription through post-translational modifications (Clausell et al., 2009).Furthermore, H1.4 plays a role in positioning the nuclear lamina, affecting the arrangement of the nuclear periphery in human lung fibroblasts, while its absence in breast cancer cells leads to reduced growth rates or necrotic features in a cell-specific manner (Sancho et al., 2008).

H1.5 is highly expressed in pluripotent stem cells (Terme et al., 2011) and demonstrates robust chromatin binding and compaction abilities (Clausell et al., 2009). Its involvement in differentiation is supported by its interactions

with factors related to differentiation and MET and EMT (Lee et al., 2004; Mackey-Cushman et al., 2011). Importantly, H1.5 is primarily associated with genes that are transcriptionally inactive, particularly those encoding proteins associated with membranes in differentiated cells (J. Y. Li et al., 2012).

2.4.2.2.2. Post-translational Modifications of Linker Histones

Linker histones can regulate gene expression through their binding affinities to DNA or other chromatin-associated proteins. Besides the distinct affinity of each isoform, this can be enhanced or inhibited through post-translational modifications. PTMs sites of linker histones crowd the regions of NTD and CTD and consist of acetylation, methylation, PARylation, ubiquitination, formylation, and citrullination, which affect the affinity of linker histones in a subtype-and modification-dependent manner (Figure 10) (Debasree et al., 2018; S. W. Harshman et al., 2013).



Figure 10. PTMs Of Linker Histone H1E. Multiple PTMs regions are present on H1E with obvious accumulation in GD. Figure adapted from (Sean W. Harshman et al., 2013).

Phosphorylation of linker histones, the most well-studied PTM, mostly occurs on the (S/T)-P-X-(K/R) of the CTD and is recognized by multiple cyclin-dependent kinases, indicating their role in the cell cycle (S. W. Harshman et al., 2013). Examples of such modifications are observed in the phosphorylation of H1.4 through glycogen synthase kinase-3, Aurora B kinase, or protein kinase A during the S-phase of the cell cycle (Hergeth & Schneider, 2015). This phosphorylation is associated with the loss of affinity of H1.4 to linker DNA and nucleosomes, which results in relaxed chromatin accessible from replication machinery (Izzo et al., 2008). Notably, cells with extreme DNA damage exhibit abundant H1 phosphorylation (Debasree et al., 2018). Facilitated open chromatin confirmation becomes accessible for DNA repair actors (S. W. Harshman et al., 2013). K26 methylation creates a binding site for HP1 and L3MBTL1, contributing to heterochromatin formation (Hergeth & Schneider, 2015). Conversely, H1.4 Ser27 phosphorylation impeded HP1 binding, illustrating the interplay between H1 modifications (Izzo et al., 2008). Linker histones undergo extensive acetylation, with sites in the GD potentially influencing DNA binding (Debasree et al., 2018). For example, GCN5 histone acetyltransferase-mediated H1.4K34 acetylation can stimulate transcription or decrease histone-chromatin affinity (S. W. Harshman et al., 2013). Another instance is arginine 54 citrullination, which results in H1 detachment from chromatin (Hergeth & Schneider, 2015). H1 formylation is involved in the DNA

damage response, whereas SUMO2/3-mediated SUMOylation has been shown to suppress totipotency in stem cells, emphasizing its importance in the transition from totipotent to pluripotent states (Hergeth & Schneider, 2015).

Table 1. PTMs of linker histones and their specific functions. Table adapted from (Hergeth & Schneider, 2015)

H1 Isoforms per Organism	**Functions**
Saccharomyces cerevisiae; 1 isoform	
Hho1p	DNA repair, gene expression
Tetrahymena thermophila; 1 isoform	
H1	Not vital, regulation of gene expression
Caenorhabditis elegans; 8 isoforms	
HIS24me	Regulation of innate immune and stress response genes
Drosophila melanogaster; 2 isoforms	
Somatic H1	Heterochromatin formation, involved in Su(var)39/HP1 pathway, JAK/STAT pathway, vital
dBigH1	Regulation of zygotic genome activation
Xenopus laevis; 5 isoforms	
B4 (germ-specific)	ATP-dependent chromatin remodelling
Chicken; 7 isoforms	
H1R	DNA damage response
Mouse; 11 isoforms	
H1a-H1e	Replication-dependent linker histones with general and specific functions
H1c, H1d, H1e (H1.2, H1.3, H1.4)	Vital in embryonic level
H1b (H1.5)	Interacts with Msx1, inhibits muscle cell differentiation
H1c (H1.c)	Heterochromatin condensation in photoreceptors
H1f0 (H1.0)	Replacement linker histone in terminal fate decision

H1x (H1.10)	Function unknown
H1oo (H1.8)	Pluripotency gene regulation in early embryonic stage
H1t2 (H1.7)	Sperm-specific
Human, 11 isoforms	
H1.1-H1.5	Replication-dependent linker histones with general and specific functions
H1.2	Recruitment of Cul4A ubiquitin ligase/PAF1, euchromatin formation and active transcription (H1.2S173p)
	Negative regulator of p53-mediated transcription
H1.3	Represor of h19 lncRNA and EMT
H1.4	H1.4K26me; heterochromatin formation via HP1 and L3MBTL1 recruitment
	H1.4K34ac; assembly of TAF, active transcription
	H1.4S172p, H1.4S187p; loss of affinity to DNA, active transcription/replication during cell cycle
H1.0	Replacement subtype in differentiated cells
H1x (H1.10)	Regulation of mitosis
H1oo, H1t, H1T2, HILS1 (H1.8, H1.6, H1.7, H1.9)	Germline-specific, unknown functions

2.5. Rahman Syndrome

The location of the HIST1H1.4 gene is on chromosome 6p22.2, and it provides the instructions for making the linker histone H1.4, also known as H1.E. A protein of linker histone family and is essential for the formation of high-order chromatin structures. It is involved in various processes such as DNA replication, DNA repair, and recombination, and plays a significant role in maintaining the stability of the genome (S. W. Harshman et al., 2013). So far identified mutations showed accumulation in the CTD region resulting in a frameshift mutation with shorter tail and a specific amino acid sequence present in every patient (Figure 11). This specific amino acid sequence is highly conserved among patients and biologically unique. Individuals with expression of pathogenic Rahman variant of H1E gene are characterized by facial gestalt and intellectual disability. These features are accompanied by abnormal brain development, detectable in MRI, cardiac anomalies, hypothyroidism and behavioral issues with different degrees among the patients (Tatton-Brown et al., 2017) (Figure 12).

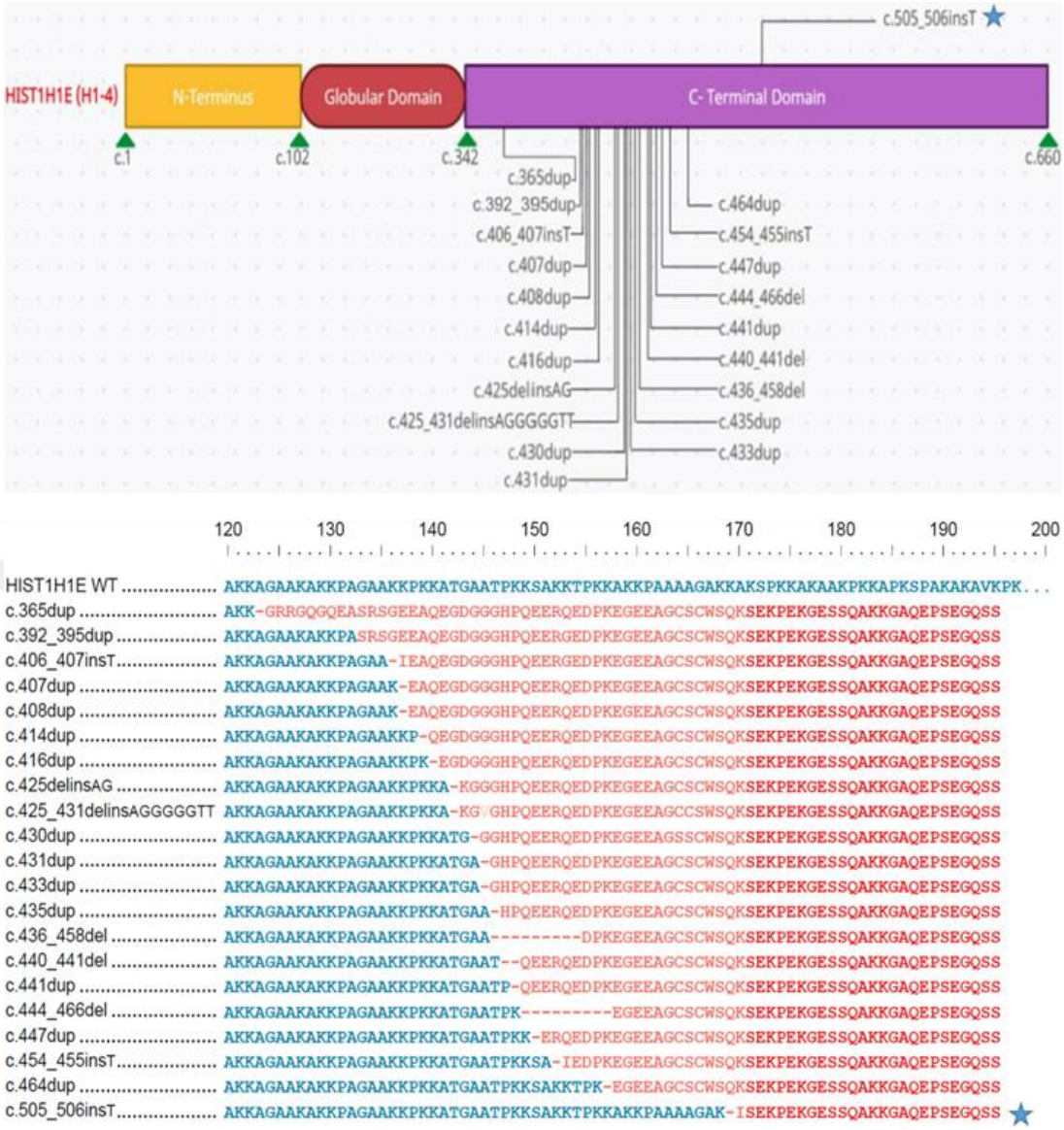

Figure 11. Mutation hotspots in H1E. Mutations in the locus accumulate in the C-terminus Domain (Adapted from (Indugula et al., 2022)

Pathogenic mutant form of HIST1H1.E gene leads to a truncated protein with reduced net positive charge, which may be less effective in neutralizing negatively charged DNA (Tatton-Brown et al., 2017).

The truncated form of the H1.4 protein may exhibit reduced efficiency in DNA binding and protein-protein interactions, as suggested by the study. Cells expressing this truncated H1.4 protein displayed a significant decrease in proliferation rate and competence, along with accelerated senescence and limited entry into the S-phase cycle, as reported in study (Xu et al., 2019). In contrast, cells expressing the mutant H1.4 protein showed proper nuclear localization and stable binding to chromatin, as per study (Xu et al., 2019). The CTD of linker histones is comprised of essential residues that undergo reversible phosphorylation, which influences chromatin dynamics and enables

chromatin condensation and/or relaxation. The presence of Rahman syndrome mutations in the CTD of the H1.4 gene leads to increased chromatin relaxation in fibroblast cells from individuals with Rahman syndrome compared to that in the control group (Xu et al., 2019). Additionally, H3 histone methylation at specific lysine residues is typically associated with appropriate chromatin compaction. However, fibroblasts from individuals with Rahman syndrome showed decreased methylation of H3K4me2, H3K9me3, and H3K27me3 in the same study. Consistent with prior investigations, a reduction in HP1β, which plays a role in heterochromatin formation by associating with methylated H3K9, was observed, suggesting a defective heterochromatin state. Additionally, nucleolar disintegration and elevated rRNA levels were observed in fibroblasts from affected individuals, as demonstrated by the loss of the nucleolar marker nucleolin, which is indicative of nuclear instability. Furthermore, a high proportion of aneuploidy has been detected in these cells (Xu et al., 2019). These results suggested a greater degree of chromatin relaxation in cells expressing truncated H1.4 (Xu et al., 2019). Enrichment analysis of cellular components revealed a significant over-representation of genes associated with neurological, immunological, and cell adhesion/membrane function pathways, which aligned with the clinical phenotypic features of the syndrome.



Figure 12. Images of individuals with Rahman Syndrome. Individuals show apparent facial gestalt (Adapted from (Tatton-Brown et al., 2017)

Analysis of methylation patterns in affected individuals showed a distinct epigenetic signature that featured a reduction in methylation levels in specific gene regions mainly expressed in the brain (Ciolfi et al., 2020). These findings

suggest that the truncated H1.4 protein influences the epigenetic regulation of genes necessary for normal neuronal cell function (Ciolfi et al., 2020). Tremblay et al. demonstrated that the overexpression of mutant H1.4 led to a unique distribution of the protein within subnuclear compartments and enlarged nuclei in rat hippocampal neurons (Tremblay et al., 2022). However, the neuronal firing rate was lower in neurons overexpressing mutant H1.4 compared to those overexpressing wild-type human H1.4 in this study (Tremblay et al., 2022).

2.6. Crossroads Of Linker Histones And EMT-MET

Linker histones, particularly H1 variants, play crucial roles in chromatin compaction and gene regulation, which in turn influence cell plasticity. These proteins are essential components of the chromatin structure, bind to DNA between nucleosomes, and contribute to higher-order chromatin organization. The dynamic nature of linker histone interactions with chromatin has been the subject of intense research in recent years, revealing their importance in various cellular processes (Funayama et al., 2006; Izzo et al., 2013). Recent studies have shown that the dynamic association and dissociation of linker histones with chromatin can modulate the accessibility of transcription factors and other regulatory proteins to the DNA. This process is particularly important during cellular reprogramming and differentiation, in which changes in chromatin structure are essential for altering gene expression patterns (Fyodorov et al., 2018). The ability of linker histones to influence chromatin accessibility has far-reaching implications for cellular plasticity as it directly affects the ability of cells to respond to environmental cues and developmental signals (Misteli, 2020).

The depletion or overexpression of specific linker histone variants has been observed to affect the efficiency of cellular reprogramming, suggesting a direct link between linker histone composition and cell plasticity. For instance, studies have demonstrated that reducing the levels of certain H1 variants can enhance the reprogramming of somatic cells into induced pluripotent stem cells (iPSCs) (Fan et al., 2005). Conversely, overexpression of specific H1 variants has been shown to impede this process, highlighting the delicate balance required for maintaining cellular plasticity (Fan et al., 2005). Furthermore, post-translational modifications of linker histones, such as phosphorylation and methylation, have been implicated in fine-tuning their interactions with chromatin, thereby providing an additional layer of regulation in cell fate decisions (Happel & Doenecke, 2009). These modifications can alter the binding affinity of linker histones for DNA and influence their interactions with other chromatin-associated proteins. For example, phosphorylation of specific residues in H1 has been linked to changes in chromatin condensation during cell cycle and cellular differentiation (Happel & Doenecke, 2009).

The role of linker histones in cell plasticity extends beyond their direct effects on the chromatin structure. Recent studies have revealed that these

proteins can also interact with various transcription factors and chromatin remodeling complexes, further influencing gene expression patterns (Funayama et al., 2006; Izzo et al., 2013). This interplay between linker histones and other regulatory proteins adds another level of complexity to the regulation of cell plasticity and highlights the importance of considering the broader chromatin context when studying cellular reprogramming and differentiation (Fyodorov et al., 2018). Moreover, the diversity of linker histone variants across different cell types and developmental stages suggests a specialized role for these proteins in maintaining cell type-specific chromatin states (Happel & Doenecke, 2009). The expression patterns of H1 variants have been shown to change during development and in response to various cellular stimuli, indicating their involvement in fine-tuning cellular plasticity in a context-dependent manner (Misteli, 2020; Terme et al., 2011). For instance, protein-level interactions of H1B with Msx1, and concomitant regulation of CER expression influence myogenesis (Lee et al., 2004). Additionally, overexpression of Msx1 has been associated with metastasis through induction of EMT in carcinoma in situ (Lee et al., 2004).

EMT and MET, the previously mentioned mechanisms of cell plasticity, are also shown to be influenced by chromatin conformation and linker histones. It was previously shown that EMT associated genes are regulated within their topologically associated domains (TADs) in chromatin indicating their need of topological remodeling for proper reorganization. Recent research alterations in linker histone expression and post-translational modifications can influence the expression of EMT-related genes, suggesting a novel epigenetic mechanism for EMT regulation (Pang et al., 2022).

For instance, the depletion of certain H1 variants has been associated with increased expression of EMT markers and enhanced cell migration. Studies have demonstrated that knockdown of H1.0 in breast cancer cells leads to upregulation of mesenchymal markers such as vimentin and N-cadherin, while simultaneously decreasing the expression of epithelial markers like E-cadherin (Torres et al., 2016). This shift in gene expression is accompanied by increased cell motility and invasiveness, which are hallmarks of EMT (Harshman et al., 2014; Torres et al., 2016). A recent study also demonstrated that H1.4 was bound to the ERK1/2 promoter, acting as a repressor, and silencing of H1.4 in lung cancer initiated EMT (Chen et al., 2024), suggesting that different H1 subtypes may play specific roles in regulating EMT in various cancer types (Izzo et al., 2013). Conversely, the overexpression of specific linker histone subtypes has been shown to suppress EMT progression in some cancer models. For example, increased expression of H1.3 has been associated with reduced metastatic potential in ovarian cancer cells through inhibition of h19, potentially through the repression of EMT-inducing transcription factors (Lv et al., 2017; Medrzycki et al., 2014). While the relationship between MET and linker histones are extremely limited besides the insights provided by the disrupted differentiation or cell fate protection incidences in abnormal expression of linker histones. Similar to the data obtained from the literature, existing RNA-seq data from the

Alotaibi lab during the EMT and MET processes of the NMuMG cell line showed distinct regulation of each linker histone (Figure 13), indicating the specific roles of linker histones for each stage.

Epithelial to mesenchymal and mesenchymal to epithelial transitions are strictly regulated biological events responsible for cell homeostasis and each one of them governs their own network neatly. It came to our realization that linker histones were part of this regulation. As shown in Figure 13, they were differentially expressed throughout the EMT and MET stages.

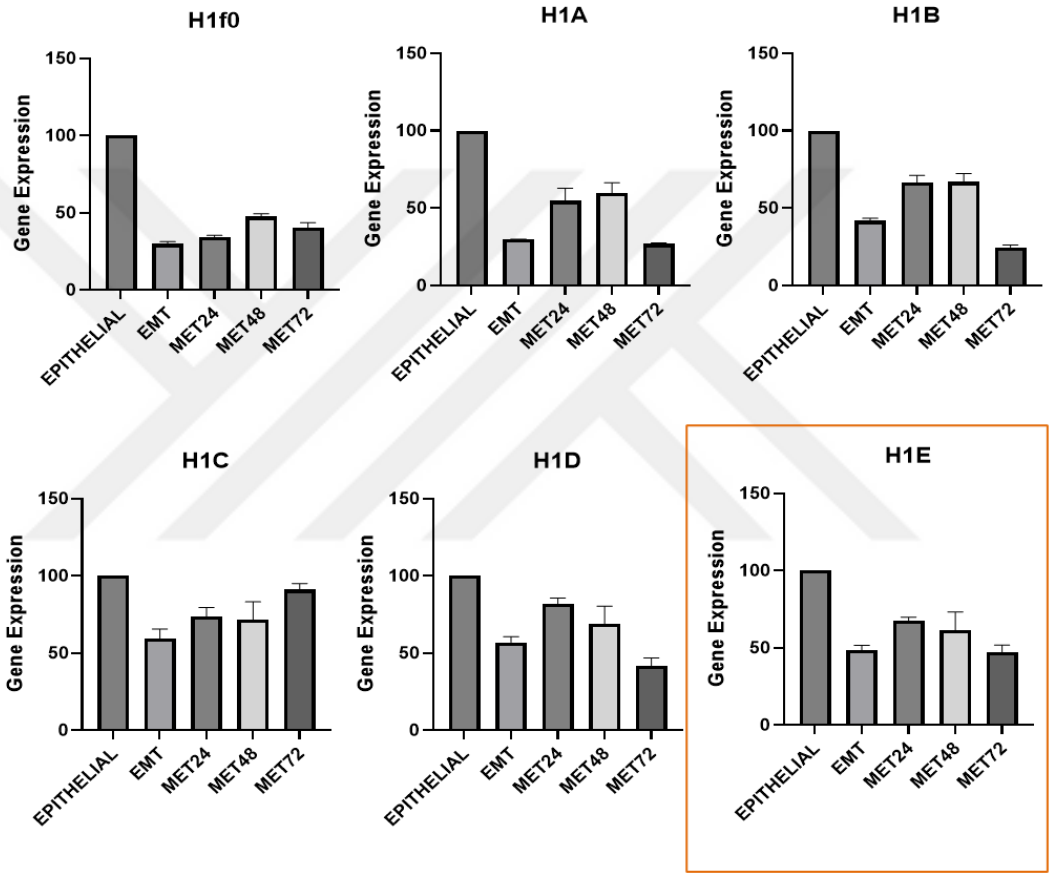

Figure 13. Differential expression of linker histones throughout the EMT-MET stages.

Almost all the linker histones showed downregulation at different levels during EMT, and only two of them, H1E, H1C, and H1D, showed relatable recovery. Questioning the role of linker histones or their subject, higher ordered chromatin on these biological events we turned our focus to linker histone H1E with the most abundant recovery in the first stages of MET.

Not only its high response to withdrawal of TGF beta but also its recent association with disease-causing human syndrome prompted us to question whether its depletion or presence of pathogenic variants would affect EMT or

MET, as its high spiked expression suggests its importance for biological events.

Post-translational modifications of H1 proteins, such as phosphorylation, methylation, and acetylation, have been shown to modulate their interactions with chromatin and other regulatory proteins (Clausell et al., 2009; Happel & Doenecke, 2009). These modifications can alter the accessibility of EMT-related genes to transcription factors and other regulatory elements, thereby providing an additional layer of control over the EMT process. For instance, the phosphorylation of H1 by cyclin-dependent kinases has been linked to increased chromatin accessibility and enhanced expression of EMT-promoting genes in certain cancer types (Clausell et al., 2009; Happel & Doenecke, 2009; Harshman et al., 2014).

Taken together with the differential expression of H1E throughout the EMT/MET process, the presence of a linker histone-caused syndrome with possible developmental decoys indicative of abnormal organs can also be a clue for the crucial role of H1.E in homeostasis of cell plasticity and EMT/MET progression.

3. MATERIALS AND METHODS

3.1. Type of Study

This study pursues an analytical approach using in vitro-supported experiments.

3.2. Time and Place of Study

This study was conducted at Izmir International Biomedicine and Genome Center between September 2023 and August 2024.

3.3. Materials of Study

3.3.1. Cell Lines & Cell Culture Reagents

Table 2. Cell lines

Cell line	Medium
NMuMG	DMEM, high Glucose; 10%FBS; 1% Penicillin/Streptomycin; 1% nonessential amino acids; 1% sodium pyruvate
MCF10A	DMEM/F12-Glutamax 5% Horse Serume 1% Hydrocortisone hEGF 4 pg/ml 1% Penicillin/Streptomycin; Insulin 10µg/ml 1 uM Forskolin

Table 3. Cell culture reagents

Materials	Cat. No	Vendor
DMEM, high glucose	41965039	Gibco
Trypsin-EDTA (0.25%), phenol red	25-200-056	Gibco
DPBS, no calcium, no magnesium	14190094	Gibco
Fetal Bovine Serum, qualified, Brazil	10270106	Gibco
MEM Non-Essential Amino Acids Solution (100X)	11140035	Gibco
Sodium pyruvate 100 mM	p04-43100	PAN-Biotech
Penicillin-Streptomycin (10,000 U/mL)	15140122	Gibco
Recombinant Human TGFβ3	100-36E-10UG	Peprotech
Insulin solution human	I9278-5ML	Sigma Aldrich
FuGENE® HD Transfection Reagent	E2311	Promega
Lipofectamine™ RNAiMAX Transfection Reagent	13778150	Invitrogen
DMSO	A3672,0100	Applichem
Lipofectamin P300 Transfection Reagent		Promega

DMEM/F12-Glutamax	31331-028	Gibco
Horse Serume	26050-070	Thermo Fisher
Hydrocortisone	H088	Sigma Aldrich
hEGF	PHG0311	Thermo Fisher
Insulin	11061-68-0	Sigma Aldrich

3.3.2. cDNA and qPCR Reagents

Table 4. cDNA and qPCR Reagents

Materials	Cat. No	Vendor
AMPIGENE® qPCR Probe Mix No-ROX	ENZ-NUC107-1000	ENZO
MicroAmp™ Fast Optical 96-Well Reaction Plate with Barcode, 0.1 mL	4346906	Applied Biosystems
MicroAmp™ Optical Adhesive Film	4360954	AppliedBiosystems
Universal Probe Library probes		Roche
RealQ Plus 2x Master Mix	APQ-A323406	Ampliqon

3.3.3. Plasmid List

Table 5. Plasmids and viral vectors used in this study.

Plasmid Name
KDC208
KDC210
TV3-1
FUCCI-ESC
AAV-Cre Virus Cat No

3.3.4. siRNA Sequence Information

Table 6. siRNA Sequence

siRNA	Sequence	Vendor
Hs_HIST1H1E_8	CTCGCTCACGCTTGCCTTCAA	Thermo Fisher
Hs_HIST1H1E_7	AGCGGCGAAGAAGCCCAAGAA	Qiagen
Hs_HIST1H1E_6	CCGCATCAAGCTGGGTCTCAA	Qiagen
Hs_HIST1H1E_3	ACCCAAGGCGGCTAAACCAAA	Qiagen
Hs_HIST1H1D_8	TTGAGATTACTTATTGTCTTT	Qiagen
Hs_HIST1H1D_7	TGGGACCAAGAAAGTGGCCAA	Qiagen
Hs_HIST1H1D_6	AAGCCGAAGGTTACAAAGGCA	Qiagen
Hs_HIST1H1D_5	CAAGGCAGTGGCAGCTTCTAA	Qiagen
Hs_HIST1H1C_7	AAGGCGGCGCCCAAGAAGAAA	Qiagen
Hs_HIST1H1C_6	AACACCGAAGAAAGCGAAGAA	Qiagen
Hs_HIST1H1C_5	GCCCAAGGTTGTCAAGCCTAA	Qiagen
Hs_HIST1H1C_4	TAGGCGAACGCCTACTTCTAA	Qiagen
Ms_HIST1H1E_3	TTCAAGTATCCTTAAACTTAA	Qiagen
Ms_HIST1H1E_2	TAGCAGATTTGTGCAGTTTAA	Qiagen
Ms_HIST1H1E_1	CAGAATGATTTAGAGATAGAA	Qiagen

3.3.5. Immunofluorescence Labelling Reagents

Table 7. Immunostaining Antibodies

Antibody	Host Species	Brand	Cat. No.
Alexa Fluor 647 Phalloidin		Invitrogen	A12380
α-Rat Alexa 568	Goat	Invitrogen	A11077
α-Mouse Alexa488	Goat	Invitrogen	A11029
α-Mouse Alexa594	Goat	Invitrogen	A11005
α-Rabbit Alexa488	Goat	Invitrogen	A11008
α-Rabbit Alexa594	Goat	Sigma	77671
α-Goat Alexa488	Donkey	Invitrogen	A32814
H3K4me3 antibody	Rabbit	Active Motif	61379
H3K27me3 antibody	Rabbit	Active Motif	39155
H3K9ac antibody	Rabbit	Active Motif	61251
H3K27ac antibody	Rabbit	Active Motif	39685
Anti E-cadherin	Mouse	BD Biosciences	BD 610181
Lamin A/C	Mouse	Abcam	Ab190380
HP1a	Rabbit	Abcam	ab109028
Lamin B1	Rabbit	Abcam	ab16048

Table 8. Immunofluorescence Labelling Reagents

Materials	Cat. No	Vendor
Formaldehyde	F8775	Sigma
Triton X-100	T8787	Sigma
DAPI	D1306	Invitrogen
Prolong Diamond Antifade Mountant solution	P36962	Thermo Fisher Scientific

3.3.6. SDS PAGE and Western Blot Reagents

Table 9. Antibodie

Antibody	Host Species	Brand	Cat. No.
Anti N-cadherin	Mouse	BD Biosciences	58169
Anti- B-Actin	mouse	Cell Signalling	61251
α-Tubulin	mouse	Abcam	ab56676
Anti E-cadherin	Mouse	BD Biosciences	BD 610181
Vimentin	Mouse	Thermo Fisher	MA5-11883
ZO-1	Rabbit	Abcam	ab276131

Table 10. Other chemicals and Reagents

Antibody	Brand	Cat. No.
30% Acrylamide/Bis	Bio Rad	1610156
TEMED	Bio Rad	1610800
Ammonium Persulfate	Bio Rad	1610700
Clarity Western ECL Substrate kit	Bio Rad	1705061

3.3.7. Other Chemicals, Consumables, and Commercial Kits

Table 11. Other Chemicals, Consumables, and Commercial kits

Materials	Cat. No	Vendor
NucleoSpin RNA kit	740955.50	Macherey-Nagel
DNA Clean & Concentrator™-5	D4014	Zymo Research
Zymoclean Gel DNA Recovery Kit	D4007	Zymo Research
Quick-DNA™ Miniprep Kit	D3025	Zymo Research
GeneRuler 1 kb DNA Ladder	SM0313	Thermo Scientific
GeneRuler 100 bp DNA Ladder	SM0321	Thermo Scientific
Agarose	A9536-500G	Sigma
Absolute Ethanol	9.200.262.500	Isolab
Ultrapure DNAse/RNAse free dH_2O	10977035	Thermo Scientific
Safe View	G108	ABM
Boric acid	10043-35-3	Merck
EDTA	E5134-500G	Sigma
Recombinant Human TGFβ3	100-36E-10UG	PEPROTECH

3.3.8. Hardware & Machines

Table 12. Hardware and machines used in this study

Machine	Vendor
pH Meter	HANNA Instruments
Toploader Balance 820 g x 0.01g	Sartorius
SimpliAmp™ Thermal Cycler	Applied Biosystems
Owl™ EasyCast™ B1A Mini Gel Electrophoresis	ThermoFisher Scientific
Microwave oven	Beko
mySPIN™ 6 Mini Benchtop Centrifuge	ThermoFisher Scientific
Vortex Mixer	ThermoFisher Scientific
Hotplate Stirrer Thermolyne	ThermoFisher Scientific
Waterbath	Nuve
Centrifuge 5810R	Eppendorf
Centrifuge MicroCL 17R	ThermoFisher Scientific
ABI 7500 Fast Thermal Cycler	ThermoFisher Scientific
NanoDrop 2000	ThermoFisher Scientific
Gel Doc XR+ System with Image Lab Software	Bio-Rad
CKX41 Inverted Microscope	Olympus
BX61 Fully Motorized Fluorescence Microscope	Olympus
Confocal Microscopy	Zeiss LSM880
S220 focused-ultrasonicator	Covaris
Bioruptor Pico Sonication device	Diagenode
Western Blot Visualization	Bio-Rad
Clonality Verification	Solentim Cell Metric X

3.3.9. Chemical Recipes

3.3.9.1.Agarose Gel Electrophoresis Solutions

10X TBE (1L)

108 g Tris
55 g Boric acid
40 ml 0.5 M pH:8 EDTA

1% Agarose Gel

0.5 g Agar
50 mL 0.5X TBE

10X TAE 1L

48.5 g Tris.
11.4 mL glacial acetic acid.
20 mL 0.5M EDTA (pH 8.0)

3.3.9.2. Western Solution

RIPA buffer (RadioImmunoPrecipitation Assay) buffer

50 Mm Tris HCl pH 8
150 mM NaCl
1% NP-40
0.5% sodium deoxycholate
+ Protease Inhibitor Cocktail
+DTT
+PMSF

10X Run Buffer 1l

30.3 g of Tris base
144.4 g of Glycine to the solution.
10 g of SDS to the solution.
10X Transfer Buffer
30.3 g of Tris base
144.4 g of Glycine to the solution

10X Transfer Buffer
Methanol 20%(v/v)
10X Transfer buffer 10%(v/v)
H2O 70%

10XTBS 1l
24.23 g Trizma HCl
80.06 g NaCl
Mix in 800 ml ultrapure water.
pH to 7.6 with pure HCl.

1X TBST
100 ml of TBS 10x
900 ml ultrapure water
1ml Tween20

Nuclear fractionation Buffers
Buffer A
10 mM HEPES
1.5 mM MgCl2,
10 mM KCl,
0.5 mM DTT,
0.05% NP40 , pH 7.9

Buffer B
5 mM HEPES,
1.5 mM MgCl2,
0.2 mM EDTA,
0.5 mM DTT,
26% glycerol (v/v), pH 7.9

Medium stripping buffer 1l
15 g glycine
1 g SDS
10 ml Tween20
Set the pH to 2.2

Harsh stripping buffer 100 ml
20 ml SDS 10%
12.5 ml Tris HCl pH 6.8 0.5M
67.5 ml ultra pure water
0.8ml ß-mercaptoethanol

3.3.9.3. Senescence Associated β galactosidase Assay

Citric acid/sodium phosphate buffer (40mM, pH6)
39.4ml of 0.1M citric acid
60.6ml of 0.2 M sodium phosphate
100ml of deionized water.

Staining Solution
10ml Citrate/sodium phosphate buffer
250ul of 200mM Potassium Ferricyanide
200mM Potassium Ferrocyanide
100ul of 200mM MgCl2
250ul of 6M NaCl
200ul of 50mg/ml X-gal in Formamide

3.4. Variables of Study

Within the scope of this study, the independent variables are the NMuMG cell line and the MCF10A cells that siRNA mediated knockdown will be performed . The vectors and siRNAs with which the cells are transfected are the dependent variables. Differentially expressed gene levels in NMuMG cells represent the dependent variable in EMT-MET conversion. Upon employment of Crispr/Cas9 protocol NMuMG cells are the dependent variable, with alteration of the cellular behavior and etc,

3.5. Tools For Data Collection

The GraphPad Prism 9 program and Microsoft Excel were used to analyze the qPCR results. Zen 3.1 program was used to analyze IF staining. Image J was used to analyze the western blot experiments. MultiScanGO software was used to analyze the SRB and BCA results.

3.6. Study Plan and Calendar

June-July 2023	Read processing
August- Dec 2023	Examination of gene expression levels of EMT and MET processes in NMuMG cells. siRNA knockdown experiments in MCF10A and NMuMG cells
Jan-April 2024	Generation of Crispr/Cas9 Haplo-insufficient and Rahman KI clones and Characterization
May-June 2024	EMT-MET experiments of Generated Clones
July- August 2024	Examining the effect of Rahman on EMT/MET and cell wellbeing.
August 2024	Writing

3.7. Data Evaluation

3.7.1. Cell Culture Maintaining and Handling

Normal Murine Mammary Gland (NMuMG) cell were cultured in DMEM supplemented with 10% FBS, 1% MEMNEAA, and 1% penicillin-streptomycin at 37 °C with 10% CO2. Cells were passaged every two days in a 1:10 ratio to avoid cellular senescence for up to four passages.

3.7.2. siRNA Transfections

siRNAs against human H1.4 and mouse H1f4 were purchased from Qiagen (Table 6). Early passage MCF10A cells, NMuMG cells, or NMuMG cells treated with TGF beta for 72 h were transfected with 20 nM siRNA using Lipofectamine RNAi Max (13778150, Invitrogen, Waltham, MA, USA) upon TGF beta withdrawal, as recommended by the manufacturer, and collected 72 h later. Candidate siRNAs were selected or eliminated based on their efficiency and phenotypic analysis of the majority or off-target effects, respectively. Efficiency levels were determined by qPCR analysis, while morphological effects were determined by IF and brightfield microscopy, and off-target effects were determined using the Blat platform and confirmed by qPCR.

3.7.3. CRISPR/Cas9 Genome Editing

CRISPR/Cas9 is a revolutionary gene-editing tool comprising guide RNA (gRNA) and Cas9 enzyme. The gRNA directs Cas9 to a specific DNA location where it creates a double-strand break. This break activates cellular repair mechanisms, particularly Homology-Directed Repair (HDR). CRISPR/Cas9-mediated HDR is a precise genome-editing technique that uses a donor DNA template to insert, delete, or replace genetic sequences at the target site. This method allows for the accurate modification of DNA sequences, making it valuable for various applications, such as correcting mutations, inserting new genes, or studying gene functions. The precision of HDR makes it a powerful tool in genetic research and potential therapeutic interventions (Li et al., 2022).

3.7.3.1. Targeting Vectors and sgRNAs

sgRNA targeting mouse H1f4 Chop-chop web tool (https://chopchop.cbu.uib.no/) and cloned into a px458 vector expressing Cas9 nuclease protein fused to green fluorescent protein (GFP) (Add gene Cat. No. 48138) according to the protocol outlined by Ran et al. Mentioned sgRNA's were produced in our laboratory previously (Abu Alhaija et al., 2024) and two of them (Table 5) were used in this study

3.7.3.2. Transformation, plasmid conformation and isolation

5ng of each plasmid was transformed into competent E. coli cells. For transformation of plasmid 50ul competent E.coli per sample was thawed on ice and mixed with 5 ng of the desired plasmid and incubated on ice for 20

minutes. Following incubation, cells were subjected to 90 s heat shock at 42C to permeabilize the membrane and force the plasmid. After heat shock, cells were rested on ice for 2 min and incubated for 1 h at 37C in antibiotic-free LB broth. Grown cultures were collected an hour later, centrifuged at 8,000 rpm for 1 min, resuspended in100 ul and spread on ampicillin-positive plates for O/N incubation at 37C.

Single colonies were selected and grown in ampicillin-positive LB broth for 16 hours. Plasmids were isolated from mini-cultures by alkaline lysis and confirmed by restriction digestion. Approved plasmid colonies were set for maxi culture, grown in 2 ml for 8 h, and later in 50 ml for 16 h. Cultures were collected the next day and plasmid extraction was performed using the Qiagen Maxi-prep kit.

3.7.3.3. Transfection targeting vector and sgRNA, FACS, Selection and Single Cell Sorting

Transfections were carried out on NMuMG cells going through passage 2 with 3 µg of the targeting vector and 1 µg of each sgRNA or an equal amount of GFPmax or empty pUC57 using FuGene HD, following the manufacturer's instructions. Cells were seeded at 4700 cells/cm2 in six well plate into three groups and were followed for 96 h.

GFP bulk sorting on 48th hour after transfection, cells were washed with 1x PBS 2 times and detached from the plates by trypsin treatment and collected in warm media. Cells were prepared for FACS sorting using a 22u pore cell strainer, pelleted at 0.3 rcf for 2 min, and resuspended in FACS buffer(10% FBS in 1X PBS). Prepared cells were sorted according to their GFP emission with the GFPmax group as the positive control and empty vector as the unstained group to eliminate possible morphologic outcomes due to stress of transfection.

Sorted cells were seeded on a 100 mm cell culture plate with their regular medium augmented by 1500ug/ml G418 as the second part of the selection. Cells were cultured on 100 mm plates for 10 days with neomycin treatment, and the success was followed up from the GFPmax group. Upon completion of selection, the cells were detached, counted as previously described, and seeded on 96 well plates by 0,7cell/ well as manual single cell cloning. After 4 h, the seeded cells were monitored and captured using the Cell Metrics instrument. Cell metrics recording was conducted for three days in rows and 14 days after cloning. Cloned originated from single cells were confirmed by the Cell metrics analysis of 14 days. Approved clones were grown to 90% confluence and passaged to larger plates upon sample collection for DNA extraction.

3.7.3.4. DNA Extraction and Genotyping

DNA extraction was performed from half of the 90% confluent 96 well plate the Invitrogen DNA extraction kit according to the manufacturer's instructions. Genotyping of candidate clones was performed using three sets of PCR followed by restriction digestion confirmation. The first round of genotyping was conducted on the 5' arm of the recombination locus containing the neomycin cassette using Primer KD419-KD420 listed above with MyTaq enzyme under the following conditions: initial denaturation at 95C 3 min and 40x Cycle of Denaturation at 95C 15 sec, annealing at 58C 10 sec, elongation at 72 °C for 15 s, and elongation at 72C for 1 min.

Clones giving positive results in the black and white PCR were checked for their 3' prime end in two steps. First, a PCR reaction with primers KD396/KD397 will be referred to as 3' PCR, with MyTaq enzyme following the following conditions: initial denaturation at 95C for 3 min and 40x Cycle of: Denaturation at 95C for 15 sec, annealing at 58C for 10 sec, elongation at 72 1 min 15 sec, and final elongation at 72C for 1 min followed by digestion of the successful amplified fragment by HindIII.

After this phase, clones were subjected to a third PCR amplification between the 3' and 5' arms using primers SD100/SD150, which will be referred to as insert PCR, with Q5 enzyme and the following conditions: 98 2 min 40x 98C 2sec, 68C 10sec, 72 1 min 50sec. 72C 2min. Amplified products were confirmed by digestion with HindIII. The last two PCR assays not only provide information on successful editing at the desired locus but also show the zygosity level of the editing. This means that partial digestion of 3 shows the undigested endogenous locus, and the edited synthetic locus as a HindIII recognition site could only be integrated by the targeting vector bearing it as a silent mutation, creating a barcode for genotyping. On the other hand, the insert PCR targeting the upstream region of neomycin gene, the region outside of the introduced targeting vector, creates PCR products of different sizes, and the presence of a 1kb band only suggests a homozygous clone or the presence of a 700bp band shows unsuccessful editing or the presence of both bands concludes that editing was successful on one allele and inefficient on the other, creating a heterozygous clone.

The same PCR reaction was used to confirm efficient Cre Recombination at the genomic level, as removal of the neomycin gene resulted in the disappearance of the 2kb band and created two bands with a 30bp difference in the heterozygous clone and a single 700bp band in the homozygous clone. After confirmation or listing of positive clones, gene editing was performed at the nucleotide level using Sanger sequencing. To determine whether the DNA of heterozygous clones was amplified with KD194/SD443, the region from the start of the neomycin gene to the outside of the 3' homology arm was targeted to ensure that the amplified fragment was obtained from the edited allele. To demonstrate the integrity of the unedited allele, PCR using SD156/SD155 was conducted. Although the intended PCR would theoretically amplify two

fragments coming from both alleles due to the 1kb difference the obtained product was unedited allele-based. Both PCR products were cut out and gel-purified to avoid non-specific contamination and sequenced using the primers listed in Table 15.

3.7.4. Adeno Associated Virus Infection and Cre recombination and Conformation

Recombination-positive clones were then subjected to AAV-Cre virus to release the endogenous promoter of the H1E locus, which was occupied by the inserted neomycin gene. Rahman H1E expression was achieved thanks to Cre recombination, which exported the neomycin gene coupled by two loxp sites heading the same direction. Viral infection was performed in two consequent doses with AAV-Cre, with 1st being registered with an MOI of 100 at 60% confluency on a 12-well plate and incubated for 16h and followed by a 1X PBS wash and virus-free medium change. 48h after administration of the first dose, the second dose was administered at the same MOI and incubated for another 16h and the same steps. Viable cells were then amplified and, as the first step conformation after Cre clones, referred to as AC, were seeded on a 12well plate with x cells/cm2 density and subjected to neomycin treatment, as described previously. Clones showing complete death were further confirmed at the genomic level, as described above. In addition, sufficient expression of Rahman H1e was confirmed at the RNA and protein levels following the procedures listed below.

3.7.5. RNA extraction and Gel electrophoresis and Cdna Generation

Total RNA was isolated from three technical replicates. The medium of the cells incubated for 72 h was aspirated and washed twice with 1X PBS. For total RNA isolation, a Nucleospin RNA extraction kit (Macherey Nagel, Germany) was used. First, lysis buffer was added to each well, according to the manufacturer's instructions. Ethanol (70%) was added to the resulting cell lysate and mixed by vortexing. It was then transferred to a NucleoSpin® RNA Column (light blue ring) provided by the kit. All the remaining cell components (cell debris, proteins, and gDNA) were eliminated. There is only one biochemical basis that allows RNA to bind to the silica column. To elute RNA from the column, 35 µL RNAse-free water was used to rehydrate the RNA.

To assess the RNA concentration and purity of each sample, the absorbance of each sample was measured at 260/280 and 260/230 nm by UV spectroscopy (Nanodrop 2000). The 260/280 ratio of RNA was approximately 2.0, and the 260/230 ratio range from 2.0-2.2.

3.7.6. RT-PCR and qPCR

RT-PCR Obtain cDNA,by previously described RNA isolation and cDNA generation methods, was diluted 1:20, and 2 µL was used for PCR amplification of target genes in a 50 µl reaction containing 0.2 µM of forward

and reverse primers (Table 5), 200 µM of dNTPs, 1x Standard Taq (Mg-free) Reaction buffer, 1.5 mM MgCl2, and 1.25 units of Taq DNA polymerase (M0320S, New England Biolabs, Ipswich, MA, USA) or 50 µl reaction containing 0.25 µM of forward and reverse primers (Table 5), 250 µM of dNTPs, 1x Q5 Reaction buffer and 1 unit of Q5 polymerase (M0320S, New England Biolabs, Ipswich, MA, USA). The PCR conditions were 98 °C for 2 min; 40 cycles of 98 °C for 20 s, 68 °C for 20 s, and 72 °C for 1 min; and 72 °C for 2 min. The amplified DNA was visualized by electrophoresis on a 2% agarose gel.

To elucidate the expression levels of interested genes Quantitative real-time PCR method was used. Throughout this study, the assay was performed using two reagents, SYBRGREEN and ENZO. RT-qPCR reactions using the RealQ Plus 2X Master Mix Green Without ROX from Amplicon were prepared by mixing 1X RealQ Plus 2X master mix, 0.2 µM of each forward and reverse primer, and 5 µl (1:20 diluted) cDNA in a 20 µl reaction volume. PCR cycling conditions were as follows: initial denaturation at 95 °C for 10 s, followed by 40 cycles of denaturation at 95 °C for 15 s, annealing at 60 °C for 30 s, and extension at 72 °C for 30 s. Fold changes in gene expression were calculated using the ΔΔCt method, with GAPDH as a reference. RT- qPCR reactions using ENZO were prepared by mixing 1X ENZO 2X master mix, 0.3 µM of each forward and reverse primers, 0.15 uM corresponding Universal Probe Library probes (Roche, Basel, Switzerland) and 2.5 µl (1:20 diluted) cDNA in a 12.5 µl reaction volume. PCR cycling conditions were as follows: initial denaturation at 95 °C for 10 s, followed by 40 cycles of denaturation at 95 °C for 15 s, annealing at 60 °C for 30 s, and extension at 72 °C for 30 s. Fold changes in gene expression were calculated using the ΔΔCt method, with GAPDH or RBM17 as a reference. In every instance Amplification was carried out in the ABI PRISM 7500 Fast qPCR System (Thermo Scientific, Waltham, MA, USA), and the primers for the corresponding genes are listed in Table 14.

3.7.7. Protein extraction and Western Blots

To assess the presence of mutated proteins or to inspect EMT-MET-related protein and senescence-related protein levels at every stage of the clones, total protein isolation with RIPA was performed, followed by Western Blot analysis. To extract total protein, cells at 80% confluency in a 100 mm plate or cells at the end of the TGF beta experiment were detached from the plates either using Trypsin or EDTA at a final concentration of 4 mM, pelleted at 0,3 rcf for 2 min, washed with 1X cold PBS, and lysed using 200ul of ice cold RIPA buffer for 30 min, followed by 10 min centrifuge at 10000xg at 4C. The supernatants were transferred to new tubes and quantified using the Pierce BCA Assay Kit. Total proteins were denatured in 4X loading dye at a final concentration of 1 at 95 °C for 5 min and loaded on 18% or 12% acrylamide gel with a protein ladder, run initially at 70 V for 20 min, and then at 170 V for one hour in a Bio-Rad system. After electrophoresis to prepare for the transfer step, the gels were soaked in transfer buffer for 10 min, while the immobilon-P membrane was soaked in methanol for 5 min for activation and 5

min in transfer buffer for equilibration. Afterward, the sandwich system was constructed following the system's recommendation (Bio-Rad) and transferred onto an immobilon-P membrane at 400mA for two hours accompanied by an ice block to prevent heating-induced heating. After blocking, the membrane was Ponceau-stained to elucidate protein degradation and equal loading. After washing Ponceau with ddH2O, 5% skimmed milk was used as a blocking reagent.

After blocking, the proteins of interest were detected using the primary antibodies listed in Table 9, the corresponding dilution factors with O/N at 4C or 1h at RT incubation, and their corresponding HRP-conjugated secondary antibodies. After each antibody treatment, membranes were washed with TBST (1xTBS, 0,1 Tween x). Finally, Clarity Western ECL Substrate kit was used for detection.

3.7.8. H1 extraction and SDS page

To elucidate the presence of the H1 isoform in protein level in the clones of interest and the absence of H1f4 in the knockout clones H1 specific protein extraction using perchloric acid was performed. Firstly 5x10^6 cells were counted and pelleted from each clone and parent cell as described before and nuclei were isolated using ice-cold nuclear fractionation Buffer A supplemented with PMSF and PIC at final concentration of 1mM and 1X respectively. The cells were incubated on a rotator for 10 minutes at 4 C and lysed by the addition of NP-40 at a final concentration of 0.3% and incubated for another 30 min under the same conditions. The released nuclei were pelleted at 10000xg and 4C for 10 min, and the supernatant containing the cytoplasmic fraction was separated into another tube. Pelleted nuclei were resuspended in 5% ice-cold perchloric acid and incubated on a rotator at 4C O/N. Following incubation, the samples were centrifuged at maximum speed for 10 min to pellet the insoluble perchloric acid proteins, and the supernatant was transferred to new tubes. 0.11x volume ice cold TCA was added to precipitate the H1 protein and incubated on ice for 10 min, followed by the addition of 1:1 10% TCA to enhance precipitation for an additional 30-minute incubation. The samples were pelleted at the maximum speed for 30 min at 4 °C and washed twice with ice-cold acetone with intermediate centrifugation. Aceton was airdried and pellets were resuspended in 8M urea.
The whole content of the isolates was loaded on 20% SDS gel and run at 180V for 4 hours for better resolution. The gels were stained with Coomassie dye o/n, destained with Coomassie destaining buffer for 2 h, and visualized using Bio-Rad.

3.7.9. Growth Curve Analysis

To determine the depth of the observed growth differences between clones, parental cell growth curve analysis was performed. Clones were seeded on 12 well plates at 20000 cells per well as duplicates for a 5-day

assay. Viable cell numbers were determined daily using the trypan blue exclusion assay. To ensure reliability, the assay was performed in triplicate.

3.7.10. Cell Cyle Analysis

After the assessment of differentiated growth patterns among cells, the clones were subjected to cell cycle analysis to detect the root cause. Cells were collected at 80% confluence, fixed with 70% ice-cold ethanol, dyed with propidium iodide , and subjected to Flow Cytometry to evaluate PI binding in the Per-CP Cy5.5 channel. To assess cell dimensions, an unstained parental sample was used, and the samples were normalized and analyzed using FlowJo v10 software (FlowJo, OH, USA). The experiment was repeated three times

3.7.11. Fluorescent, ubiquitination-based cell-cycle indicators (Fucci) Transfection and Cell cycle Analysis

The radical results obtained from the PI-based cell cycle analysis created the necessity confirmed the results of a different assay with a lower error rate. This assay was determined to be Fucci-based cell cycle analysis. The Fucci system, in contrast with PI, which only targets and binds DNA of samples, evaluates its content according to the density of emission, creates a low trust range, and targets the specific cyclins of each cell cycle stage, creating trustworthy results. The fluorescent ubiquitin cell cycle indicator (FUCCI)-based system allows for live and in vivo observation of cell cycle progression. Based on the mutually exclusive activity of two fluorescently labeled proteins, cdt1 and gemini,n, during the G0/1 and S/G2/M phases of the cell cycle, individual cells can be assigned to their respective cell cycle phases by fluorescence imaging of the nucleus (Figure 14).

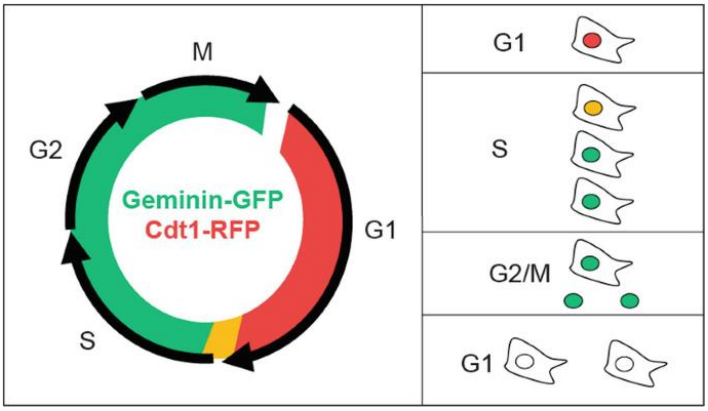

Figure 14. Illustration of the principle of action of the Fucci system.

First, every clone and parental cell were plated in six-well plated at 12500cells/cm2 density. The following day, cells were transfected with 5 µg of Fucci plasmid using Lipofectamine P3000 Reagent, as recommended by the manufacturer. 48h after transfection, cells were selected with 500 ug/ml

hygromycin for 7 days and 800ug/ml for 4 days to ensure the viability of only clones with genome-integrated Fucci to obtain a stable transfected line for further experiments.

3.7.12. EMT MET experiments

To analyze the effect of downregulated H1e or its absence, and the effects of Rahman and other mutations on EMT and MET processes, clones were seeded at 6250/cm2 density and treated with 2,5ng/ml TGF beta TGFβ3 (100-36E, Pep Rotech, London, UK) for 96h and collected for the EMT group. For the MET group, cells were treated with equal amounts of TGFβ and after 96 h washed with 1XPBS three times to remove TGFβ from the environment and incubated for another 96h to allow mesenchymal to epithelial transition. As a control for the transition, an untreated group vehicle was also used in the experiment under the same seeding conditions and 96h of incubation at 37C with 10% CO2. All groups were followed up for the entire experiment using bright-field microscopy images, and RNA, protein, and slides for IF staining were collected at the end of each stage.
TGFβ3 was dissolved in a buffer containing purified water to a final concentration of 7.5% 19 BSA and 1.2 M HCl and stored at -20 °C for further experiments

3.7.13. Immunostaining

Clones in the EMT, MET, and control groups were washed with 1X PBS and fixed with 4% formaldehyde (F8775, Sigma) for 10 min at room temperature, washed twice with PBST(1XPBS,0.1%Triton X), and permeabilized with 0.5% Triton X-100 (T8787, Sigma) for 5 min. The clones were then incubated with primary antibodies in PBS containing 5% BSA (1:200) for one hour at room temperature. Afterward, the fluorescence-conjugated secondary antibody was applied for an additional hour after washing in PBS. Nuclei were visualized with DAPI (1:1000, Invitrogen) and mounted with ProLong Diamond Antifade Mounting Solution (P36962, Thermo Fisher Scientific, Waltham, MA, USA). Confocal microscopy was performed using an LSM 880 microscope equipped with the ZEN software (Zeiss, Oberkochen, Germany). All the antibodies, targeted proteins, and compatible secondary antibodies are listed in Table X.

3.7.14. SA-β-Galactosidase Assay

TGF-β-treated and untreated cells were collected at the end of the experiment and washed three times with 1XPBS. Cells were fixed for 5 min, and the appropriate amount of X-gal was measured and mixed with SA-β-Galactosidase Assay buffer, and the pH was fixed at approximately 6.0.

The fixed cells were washed three times with 1xPBS, and 1 ml of the solution was dispersed into each well. As a positive control, senescent Huh7 cells were treated with doxorubicin.

3.7.15. Xenograft on Zebrafish larva

To assess the migratory and invasive abilities of clone 10, both BC and AC versions accompanied by parental cells on passage two were grafted on zebrafish larvae following the protocol developed by (Au - Martinez-Lopez et al., 2021) with minor modifications (Figure 15). The injected larvae were examined 24 h after the injection to ensure the integrity of the injected yolk. Approved larvae were followed for four days post injection (4dpi) and the results were obtained by confocal microscopy imaging. Exclaimed data was analyzed on GraphPad Prism 10.2.3

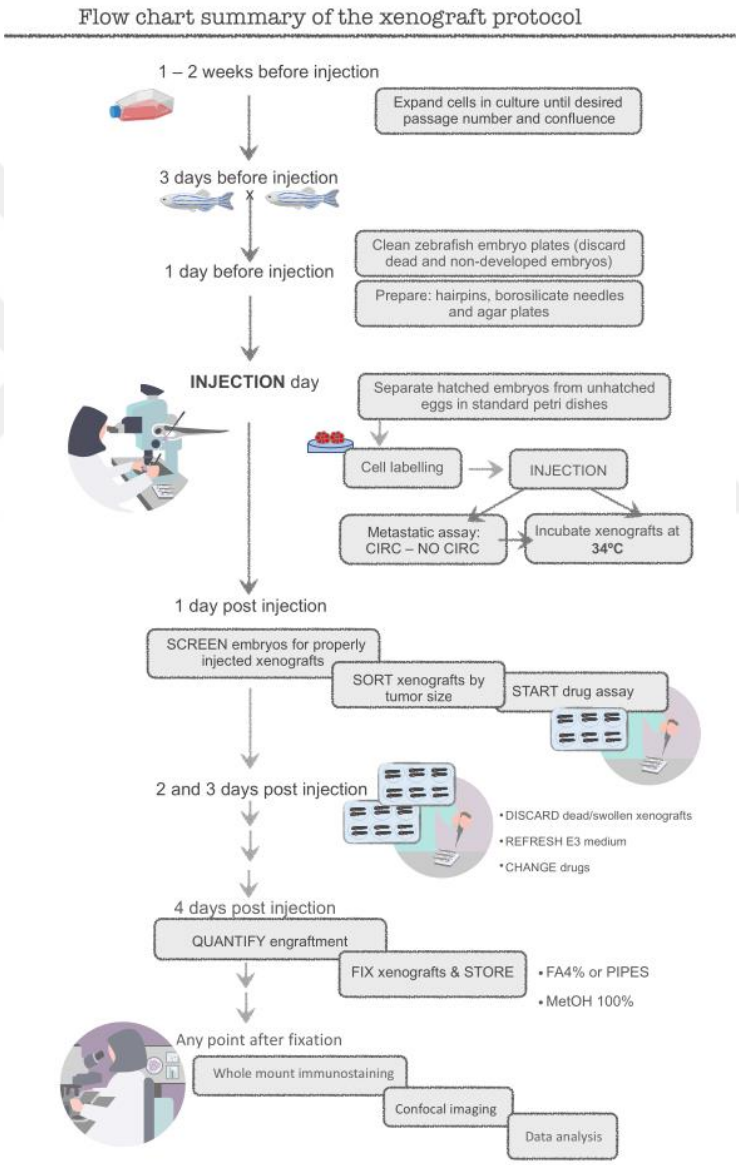

Figure 15. Xenograft Workflow. Figure adapted from (Au - Martinez-Lopez et al., 2021).

3.8. Limitation of the Study

Obtaining H1e knockout clone. None of the 255 clones screened was positive for a single knockout of H1e. Obtained 3 homozygous cloned also showed deletion of other linker isoforms.

3.9. Ethics Committee Approval

This study was approved by the IBG Local Ethics Committee protocol number 2023-018.

4. RESULTS

4.1. siRNA Mediated Silencing of linker histones on MCF10A

To assess the potential role of linker histones in MCF10A well-being and EMT, siRNA-mediated depletion of three different linker histones was employed. First, we investigated the effects of H1C depletion. H1C was shown to arrest cell cycle at G1 phase and altering the nucleosome spacing of genome in one study (Sancho, 2008). In another study, it was shown to influence human telomerase enzyme expression and activity through RNA-RNA interactions (Ivanyi-Nagy et al., 2018). According to our results, H1.C depletion dramatically affected the survival and growth rate of cells but did not cause any EMT effect. On the contrary silencing of H1C caused upregulation in both epithelial and mesenchymal markers, CDH1 and CDH2, respectively (Figure 16).

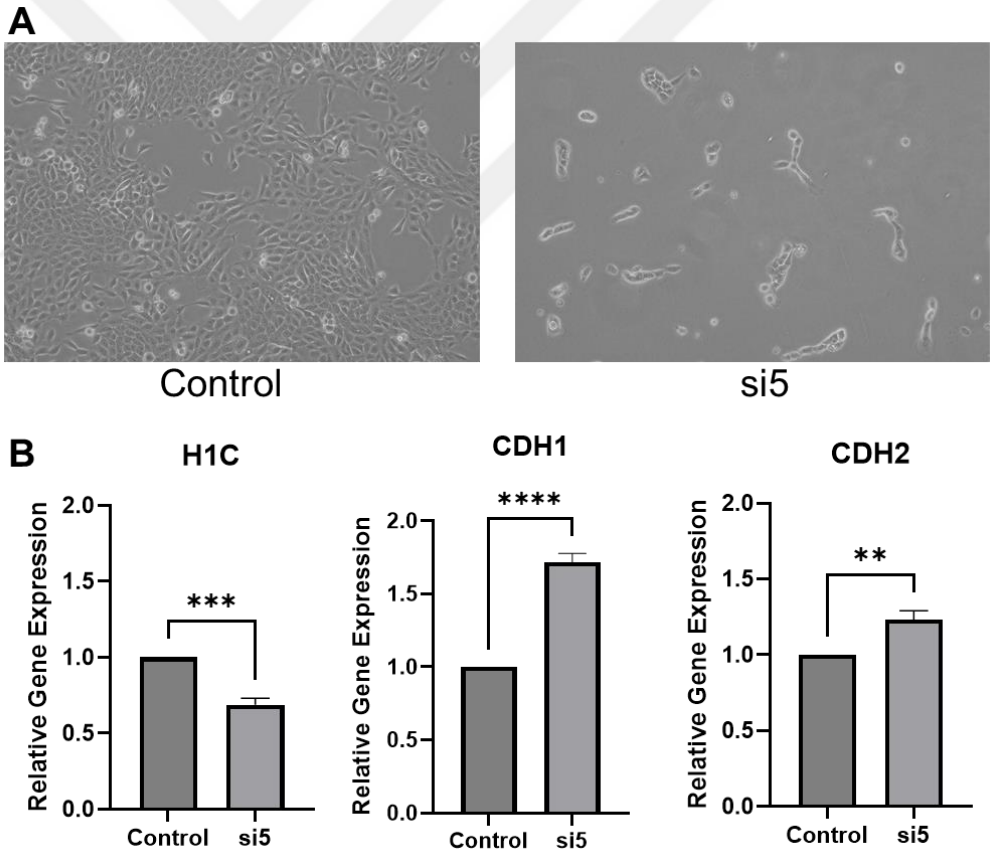

Figure 16. H1C Depletion Does Not Promote EMT. A. Silencing of H1C did not create an EMT phenotype but caused an increase cellular death and retarded growth. B. In RNA level H1C depletion resulted in increased expression of both CDH1 and CDH2. The data was analyzed using Student's t test. ($p > 0.05$ *, $p \leq 0.05$ **, $p \leq 0.01$ *** and $p \leq 0.001$ ****)

Similarly, the depletion of another linker variant, H1D, resulted in increased death, but not in any EMT phenotype, with increased expression of CDH1 and CDH2 (Figure 17). On the other hand, siRNA mediated knockdown of linker histone H1E did resulted in EMT phenotype with increased death (Figure 18).

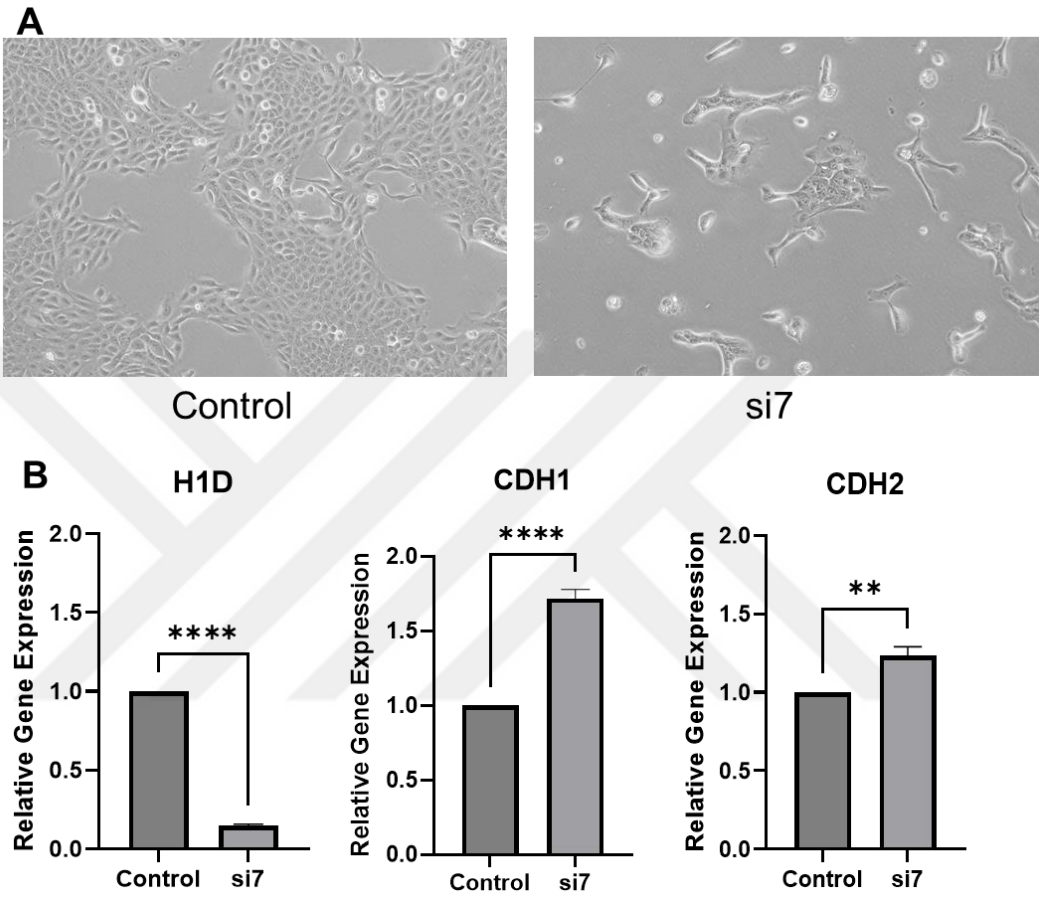

Figure 17. H1D Depletion Does Not Promote EMT. Silencing of H1C did not create an EMT phenotype but caused an increase in both CDH1 and CDH2. The data was analyzed using Student's t test. ($p > 0.05$ *, $p \leq 0.05$ **, $p \leq 0.01$ *** and $p \leq 0.001$ ****)

Upon depletion of H1E, a gain of spindle-like morphology was observed in MCF10A cells with decreased expression levels of CDH1 but no significant change in the expression of the mesenchymal marker CDH2 (Figure 18).

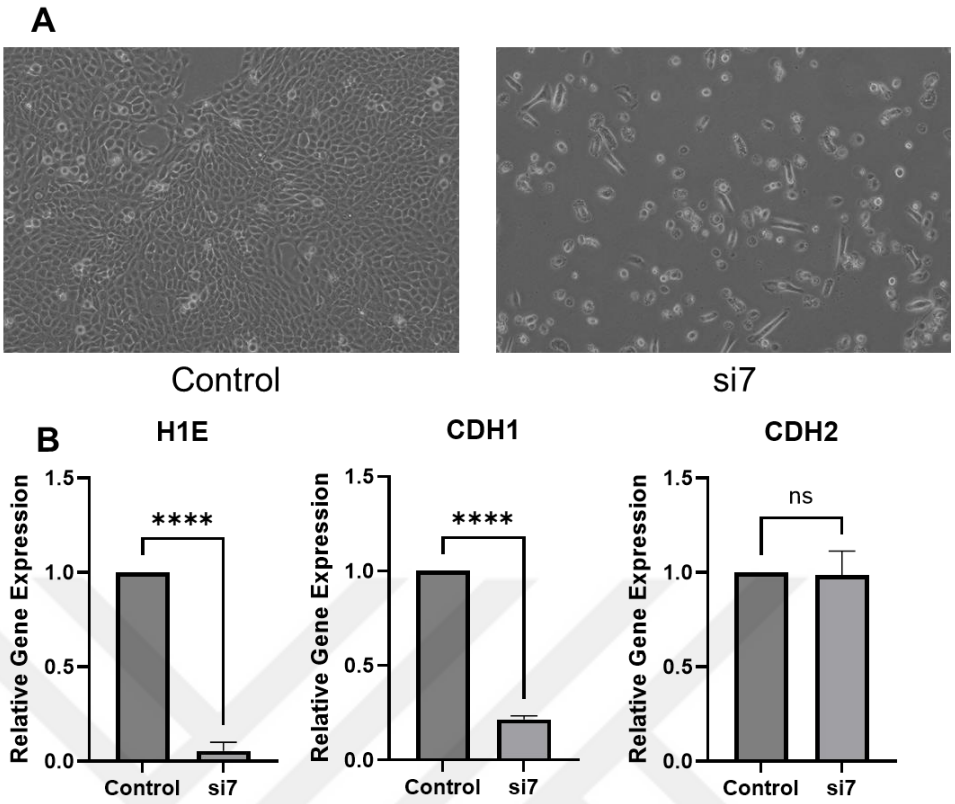

Figure 18. H1E depletion promoted an EMT-like phenotype. The silencing of H1E created an EMT phenotype with a decrease in CDH1 expression. The data was analyzed using Student's t test. ($p > 0.05$ *, $p \leq 0.05$ **, $p \leq 0.01$ *** and $p \leq 0.001$ ****)

After observing the decreased cell number after siRNA treatment, the cells were employed for cell viability inspection via the SRB assay. The results showed a slight drop in the survival rate of the cells, as shown in Figure 19, indicating that the observed decrease could be the result of cell cycle-related disruptions.

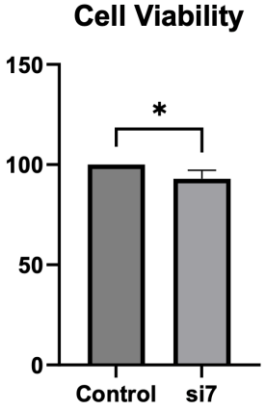

Figure 19. H1E depletion influenced cell viability. Silencing of H1E affected cell viability. The data was analyzed using Student's t test. ($p > 0.05$ *, $p \leq 0.05$ **, $p \leq 0.01$ *** and $p \leq 0.001$ ****)

As expected, the cell cycle assay showed cell cycle arrest in the G1 phase of the cell cycle (Figure 20). As suggested by previous linker histone studies, H1E, as well as other linker histones, plays a prominent role in the progression of the cell cycle by setting up the chromatin into the right configuration for replication of DNA.

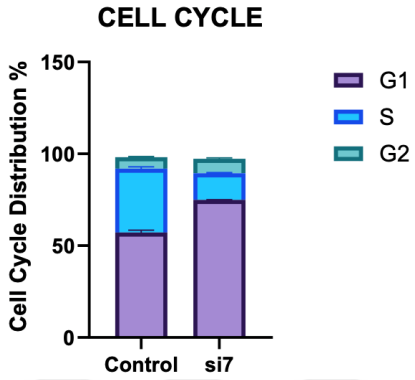

Figure 20. H1E depletion influences the cell cycle. The silencing of H1E arrested the cell cycle at the G1 phase.

Taken together, H1E was the only linker histone among the investigated proteins that influenced epithelial integrity in human mammary gland cells. The obtained results are in line with the literature that claims that loss of H1E drives EMT in lung cancer cell lines, as well as disruptions in the cell cycle with deadly features (Chen et al., 2024; Sancho et al., 2008).

4.2. Silencing of H1E linker histone in Normal Murine Mammary Gland

The Normal Murine Mammary Gland (NMuMG) cell line is a widely accepted model for EMT and MET studies. Owing to their high plasticity, these cells can undergo EMT upon proper treatment, while under optimal conditions, they display total epithelial features. Unlike NMuMG cells, MCF10A cell line is widely known for its heterogeneous population that gives rise to epithelial and mesenchymal cells even under optimal conditions, synchronously. To confirm that the effects of H1E depletion in MCF10A cell lines were not affected by their heterogeneous nature, we performed siRNA-mediated knockdown assays on NMuMG cells. Further experiments were designed according to the mouse cell line to avoid the possible background effects of MCF10A heterogeneity.

4.2.1. Selection of siRNA for subsequent experiments

For the knockdown experiments, four different siRNAs targeting H1E were used, and their efficiency was validated in NMuMG cells by measuring H1E mRNA levels. Knockdown experiments were conducted in two stages, epithelial and mesenchymal. For epithelial knockdown, non-treated NMuMG cells at passage 2 were used to assess the effects of H1E depletion on the epithelial state. For mesenchymal cell knockdown, three days prior to

transfection, NMuMG cells at passage 2 were treated with TGF-β to induce EMT. To assess the effects of depletion on mesenchymal-to-epithelial transition cells, cells were transfected with siRNAs against H1E on the same day as TGF-β withdrawal, while in a mesenchymal state. Different siRNAs displayed different phenotypes shown in Figure 21.

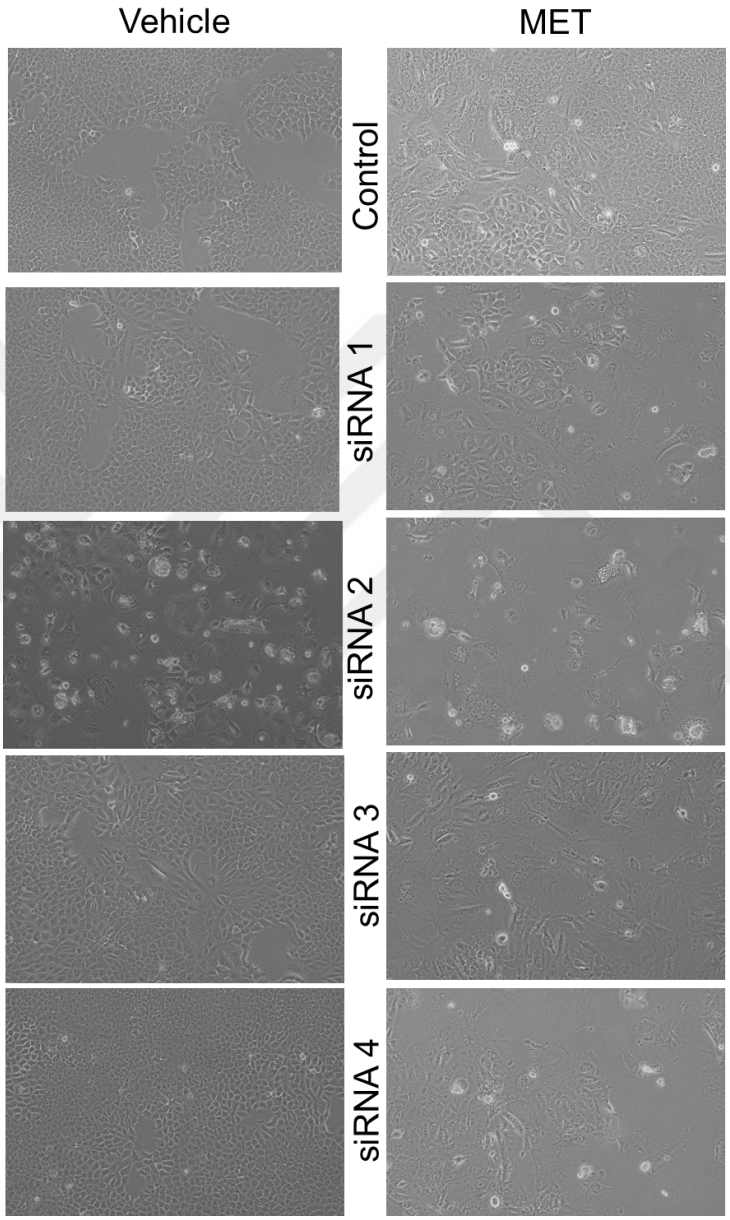

Figure 21. Knockdown with different siRNAs resulted in different phenotypic responses.

The results showed that only one siRNA, which also created a strange morphology, showed efficient knockdown in two stages, as shown in Figure 22A and B. Since linker histones show high similarity at the nucleotide level, we checked for possible off-target effects of the selected siRNA by aligning

seven somatic linker histones and showed that the target sequence of the selected siRNA did not show any match with the other isoforms (Figure 22 C).

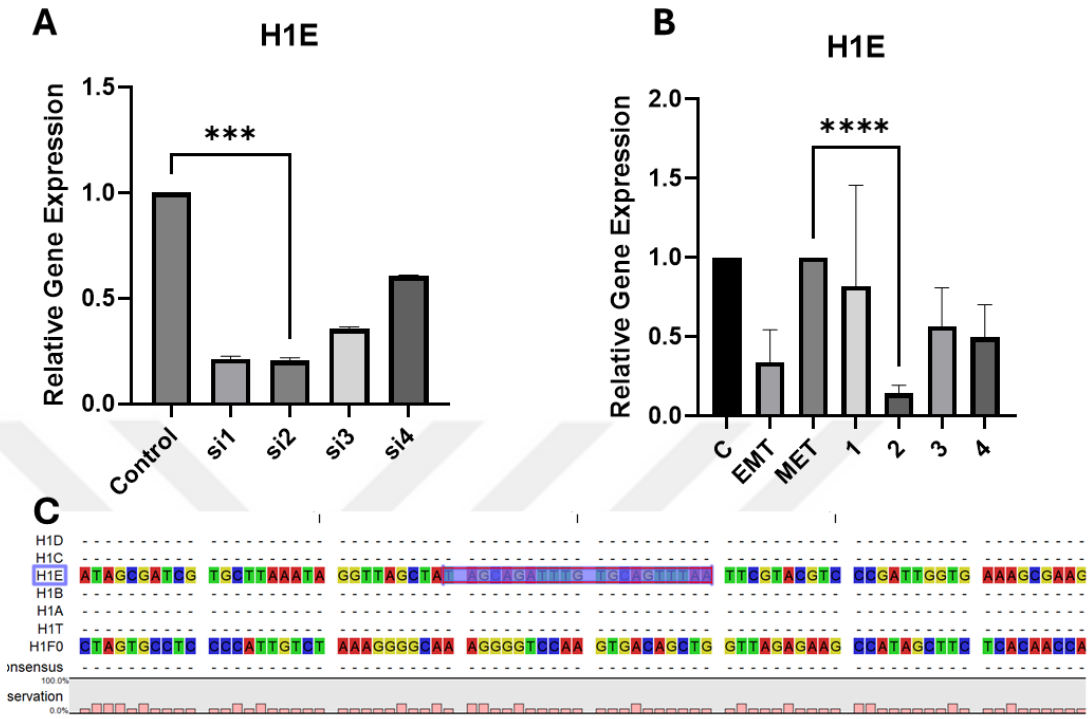

Figure 22. Knockdown efficiencies and targeting sequences of siRNA2 aligned with linker isoforms. A. NMuMG cells in vehicle state or recovering from TGF 3 treatment were transfected with either control or H1E targeting siRNAs, after 72 h, cells were collected, RNA was isolated and and efficiency levels were measured by qPCR A and B respectively. C. Alignment of linker histone isoforms. Selection shows the target sequence of siRNA2. The data was analyzed using Student's t test. ($p > 0.05$ *, $p \leq 0.05$ **, $p \leq 0.01$ *** and $p \leq 0.001$ ****)

4.2.2. Depletion of H1E in NMuMG Cells Results in EMT-like Phenotype

The subsequent knockdown of H1E resulted in an EMT-like phenotype. When this arrest was further investigated, we observed that knockdown of the H1E gene did not only result in downregulation of the CDH1 gene, a major indicator of epithelial to mesenchymal transition, but also resulted in downregulation of CDH2, which would show an increase in typical transition (Figure 23 A). In morphology wise cells lost their epithelial cobblestone features and cell-cell adhesion in time dependent manner as shown in Figure 23 B.

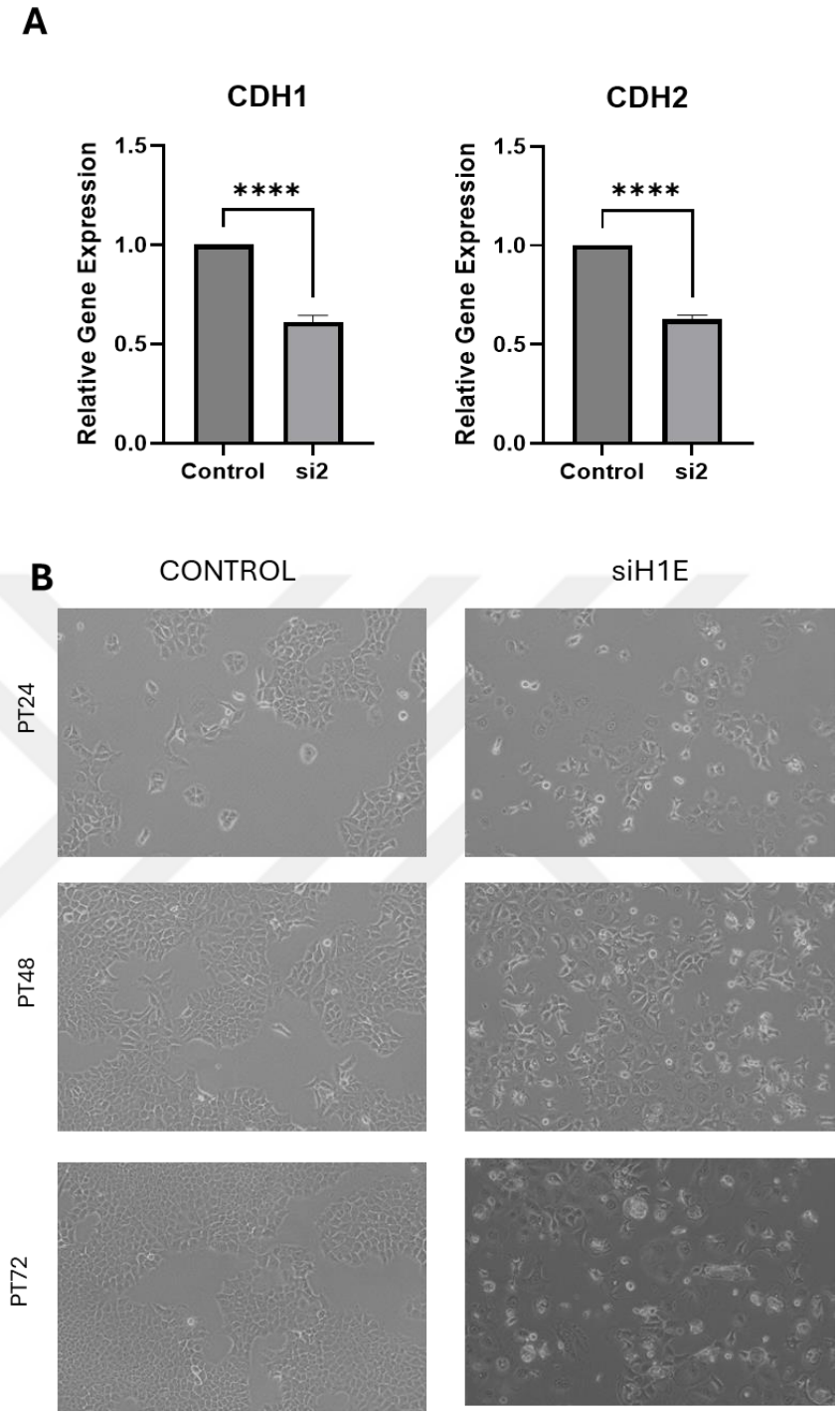

Figure 23. Depletion of H1E in NMuMG cells resulted in an EMT-like phenotype. A. CDH1 levels of siH1E showed mild drop together with CDH2 levels creating conflict. B Cells displayed an elongated morphology accompanied by the formation of strange vesicules and enlarged cytoplasm. The data was analyzed using Student's t test. ($p > 0.05$ *, $p \leq 0.05$ **, $p \leq 0.01$ *** and $p \leq 0.001$ ****)

When the localization of E-cadherin and the status of stress fibers were inspected by immunostaining of the corresponding proteins, an EMT-like pattern was observed (Figure 24). Upon initiation of EMT, E-cadherin is either

expected to be diminished or delocalized from the cell membrane into the cytoplasm. Similar features were present in H1E depleted group, with dispersion of E-cadherin throughout the cell body, indicating partial delocalization and accumulation of E-cadherin in the cytoplasm. Similarly, increased formation of stress fibers was observed through overall staining with the phalloidin antibody.

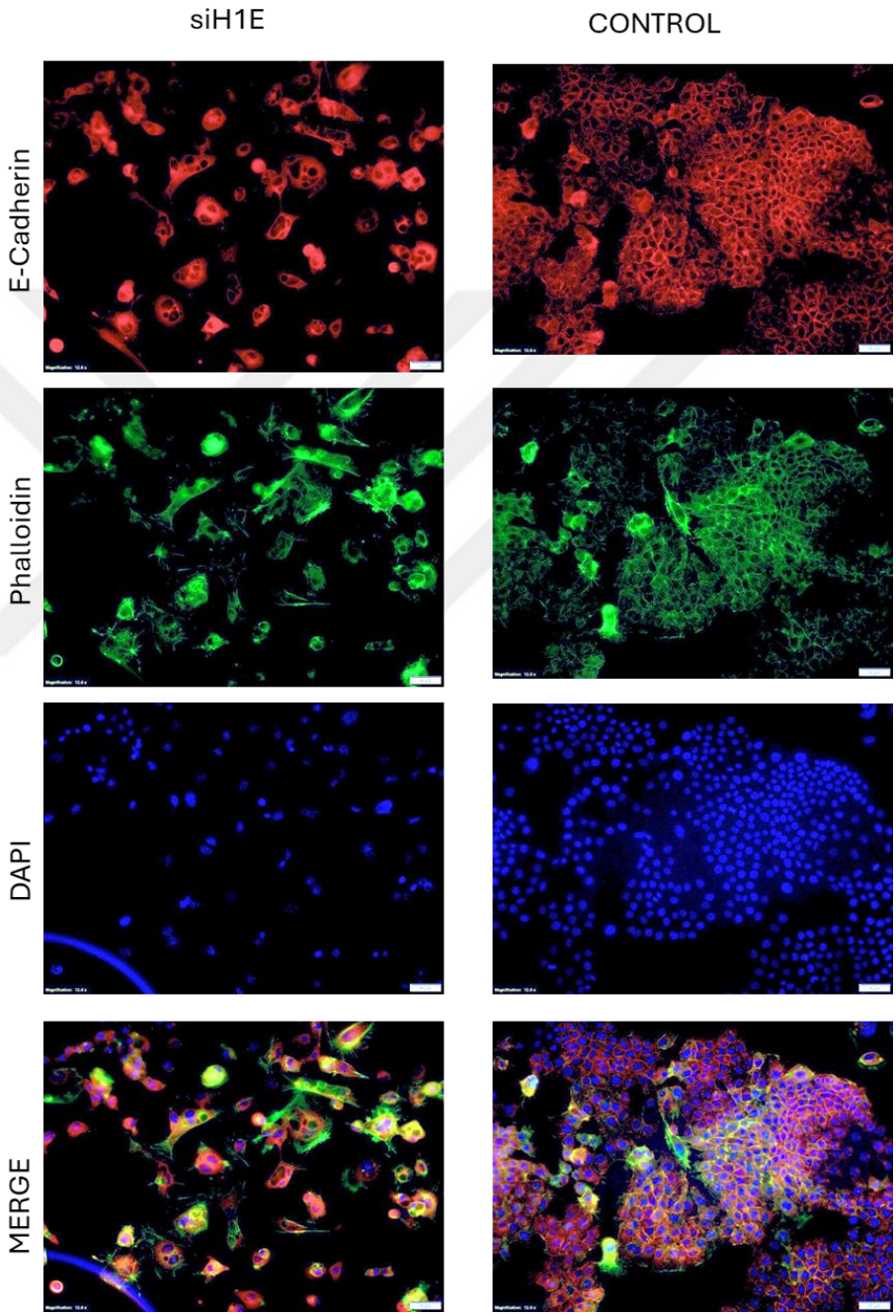

Figure 24. Immunofluorescence Imaging confirmed an EMT-like phenotype. Immunofluorescence staining showed delocalized E-cadherin from the membrane, and phalloidin staining showed the stress fibers and unusual morphology of H1E depleted cells unable to recover from TGF-β treatment.

4.2.3. Generation of FUCCI Clones and Assessment of Cell Cycle in Knockdown

Because of the close relationship between linker histones and cell cycle processes and observed G1 arrest in human cell lines, we also employed cell cycle analysis for knockdown in NMuMG cells (Brown et al., 1996; Sancho, 2008).

Due to couple setbacks the cell cycle assay for NMuMG cells was performed utilizing FUCCI system. The Fucci system, in contrast with PI, which only targets and binds DNA of samples, evaluates its content according to the density of emission, creates a low trust range, and targets the specific cyclins of each cell cycle stage, creating trustworthy results. The fluorescent ubiquitin cell cycle indicator (FUCCI)-based system allows for live and in vivo observation of cell cycle progression. Based on the mutually exclusive activity of two fluorescently labeled proteins cdt1 and geminin during the G0/1 and S/G2/M phases of the cell cycle, individual cells can be assigned to their respective cell cycle phase by fluorescence imaging of the nucleus (Fischer & Thievessen, 2023).

Prior to siRNA treatment, the cells were transfected with the Fucci-ESC plasmid and used for antibiotic selection. Upon completion of selection, the cells were treated with siRNAs as described previously and employed for fluorescence-activated flow cytometry.

In agreement with previous results, knockdown of H1E resulted in G1 cell cycle arrest (Figure 25). During the cell cycle, it has been reported previously that linker histones are phosphorylated and lose their affinity to chromatin. This reaction results in conformational changes and chromatin accessibility to the replication machinery of the cell. Interestingly, the increased S phase of the cell cycle could be indicative of active and aberrant replication in the absence of H1E. Additionally, abnormal DNA replication is a known cause G1 arrest through activation of pathways involving p53, in the G1 checkpoint. G1 arrest mostly acts as a DNA repair window for the cell, where either the damage in DNA is repaired or the cell is forced to undergo apoptosis. It is worth noting that the unusual phenotype of the cell together with G1 arrest could be indicative of damaged DNA in the absence of H1E, which could result in an open conformation through the perturbation of higher-order chromatin and vulnerability to DNA-damaging reagents. Further experiments are needed to validate the genomic integrity and cause of cell cycle arrest (Hergeth & Schneider, 2015).

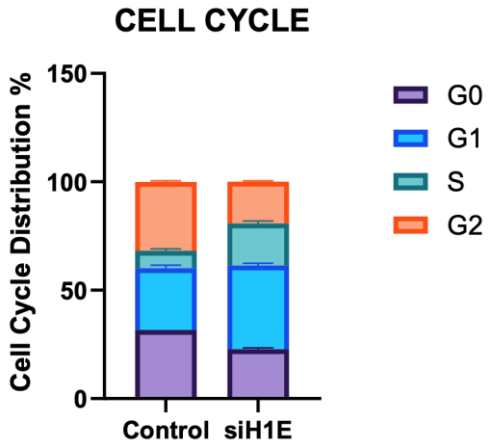

Figure 25. H1E depletion in NMuMG cells resulted in G1 arrest. The FUCCI-based system showed an accumulation of cells in the G1 phase in the absence of H1E.

4.2.4. Depletion of H1E in NMuMG Cells Obstracts MET and Results in Mesenchymal-like Phenotype

To investigate the function and necessity of H1E in the onset of MET, NMuMG cells, treated with TGF-β for three days and gained mesenchymal traits, were treated with siH1E upon withdrawal of TGF-β from the culture media (Figure 26). Knockdown of the H1E gene at the start of the Mesenchymal to Epithelial transition resulted in arrest of the mesenchymal state and inhibited the transition. MET obstruction was first observed using phase contrast imaging. siRNA-transfected cells exhibited vesicular enlarged cytoplasm with loss of apical polarity (Figure 27). They failed to gain cobblestone morphology, as observed in the control group after 72h absence of TGF-β. The displayed features of the knockdown group failed to match the exact EMT phenotype at the RNA level, and an inability of CDH1 levels to recover was observed (Figure 28).

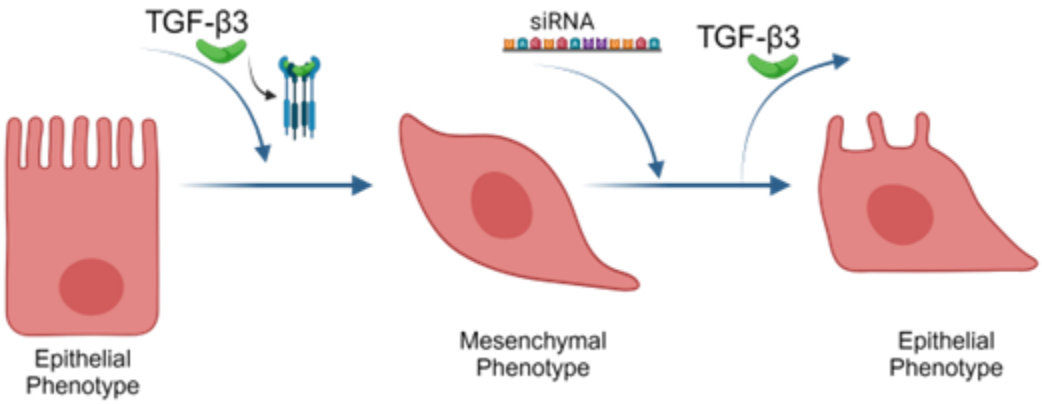

Figure 26. Illustration of H1E silencing on the onset of MET. Cells treated with TGF-β3 for 72 h were treated with siRNAs targeting the H1E transcript after withdrawal of growth factor.

We observed the inability of Fibronectin and ITGA5 to return to physiological expression levels, and HNF4A and CTNNB1 to regain their active expression, as expected (Figure 28). Vimentin on the other hand, type III intermediate filament that maintains cell integrity, and is associated with cell migration, motility and adhesion, and its overexpression is found to drive EMT in many cancers, remained behind even the levels of control group (Wu et al., 2018). This raises questions about the arrest of EMT, but also indicates that, together with the observed atypical phenotype, cells are standing in between the two states.

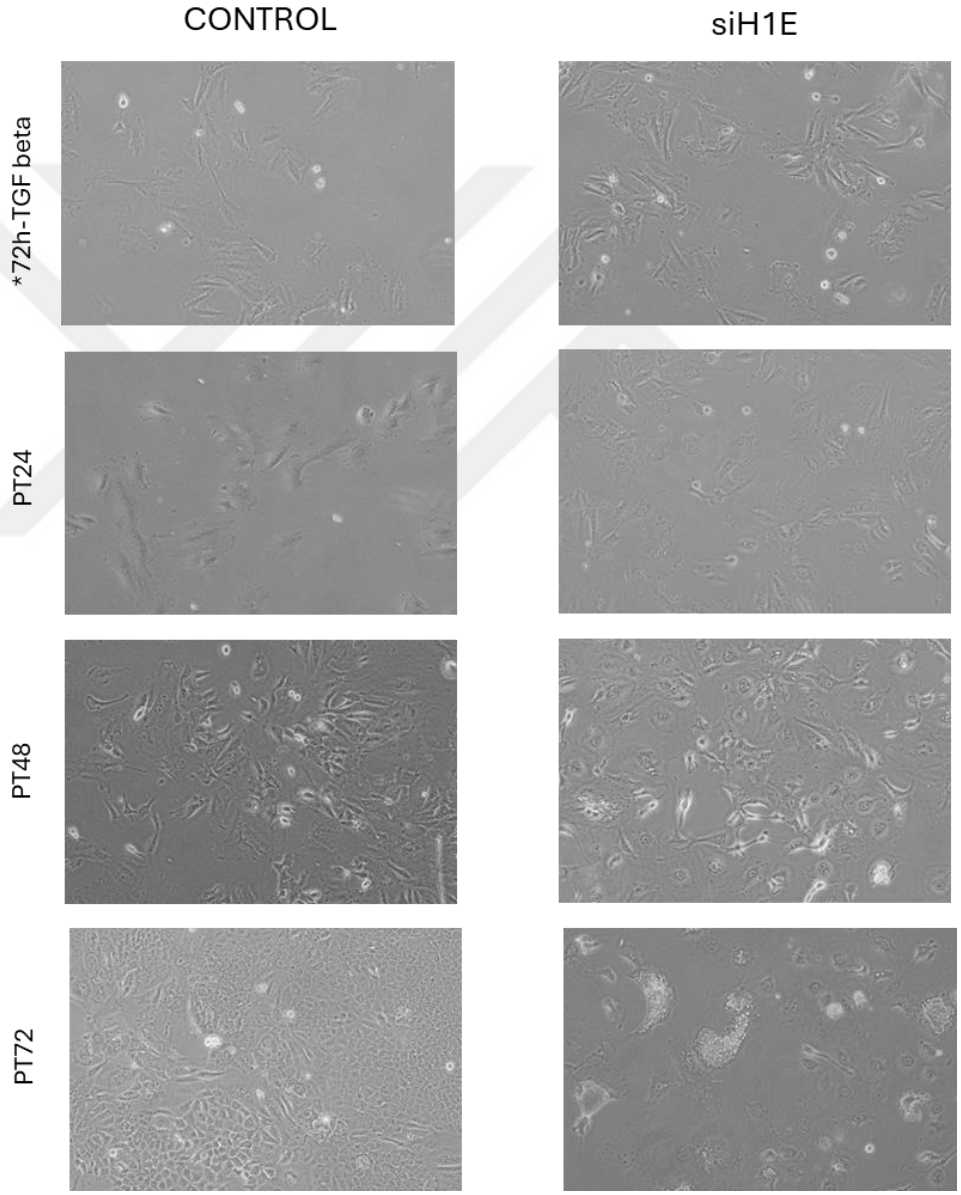

Figure 27. H1E knockdown arrested cells in the mesenchymal-like state by obstructing the Mesenchymal-Epithelial Transition. Phase-contrast images of either control or siH1E treated samples at certain time points.* Transfection time. The data was analyzed using multiple unpaired t test. ($0.05 < p \leq 0.001$ *)

In addition, immunofluorescence staining of E-cadherin showed that the recovered amount was not able to relocalize to the membrane but accumulated in the cytoplasm. Thus TGF- beta treatment-induced stress fibers were still present, as shown by phalloidin staining in Figure 29. 72 h after its withdrawal. In contrast, the control group showed successful recovery of E-cadherin at the RNA level and its relocation to the membrane, accompanied by the disappearance of stress fibers. To further confirm the obstruction of MET, we examined a couple of epithelial and mesenchymal markers.

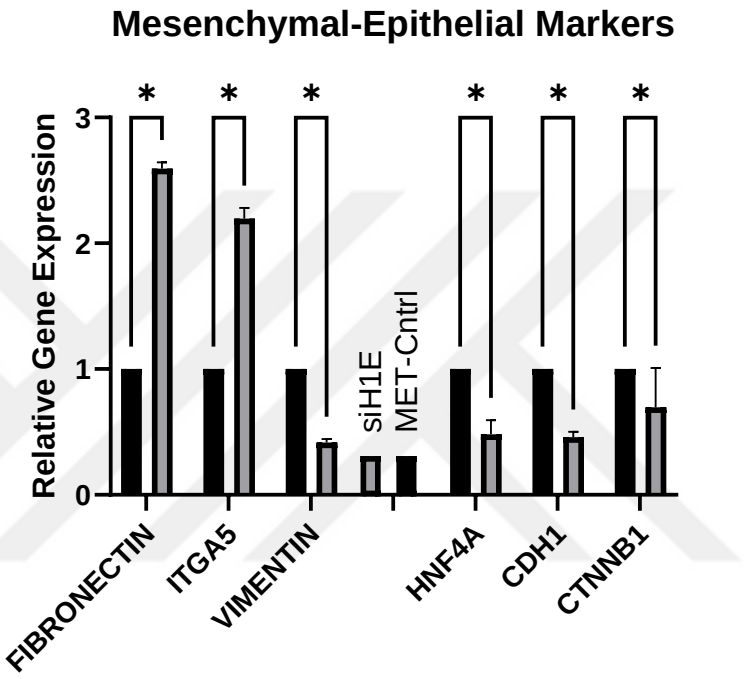

Figure 28. H1E knockdown arrested cells in the mesenchymal-like state by obstructing the Mesenchymal-Epithelial Transition. Early passage NMuMG cells were transfected with either control or H1E targeting siRNAs, after 72 h, cells were collected, RNA was isolated and expression levels of both mesenchymal markers like Fibronectin, ITGA5, Vimentin and epithelial markes like HNF4A, CDH1and CTNNB1 was measured. ($0.05 < p \leq 0.001$ *)

In line with the qPCR and morphological assessment, immunostaining of E-cadherin protein showed its inability to reach membrane but accumulated in the cytoplasm of the cells. Besides the persistent presence of stress fiber by phalloidin antibody showing the still present mesenchymal character and halted MET (Figure 29).

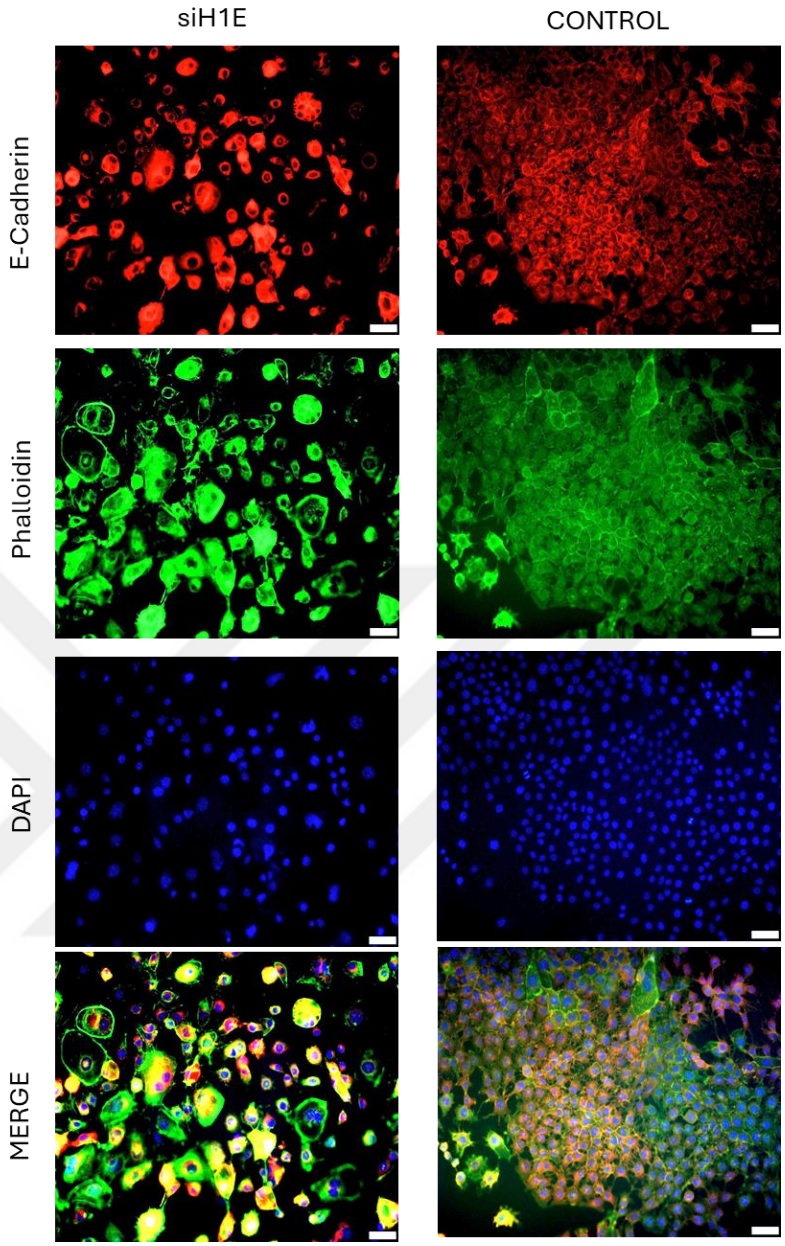

Figure 29. In the absence of H1E, E-cadherin failed to localize to the cell membrane. Immunofluorescence staining showed delocalized E-cadherin from the membrane, and phalloidin staining showed the stress fibers and unusual morphology of H1E depleted cells unable to recover from TGF-β treatment.

4.2.5. Assessment of Senescence in Knockdown

H1E depleted cells underwent dramatic morphological changes with enlarged cytoplasm, multinuclear anatomy, and multiple vesicles. Since the morphological assessments of the treated clones were similar to senescence features, we questioned whether the depletion of H1E could accelerate or generate cellular senescence and performed an SA-beta-galactosidase assay

with MET knockdown cells and non-treated MET cells as negative controls and Huh7 dox-treated cells as positive controls (Figure 30).

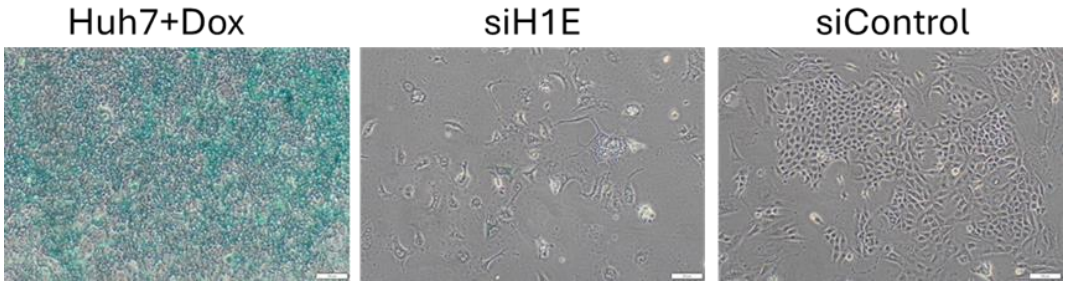

Figure 30. Cells arrested in the mesenchymal state after silencing of H1E showed a senescence tendency. H1E depleted cells showed a slight affinity for x-gal.

Cells showed slight reactivity, which was not enough to indicate the senescent state. This indicated that the displayed phenotype and arrest of EMT were not caused by SAHF formation. but most probably by disruption of chromatin levels.

4.3. Development of linker histone H1E knockout NMuMG cell lines

H1E linker histone as mentioned above belongs to one of the most divergent and heterogeneous histones among histone families that are evolutionarily conserved. In addition to the well-known architectural roles of linker histones, each of the 11 isoforms also has different biological roles, depending on the cell in which they are present and their state (Hergeth & Schneider, 2015; Izzo et al., 2008). Similarly, our previous studies have shown that linker histones undergo dramatic changes in expression during EMT and MET (Figure 31). To further investigate the role of linker histones in EMT-MET, we focused on linker histones with disease-causing mutations.

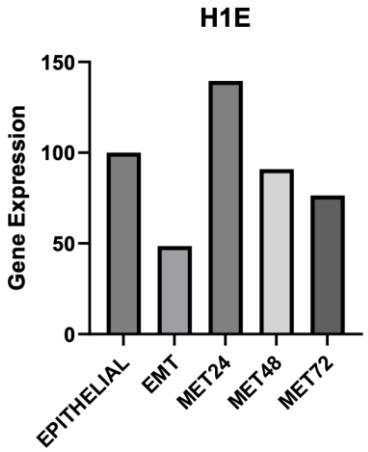

Figure 31. H1E levels change throughout of EMT-MET. RNA-seq data showing differential expression of H1E during transitions.

4.3.1. CRISPR/Cas9 strategy and Vector Design

After obtaining the knockdown results with MET obstructing ability of H1E in the absence of itself, we generated H1E knockout cells using CRISPR/Cas9 technology utilized with Homology-Directed Repair to not only display knockouts but also knock in a human H1E gene harboring c.430dupG, a mutation recently associated with Rahman Syndrome and later nominated as HIST1H1E syndrome (Figure 32). As HDR-mediated CRISPR/Cas9 focuses on the knock-in of artificial genes and not knock-out, we designed our HDR template to ensure knockout of H1E in first-generation clones. To achieve this, 5' homology arms were designed to cover the area spinning between the promoter and the coding sequence of H1E, and a neomycin gene followed by polyadenylation signals was placed immediately thereafter. This neomycin cassette arrests the promoter of H1E and fully inhibits its transcription via polyadenylation signals. This would not only allow generation of knock-out acting knock-in clones but would also allow for geneticin selection on transfected cells and narrow down the chances of unnecessary genotyping. In the HDR template, the neomycin cassette was followed by an HA tag coding sequence for later protein-related experiments, followed by the human H1E gene, which harbors the most frequent mutation observed in HISTH1E patients, c.430dupG. The 3' homology arm is 300bp long after the coding sequence (CDS). The designed vectors were synthesized commercially by the Eurofins Company.

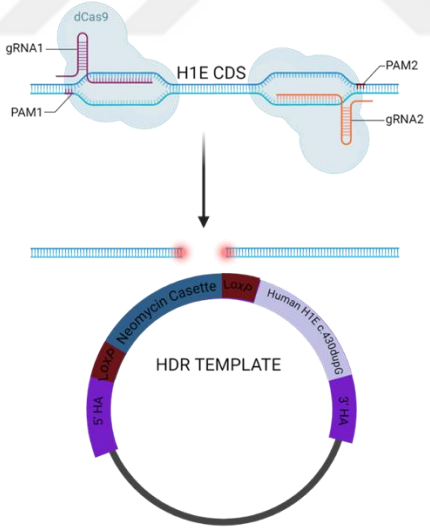

Figure 32. Illustration of HDR directed Crispr/Cas9 genome editing of H1E locus.

As per sgRNA, two sgRNAs were designed to target the start and end of the H1E gene with appropriate PAM sequences coding Cas9 and GFP proteins. The presence of GFP protein in the sgRNA was designed to create a transient expression in the first days of transfection, enabling sorting of cells according to the GFP signal and ensuring the collection of sgRNA-transfected cells, scaling down the chances of wasteful genotyping. The synthesized

plasmids were transformed into competent E. coli cells grown on ampicillin-positive LB Agar O/N plates. Single colonies were selected and grown in ampicillin-positive LB broth for 16 hours. Plasmids were isolated from mini-cultures by alkaline lysis . Approved plasmid colonies were set for maxi culture, grown in 2 ml for 8 h, and later in 50 ml for 16 h. Cultures were collected the next day and plasmid extraction was performed using the Qiagen Maxi-prep kit.

4.3.2. CRISPR/Cas9 Editing of NMuMG cell, Single Cell Cloning and Genotyping

NMuMG cells at passage two were transfected with two sgRNAs targeting the HIST1H1E gene and an HDR template TV3-1 that replaced the wild-type gene with the CTD-mutated human gene harboring a neomycin cassette that arrests the endogenous promoter. After 96 h, the transfected cells were analyzed and collected by fluorescence-activated flow cytometry as GFP-positive bulk populations and subjected to neomycin selection for 10 days at low density on 100 mm diameter plates with scramble transfected control cells. Untransfected, untreated daughter cells were frozen immediately for use as the parental group in subsequent experiments. Upon completion of the selection, bulk cells were cloned manually into 96 well plates and their growth and clonality were monitored and analyzed by Solentim Cell metrics for 15 days. Approved clones were grown further, and DNA was collected from each clone for the genotyping (Figure 33) by multi-step PCRs (Figure 34).

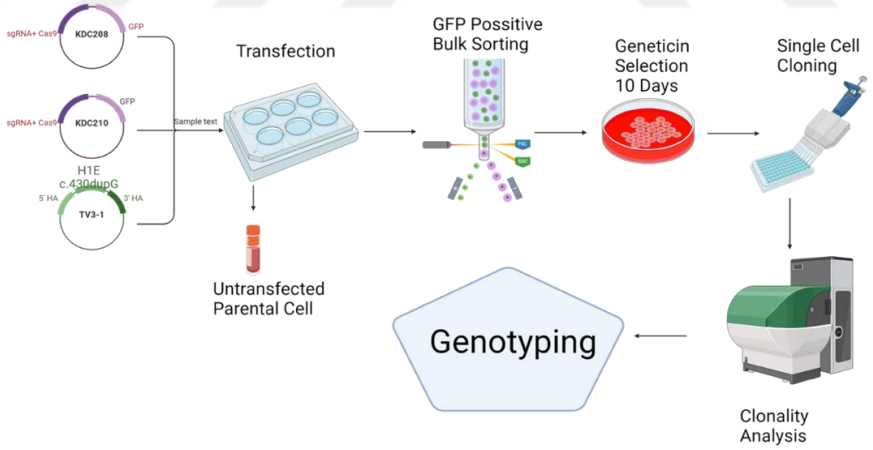

Figure 33. Workflow of CRISPR/Cas9 edited clone generation.

The first round of genotyping was conducted on the 5' arm of the recombination locus containing the neomycin cassette using Primer KD419-KD420, which targeted the 5' upstream locus of the H1E gene outside the introduced construct and the neomycin cassette, giving positive results only for the proper recombination of 5' prime clones. Clones yielding positive results in the black and white PCR, as shown in Figure 35A-C, were checked for their 3'-prime end in two steps. First, PCR was performed using the KD396/KD397

primers, followed by digestion of the successfully amplified fragment by HindIII. Similar to the 5' PCR, 3' screening also targeted the 3' endogenous part of the H1E locus outside the given construct and downstream of the neomycin gene, amplifying both mutated and endogenous genes. Successful PCR, shown in Figure 35A-C, was performed for HindIII digestion to separate human and mouse genes, successfully recombining the locus and recombination null locus, respectively. Fact possible thanks to silent mutation creating a HindIII recognition sequence integrated in the introduced HDR template, giving the opportunity to separate the two alleles and conformation of the zygosity of the recombination (Figure 35).

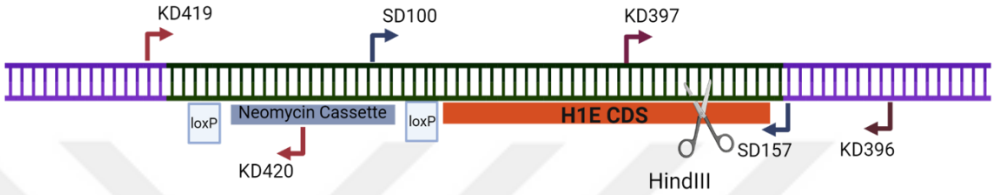

Figure 34. Schematic representation of genotyping and genotyping analysis of approved single-cell clones.

A total of 250 clones collected from four different transfections resulted in either heterozygous clones or incorrectly recombined cells. As a result, subsequent experiments were performed with heterozygous clones selected randomly from the first set of positives. Genotyping analysis was repeated once more on the selected clones as described previously and is shown in Figure 35 together with the clonal reports of the clones.

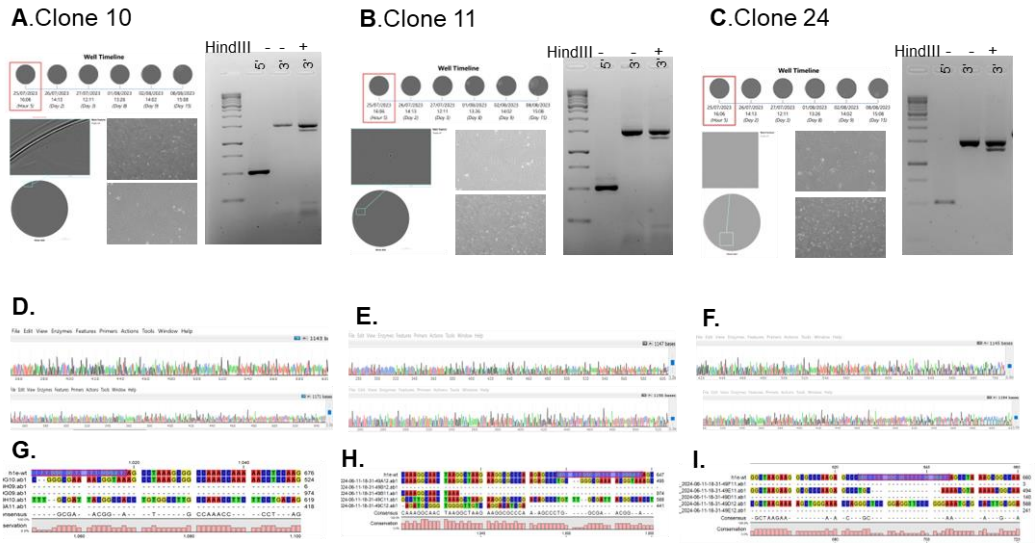

Figure 35. Final Genotyping Of Selected Clones. A-C. Clonality analysis and morphological assessment of clones after single-cell cloning and genotyping results. Sanger sequencing results of clones for endogenous wildtype allele and Crispr-Cas9 edited mutant allele. G-I. Sequencing results were aligned to the H1E gene, with the highlighted target sequence of sgRNA 210 showing a two bp deletion.

To confirm the recombination at the nucleotide level, SD155 and SD156 primers were used to amplify the endogenous wild-type allele, and PCR using KD194 and KD396 primers was used to amplify the recombined mutant human allele, and the products were subjected to Sanger sequencing (Figure 35D-F). The sequencing results showed successful recombination and integration of the mutant gene into the desired locus without further mutations. Although on behalf of the endogenous wild-type allele, a single nucleotide deletion was spotted on two of the clones (Figure 35G-I), creating a frameshift mutation resulting in a shorter CTD tail that did not dramatically affect its charge (Figure 36). Clones without dramatic charge differences were considered safe for the subsequent experiments. On the other hand, clone 24 showed a 16 bp deletion in the WT allele, creating a dramatic change in the WT protein, which was considered another function disturbing mutation, and the clone continued to the later experiments as another group of truncated mutations.

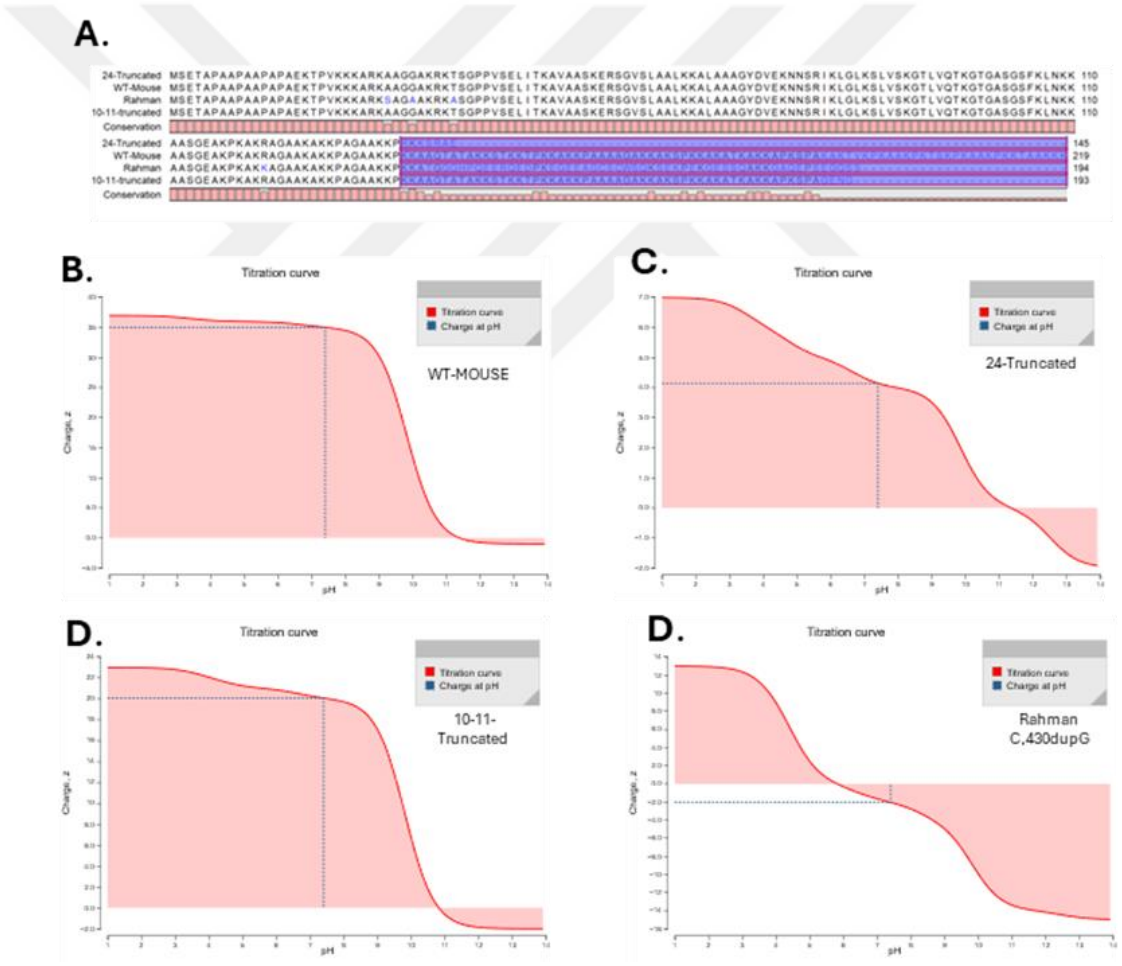

Figure 36. Amino Acid Sequence of clones and charge differences of CTD tails. A. Amino acid sequences of clones constructed from the Sanger sequencing results of endogenous wild-type allele. The selection shows the C-Terminal Domain of each protein. B. Titration curve of WT-Mouse H1E CTD showing its charge z:30. C. Titration curve of 24-Mouse Truncated H1E CTD showing its charge z:4. D. Titration curve of 10-11-Mouse Truncated H1E CTD showing its charge z:20. E. Titration curve of Rahman c.430dupG Truncated H1E CTD showing its charge z: -4

It is worth noting that although the mutation in 24 caused a 74 amino acid shorter CTD tail, the charge did not decrease as much as in the case of the Rahman mutation (Table 13).

CLONE NUBMER	GENOTYPE	NOTE	CTD Charge
Parental	Homozygous	-	30
10	Heterozygous	2bp deletion	20
11	Heterozygous	2bp deletion	20
24	Heterozygous	16bp deletion	4

Table 13. List of clones for further experiments

4.4. Proliferation Rate and Cell Cycle Analysis Of BC Clones

Although no significant change was observed in the epithelial or mesenchymal gene expression patterns of the clones, since the H1E linker histone belongs to the cell cycle-dependent linker histone proliferation rate, the cell cycle of the clones was also inspected. First, for the detection of the proliferation pattern, clones on early passage were seeded in equal numbers in five wells of 12-well plates, each with control of the parental cell. The proliferation rate was determined using the trypan blue exclusion assay for five subsequent days. The experiment was independently repeated thrice, with two replicates. Clones 10 and 11 did not show any significant regression of growth, as shown in Figure 37, although clone 24 showed a slower growth. This not only decreased the dosage of the linker protein, which was shown to be ineffective in two other clones but was also due to the presence of the truncated H1E protein.

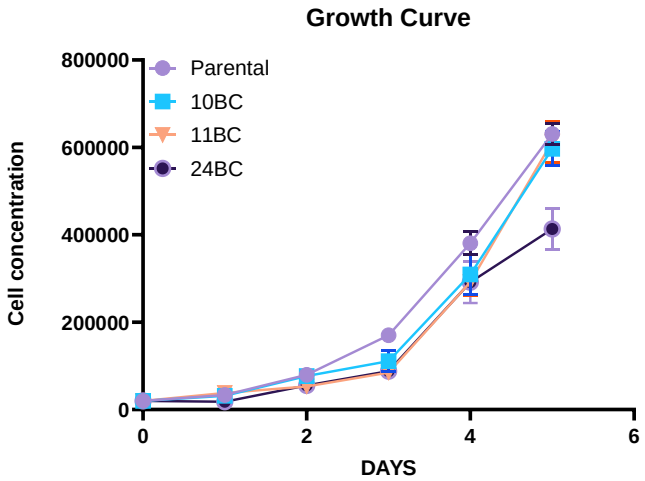

Figure 37. Half-dose depletion of H1E or its Truncation did not affect the growth rate, but deletion of the CTD resulted in retarded growth. Growth Curve of BC clones showing only slight retardation in truncated 24.

As per cell cycle analysis, cells at early passage were seeded in 6-well plates at equal numbers and grown to 80% confluency. Later, cells were fixed with ethanol, stained with PI, and measured using FACS Canto I, with parental cells as a control. The collected results were analyzed using FlowJo Software. Consistent with the proliferation rate, cell cycle analysis did not show any significant differences compared to the parental cells for clones 10 and 11. As per the clone 24 cell cycle analysis, no significant difference was observed without explaining the observed retardation of proliferation (Figure 38).

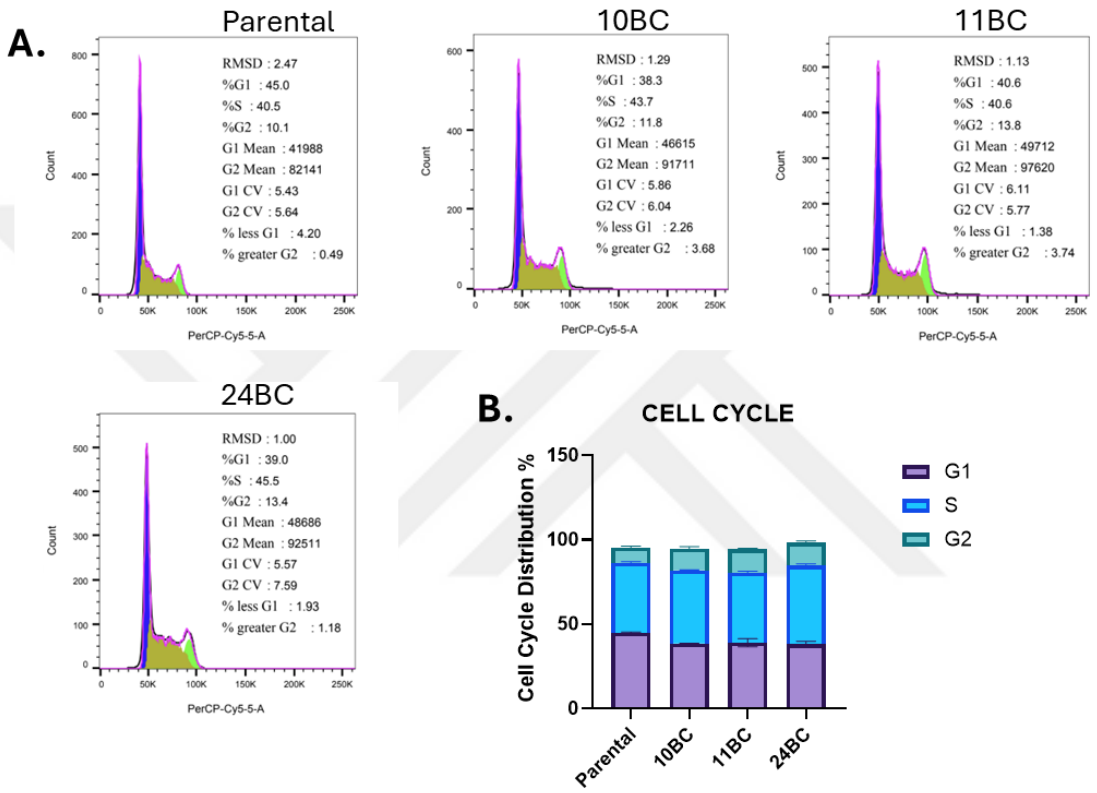

Figure 38. Half-dose depletion of H1E or its Truncation did not affect the Cell Cycle. A. Individual FACS profiles from a representative experiment are displayed. Analysis of DNA content was carried out using the Per-CP Cy5.5 channel by flow cytometry. B. Percentage of cell cycle distribution results representing the average of three independent experiments.

4.5. EMT-MET Experiments Of BC Clones

Cell plasticity is an elegant but vitally critical trait for the generation and maintenance of tissue homeostasis. As mentioned above, NMuMG cells are a globally accepted EMT-MET model because of their high cellular plasticity and fast and morphologically observable response to the presence and withdrawal of TGF beta. To elucidate whether the haploinsufficiency of H1E linker histone affected the plasticity ability of the NMuMG cells, clones were employed for EMT experiments upon introduction of TGF-β3.

4.5.1. Epithelial to Mesenchymal Transition of BC Clones

To detect the effect of decreased H1E amount or presence of truncated protein on EMT, the three clones were treated with 2.5ng/ml TGF beta for 96h and cells were either collected for RNA and protein extraction or fixed and stained for major epithelial and mesenchymal markers. As a first insight, typical EMT is defined by morphological changes. Due to the loss of apicobasal polarity and tight junctions, epithelial cells lose their cobblestone morphology and gain a spindle-like, elongated shape able to migrate through tissues in complex systems (Kalluri & Weinberg, 2009). As shown in Figure 39, the cells exhibited a typical fibroblast-like spindle-like mesenchymal morphology upon treatment with TGF beta.

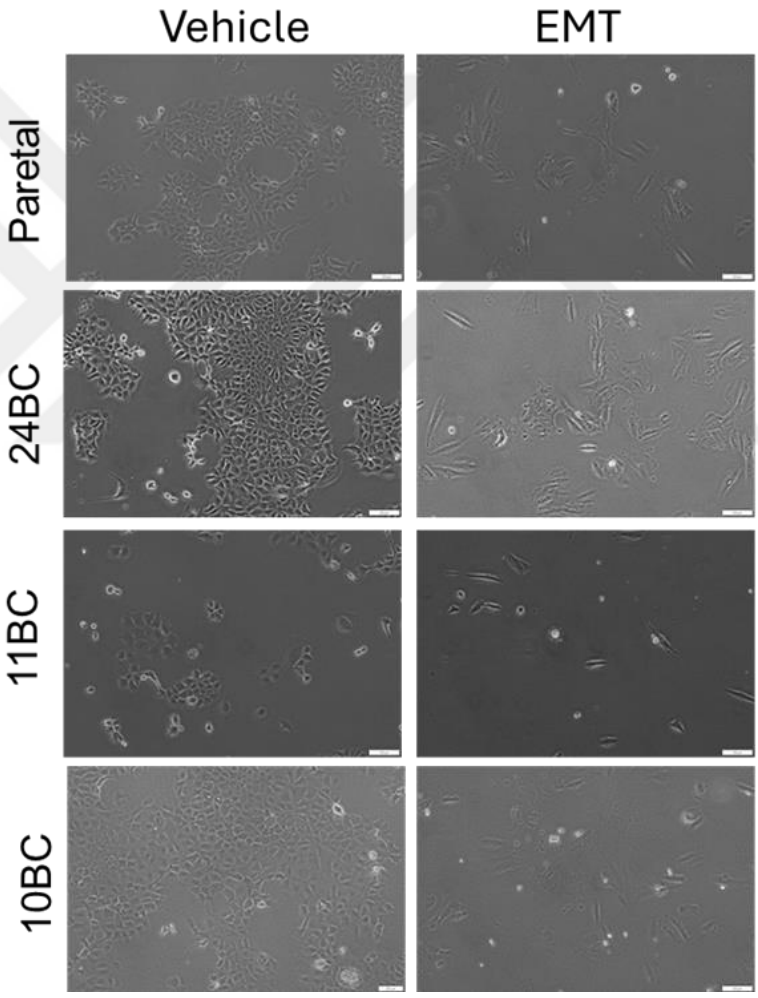

Figure 39. 10BC successfully completed epithelial-to-mesenchymal transition. Upon treatment with TGF-β cell displayed downregulated epithelial markers accompanied by upregulation of mesenchymal markers. Apart from vimentin, which did not show statistically significant upregulation.

In RNA level hallmark of EMT phenotype is the dramatic downregulation of epithelial guardian CDH1. The downregulation of the major epithelial

adhesion molecule CDH1 is followed by the downregulation of epithelial markers and the upregulation of mesenchymal markers (Kalluri & Weinberg, 2009). As hinted from the morphological assessment, in RNA-level cells also exhibited a typical EMT transcriptomic signature as per the investigated genes. As shown in Figures 40,41 and 43, in each clone, mesenchymal markers such as fibronectin, vimentin, and ITGA5 were significantly increased, while epithelial markers such as Cdh1, Ahr , CTNNB1, and Klf4 were significantly downregulated, confirming the transition at the RNA level.

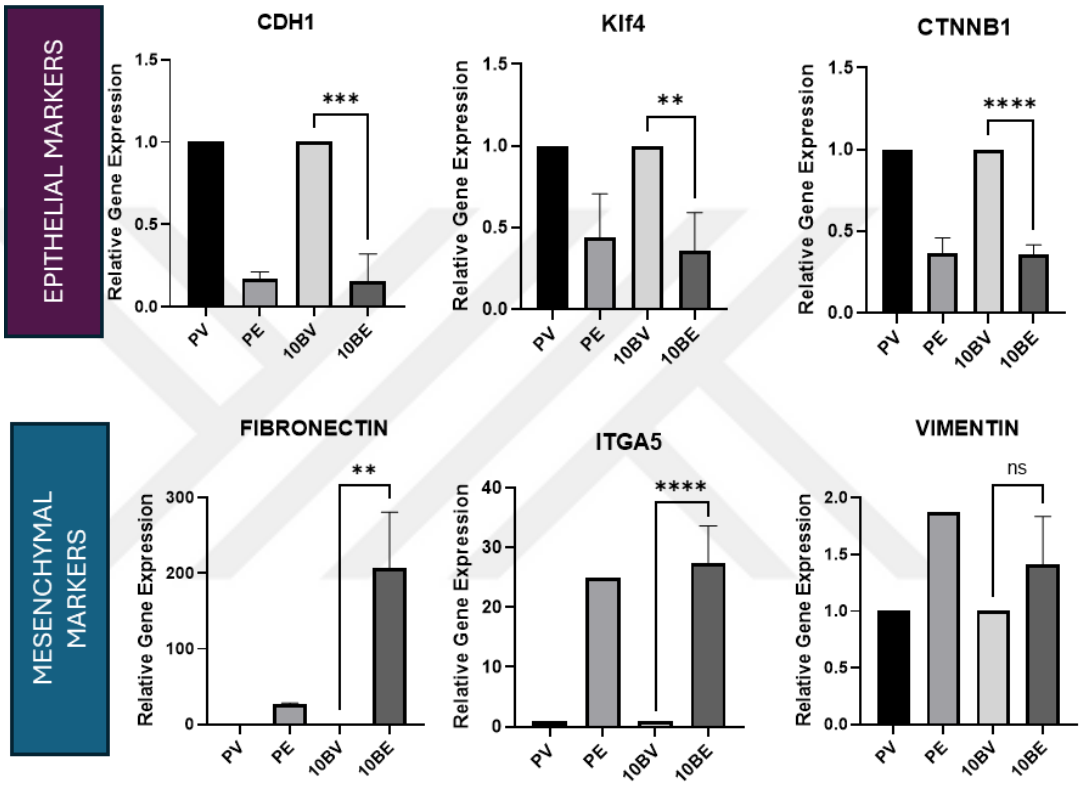

Figure 40. 10BC successfully completed epithelial-to-mesenchymal transition. Upon treatment with TGF-β cell displayed downregulated epithelial markers accompanied by upregulation of mesenchymal markers. With the exception of vimentin, which did not show statistically significant upregulation. The data was analyzed using Student's t test. ($p > 0.05$ *, $p \leq 0.05$ **, $p \leq 0.01$ *** and $p \leq 0.001$ ****)

Besides the morphological assessment and the concomitant downregulation and upregulation of epithelial and mesenchymal markers, respectively, vimentin did not show significant upregulation in clone 10 or 24 (Figure 40/42). Considering the downregulation of vimentin in MET knockdowns, this inability to upregulate vimentin could be caused by the absence or lowered dosage of H1E.

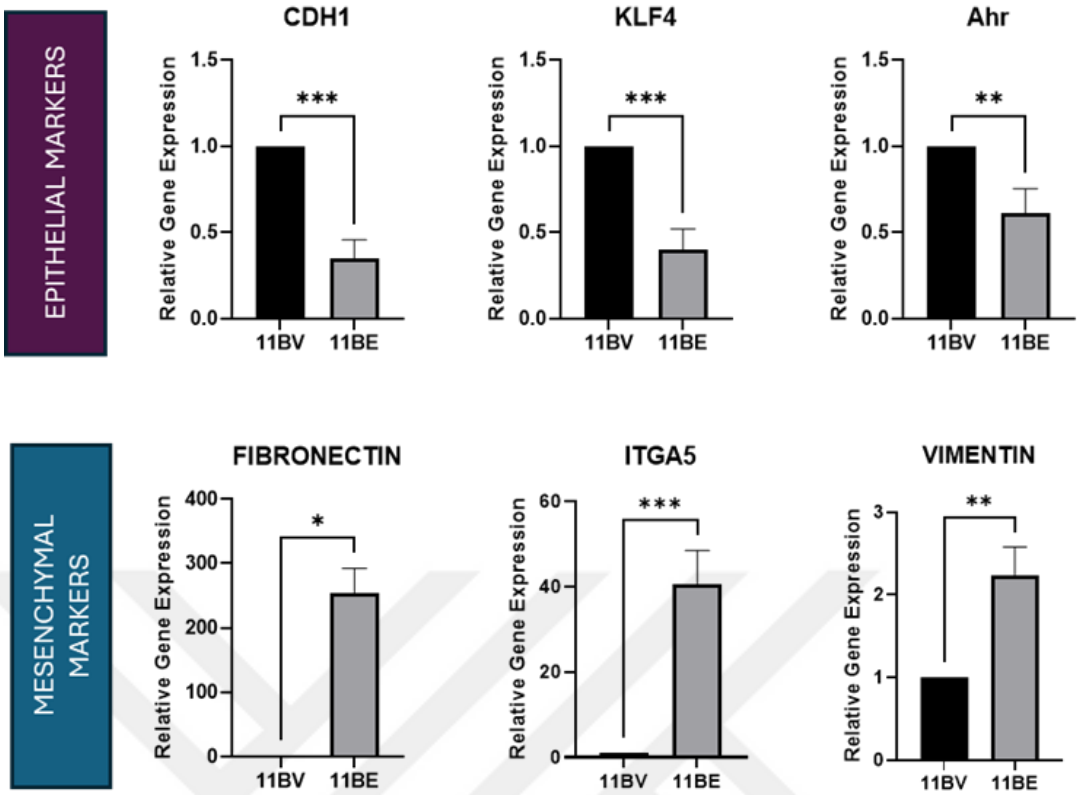

Figure 41. 11BC Successfully Completed Epithelial-To-Mesenchymal Transition. Upon treatment with TGF-β cell displayed downregulated epithelial markers accompanied by upregulation of mesenchymal markers. The data was analyzed using Student's t test. ($p > 0.05$ *, $p \leq 0.05$ **, $p \leq 0.01$ *** and $p \leq 0.001$ ****)

Beside the slight differences all examined clones were able to transition from epithelial to mesenchymal state. Although the integrity of the epithelial state of the clones in the first place was not consistent with the siRNA-mediated knockdown of H1E either in NMuMG cells or in the MCF10A cell line, the differences and protected plasticity were attributed to differential levels of silencing in the two experimental groups. Where in siRNA mediated knockdown assays resulted almost fully diminishment H1E with a ~95% reduction in its expression, Crispr/Cas9 generated clones were only able to reduce the expression levels by 50%. This change indicates that the effects of H1E on cell plasticity occur in a dose-dependent manner.

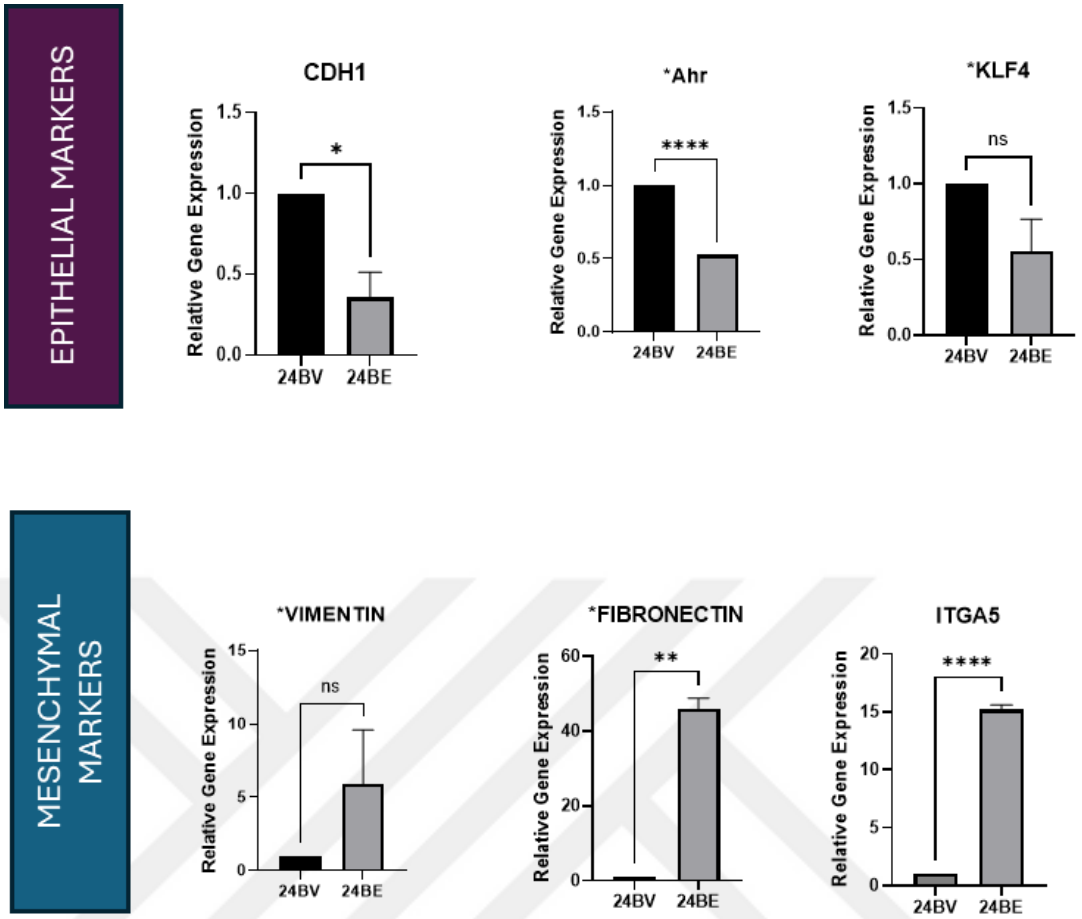

Figure 42. 24BC Successfully Completed Epithelial-To-Mesenchymal Transition. Upon treatment with TGF-β cell displayed downregulated epithelial markers accompanied by upregulation of mesenchymal markers. The data was analyzed using Student's t test. ($p > 0.05$ *, $p \leq 0.05$ **, $p \leq 0.01$ *** and $p \leq 0.001$ ****)

4.5.2. Mesenchymal to Epithelial Transition of BC Clones

For mesenchymal to epithelial transition, EMT was induced in clones with 96h TGF-beta treatment, and for induction of MET, transitioned mesenchymal cells were washed three times with 1XPBS and grown in normal media without supplementation with TGF-β. The resulting cells were examined by phase-contrast imaging, immunostaining for morphological assessment, and qPCR for their transcriptomic patterns. As shown in Figure 43, upon withdrawal of TGF-β cells, epithelial features with cobblestone morphology and increased cell-cell adhesion were observed.

Immunofluorescence staining showed the recovery of E-cadherin on the membrane and disappearance of stress fibers, as observed by phalloidin staining (Figure 44A-46A).

Similarly RNA levels of mesenchymal markers such as vimentin, fibronectin and ITGA5 showed downregulation followed by upregulation of CDH1, Klf4 and Ahr, epithelial genes showing onset of MET (Figure 44-46B).

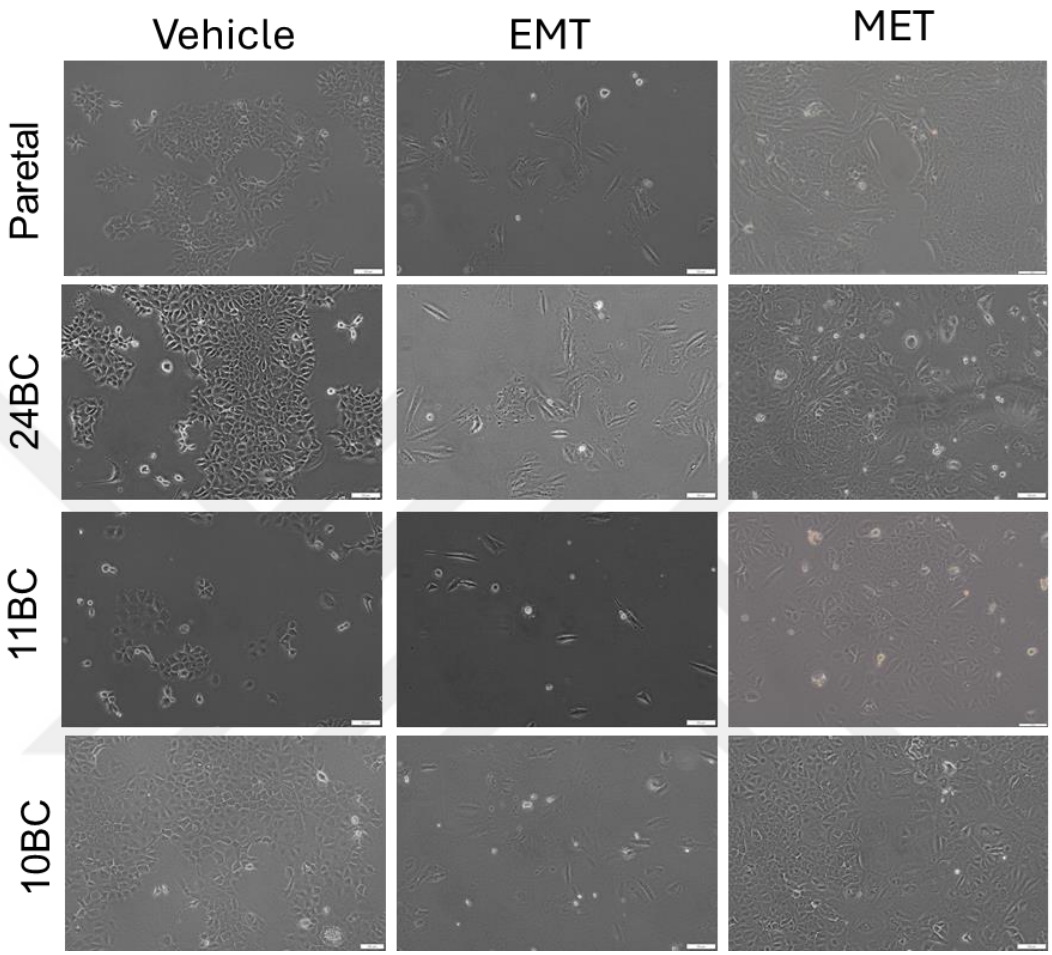

Figure 43. BC Clones Successfully Completed The Mesenchymal To Epithelial Transition. Phase-contrast microscopy images showing complete transitions.

The behavior of siRNA-mediated knockdown and heterozygous knockout clones in response to TGF-β withdrawal is not consistent. Arrest at the mesenchymal level was not observed in any of the clones. This effect was attributed to protein expression level of H1E. In knockdown experiments, H1e levels were 95% silenced, whereas this ratio could only reach up to 50% in CRISPR-generated clones. Thus, this difference also provides the first evidence of the functionality of the endogenous WT allele. As per 10 and 11, due to the low drop in charge functionality of the linker histone, even for 24, the deletion mutation was not enough to disrupt MET and potentially cause loss of function mutation.

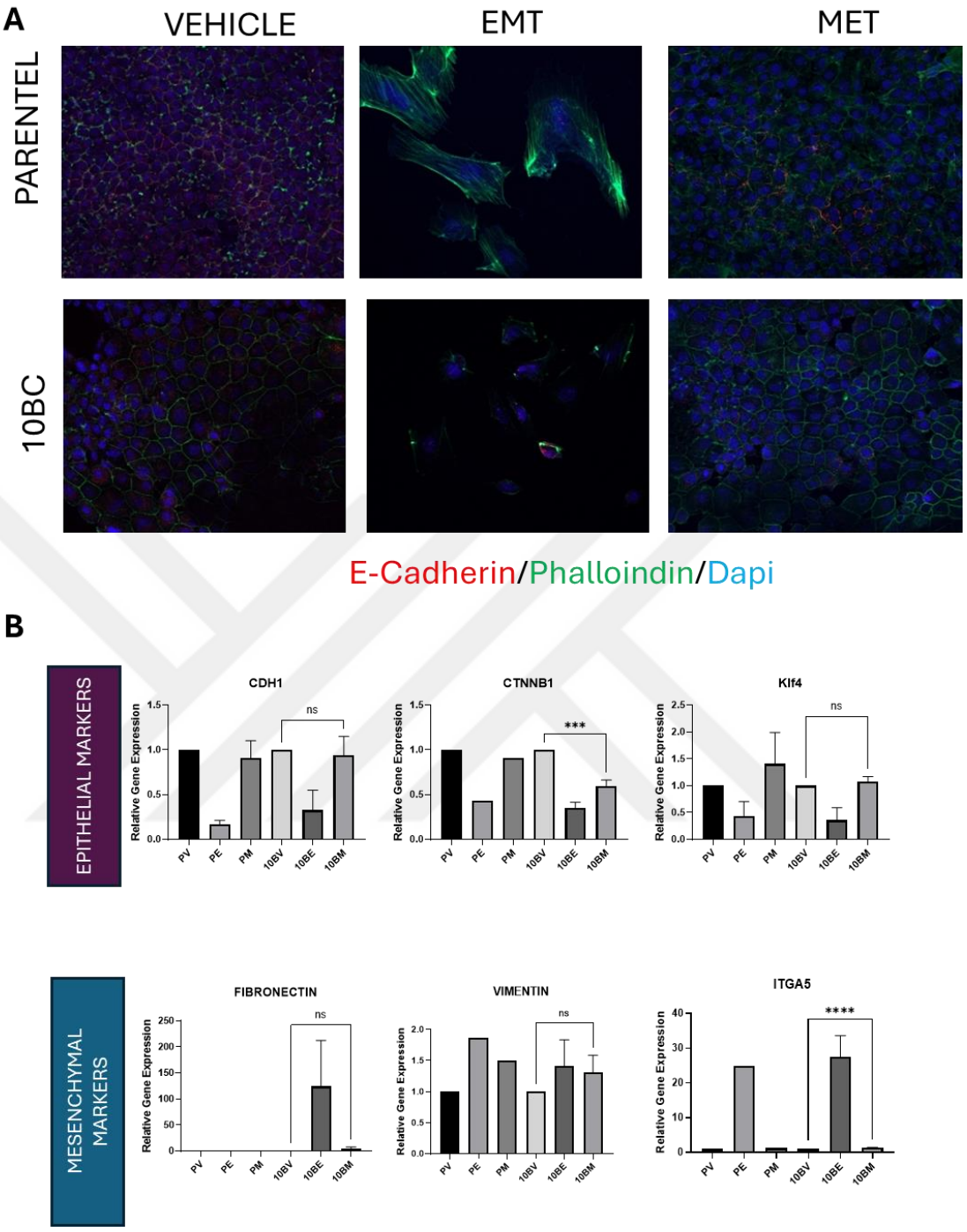

Figure 44. 10BC Successfully Completed The Mesenchymal-To-Epithelial Transition. Upon withdrawal of TGF-β cells displayed downregulated epithelial markers accompanied by upregulation of mesenchymal markers. With the exception of vimentin, which did not show statistically significant upregulation. The data was analyzed using Student's t test. ($p > 0.05$ *, $p \leq 0.05$ **, $p \leq 0.01$ *** and $p \leq 0.001$ ****)

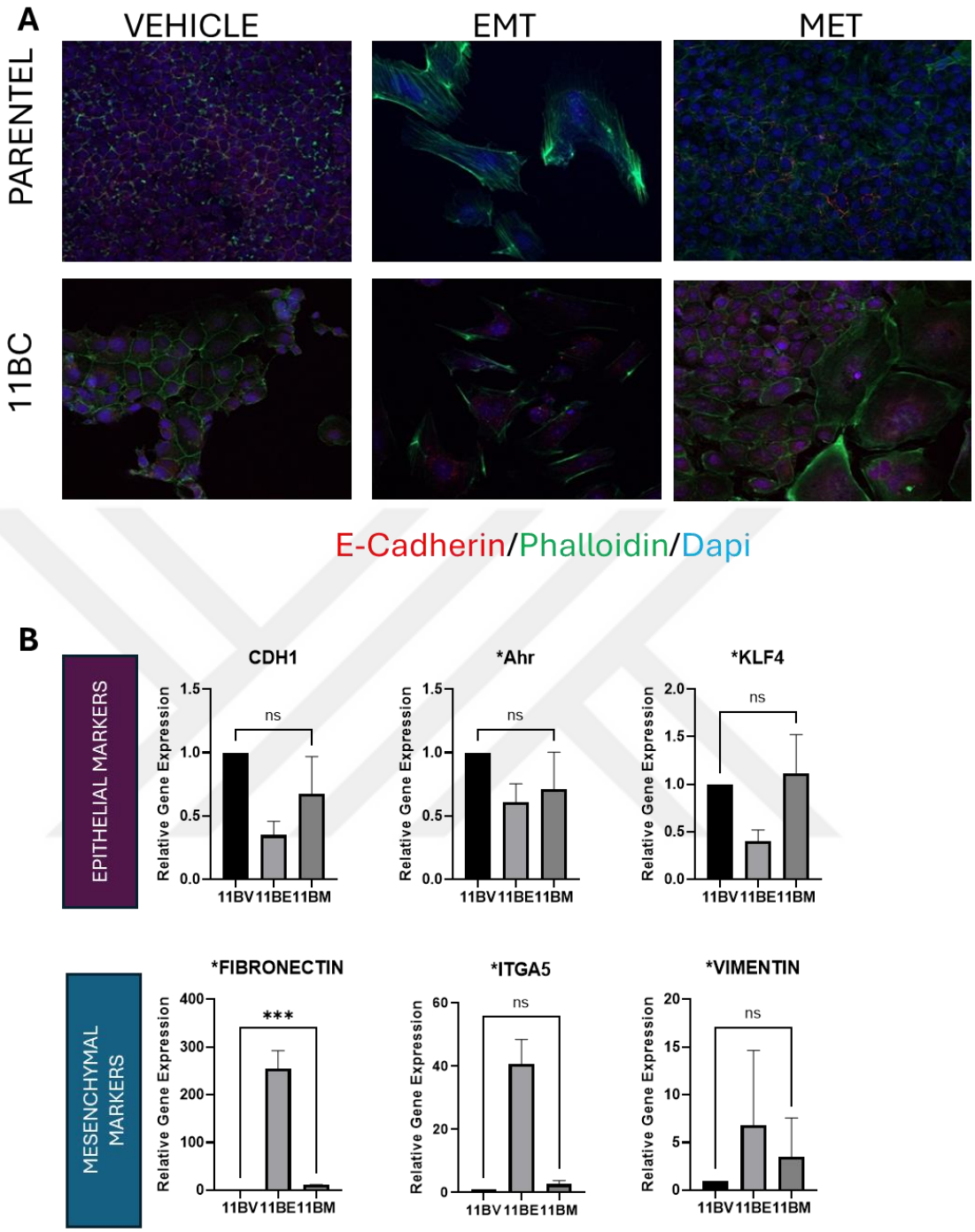

Figure 45. 11BC Successfully Completed The Mesenchymal To Epithelial Transition. Upon withdrawal of TGF-β cells displayed downregulated epithelial markers accompanied by upregulation of mesenchymal markers. With the exception of vimentin, which did not show statistically significant upregulation. The data was analyzed using Student's t test. ($p > 0.05$ *, $p \leq 0.05$ **, $p \leq 0.01$ *** and $p \leq 0.001$ ****)

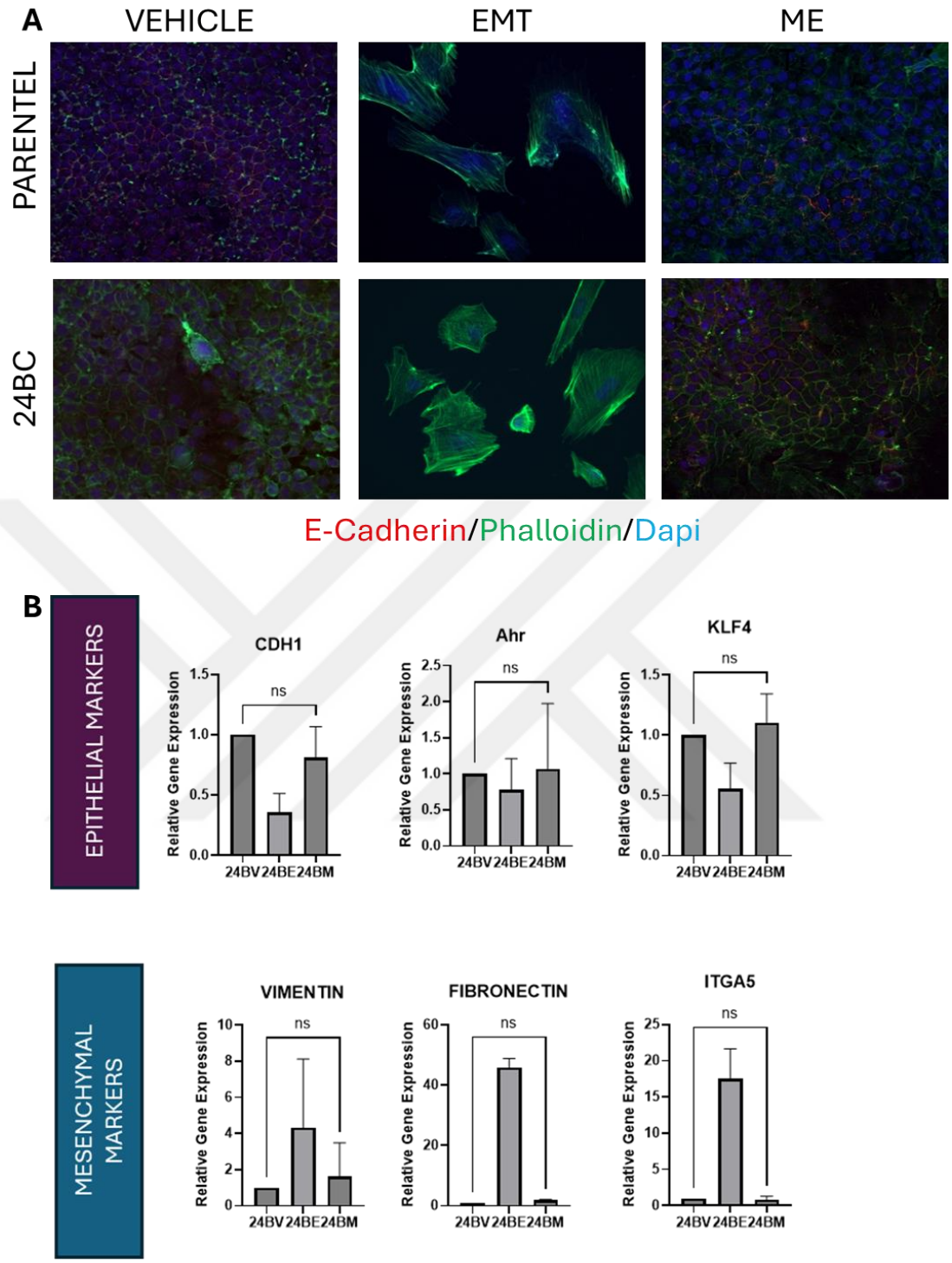

Figure 46. 24BC Successfully Completed The Mesenchymal To Epithelial Transition. Upon withdrawal of TGF-β cells displayed downregulated epithelial markers accompanied by upregulation of mesenchymal markers. The data was analyzed using Student's t test. ($p > 0.05$ *, $p \leq 0.05$ **, $p \leq 0.01$ *** and $p \leq 0.001$ ****)

4.6. Generation And Validation of Clones With RAHMAN H1E mutation expression

4.6.1. Adeno-Associated Cre Virus Infection

As mentioned above, the first generation of CRISPR-Cas9 clones, owing to the presence of floxed neomycin at the 5' upstream region, ends up as a knockout locus. Not only the presence of neomycin gene but also two polyadenylation signals following the CDS of neomycin ensured the silencing of the downstream human H1E gene. To rescue the expression of the human H1e gene with the Rahman mutation, the cells were infected with adeno-associated Cre virus to enable Cre recombination. Cre-mediated excision of floxed neomycin and polyadenylation signals rescued the occupied endogenous promoter, ensuring physiological expression levels of the mutated gene (Figure 47).

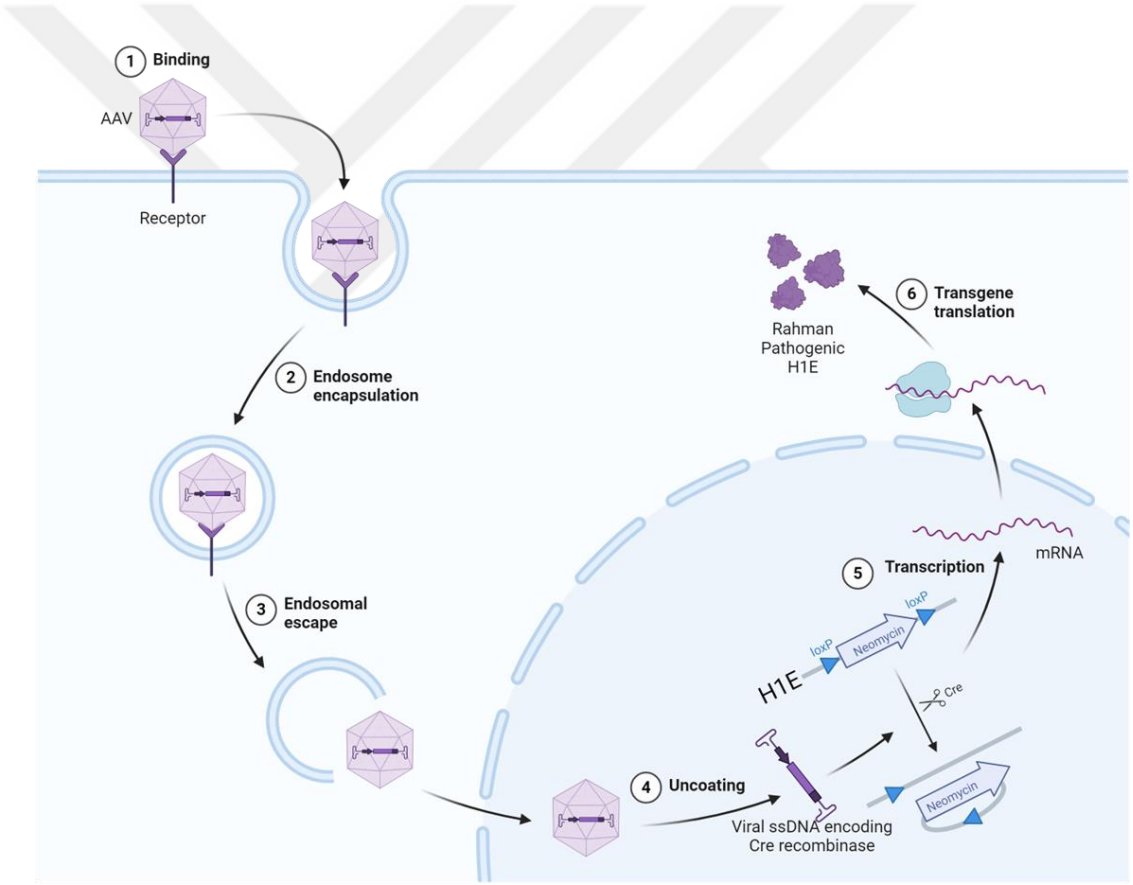

Figure 47. Schematic illustration of AAV-Cre infection, Cre-recombination, and initiation of Pathogenic Rahman Variant expression.

4.6.2. Validation of Cre Recombination and Expression of Mutant Protein

Half of the double-infected cells were selected for neomycin selection to ensure the effectiveness of the AAV-iCre infection and Cre recombination. After observing the complete death of non-resistant cells, DNA and RNA were

collected to ensure recombination at the molecular level. The collected gDNA was used for the first genotyping PCRs and for PCR utilizing the SD100/SD157, amplifying the region spinning from the 5' endogenous locus until the edges of the 3' Homology Arm, including the neomycin cassette. As shown in Figure 48A comparison with the cells pre Cre Recombination, as from now on will be mentioned as BC aka before Cre clones, loss of 5' screening PCR product was observed. This loss alone shows that effective Cre recombination, as the excision of the neomycin gene causes the loss of reverse primer targets for this gene. Subsequently, the 3' locus was checked to ensure that it was unaffected by recombination, as expected.

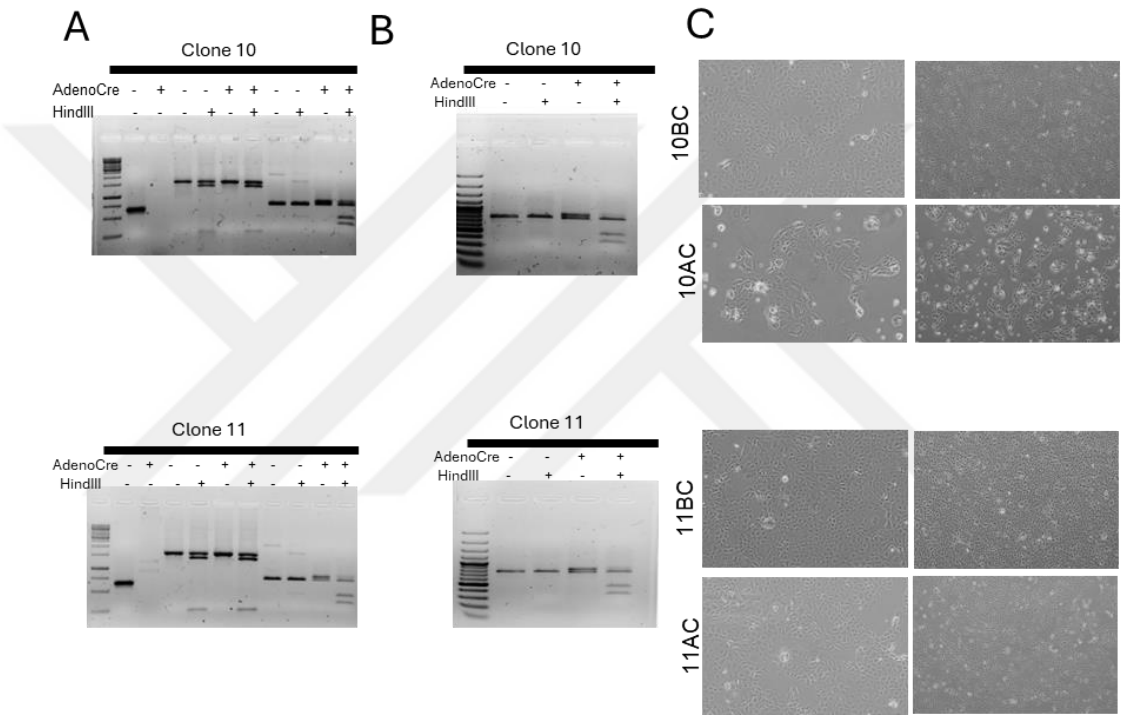

Figure 48. Verification Of Cre Efficiency At The Genomic And RNA Levels By RT-PCR And Assessment Of Morphological Changes In Cells In Response To Rahman Protein. A. Genomic level conformation of integrity in the locus of interest and efficient Cre-recombination. B. RNA level confirmation of pathogenic Rahman H1E expression through a PCR utilizing cDNA and primers targeting the CDS region of both alleles. C. Morphological response of the clones to presence of pathogenic Rahman variant.

To further confirm the recombination, SD100/SD157 PCR was employed, showing in the BC clones the 2009bp band, the H1E locus was amplified together with the neomycin cassette, and the 742 bp band showing the endogenous WT H1E allele due to heterozygosity. In the BC samples, the product of the mutated allele was confirmed by HindIII digestion. After Cre recombination, replacement of the 2009bp band with a 784bp band and its digestion are shown in Figure 48A, confirming Cre recombination at the genomic level. To ensure the expression of mutated genes, RNA was collected

from both AC and BC clones, used for the generation of cDNA, and used for SD100/SD157 PCR. The results of RT-PCR showed a single band in BC clones representing endogenous WT allele expression, and later in AC clones the second 784bp band representing the expression of the mutation, which was further confirmed by HindIII digestion, as shown in Figure 48B.

In addition to elucidate possible morphological responses to presence of the pathogenic protein we employed phase-contrast microscopy imaging. As shown in Figure 48C clone 11 did not present visible features while clone 10 showed enlarged cytoplasm, binucleation and unusual vesicle around the nucleus.

Finally, to ensure the proper translation of the mutated transcript into protein and its correct localization, which would also suggest its proper function, Western Blot and immunofluorescence staining targeting the HA tag of the mutated protein were performed. As shown in Figure 49A, the mutated protein was detected in both clones, raising concerns regarding the difference between the amounts of the two proteins. 11 AC showed almost three times more protein presence than clone 10 AC raising questions about the integrity of the clones and possible random integration concerns in clone 11 (Figure 49B).

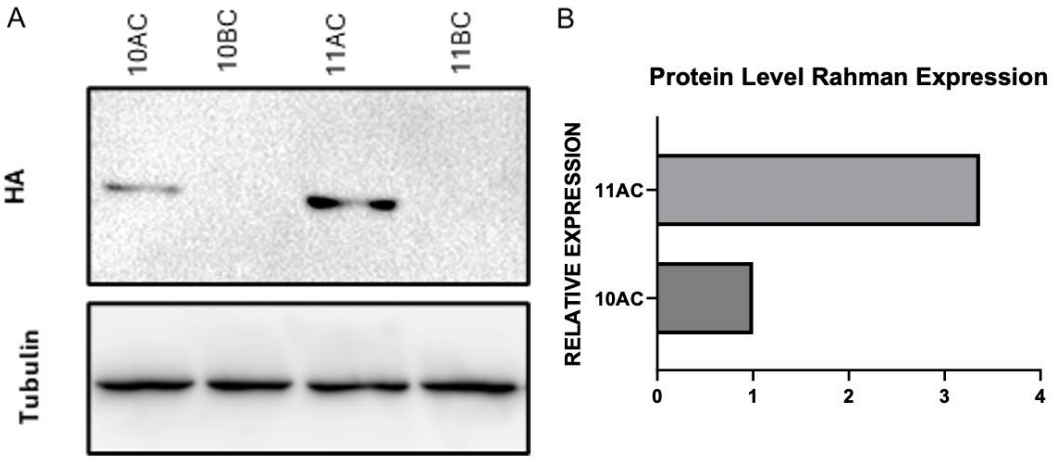

Figure 49. Verification Of Cre Efficiency At The Protein Level. A. Western Blot images showing the absence of pathogenic H1E in BC clones and its presence in AC clones, tagged and targeted by anti-HA. B. Clone 11 displayed three-fold more protein expression.

Similar results were obtained with IF staining 11 showing a more intense signal in contrast to 10; however, in both cases, staining was observed inside the nucleus in proper localization, which was also confirmed by Lamin B1 staining showing the borders of the nucleus in each case. Interesting results were obtained, Lamin b1 staining showed dispersed lamination in AC clones. Result indeed was obtained previously with different Rahman clones in our

laboratory; however, the means and mechanisms remain to be understood (Figure 50).

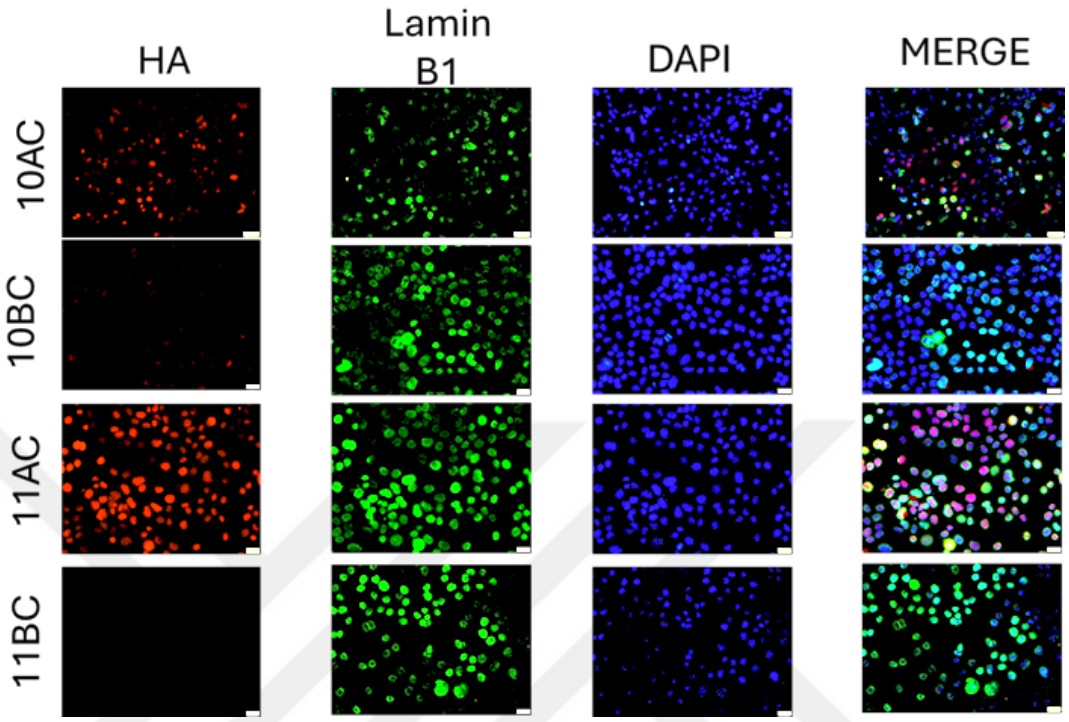

Figure 50. Verification Of Proper Pathogenic Variant Localization. Anti-HA staining showed in Lamin border localization inside the nucleus. The cells showed defects in lamination.

4.7. Proliferation Rate And Cell Cycle Analysis

After Cre Recombination, clone 10 showed retarded growth compared to the BC and parental cells. Together with the fact that H1E belongs to the family of cell cycle-dependent linker histones, the trypan blue exclusion assay for proliferation rate and PI-based cell cycle analysis was performed as described previously. As shown in Figure 51, clone 11 AC showed a slight retardation of growth, whereas clone 10 AC showed dramatically slower growth and death, as can be observed from the decreasing number of cells in the later days of the growth curve. As perse of Cell cycle analysis while clone 11 showed physiological cell cycle clone 10 AC showed a dramatic change and G2 arrest in all individual replicates (Figure 52).

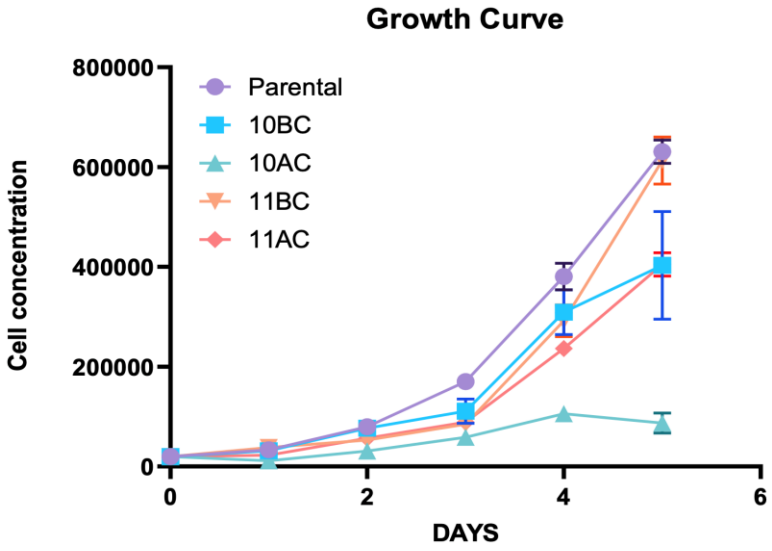

Figure 51. Clone 10 Showed Dramatic Growth Arrest In Response To Pathogenic Protein Expression.

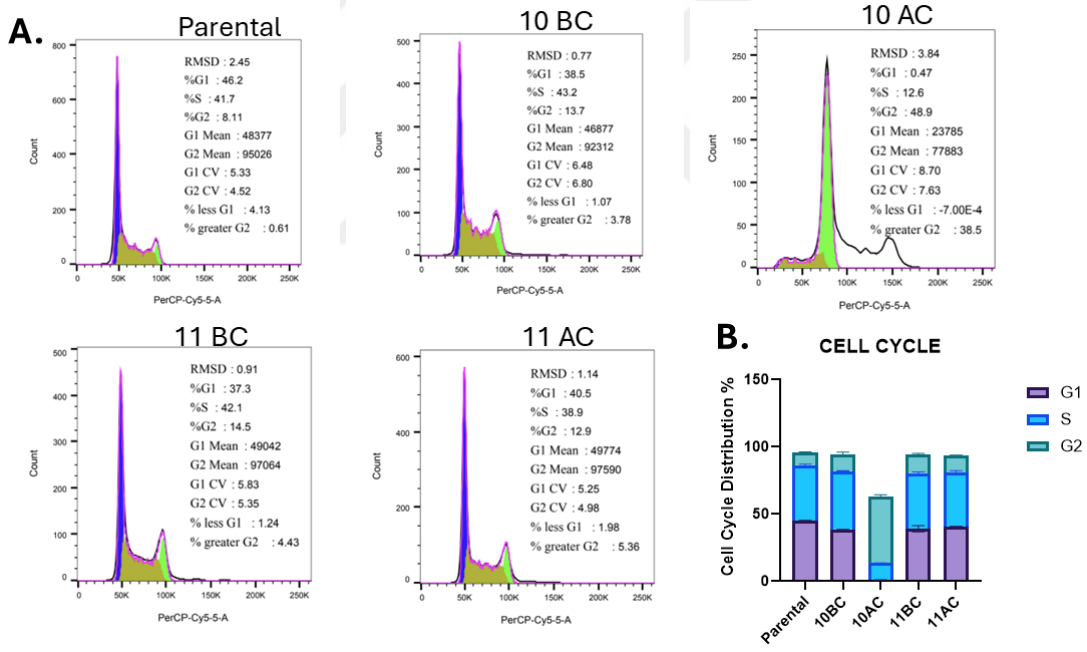

Figure 52. Clone 10 Showed Dramatic Cell Cycle Arrest In Response To Pathogenic Protein Expression.

4.8. EMT-MET Experiments of AC Clones

4.8.1. Epithelial to Mesenchymal Transition of AC Clones

As described previously to assess the effect of Rahman mutation on epithelial to mesenchymal transition two clones were treated with 2.5ng/ml TGF beta for 96h and cells were either collected for RNA and protein extraction or fixed and stained for major epithelial and mesenchymal markers. As shown

in Figure 53, 11 exhibited a typical spindle-like mesenchymal morphology, whereas 10 exhibited a more fibroblast-like morphology with enlarged cytoplasm and an increase in binucleation upon treatment with TGF beta.

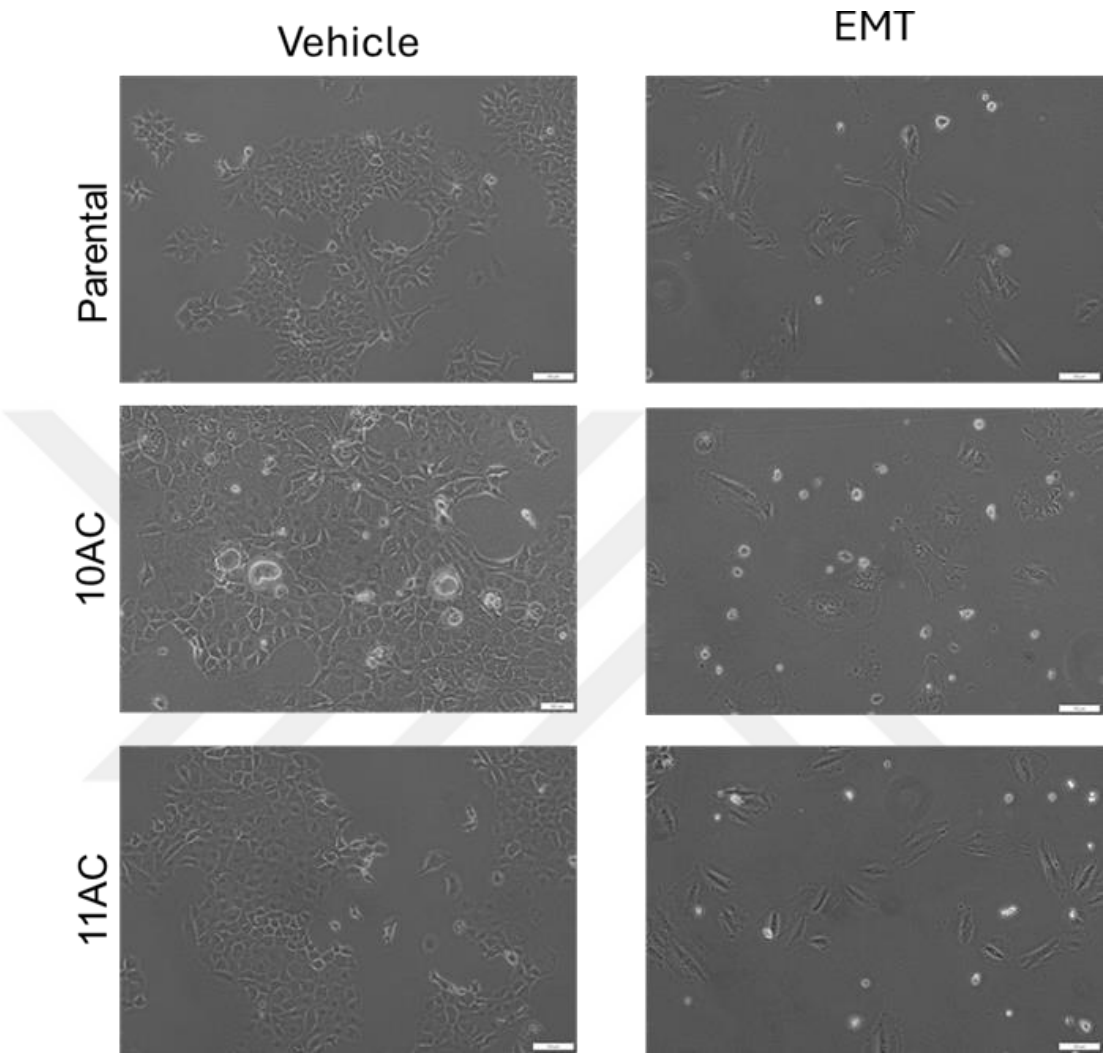

Figure 53. Rahman Clones Were Able To Undergo EMT. Phase-contrast images of the cells displayed a spindle-like morphology for 11 and a more enlarged shape for 10 upon treatment with TGF-β3.

In RNA level both clones also exhibited a typical EMT transcriptomic signature as per investigated genes. As shown in Figure 54 and 55 mesenchymal markers such as fibronectin, vimentin, and ITGA5 showed significant increases, while epithelial markers such as Cdh1, Ahr, CTNNB1, and Klf4 were significantly downregulated, confirming successful epithelial-mesenchymal transition at the RNA level.

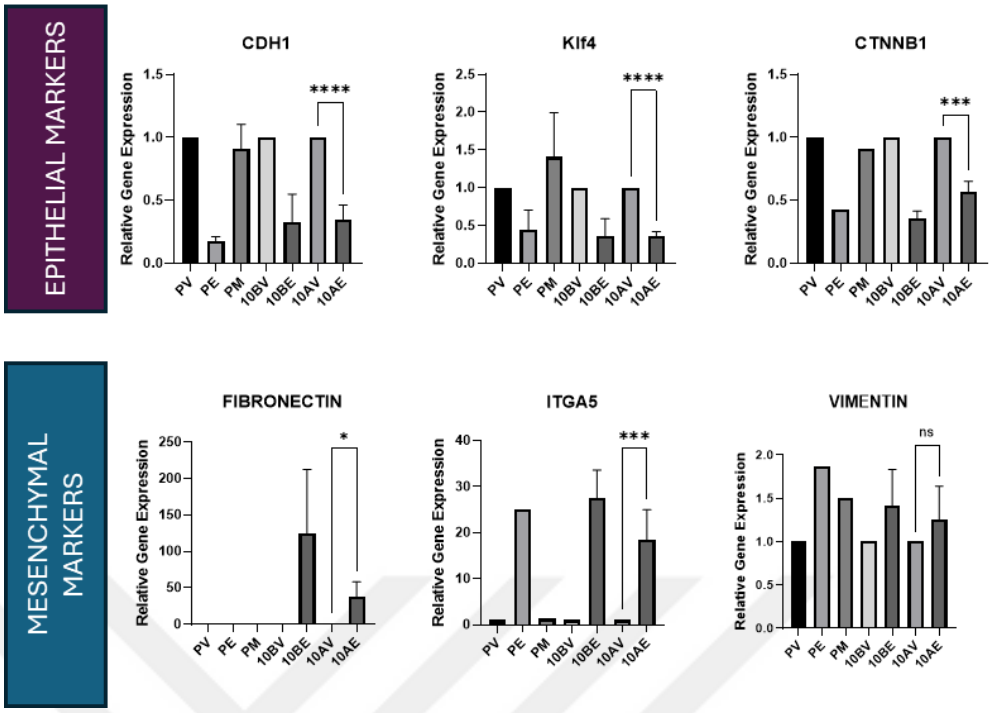

Figure 54. 10AC Cells Were Able To Undergo EMT. Epithelial markers were significantly downregulated, while mesenchymal markers were upregulated. The data was analyzed using Student's t test. ($p > 0.05$ *, $p \leq 0.05$ **, $p \leq 0.01$ *** and $p \leq 0.001$ ****)

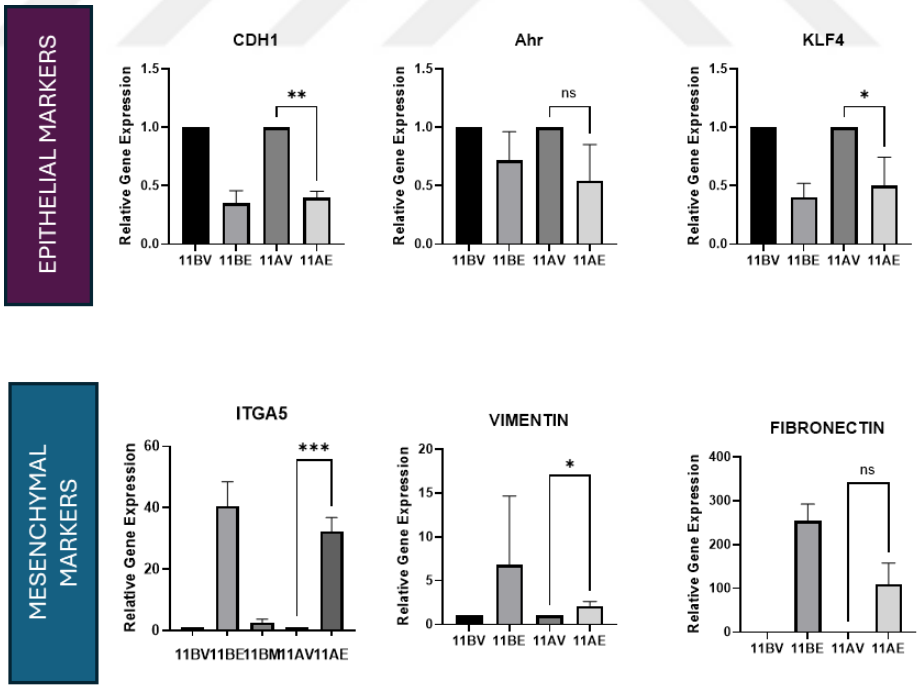

Figure 55. 11AC Cells Were Able To Undergo EMT. Epithelial markers were significantly downregulated, while mesenchymal markers were upregulated. The data was analyzed using Student's t test. ($p > 0.05$ *, $p \leq 0.05$ **, $p \leq 0.01$ *** and $p \leq 0.001$ ****)

4.8.2. Mesenchymal to Epithelial Transition of AC Clones

For mesenchymal to epithelial transition, EMT was induced in clones with 96h TGF-beta treatment, and for induction of MET, transitioned mesenchymal cells were washed three times with 1XPBS and grown in normal media without supplementing TGF-β. The resulting cells were examined by phase-contrast imaging, immunostaining for morphological assessments, and qPCR for their transcriptomic pattern. Unexpectedly, the results differed among the clones (Figure 56). As shown in Figure 56 upon withdrawal of TGF-β clone 11 quickly gained epithelial features with cobblestone morphology and increased cell-cell adhesion. At the RNA level, Clone 11 AC, showed typical mesenchymal epithelial transition with a decrease in mesenchymal markers such as vimentin, fibronectin, and ITGA5, and an increase in epithelial markers such as Cdh1, CTNNB1,Ahr (Figure 57). While clone 10AC had quite opposite results (Figure 58). Also, immunofluorescence staining showed relocalization of E-cadherin on membrane and vanishment of stress fibers observed by phalloidin staining (Figure 59).

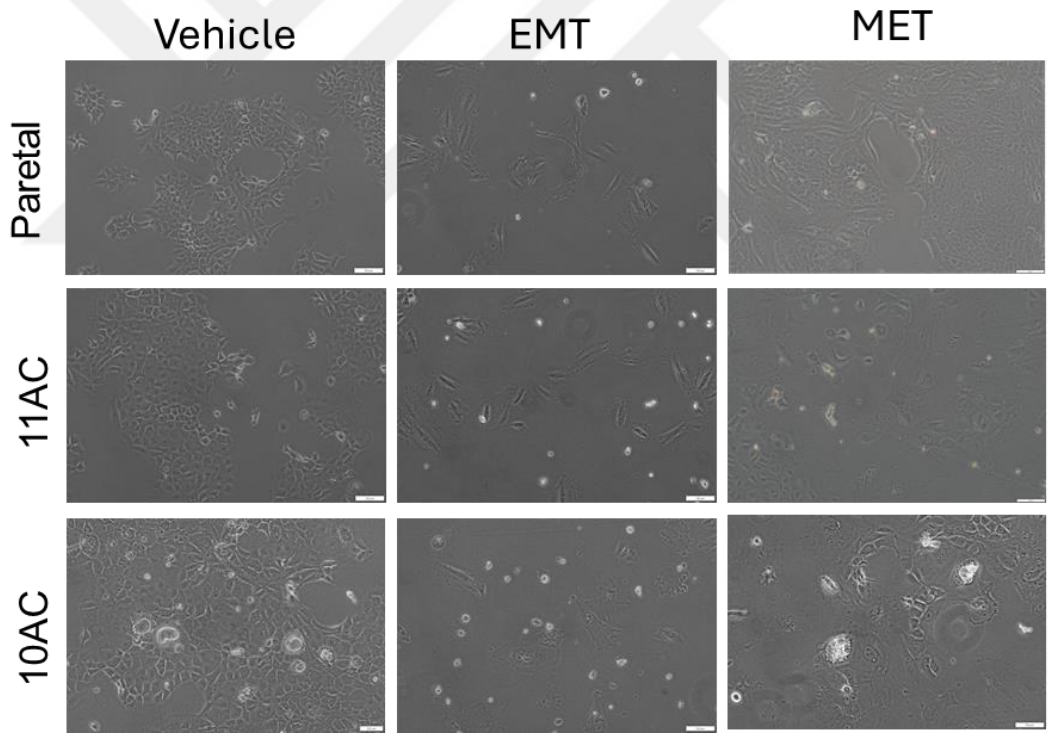

Figure 56. Phase-Contrast Microscopy Images Showing Different Responses Of Rahman Clones To TGF-β3 Withdrawal.

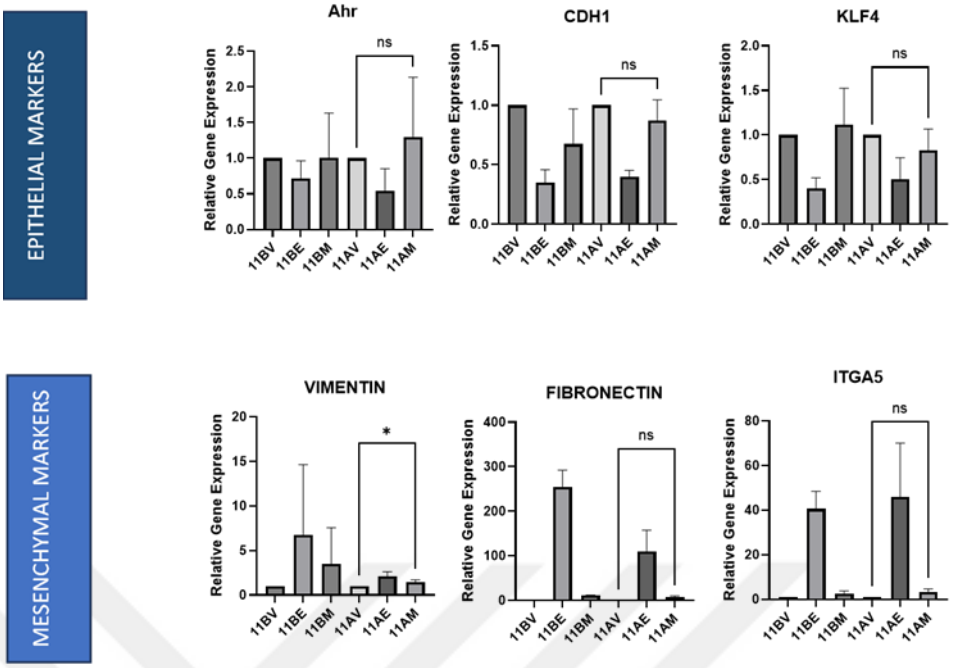

Figure 57. 11AC Successfully Completed The Mesenchymal-To-Epithelial Transition. After the withdrawal of TGF-β3 cells, they quickly recovered their epithelial features and lost their mesenchymal abilities. The data was analyzed using Student's t test. ($p > 0.05$ *, $p \leq 0.05$ **, $p \leq 0.01$ *** and $p \leq 0.001$ ****)

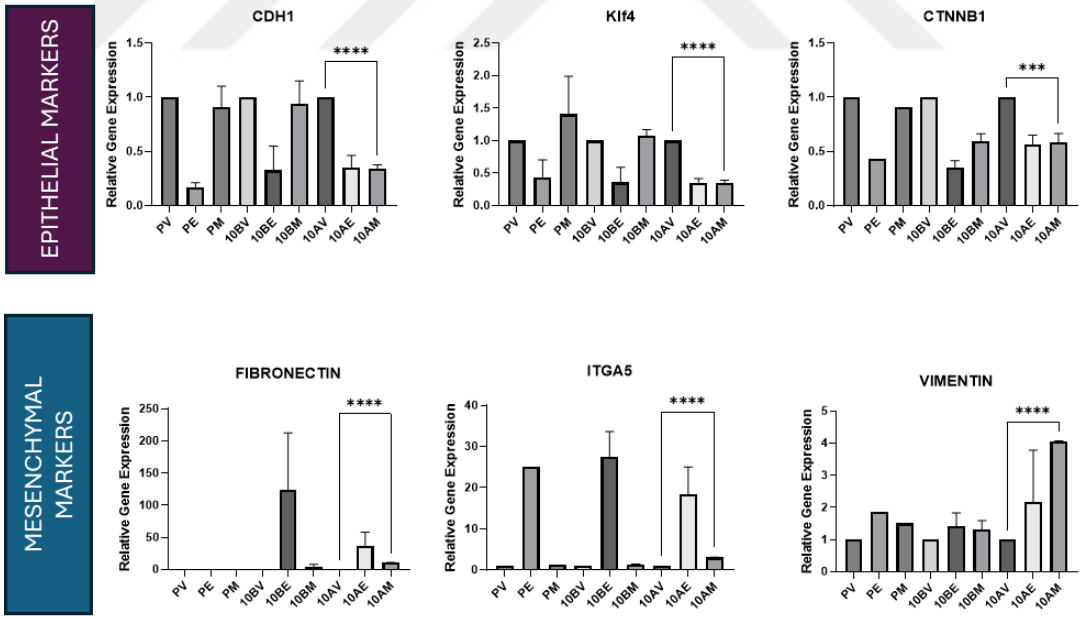

Figure 58. 10AC Was Not Able To Complete Mesenchymal To Epithelial Transition Successfully. Upon withdrawal of TGF-β, cells failed to regain epithelial features instead of the constant expression of vimentin. The data was analyzed using Student's t test. ($p > 0.05$ *, $p \leq 0.05$ **, $p \leq 0.01$ *** and $p \leq 0.001$ ****)

On the other hand, clone 10 failed to complete the Mesenchymal to Epithelial transition, and cells were arrested in the mesenchymal form in phase-contrast imaging (Figure 56) with increased death. In immunofluorescence imaging, E-cadherin failed to localize to the membrane, and stress fibers remained the same as in the TGFβ3-treated group (Figure 59) .

At the RNA level, the expression of all the inspected epithelial genes failed to recover to their previous levels, while the levels of the mesenchymal genes remained or were even higher, like vimentin (Figure 58).
Interestingly, both the knockdown and 10AC groups showed the same response to TGF-β withdrawal by being arrested at the mesenchymal level. Although the mechanisms by which the pathogenic variant causes the syndrome are not fully understood, this result raised interest in whether it could be a loss-of-function mutation causing a compound negative effect. However, the presence of MET-capable clones was problematic, and clones need to be verified again.

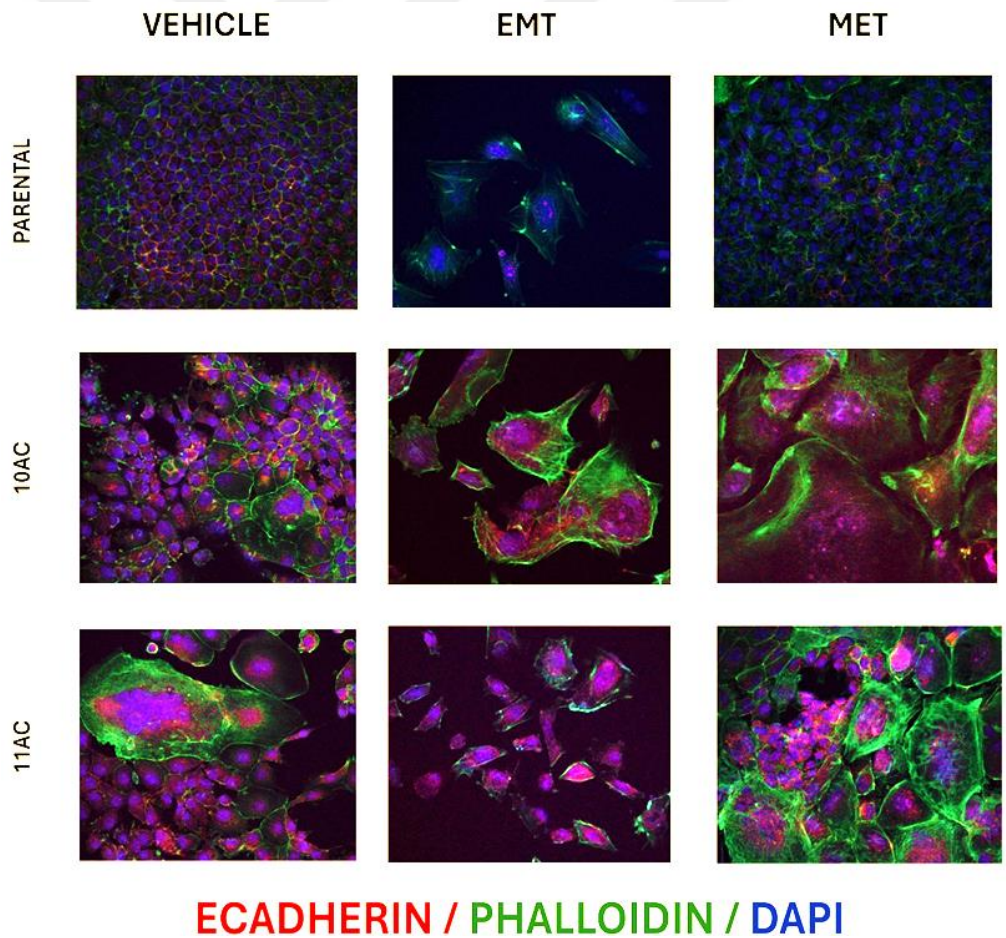

Figure 59. Immunofluorescence staining of clones in each state of the transition anti-E-cadherin and anti-phalloidin. 10AC cells showed accumulation of E-cadherin in the cytoplasm even before treatment with TGF-β3.

4.9. Genotyping of Linker Histone Isoforms

After identifying several differences among the clones, we checked the genomic integrity of the linker histone isoforms and their expression levels. To determine the genomic integrity, PCR was performed for each one of the four isoforms. (Figure 60).

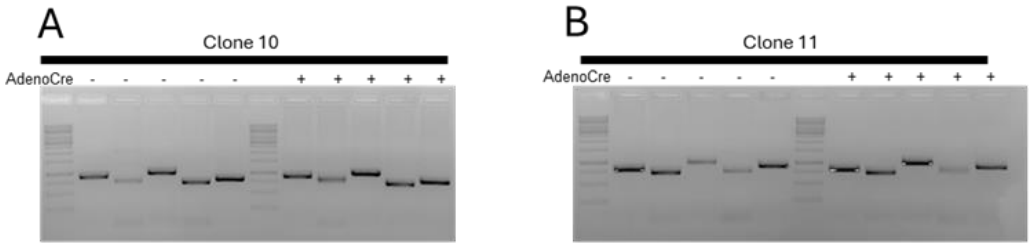

Figure 60. Genomic Examination Of Different Linker Histone Isoforms By Genomic PCR Showed Dosage Depletion Of H1D In Clone 11. Examination of linker isoforms of clone (A) 10. Lane 1 MW1KB, lane2 H1T, lane 3 H1E, lane 4 H1D, lane 5 H1C, and lane 6 H1A. Examination of the linker isoforms of clone (B)11. Lane 1 MW1KB, lane2 H1A, lane 3 H1C, lane 4 H1D, lane 5 H1E, and lane 6 H1T. Examination of 5' regulatory region of linker histones. Lane 1 MW1KB, lane 2 H1F0, lane 3 H1D, lane 4 H1A, lane 5 H1B, lane 6 H1C.

Four isoforms, H1A, H1D, H1C, and H1T, were selected based on their sequence similarity with each other and with the H1E gene. The obtained results showed the physiological amplicon size and amount of linker histones in clone 10 (Figure 60A). As per clone 11, although the resulting amplicons were of the expected size, the amount of linker histone H1D showed a decrease in the BC state and gain of physiological amount in the AC state (Figure 60B). Later, the expression levels of the isoforms for each clone were checked by qPCR, and downregulation of H1D in the BC state was also observed, indicating a possible impairment of the locus (Figure 61).

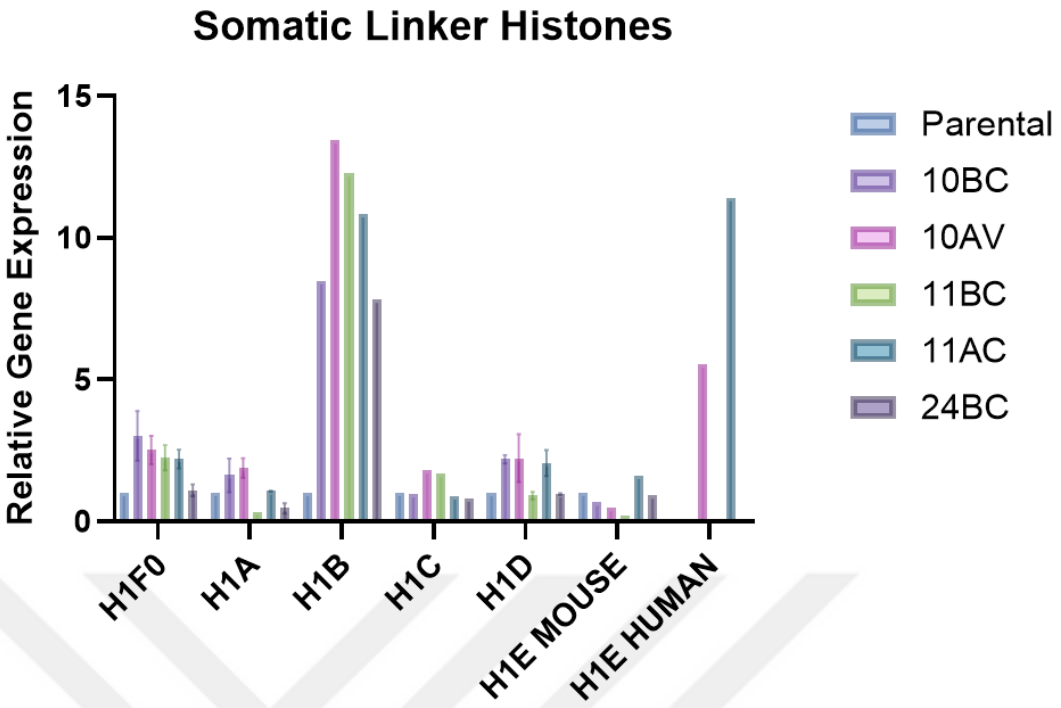

Figure 61. H1D was downregulated in clone 11BC, which was consistent with a decrease in genomic screening.

Since other histones also showed differential expression levels we went on for clone 10 and performed Sanger sequencing for the genomic PCR products of linker histones H1A, H1D, and H1C. A silent mutation was observed in the linker histone H1D without affecting the amino acid sequence, and the clone was accepted as the only off-target-free sample.

To further elucidate the differential expression of linker histones for possible Cas9 off-target effects, we amplified the 5' regulatory regions of linker histones H1A, H1B, H1C, H1D, and H1F0 (Figure 62A). The results showed impairment of the linker histone H1F0's 5' region, most probably in a heterozygous manner, as can be seen in Figure 62A, with the presence of the desired and multiple amplicons from clone 11. In contrast, clone 10 showed a single expected band, indicating locus integrity. To further check the status of linker histones in protein level fractional protein isolation, perchloric acid linker histone extraction was performed. Obtained linker histones were run on 20% gel and analyzed through Coomassie staining (Figure 62B). Presence of linker histones were detected without recognizable differences.

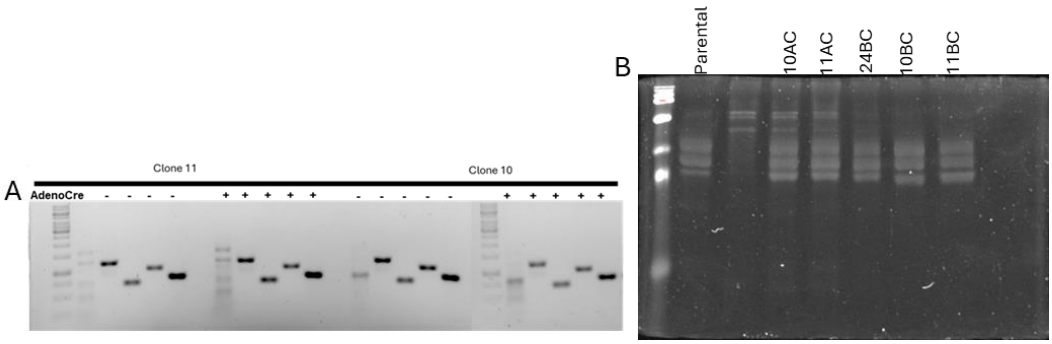

Figure 62. Clone 11 showed disruptions in 5' regulatory region of H1f0 but no difference was detected in overall protein levels of linker histones. A. 5' regulatory regions of H1.0, H1A, H1C, H1D, H1B for 11 BC/AC and 10BC/AC respectively. B. The perchloric acid extraction method was used to obtain and elucidate the expression of linker histones.

4.10. Pathogenic H1E Variant Impaired Cell Plasticity And Accelerated Senescence

After eliminating clone 11, we further investigated the arrested mesenchymal state of clone 10 by inspecting the further epithelial and mesenchymal markers both at RNA and protein level.

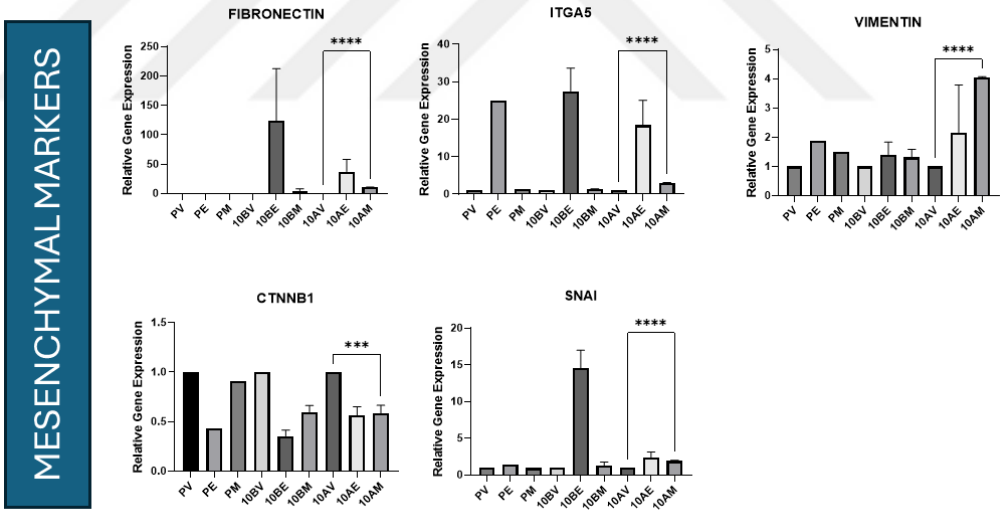

Figure 63. 10 AC Retained Mesenchymal Gene Pattern. Removal of TGF-β could not initiate MET, mesenchymal gene expression was prominent. The data was analyzed using Student's t test. ($p > 0.05$ *, $p \leq 0.05$ **, $p \leq 0.01$ *** and $p \leq 0.001$ ****)

Sustained expression of mesenchymal markers such as Fibronectin, ITGA5, and Snail was prominent in RNA level. While vimentin did not only retained its high expression levels but also displayed even higher levels of expression even after removal of TGF-β (Figure 63).

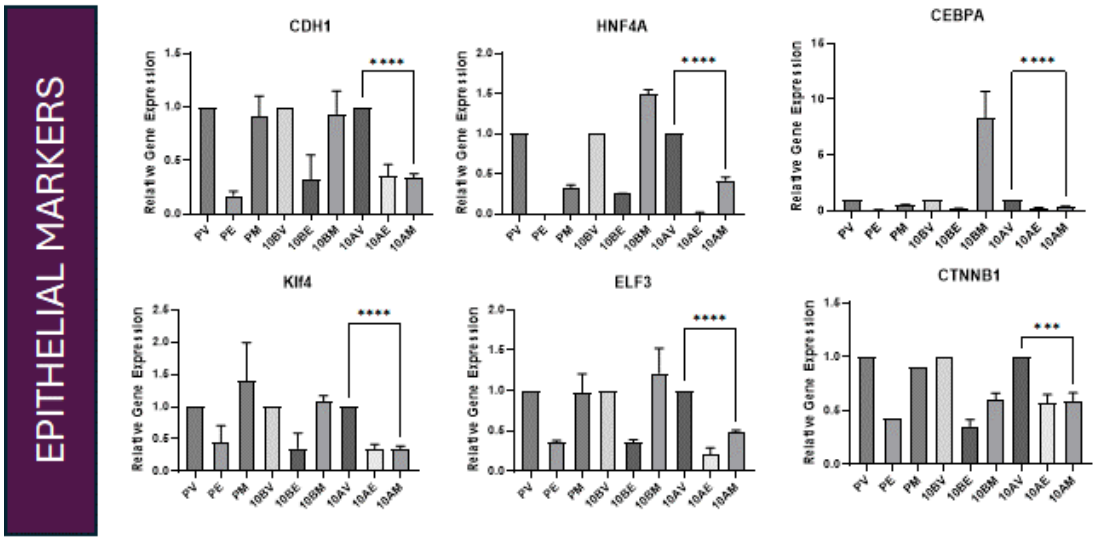

Figure 64. 10 AC Failed to Gain Epithelial Gene Expression Patter. Removal of TGF-β could not initiate MET, mesenchymal gene expression was prominent. The data was analyzed using Student's t test. ($p > 0.05$ *, $p \leq 0.05$ **, $p \leq 0.01$ *** and $p \leq 0.001$ ****)

On the side of the epithelial markers both Elf3 and HNF4A showed slight upregulation in RNA level but not enough to create a MET pattern. On the other hand Klf4 and CEBPA remained in similar levels with TGF-β treated cells while CDH1 levels showed slightly further downregulation (Figure 64).

Protein levels of E-cadherin did not change in western blots (Figure 65). Taken together with the IF results, this could be explained by the presence of E-cadherin protein in the cytoplasm of the cells and not in the membrane (Figure 66). Accumulation of E-cadherin in the cytoplasm of the cell even after withdrawal of TGF-β3 might indicate the inability of β-catenin to form a complex with E-cadherin on the cell membrane, or the inability of E-cadherin to be marked for degradation. Considering the decrease in the RNA levels of CDH1 and CTNNB1, disruptions in the protein level recycling mechanism of E-cadherin appear to be more logical.

Another epithelial marker, zonula occludens-1 (ZO-1), is a tight junction protein that plays a critical role in the formation and maintenance of tight junctions in epithelial cells, showing complete depletion in BC clones, but no major differences in AC. On the other hand, the mesenchymal marker N-cadherin shows a typical behavior of increased expression in TGF- beta treatment of clones and diminishes after withdrawal, except for 10AC, which keeps increasing its endogenous N-cadherin levels, indicative of an arrested mesenchymal character (Figure 65).

In addition, another conflicting result was observed in the protein levels of the mesenchymal marker vimentin. Which shows typical expression in parental and BC clone, while is already enhanced in 10 AC clone even before

the treatment of TGF-β3 and shows constative enhanced expression throughout the transitional states.

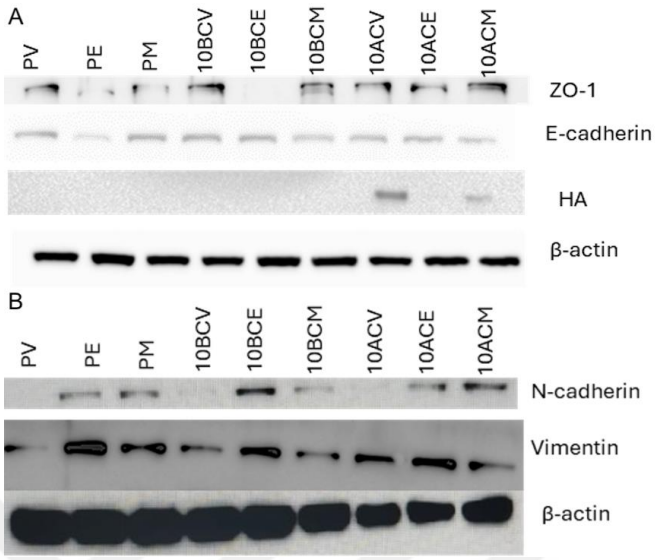

Figure 65. Inability of 10 AC to complete MET was also apparent at the protein level.

Linker histones are closely associated with senescence and cell-cycle checkpoints. Previous studies have shown that patients with Rahman mutations exhibit accelerated cellular senescence and cell cycle arrest. In this study, we also observed cell cycle arrest at the G2 phase, which raised questions regarding the senescence state of the cells. In particular, cells treated with TGF-β showed an enlarged cytoplasm, delayed growth, and increased cell death. Taken together, the fact that TGF- beta does not only activates EMT, but also induces apoptosis and senescence in different percentages according to the health and type of cell line (Spender et al., 2009), we wanted to elucidate whether cells treated with TGF-β showed senescent features (Tominaga & Suzuki, 2019). To this end, a senescence-associated β-galactosidase assay was performed on cells treated with or without TGF-β. As shown in Figure 67 Parental cells treated with or without TGF-β showed almost no reaction to the given X-gal, with no production of blue color. On the other hand, clone 11, although it did not show any arrest in cell cycle assays, reacted both in the BC and AC states regardless of the TGF-β treatment. This phenomenon could be explained by the disruption of other linker isoforms, as these proteins are also associated with senescence pathways. In contrast, clone 10 showed no reaction in the BC state, but responded in the AC state, which was seemingly increased by TGF-β treatment. This can be explained by the insufficiency of single-allele knockout of the H1E linker histone, which is easily compensated by other histones, but the presence of a pathogenic variant that clogs the compensation mechanism and perturbs chromatin organization could also activate the senescence pathway.

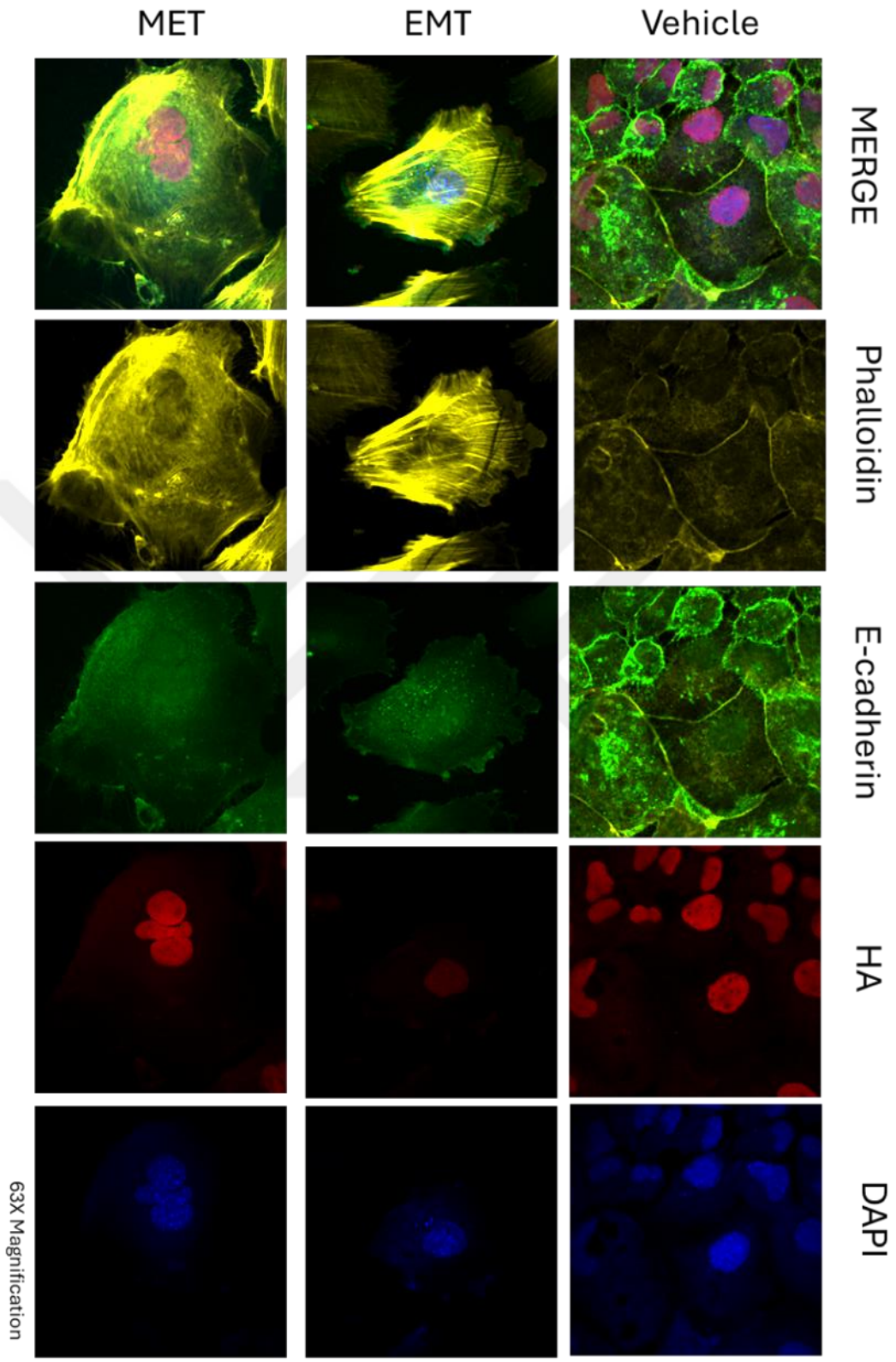

Figure 66. IF staining results of clone 10 AC showing halted MET.

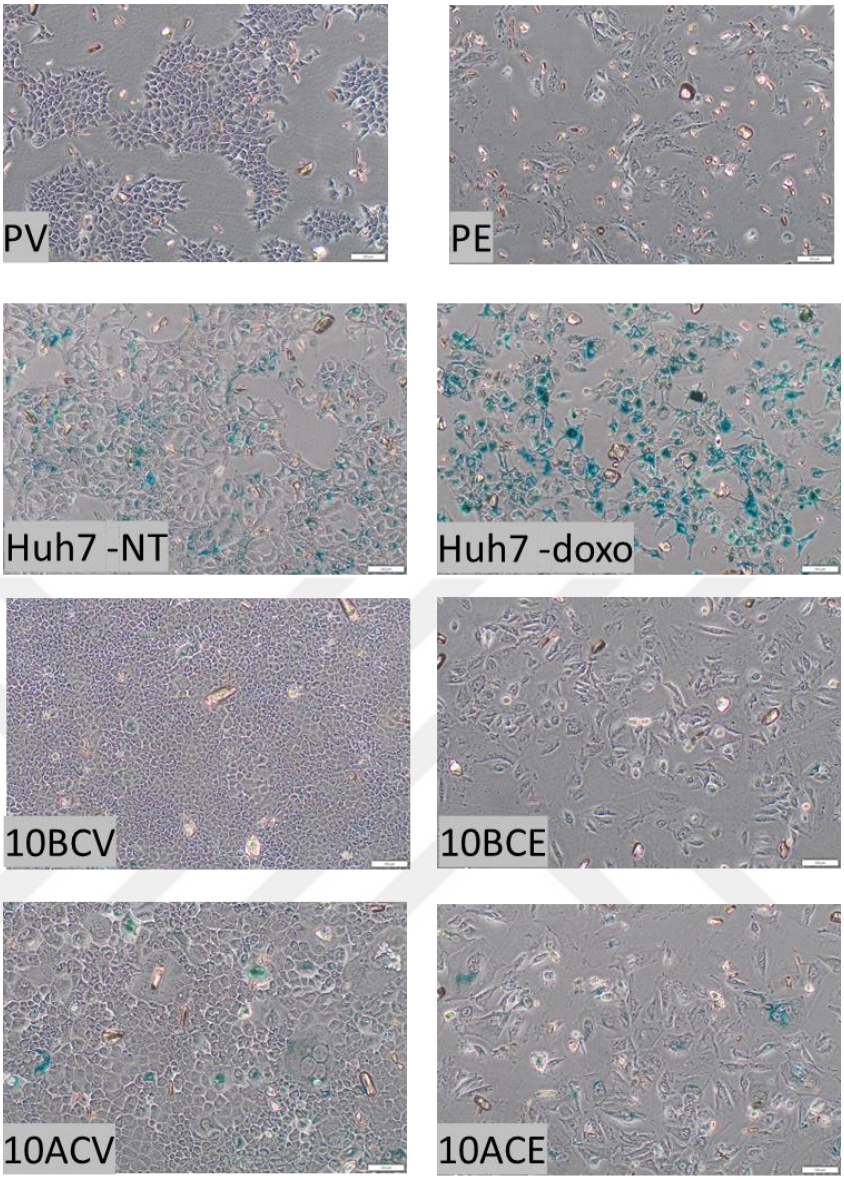

Figure 67. 10AC Showed β-Galactosidase Activity, Indicating Senescence.

4.11. Pathogenic H1E Variant Caused Migration and Invasion in Zebrafish

Intrigued by the presence of increased mesenchymal markers at the protein level, we questioned the epithelial integrity of 10 AC cells, even without TGF-β3 treatment. Since increased levels of N-cadherin and vimentin are closely associated with the gain of migratory abilities, we tested this feature using a zebrafish xenograft approach. 10 BC and AC cells together with Parental as negative control and MCF7 positive control on passage two were injected into the yolk sac of three-day old zebrafish embryos. Results were obtained at 4dpi (Figure 68).

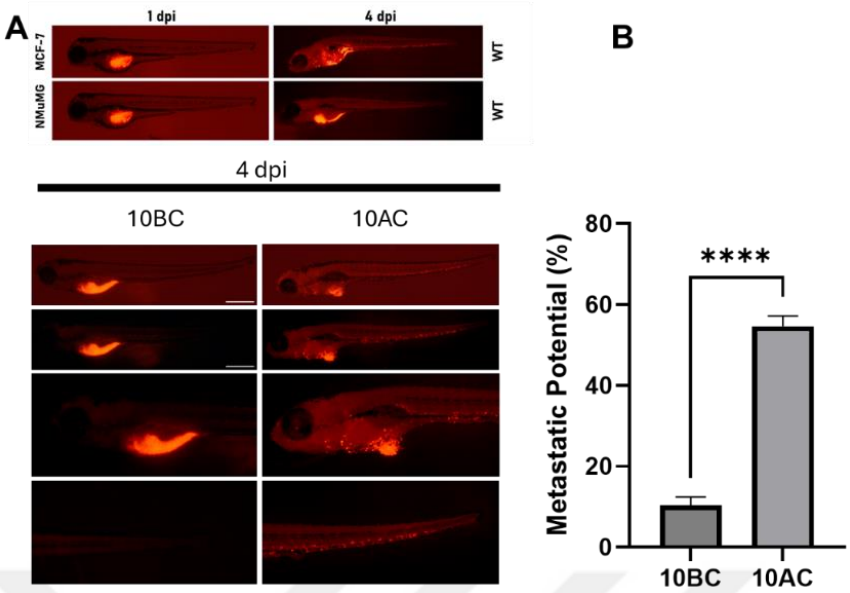

Figure 68. 10AC Exhibited Enhanced Motility And Metastatic Features In Zebrafish. The data was analyzed using Student's t test. ($p > 0.05$ *, $p \leq 0.05$ **, $p \leq 0.01$ *** and $p \leq 0.001$ ****)

Injected 10 BC cells did not show any movement and acted as parental cells, which is described by their non-motility in zebrafish. In contrast, 10AC, which displays dispersed E-cadherin in the cytoplasm, increased N-cadherin and vimentin protein levels following the injection passed through the yolk sac tissue and entered the caudal vein of the fish. It not only remained in the bloodstream and migrated through the circulatory system, but also passed through the endothelia, invaded the neighboring muscle tissue, and colonized. 10 AC not only showed migratory and invasive abilities but also was able to metastasize in distant tissues, showing higher levels of motility than the MCF-7 metastatic breast cancer cell line.

4.12. Linker histone compensation in 10AC

Mechanisms by which linker histones compensate for their loss are still unclear. However, histone depletion assays provide prominent evidence of this kin regulation. In 10AC when we investigated the expression status of other linker histones we saw that changes in the cells were cell and transition dependent. We saw that, H1.D, the epithelial integrity-related linker histone was not able to lower its expression or triad to compensate for the loss or functional presence of the linker histone (Figure 69). A recent study has shown that H1.D acts as a negative regulator of lncRNA h19, and its expression is associated with EMT (Hu et al., 2018; Medrzycki et al., 2014). This linker is not expected to be found in mesenchymal cells, because of its positive association with epithelial integrity. The high presence of this linker might be the reason for enhanced senescence in the EMT state of the cell owing to increased stress with multiple signals present.

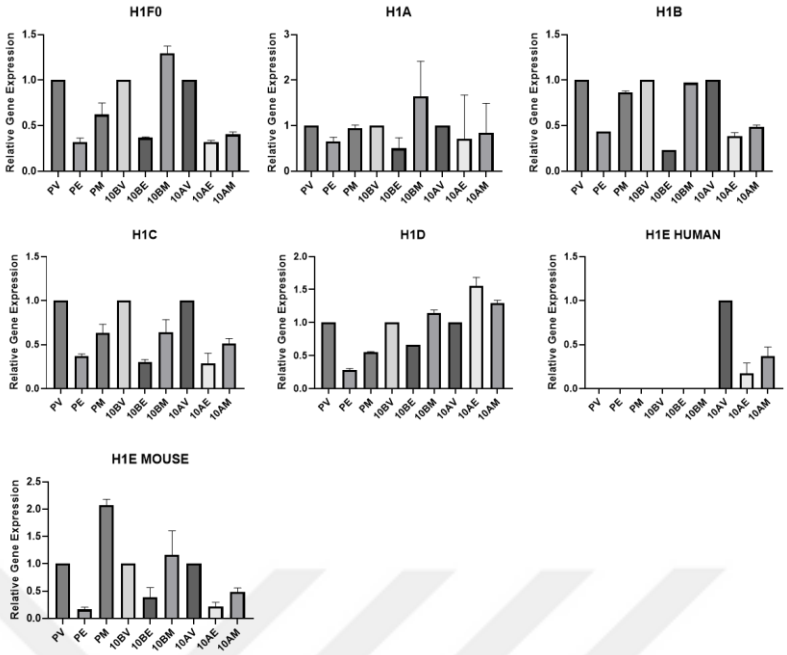

Figure 69. 10AC showed differential expression of isoforms during EMT and MET. H1D seems to try rescue epithelial phenotype or halt the EMT in the first place. The data was analyzed using Student's t test. ($p > 0.05$ *, $p \leq 0.05$ **, $p \leq 0.01$ *** and $p \leq 0.001$ ****)

5. DISCUSSION

Linker histones play a crucial role in chromatin organization and gene regulation, but their specific functions in cellular processes such as epithelial-mesenchymal transition (EMT) and mesenchymal-epithelial transition (MET) remain poorly understood. This study investigates the impact of depleting three different linker histone isoforms (H1C, H1D, and H1E) in human mammary epithelial cells (MCF10A) and mouse mammary gland cells (NMuMG). This study revealed a particularly intriguing role for the H1E isoform in maintaining epithelial integrity and regulating cell plasticity. Furthermore, this study explored the effects of a pathogenic mutation in H1E associated with Rahman syndrome, providing insights into the potential mechanisms underlying this developmental disorder. By examining the consequences of H1E depletion and mutation on EMT and MET processes, cell cycle progression, and cellular phenotypes, this study contributes to our understanding of linker histone functions in cellular plasticity and highlights the complex interplay between epigenetic regulators and cell fate decisions.

After depletion of three different linker histones in the human mammary cell line MCF10A, the cells responded to EMT only in the absence of one isoform. The first trial was performed with H1C, which was previously associated with post-transcriptional regulation of the human telomerase enzyme and the cell cycle (Ivanyi-Nagy et al., 2018; Sancho, 2008). Consistently, depletion of H1C resulted in increased death and retarded growth with no indication of the importance of EMT regulatory markers, wherein CDH1, whose downregulation is considered a hallmark of EMT, was upregulated. The other inspected linker isoform, H1D, showed similar results as H1C upon depletion. Previous studies have shown that H1D acted as negative regulator of H19, a lncRNA whose expression was positively associated with EMT in ovarian cancer and glioma tissues (Hu et al., 2018; Lv et al., 2017; Medrzycki et al., 2014). Inconsistent with previous data, our results showed increased cell death and increased expression of the epithelial and mesenchymal markers CDH1 and CDH2, respectively. The reason for this could be either the accumulated number of destructive mutations in cancerous cell lines or the tissue specificity of the linker histones. In contrast, depletion of H1E in MCF10A cells resulted in an EMT-like phenotype, which was followed by significant downregulation of CDH1. Consistent with a recent data showing that H1.E silencing resulted in the initiation of EMT and increased the migration ability of lung cancer cell lines (Chen et al., 2024). In another study, shRNA-mediated silencing of H1E resulted in an unidentified necrosis-like phenotype, with minor effects on the cell cycle (Sancho, 2008). In our study, depletion of H1E resulted in a significant decrease in the viability of cells with an EMT-like morphology and arrested the cell cycle in the G1 phase. Linker histones are closely associated with cell cycle progression and regulation of the chromatin state for access to the replication machinery (Hergeth & Schneider, 2015; Mayor et al., 2015). Specific linker, histone H1.E was found to be highly

phosphorylated in G1, with a peak in the S phase of the cell cycle, to lose its affinity for DNA and other nucleosome-associated proteins to ensure relaxed conformation and access to DNA replication machinery (Gréen et al., 2011). In its absence or prolonged relaxation, chromatin also creates vulnerability to DNA Damaging agents. Interestingly, the majority of G1 arrest is a profound of DNA damage response (Lai et al., 2021). Taken together, the observed G1 arrest and retarded growth could be due to severe damage occurring in the genetic material of the cells in the absence of H1E. This could also cause the loss of epithelial integrity as a stress response or evasion of apoptosis (Rajabi et al., 2024). Features that would not occur only in response to DNA damage but could also be induced through loss of H1E caused perturbation of chromatin and disturbances in higher chromatin order. Since TAD organization was shown to be distinct for mesenchymal and epithelial cells and organized strictly and separately, it could support the chromatin level perturbation caused by EMT (Pang et al., 2022). Why the other linkers did not respond to this was or the determination of the inner cause of this phenotype remains to be discovered. Inspection of histone compensation and validation of chromatin-level integrity is needed.

Due to the high heterogeneity of MCF10A cells and the differential expression of linker histones in the Normal Murine Mammary Gland (NMuMG), H1E depletion was repeated in these cells. NMuMG cells are a widely used EMT-MET model because of their high plasticity, homogenous epithelial characteristics, and easy and quick experimental advantages. Similar to the MCF10A results, H1E depletion generated an EMT-like phenotype, but with the downregulation of CDH1, a hallmark EMT, and CDH2, a mesenchymal marker typically expected to be upregulated. Nevertheless, our study revealed a strong association between linker histone H1E and the epithelial state of NMuMG cells. Our research demonstrated that a 90% reduction in H1E in epithelial cells led to loss of cell integrity, as evidenced by the acquisition of a distinct phenotype. First, the observed phenotype raised concerns about the induction of senescence in response to H1E depletion, as previous studies have shown that linker histones are closely related to SAHF formation or are absent in the senescent state (Funayama, Saito et al., 2006). However, the senescence assay yielded negative results, which indicated that the observed phenotype was not due to senescence. Furthermore, shRNA-mediated H1E knockdown in human mammary cell lines confirmed that protein depletion resulted in a necrotic-like phenotype with negative apoptosis results and increased cell death (Sancho, 2008), which was not fully consistent with our findings. Despite the unusual phenotype displayed by the cells, we did not observe a necrotic rate of cell death compared with the control group. This could be due to the limited time of siRNA transfection, which does not go further than three days in contrast to shRNA knockdowns, and the possibility of long-term monitoring. Notably, a recent study published in 2024 showed that H1e depletion in small nuclear lung carcinoma cells induced EMT (Chen, Yang et al., 2024), which is consistent with our findings. Overexpression of H1.4 inhibited growth and migration. Taken together, these results confirm our mesenchymal-like phenotype and suggest different cell-dependent roles for

the linker histones. Despite the limited data on the role of H1E in the regulation of EMT and cell plasticity, its role in MET has not been investigated. In this study, we showed that H1E silencing did not only disrupted the epithelial integrity of untreated cells and halted the mesenchymal-to-epithelial transition in mesenchymal NMuMG cells. Linker histones have been previously associated with the MET process because of their roles in development and differentiation; however, there is no evidence of their role in this process. Our results only created conflict regarding the differential expression of CDH1 at the RNA and protein levels. As shown at the RNA level, CDH1 showed decreased fulfilling of the EMT hallmark, whereas staining of cells in the immunostaining assay was positive for anti-E-cadherin. Although E-cadherin was present in the cell, it was delocalized in the cytoplasm, showing a loss of function as an adherency protein. According to these results, E-cadherin accumulated in the cell cytoplasm, raising questions regarding the integrity of the E-cadherin degradation cascade, which could be affected by the absence of H1E. Nevertheless, H1E depletion disrupted the epithelial integrity and high plasticity of NMuMG cells and halted their transition with the generation of an interesting morphology.

Recently, a frameshift mutation in the CTD tail of the H1E linker histone was found to cause a syndrome with distinct features, abnormal organ development, and severe intellectual disability. Since the known regulatory roles of H1E in development and organogenesis and the newly discovered provital role in guarding epithelial integrity, we wanted to investigate the possible effects of pathogenic Rahman variants on EMT and MET processes. Using HDR mediated Crispr/Cas9 genome editing, we generated clones, heterozygous knockout, and transgenic NMuMG cells harboring H1e c.430dupG, which is the most frequent Rahman mutation. Owing to the design of the HDR template with the presence of the neomycin cascade at the 5' locus, after the successful integration of the synthetic gene in the loci, the neomycin gene would arrest the expression of the H1E gene by occupying its endogenous promoter. The first generated heterozygous knockout clones acted mostly like normal NMuMG cells as a result of proliferation and the cell cycle, and showed a perfectly normal pattern, with the exception of 24, which showed delayed growth. Sanger sequencing showed that clone 24 had several deletions due to the unwanted effects of sgRNAs. These deletions caused a frameshift mutation with 74 amino acid depletion, almost completely erasing the CTD tail. This clone was accepted as another function disturbing-mutation and continued the experiment. For the other two clones, 10 and 11 had a 2 bp deletion in the endogenous wild-type allele of H1e, creating a frame mutation resulting in a shorter Rahman CTD tail, but with a smaller drop in charge, from 30 to 20, and different amino acid sequences. Recent in silico studies have shown that even a drop to half of the charge would not inhibit chromatin condensation through the inability of linker binding on the nucleosome (Matthew Watson 2024), and unpublished data from our and collaborator laboratories' in vitro results showed that even in the complete deletion of the CTD tail, linker histones still showed some affinity to nucleosomes through its globular domain. Another study demonstrated that

the removal of the majority of the CTD tail did not have any effect on cell survival and well-being (Lu et al., 2009; Lu & Hansen, 2004); therefore, we concluded that the mutation was ineffective, as per the EMT and MET experiments and continued the subsequent experiments. Clone 24 was almost completely depleted from the CTD tail.

Typical EMT is characterized by spindle-shaped morphology, a decrease in epithelial markers such as CDH1, and an increase in mesenchymal markers such as vimentin and fibronectin at the molecular level (Yang, Antin et al. 2020). All of these typical behaviors were observed in BC clones treated with TGF-β, with the exception of vimentin in clones 24 and 10. They did not show a significant upregulation of vimentin upon induction of EMT with TGF-β. This could be because of its upregulation in the vehicle state. When the MET processes of the clones were examined, they did not exhibit any atypical behavior at the morphological level. At the molecular level, they showed an upregulation in the expression of epithelial markers and a decrease in most of the observed mesenchymal markers. However, clone 11 was not fully capable of decreasing fibronectin expression, although it was not accompanied by any other mesenchymal markers associated with metastasis (Ju, Godet et al. 2017). The contrasting results for haplo-insufficient clones in the knockdown assays were attributed to the level of H1E inhibition. Knockdown experiments using siRNA showed almost complete reduction of H1E, whereas heterozygous clones were only able to reduce H1E expression by half. These results suggested that the effects of H1E depletion on cell plasticity and epithelial integrity occurred in a dose-dependent manner.

To investigate the effects of pathogenic Rahman mutations, cells were subjected to Cre recombination and the efficiency of the procedure was examined at the genomic, RNA, and protein levels. The expression of the Rahman mutation was verified in both cases, with concerns regarding different expression levels. Later, proliferation and cell cycle experiments revealed distinct differences between the clones. G2 arrest and serious growth retardation were observed in clone 10 and Rahman patients, while clone 11 showed different health features. Later in the EMT and MET experiments, while both clones were able to undergo EMT, 11 successfully completed the epithelial transition and 10 were arrested in the mesenchymal state. Based on this, we genotyped other linker histone isoforms for possible off-target effects of sgRNA, endangering clone integrity.

Indeed, we found a dosage decrease in the genomic PCRs of clone 11 targeting the linker histone H1D, which was confirmed at the RNA level by qPCRs. We attempted to show a decrease in protein levels with nuclei isolation and linker extraction by perchloric acid; however, the results were not conclusive due to difficulties in amount equalization.

After eliminating clone 11, we accepted clone 10 as an appropriate transgenic model with Rahman expression and further focused on EMT arrest. To further confirm the arrest at the mesenchymal level, we measured the

protein levels of E-cadherin, ZO-1, and N-cadherin, together with the Rahman protein. Rahman protein showed to decrease in TGF-beta treated group consistent with the RNA-seq results of parental cells and return of expression was observed. E-cadherin was not significantly altered as an EMT marker, consistent with IF staining, which showed accumulation of E-cadherin in the cytoplasm. The expression of N-cadherin, which is expressed at the vehicle level, was increased by TGF-β treatment and continued to increase even after its withdrawal. In addition, enhanced protein levels of vimentin, a mesenchymal marker closely associated with migration, in all states of clone 10AC both explained the undetected change in RNA level but also raised questions about the epithelial integrity of the cells. Again, not only showing mesenchymal arrest but also the ability of 10 AC clones to migrate in zebrafish xenografts, especially the ability of 10 AC to form tumor-like structures, even without treatment, indicated arrest in the intermediate state. However, further validation is required in this regard.

Taking a closer look at the EMT process of the cells, we observed that they did not display a typical spindle EMT morphology but exhibited enlarged cytoplasm with accumulation of E-cadherin in the cytoplasm both in TGF-β-treated and untreated cells, raising questions about the outcome of treatment. As a well-known event TGF-β treatment not only induces EMT but also promotes apoptosis and senescence in every instance. The only reason for the different outcomes from different cells is that the plasticity level of the treated cells acts as a determinant by which percentage each event will take place. NMuMG cells for example due to their high level of plasticity respond to TGF-b with ~70% EMT, 20% Apoptosis and 10% Senescence. Taking into consideration the results of knockdown assays and questioning the integrity of plasticity levels, especially due to the observed inability to complete MET, we checked the senescence status of the cells and observed that 10 AC already exhibited senescence features and showed higher reactivity upon TGF-β treatment. Accelerated senescence features were concomitant with fibroblast collected from patients which also showed cell cycle disturbances (For instance (Flex et al., 2019)), EMT and MET features have not been explored previously in patient samples, and it was thought that EMT and MET are major stars of development; this kind of drastic effect would be lethal and unrealistic. However, the differences between EMT MET types and the favor of linker histones acting differently in every cell type might bypass the lethal effects in early development, and milder disturbances of the program could explain abnormal organ development. Further experiments on human cell lines are required to confirm these hypotheses.

Senescence could be an indicator of DNA damage in Rahman clones, which could be caused by the vulnerability of DNA in the absence or functional disturbances of the H1E linker histone. In that case H1E is especially important for protection from cell cycle through its long CTD tail and ability to form condensed heterochromatin structures that would protect the genetic material of the cells from the radical reagents. Positivity of clones and senescence negative feature of knockdown experiment could be due to the accumulation

of damages in long -term culturing conditions in contrast with transient knock down assay, where they cannot accumulate enough to induce senescence (Funayama et al., 2006; Tominaga & Suzuki, 2019).

Strangely, the arrest of 10A cells and siRNA in the mesenchymal state were similar to each other. It is unclear whether the Rahman mutation acted as a loss-of-function mutation or created a double-compound effect. The fact that Rahman clones and depleted groups share the same effect suggests a double-negative effect, where the Rahman protein neutralizes the functionality of WT H1E. However, the distinct and unique amino acid sequence present in every individual with the syndrome, even because of different mutations, should not be overlooked. Further investigation of this peptide alone may prove its biological importance or irrelevance. Generation of homozygous knockout clones would provide better insights into this subject. However, strangely enough, none of the positive clones were intact linkers. Very few homozygous clones were obtained from the experiments conducted in this study. Each individual bore a PCR-level visible deletion. Together with the fact that a clone bearing an additional mutation displayed healthier features in our study, this suggests a more complex and vital compensation mechanism within linker histones.

On the other hand, linker histones are considered as main architects and guardians of higher order chromatin. Since the compaction relies solely on their interactions with each other and other chromatin related proteins. They are responsible for the integrity and protection of genetic material, maintenance of cellular homeostasis through conformational changes in chromatin structure to regulate gene expression, and modulation of cell growth and proliferation, granting plasticity to chromatin. Depletion of or function-related gain of mutation on this kind of chromatin organizer would disrupt the chromatin higher order and could change the overall gene expression due to the uncontrollable access of transcription factors to various regions of the destructed architecture.

Although in the case of different linker histones the outcome was different but not unresponsive could be explained through the preferable different function nature of linker histones

Linker histones continuously perturb the chromatin to create optimum conditions, with continuous crosstalk within each other since all of them are associated with moderately different functions. For example, although most linker histones are positioned in similar ways, avoiding active regulatory regions and creating heterochromatin-like compact structures, the linker histone H1.A was found to favorize some active chromodomains and associate with euchromatin-like relaxed structures enhancing active gene expression. Similar preferences of linker histones are also present in TAD, A/B compartmentalization. A H1 silencing study showed that H1.C was depleted from both compartments and re-compartmentalized in compartment A, whereas H1E compartmentalized in Compartment B and kept decreasing in

compartment A (Serna-Pujol et al., 2022). Previously it was also shown that epithelial genes and mesenchymal genes have their own distinct TAD's with mesenchymal genes upon activation move between A/B (Pang et al., 2022). Different effects of linker histones could be due to that kind of role in the compartmentalization and dysregulation of gene expression through disrupted higher order chromatin.

In addition, TAD-related outcomes could also be possible for Rahman mutations. In the case of the mutation, loss of protein charge or possible loss or gain of function through its distinct amino acid sequence could result in loss of previous functions through loss of affinity. Or irregular interaction with TAD compartments or already occupiers of the TAD that could result in the same outcome as the loss of cellular plasticity.

This study provides valuable insights into the role of linker histone H1E in the epithelial-mesenchymal transition (EMT) and mesenchymal-epithelial transition (MET). Our findings revealed a complex interplay between H1E and cellular phenotypes, particularly in the context of the Rahman mutation. The observed mesenchymal arrest in cells expressing the Rahman mutation suggests a potential mechanism for the developmental abnormalities associated with the Rahman syndrome. Furthermore, the similarities between H1E-depleted cells and those expressing the Rahman mutation indicated a possible loss-of-function or compound effect of the mutation. These results highlight the importance of linker histones in maintaining cellular identity and regulating EMT/MET processes. However, this study also raises new questions about the compensatory mechanisms among linker histone variants and the cell type-specific effects of H1E depletion or mutation. Future research should focus on generating homozygous knockout models, investigating their effects in human cell lines, and exploring their potential implications for organ development and cancer progression. Overall, this study contributes to our understanding of linker histone function and opens new avenues for research on epigenetic regulation of cellular plasticity and developmental disorders.

6. CONCLUSION AND SUGGESTIONS

The study provides significant insights into the role of linker histone H1E in epithelial-mesenchymal transition (EMT) and mesenchymal-epithelial transition (MET) processes, as well as its implications for cellular plasticity and development. This study demonstrated that H1E depletion in human mammary epithelial cells (MCF10A) and mouse mammary gland cells (NMuMG) results in an EMT-like phenotype, suggesting a crucial role for H1E in maintaining epithelial integrity. Notably, the effects of H1E depletion on cell plasticity and epithelial integrity appear to be dose-dependent, with complete depletion leading to more severe phenotypes compared to partial reduction.

Investigation of the Rahman syndrome-associated H1E mutation revealed complex effects on EMT and MET processes, including mesenchymal arrest and accelerated senescence features. This study suggests that the Rahman mutation may act as a loss-of-function mutation or create a double-compound effect, potentially explaining the developmental abnormalities associated with Rahman syndrome. These findings highlight the importance of linker histones in maintaining cellular identity and regulating EMT/MET processes, with potential implications in organ development and cancer progression.

Future research directions should focus on conducting RNA-seq analysis to better understand the effects of both H1E silencing and pathogenic variants on MET, as well as performing ATAC-seq to examine and confirm chromatin-level disruptions caused by H1E depletion or mutation. Additionally, pull-down assays for wild-type H1E and its pathogenic variant should be carried out to investigate possible alterations in protein-level interactions. Cut&Run techniques could be utilized to determine the localization patterns of wild-type H1E and pathogenic H1E on chromatin.

Further studies should include generating homozygous knockout models to elucidate the role of H1E and its variants, investigating the effects of H1E depletion and mutation in human cell lines to better understand their relevance to human development and disease, and exploring the compensatory mechanisms among linker histone variants and their cell-type-specific effects. Examining the potential implications of H1E dysfunction on organ development and cancer progression would also be valuable. These future studies will contribute to a more comprehensive understanding of linker histone function and its role in epigenetic regulation of cellular plasticity and developmental disorders. These findings may have significant implications for the understanding of various biological processes and disease mechanisms.

7. REFERENCES

Abu Alhaija, A. A., Lone, I. N., Sekeroglu, E. O., Batur, T., Angelov, D., Dimitrov, S., Hamiche, A., Firat Karalar, E. N., Ercan, M. E., & Yagci, T. (2024). Development of a mouse embryonic stem cell model for investigating the functions of the linker histone H1-4. *FEBS Open bio*, *14*(2), 309-321.

Acloque, H., Adams, M. S., Fishwick, K., Bronner-Fraser, M., & Nieto, M. A. (2009). Epithelial-mesenchymal transitions: the importance of changing cell state in development and disease. *J Clin Invest*, *119*(6), 1438-1449. https://doi.org/10.1172/jci38019

Adhikary, A., Chakraborty, S., Mazumdar, M., Ghosh, S., Mukherjee, S., Manna, A., Mohanty, S., Nakka, K. K., Joshi, S., De, A., Chattopadhyay, S., Sa, G., & Das, T. (2014). Inhibition of epithelial to mesenchymal transition by E-cadherin up-regulation via repression of slug transcription and inhibition of E-cadherin degradation: dual role of scaffold/matrix attachment region-binding protein 1 (SMAR1) in breast cancer cells. *J Biol Chem*, *289*(37), 25431-25444. https://doi.org/10.1074/jbc.M113.527267

Akhmetkaliyev, A., Alibrahim, N., Shafiee, D., & Tulchinsky, E. (2023). EMT/MET plasticity in cancer and Go-or-Grow decisions in quiescence: the two sides of the same coin? *Molecular Cancer*, *22*(1), 90. https://doi.org/10.1186/s12943-023-01793-z

Alexanian, A. R. (2015). Epigenetic modulators promote mesenchymal stem cell phenotype switches. *Int J Biochem Cell Biol*, *64*, 190-194. https://doi.org/10.1016/j.biocel.2015.04.010

Alotaibi, H., Basilicata, M. F., Shehwana, H., Kosowan, T., Schreck, I., Braeutigam, C., Konu, O., Brabletz, T., & Stemmler, M. P. (2015). Enhancer cooperativity as a novel mechanism underlying the transcriptional regulation of E-cadherin during mesenchymal to epithelial transition. *Biochim Biophys Acta*, *1849*(6), 731-742. https://doi.org/10.1016/j.bbagrm.2015.01.005

Arnold, S. J., Hofmann, U. K., Bikoff, E. K., & Robertson, E. J. (2008). Pivotal roles for eomesodermin during axis formation, epithelium-to-mesenchyme transition and endoderm specification in the mouse. *Development*, *135*(3), 501-511. https://doi.org/10.1242/dev.014357

Artavanis-Tsakonas, S., Rand, M. D., & Lake, R. J. (1999). Notch signaling: cell fate control and signal integration in development. *Science*, *284*(5415), 770-776. https://doi.org/10.1126/science.284.5415.770

Atiya, H. I., Gorecki, G., Garcia, G. L., Frisbie, L. G., Baruwal, R., & Coffman, L. (2023). Stromal-Modulated Epithelial-to-Mesenchymal Transition in Cancer Cells. *Biomolecules*, *13*(11). https://doi.org/10.3390/biom13111604

Au - Martinez-Lopez, M., Au - Póvoa, V., & Au - Fior, R. (2021). *JoVE*(172), e62373. https://doi.org/doi:10.3791/62373

Avilion, A. A., Nicolis, S. K., Pevny, L. H., Perez, L., Vivian, N., & Lovell-Badge, R. (2003). Multipotent cell lineages in early mouse development depend on SOX2 function. *Genes Dev*, *17*(1), 126-140. https://doi.org/10.1101/gad.224503

Barriere, G., Fici, P., Gallerani, G., Fabbri, F., & Rigaud, M. (2015). Epithelial Mesenchymal Transition: a double-edged sword. *Clinical and Translational Medicine*, *4*(1), 14. https://doi.org/10.1186/s40169-015-0055-4

Bataille, F., Rohrmeier, C., Bates, R., Weber, A., Rieder, F., Brenmoehl, J., Strauch, U., Farkas, S., Fürst, A., Hofstädter, F., Schölmerich, J., Herfarth, H., & Rogler, G. (2008). Evidence for a role of epithelial mesenchymal transition during pathogenesis of fistulae in Crohn's disease. *Inflamm Bowel Dis*, *14*(11), 1514-1527. https://doi.org/10.1002/ibd.20590

Bedi, U., Mishra, V. K., Wasilewski, D., Scheel, C., & Johnsen, S. A. (2014). Epigenetic plasticity: a central regulator of epithelial-to-mesenchymal transition in cancer. *Oncotarget*, *5*(8), 2016-2029. https://doi.org/10.18632/oncotarget.1875

Bednar, J., Garcia-Saez, I., Boopathi, R., Cutter, A. R., Papai, G., Reymer, A., Syed, S. H., Lone, I. N., Tonchev, O., Crucifix, C., Menoni, H., Papin, C., Skoufias, D. A., Kurumizaka, H., Lavery, R., Hamiche, A., Hayes, J. J., Schultz, P., Angelov, D.,…Dimitrov, S. (2017). Structure and Dynamics of a 197 bp Nucleosome in Complex with Linker Histone H1. *Molecular Cell*, *66*(3), 384-397.e388. https://doi.org/https://doi.org/10.1016/j.molcel.2017.04.012

Bertolino, E., Reinitz, J., & Manu. (2016). The analysis of novel distal Cebpa enhancers and silencers using a transcriptional model reveals the complex regulatory logic of hematopoietic lineage specification. *Developmental biology*, *413*(1), 128-144. https://doi.org/https://doi.org/10.1016/j.ydbio.2016.02.030

Bobde, R. C., Saharan, K., Baral, S., Gandhi, S., Samal, A., Sundaram, R., Kumar, A., Singh, A. K., Datta, A., & Vasudevan, D. (2021). In Vitro Characterization of Histone Chaperones using Analytical, Pull-Down and Chaperoning Assays. *J Vis Exp*(178). https://doi.org/10.3791/63218

Bogachek, M. V., De Andrade, J. P., & Weigel, R. J. (2015). Regulation of epithelial-mesenchymal transition through SUMOylation of transcription factors. *Cancer Res*, *75*(1), 11-15. https://doi.org/10.1158/0008-5472.Can-14-2824

Bort, R., Signore, M., Tremblay, K., Martinez Barbera, J. P., & Zaret, K. S. (2006). Hex homeobox gene controls the transition of the endoderm to a pseudostratified, cell emergent epithelium for liver bud development. *Dev Biol*, *290*(1), 44-56. https://doi.org/10.1016/j.ydbio.2005.11.006

Bouchard, M., Souabni, A., Mandler, M., Neubüser, A., & Busslinger, M. (2002). Nephric lineage specification by Pax2 and Pax8. *Genes Dev*, *16*(22), 2958-2970. https://doi.org/10.1101/gad.240102

Brabletz, T., Kalluri, R., Nieto, M. A., & Weinberg, R. A. (2018). EMT in cancer. *Nature Reviews Cancer*, *18*(2), 128-134. https://doi.org/10.1038/nrc.2017.118

Brown, D. T., Alexander, B. T., & Sittman, D. B. (1996). Differential effect of H1 variant overexpression on cell cycle progression and gene expression. *Nucleic Acids Res*, *24*(3), 486-493. https://doi.org/10.1093/nar/24.3.486

Buijs, J. T., Henriquez, N. V., van Overveld, P. G., van der Horst, G., Que, I., Schwaninger, R., Rentsch, C., Ten Dijke, P., Cleton-Jansen, A. M., Driouch, K., Lidereau, R., Bachelier, R., Vukicevic, S., Clézardin, P., Papapoulos, S. E., Cecchini, M. G., Löwik, C. W., & van der Pluijm, G. (2007). Bone morphogenetic protein 7 in the development and treatment of bone metastases from breast cancer. *Cancer Res*, *67*(18), 8742-8751. https://doi.org/10.1158/0008-5472.Can-06-2490

Buijs, J. T., Rentsch, C. A., van der Horst, G., van Overveld, P. G., Wetterwald, A., Schwaninger, R., Henriquez, N. V., Ten Dijke, P., Borovecki, F., Markwalder, R., Thalmann, G. N., Papapoulos, S. E., Pelger, R. C., Vukicevic, S., Cecchini, M. G., Löwik, C. W., & van der Pluijm, G. (2007). BMP7, a putative regulator of epithelial homeostasis in the human prostate, is a potent inhibitor of prostate cancer bone metastasis in vivo. *Am J Pathol*, *171*(3), 1047-1057. https://doi.org/10.2353/ajpath.2007.070168

Burgess, R., Rawls, A., Brown, D., Bradley, A., & Olson, E. N. (1996). Requirement of the paraxis gene for somite formation and musculoskeletal patterning. *Nature*, *384*(6609), 570-573. https://doi.org/10.1038/384570a0

Cano, A., Pérez-Moreno, M. A., Rodrigo, I., Locascio, A., Blanco, M. J., del Barrio, M. G., Portillo, F., & Nieto, M. A. (2000). The transcription factor snail controls epithelial–mesenchymal transitions by repressing E-cadherin expression. *Nature cell biology*, *2*(2), 76-83.

Caterino, T. L., & Hayes, J. J. (2011). Structure of the H1 C-terminal domain and function in chromatin condensation. *Biochem Cell Biol*, *89*(1), 35-44. https://doi.org/10.1139/O10-024

Chaffer, C. L., Thompson, E. W., & Williams, E. D. (2007). Mesenchymal to Epithelial Transition in Development and Disease. *Cells Tissues Organs*, *185*(1-3), 7-19. https://doi.org/10.1159/000101298

Chalmers, A. D., Lachani, K., Shin, Y., Sherwood, V., Cho, K. W. Y., & Papalopulu, N. (2006). Grainyhead-like 3, a transcription factor identified in a microarray screen, promotes the specification of the superficial layer of the embryonic epidermis. *Mechanisms of Development*, *123*(9), 702-718. https://doi.org/https://doi.org/10.1016/j.mod.2006.04.006

Chambers, I., Colby, D., Robertson, M., Nichols, J., Lee, S., Tweedie, S., & Smith, A. (2003). Functional expression cloning of Nanog, a pluripotency sustaining factor in embryonic stem cells. *Cell*, *113*(5), 643-655. https://doi.org/10.1016/s0092-8674(03)00392-1

Chea, H. K., Wright, C. V., & Swalla, B. J. (2005). Nodal signaling and the evolution of deuterostome gastrulation. *Dev Dyn*, *234*(2), 269-278. https://doi.org/10.1002/dvdy.20549

Chen, J., Zheng, X., Rao, N., Huang, Y., Liu, J., Li, Y., & Zhang, J. (2021). Key Markers and Epigenetic Modifications of Dental-Derived Mesenchymal Stromal Cells. *Stem Cells International*, *2021*(1), 5521715. https://doi.org/https://doi.org/10.1155/2021/5521715

Chen, Q., Yang, M., Duan, X., Zhang, J., Shi, F., Chen, R., & Li, Y. (2024). Linker Histone H1.4 Inhibits the Growth, Migration and EMT Process of Non-Small Cell Lung Cancer by Regulating ERK1/2 Expression. *Biochem Genet*. https://doi.org/10.1007/s10528-024-10760-2

Chen, S., Saeed, A. F. U. H., Liu, Q., Jiang, Q., Xu, H., Xiao, G. G., Rao, L., & Duo, Y. (2023). Macrophages in immunoregulation and therapeutics. *Signal Transduction and Targeted Therapy*, *8*(1), 207. https://doi.org/10.1038/s41392-023-01452-1

Cheng, G. Z., Zhang, W. Z., Sun, M., Wang, Q., Coppola, D., Mansour, M., Xu, L. M., Costanzo, C., Cheng, J. Q., & Wang, L. H. (2008). Twist is transcriptionally induced by activation of STAT3 and mediates STAT3 oncogenic function. *J Biol Chem*, *283*(21), 14665-14673. https://doi.org/10.1074/jbc.M707429200

Ciolfi, A., Aref-Eshghi, E., Pizzi, S., Pedace, L., Miele, E., Kerkhof, J., Flex, E., Martinelli, S., Radio, F. C., Ruivenkamp, C. A. L., Santen, G. W. E., Bijlsma, E., Barge-Schaapveld, D., Ounap, K., Siu, V. M., Kooy, R. F., Dallapiccola, B., Sadikovic, B., & Tartaglia, M. (2020). Frameshift mutations at the C-terminus of HIST1H1E result in a specific DNA hypomethylation signature. *Clin Epigenetics*, *12*(1), 7. https://doi.org/10.1186/s13148-019-0804-0

Ciruna, B., & Rossant, J. (2001). FGF signaling regulates mesoderm cell fate specification and morphogenetic movement at the primitive streak. *Dev Cell*, *1*(1), 37-49. https://doi.org/10.1016/s1534-5807(01)00017-x

Clausell, J., Happel, N., Hale, T. K., Doenecke, D., & Beato, M. (2009). Histone H1 Subtypes Differentially Modulate Chromatin Condensation without Preventing ATP-Dependent Remodeling by SWI/SNF or NURF. *PLoS One*, *4*(10), e0007243. https://doi.org/10.1371/journal.pone.0007243

Clevers, H. (2006). Wnt/beta-catenin signaling in development and disease. *Cell*, *127*(3), 469-480. https://doi.org/10.1016/j.cell.2006.10.018

Clevers, H., & Watt, F. M. (2018). Defining adult stem cells by function, not by phenotype. *Annual review of biochemistry*, *87*(1), 1015-1027.

Cooper, C. D., Newman, J. A., Aitkenhead, H., Allerston, C. K., & Gileadi, O. (2015). Structures of the Ets Protein DNA-binding Domains of Transcription Factors Etv1, Etv4, Etv5, and Fev: DETERMINANTS OF DNA BINDING AND REDOX REGULATION BY DISULFIDE BOND FORMATION. *J Biol Chem*, *290*(22), 13692-13709. https://doi.org/10.1074/jbc.M115.646737

Cowan, C. E., Kohler, E. E., Dugan, T. A., Mirza, M. K., Malik, A. B., & Wary, K. K. (2010). Kruppel-like factor-4 transcriptionally regulates VE-

cadherin expression and endothelial barrier function. *Circ Res*, *107*(8), 959-966. https://doi.org/10.1161/circresaha.110.219592

Cui, N., Hu, M., & Khalil, R. A. (2017). Biochemical and Biological Attributes of Matrix Metalloproteinases. *Prog Mol Biol Transl Sci*, *147*, 1-73. https://doi.org/10.1016/bs.pmbts.2017.02.005

Dai, Y., & Faller, D. V. (2008). Transcription Regulation by Class III Histone Deacetylases (HDACs)-Sirtuins. *Transl Oncogenomics*, *3*, 53-65. https://doi.org/10.4137/tog.s483

Darsigny, M., Babeu, J. P., Dupuis, A. A., Furth, E. E., Seidman, E. G., Levy, E., Verdu, E. F., Gendron, F. P., & Boudreau, F. (2009). Loss of hepatocyte-nuclear-factor-4alpha affects colonic ion transport and causes chronic inflammation resembling inflammatory bowel disease in mice. *Plos One*, *4*(10), e7609. https://doi.org/10.1371/journal.pone.0007609

Dave, N., Guaita-Esteruelas, S., Gutarra, S., Frias, A., Beltran, M., Peiro, S., & de Herreros, A. G. (2011). Functional cooperation between Snail1 and twist in the regulation of ZEB1 expression during epithelial to mesenchymal transition. *Journal of Biological Chemistry*, *286*(14), 12024-12032.

Debasree, D., Khaja Mohieddin, S., & Ananda, M. (2018). Histone Chaperones Regulate Mammalian Gene Expression. In U. Fumiaki (Ed.), *Gene Expression and Regulation in Mammalian Cells* (pp. Ch. 4). IntechOpen. https://doi.org/10.5772/intechopen.71924

Debaugnies, M., Rodríguez-Acebes, S., Blondeau, J., Parent, M.-A., Zocco, M., Song, Y., de Maertelaer, V., Moers, V., Latil, M., Dubois, C., Coulonval, K., Impens, F., Van Haver, D., Dufour, S., Uemura, A., Sotiropoulou, P. A., Méndez, J., & Blanpain, C. (2023). RHOJ controls EMT-associated resistance to chemotherapy. *Nature*, *616*(7955), 168-175. https://doi.org/10.1038/s41586-023-05838-7

Dengler, V. L., Galbraith, M., & Espinosa, J. M. (2014). Transcriptional regulation by hypoxia inducible factors. *Crit Rev Biochem Mol Biol*, *49*(1), 1-15. https://doi.org/10.3109/10409238.2013.838205

Dhawan, A., Taylor, R. M., Cheeseman, P., De Silva, P., Katsiyiannakis, L., & Mieli-Vergani, G. (2005). Wilson's disease in children: 37-year experience and revised King's score for liver transplantation. *Liver Transpl*, *11*(4), 441-448. https://doi.org/10.1002/lt.20352

Dong, P., Xiong, Y., Watari, H., Hanley, S. J. B., Konno, Y., Ihira, K., Yamada, T., Kudo, M., Yue, J., & Sakuragi, N. (2016). MiR-137 and miR-34a directly target Snail and inhibit EMT, invasion and sphere-forming ability of ovarian cancer cells. *Journal of Experimental & Clinical Cancer Research*, *35*(1), 132. https://doi.org/10.1186/s13046-016-0415-y

Dongre, A., & Weinberg, R. A. (2019). New insights into the mechanisms of epithelial-mesenchymal transition and implications for cancer. *Nat Rev Mol Cell Biol*, *20*(2), 69-84. https://doi.org/10.1038/s41580-018-0080-4

Dongre, A., & Weinberg, R. A. (2019). New insights into the mechanisms of epithelial–mesenchymal transition and implications for cancer. *Nature*

reviews Molecular cell biology, *20*(2), 69-84. https://doi.org/10.1038/s41580-018-0080-4

Dragonetti, M., Turco, C., Benedetti, A., Goeman, F., Forcato, M., Scalera, S., Allegretti, M., Esposito, G., Fazi, F., Blandino, G., Donzelli, S., & Fontemaggi, G. (2024). The lncRNAMALAT1-WTAP axis: a novel layer of EMT regulation in hypoxic triple-negative breast cancer. *Cell Death Discovery*, *10*(1), 276. https://doi.org/10.1038/s41420-024-02058-4

Dudley, A. T., & Robertson, E. J. (1997). Overlapping expression domains of bone morphogenetic protein family members potentially account for limited tissue defects in BMP7 deficient embryos. *Dev Dyn*, *208*(3), 349-362. https://doi.org/10.1002/(sici)1097-0177(199703)208:3<349::Aid-aja6>3.0.Co;2-i

Duncan, E. J., Gluckman, P. D., & Dearden, P. K. (2014). Epigenetics, plasticity, and evolution: How do we link epigenetic change to phenotype? *Journal of Experimental Zoology Part B: Molecular and Developmental Evolution*, *322*(4), 208-220. https://doi.org/https://doi.org/10.1002/jez.b.22571

Emilia, M., Alexandra Eugenia, B., Ana Maria, O., Monica Teodora, N., Carolina, C., & Gheorghita, I. (2020). Schwann Cell Plasticity in Peripheral Nerve Regeneration after Injury. In J. B. Stavros, H. R. Fabian, & L. Welwin (Eds.), *Demyelination Disorders* (pp. Ch. 3). IntechOpen. https://doi.org/10.5772/intechopen.91805

Erami, Z., Herrmann, D., Warren, S. C., Nobis, M., McGhee, E. J., Lucas, M. C., Leung, W., Reischmann, N., Mrowinska, A., Schwarz, J. P., Kadir, S., Conway, J. R. W., Vennin, C., Karim, S. A., Campbell, A. D., Gallego-Ortega, D., Magenau, A., Murphy, K. J., Ridgway, R. A.,…Timpson, P. (2016). Intravital FRAP Imaging using an E-cadherin-GFP Mouse Reveals Disease- and Drug-Dependent Dynamic Regulation of Cell-Cell Junctions in Live Tissue. *Cell Rep*, *14*(1), 152-167. https://doi.org/10.1016/j.celrep.2015.12.020

Fan, Y., Nikitina, T., Zhao, J., Fleury, T. J., Bhattacharyya, R., Bouhassira, E. E., Stein, A., Woodcock, C. L., & Skoultchi, A. I. (2005). Histone H1 depletion in mammals alters global chromatin structure but causes specific changes in gene regulation. *Cell*, *123*(7), 1199-1212. https://doi.org/10.1016/j.cell.2005.10.028

Fan, Y., Sirotkin, A., Russell, R. G., Ayala, J., & Skoultchi, A. I. (2001). Individual somatic H1 subtypes are dispensable for mouse development even in mice lacking the H1(0) replacement subtype. *Mol Cell Biol*, *21*(23), 7933-7943. https://doi.org/10.1128/mcb.21.23.7933-7943.2001

Fang, H., Clark, D. J., & Hayes, J. J. (2012). DNA and nucleosomes direct distinct folding of a linker histone H1 C-terminal domain. *Nucleic Acids Res*, *40*(4), 1475-1484. https://doi.org/10.1093/nar/gkr866

Fatma, H., Jameel, M., Akhtar, K., Ansari, M. A., & Siddique, H. R. (2023). Implication of Lupeol in compensating Sorafenib-induced perturbations of redox homeostasis: A preclinical study in mouse model. *Life Sci*, *322*, 121647. https://doi.org/10.1016/j.lfs.2023.121647

Fischer, L., & Thievessen, I. (2023). FUCCI Reporter Gene-Based Cell Cycle Analysis. In O. Friedrich & D. F. Gilbert (Eds.), *Cell Viability Assays: Methods and Protocols* (pp. 371-385). Springer US. https://doi.org/10.1007/978-1-0716-3052-5_24

Fischle, W., Wang, Y., Jacobs, S. A., Kim, Y., Allis, C. D., & Khorasanizadeh, S. (2003). Molecular basis for the discrimination of repressive methyl-lysine marks in histone H3 by Polycomb and HP1 chromodomains. *Genes Dev*, *17*(15), 1870-1881. https://doi.org/10.1101/gad.1110503

Flex, E., Martinelli, S., Van Dijck, A., Ciolfi, A., Cecchetti, S., Coluzzi, E., Pannone, L., Andreoli, C., Radio, F. C., Pizzi, S., Carpentieri, G., Bruselles, A., Catanzaro, G., Pedace, L., Miele, E., Carcarino, E., Ge, X., Chijiwa, C., Lewis, M. E. S.,…Tartaglia, M. (2019). Aberrant Function of the C-Terminal Tail of HIST1H1E Accelerates Cellular Senescence and Causes Premature Aging. *Am J Hum Genet*, *105*(3), 493-508. https://doi.org/10.1016/j.ajhg.2019.07.007

Freire-de-Lima, L., Gelfenbeyn, K., Ding, Y., Mandel, U., Clausen, H., Handa, K., & Hakomori, S. I. (2011). Involvement of O-glycosylation defining oncofetal fibronectin in epithelial-mesenchymal transition process. *Proc Natl Acad Sci U S A*, *108*(43), 17690-17695. https://doi.org/10.1073/pnas.1115191108

Fukagawa, A., Ishii, H., Miyazawa, K., & Saitoh, M. (2015). δEF1 associates with DNMT1 and maintains DNA methylation of the E-cadherin promoter in breast cancer cells. *Cancer Med*, *4*(1), 125-135. https://doi.org/10.1002/cam4.347

Funayama, R., Saito, M., Tanobe, H., & Ishikawa, F. (2006). Loss of linker histone H1 in cellular senescence. *J Cell Biol*, *175*(6), 869-880. https://doi.org/10.1083/jcb.200604005

Fyodorov, D. V., Zhou, B. R., Skoultchi, A. I., & Bai, Y. (2018). Emerging roles of linker histones in regulating chromatin structure and function. *Nat Rev Mol Cell Biol*, *19*(3), 192-206. https://doi.org/10.1038/nrm.2017.94

Gabbiani, G. (2003). The myofibroblast in wound healing and fibrocontractive diseases. *J Pathol*, *200*(4), 500-503. https://doi.org/10.1002/path.1427

Giné, E., Crespo, M., Muntañola, A., Calpe, E., Baptista, M. J., Villamor, N., Montserrat, E., & Bosch, F. (2008). Induction of histone H1.2 cytosolic release in chronic lymphocytic leukemia cells after genotoxic and non-genotoxic treatment. *Haematologica*, *93*(1), 75-82. https://doi.org/10.3324/haematol.11546

Gonzalez, D. M., & Medici, D. (2014). Signaling mechanisms of the epithelial-mesenchymal transition. *Sci Signal*, *7*(344), re8. https://doi.org/10.1126/scisignal.2005189

Gravdal, K., Halvorsen, O. J., Haukaas, S. A., & Akslen, L. A. (2007). A Switch from E-Cadherin to N-Cadherin Expression Indicates Epithelial to Mesenchymal Transition and Is of Strong and Independent Importance for the Progress of Prostate Cancer. *Clinical Cancer Research*, *13*(23), 7003-7011. https://doi.org/10.1158/1078-0432.Ccr-07-1263

Gréen, A., Sarg, B., Gréen, H., Lönn, A., Lindner, H. H., & Rundquist, I. (2011). Histone H1 interphase phosphorylation becomes largely established in

G1 or early S phase and differs in G1 between T-lymphoblastoid cells and normal T cells. *Epigenetics Chromatin*, *4*, 15. https://doi.org/10.1186/1756-8935-4-15

Gregory, P. A., Bert, A. G., Paterson, E. L., Barry, S. C., Tsykin, A., Farshid, G., Vadas, M. A., Khew-Goodall, Y., & Goodall, G. J. (2008). The miR-200 family and miR-205 regulate epithelial to mesenchymal transition by targeting ZEB1 and SIP1. *Nature cell biology*, *10*(5), 593-601.

Grille, S. J., Bellacosa, A., Upson, J., Klein-Szanto, A. J., Van Roy, F., Lee-Kwon, W., Donowitz, M., Tsichlis, P. N., & Larue, L. (2003). The protein kinase Akt induces epithelial mesenchymal transition and promotes enhanced motility and invasiveness of squamous cell carcinoma lines. *Cancer Research*, *63*(9), 2172-2178.

Hampton, H. R., & Chtanova, T. (2016). The lymph node neutrophil. Seminars in immunology,

Hao, F., Kale, S., Dimitrov, S., & Hayes, J. J. (2021). Unraveling linker histone interactions in nucleosomes. *Curr Opin Struct Biol*, *71*, 87-93. https://doi.org/10.1016/j.sbi.2021.06.001

Happel, N., & Doenecke, D. (2009). Histone H1 and its isoforms: contribution to chromatin structure and function. *Gene*, *431*(1-2), 1-12. https://doi.org/10.1016/j.gene.2008.11.003

Harshman, S. W., Hoover, M. E., Huang, C., Branson, O. E., Chaney, S. B., Cheney, C. M., Rosol, T. J., Shapiro, C. L., Wysocki, V. H., Huebner, K., & Freitas, M. A. (2014). Histone H1 phosphorylation in breast cancer. *J Proteome Res*, *13*(5), 2453-2467. https://doi.org/10.1021/pr401248f

Harshman, S. W., Young, N. L., Parthun, M. R., & Freitas, M. A. (2013). H1 histones: current perspectives and challenges. *Nucleic Acids Research*, *41*(21), 9593-9609. https://doi.org/10.1093/nar/gkt700

Harshman, S. W., Young, N. L., Parthun, M. R., & Freitas, M. A. (2013). H1 histones: current perspectives and challenges. *Nucleic Acids Res*, *41*(21), 9593-9609. https://doi.org/10.1093/nar/gkt700

Hartman, P. G., Chapman, G. E., Moss, T., & Bradbury, E. M. (1977). Studies on the role and mode of operation of the very-lysine-rich histone H1 in eukaryote chromatin. The three structural regions of the histone H1 molecule. *Eur J Biochem*, *77*(1), 45-51. https://doi.org/10.1111/j.1432-1033.1977.tb11639.x

Hatini, V., Huh, S. O., Herzlinger, D., Soares, V. C., & Lai, E. (1996). Essential role of stromal mesenchyme in kidney morphogenesis revealed by targeted disruption of Winged Helix transcription factor BF-2. *Genes Dev*, *10*(12), 1467-1478. https://doi.org/10.1101/gad.10.12.1467

Hendzel, M. J., Lever, M. A., Crawford, E., & Th'ng, J. P. (2004). The C-terminal domain is the primary determinant of histone H1 binding to chromatin in vivo. *J Biol Chem*, *279*(19), 20028-20034. https://doi.org/10.1074/jbc.M400070200

Hergeth, S. P., & Schneider, R. (2015). The H1 linker histones: multifunctional proteins beyond the nucleosomal core particle. *EMBO Rep*, *16*(11), 1439-1453. https://doi.org/10.15252/embr.201540749

Herzlinger, D., Koseki, C., Mikawa, T., & al-Awqati, Q. (1992). Metanephric mesenchyme contains multipotent stem cells whose fate is restricted after induction. *Development*, *114*(3), 565-572. https://doi.org/10.1242/dev.114.3.565

Hiragami-Hamada, K., & Nakayama, J. I. (2019). Do the charges matter?-balancing the charges of the chromodomain proteins on the nucleosome. *J Biochem*, *165*(6), 455-458. https://doi.org/10.1093/jb/mvz004

Hlubek, F., Spaderna, S., Schmalhofer, O., Jung, A., Kirchner, T., & Brabletz, T. (2007). Wnt/FZD signaling and colorectal cancer morphogenesis. *Front Biosci*, *12*, 458-470. https://doi.org/10.2741/2075

Hogan, Brigid L. M., Barkauskas, Christina E., Chapman, Harold A., Epstein, Jonathan A., Jain, R., Hsia, Connie C. W., Niklason, L., Calle, E., Le, A., Randell, Scott H., Rock, J., Snitow, M., Krummel, M., Stripp, Barry R., Vu, T., White, Eric S., Whitsett, Jeffrey A., & Morrisey, Edward E. (2014). Repair and Regeneration of the Respiratory System: Complexity, Plasticity, and Mechanisms of Lung Stem Cell Function. *Cell Stem Cell*, *15*(2), 123-138. https://doi.org/10.1016/j.stem.2014.07.012

Hong, K. O., Kim, J. H., Hong, J. S., Yoon, H. J., Lee, J. I., Hong, S. P., & Hong, S. D. (2009). Inhibition of Akt activity induces the mesenchymal-to-epithelial reverting transition with restoring E-cadherin expression in KB and KOSCC-25B oral squamous cell carcinoma cells. *J Exp Clin Cancer Res*, *28*(1), 28. https://doi.org/10.1186/1756-9966-28-28

Hu, Q., Yin, J., Zeng, A., Jin, X., Zhang, Z., Yan, W., & You, Y. (2018). H19 Functions as a Competing Endogenous RNA to Regulate EMT by Sponging miR-130a-3p in Glioma. *Cell Physiol Biochem*, *50*(1), 233-245. https://doi.org/10.1159/000494002

Huang, L., Sun, J., Ma, Y., Chen, H., Tian, C., & Dong, M. (2024). MSI2 regulates NLK-mediated EMT and PI3K/AKT/mTOR pathway to promote pancreatic cancer progression. *Cancer Cell International*, *24*(1), 273. https://doi.org/10.1186/s12935-024-03444-9

Hübner, M. R., & Spector, D. L. (2010). Role of H3K27 demethylases Jmjd3 and UTX in transcriptional regulation. *Cold Spring Harb Symp Quant Biol*, *75*, 43-49. https://doi.org/10.1101/sqb.2010.75.020

Hynes, R. O. (2002). Integrins: bidirectional, allosteric signaling machines. *Cell*, *110*(6), 673-687. https://doi.org/10.1016/s0092-8674(02)00971-6

Hynes, R. O. (2009). The Extracellular Matrix: Not Just Pretty Fibrils. *Science*, *326*(5957), 1216-1219. https://doi.org/doi:10.1126/science.1176009

Ikenouchi, J., Sasaki, H., Tsukita, S., Furuse, M., & Tsukita, S. (2008). Loss of occludin affects tricellular localization of tricellulin. *Mol Biol Cell*, *19*(11), 4687-4693. https://doi.org/10.1091/mbc.e08-05-0530

Iking-Konert, C., Ostendorf, B., Sander, O., Jost, M., Wagner, C., Joosten, L., Schneider, M., & Hänsch, G. (2005). Transdifferentiation of polymorphonuclear neutrophils to dendritic-like cells at the site of inflammation in rheumatoid arthritis: evidence for activation by T cells. *Annals of the rheumatic diseases*, *64*(10), 1436-1442.

Indugula, S. R., Ayala, S. S., Vetrini, F., Belonis, A., & Zhang, W. (2022). Exome sequencing identified a novel HIST1H1E heterozygous protein-truncating variant in a 6-month-old male patient with Rahman syndrome: A case report. *Clinical Case Reports*, *10*(2), e05370. https://doi.org/https://doi.org/10.1002/ccr3.5370

Ingham, P. W., & McMahon, A. P. (2001). Hedgehog signaling in animal development: paradigms and principles. *Genes Dev*, *15*(23), 3059-3087. https://doi.org/10.1101/gad.938601

Ivanyi-Nagy, R., Ahmed, S. M., Peter, S., Ramani, P. D., Ong, P. F., Dreesen, O., & Dröge, P. (2018). The RNA interactome of human telomerase RNA reveals a coding-independent role for a histone mRNA in telomere homeostasis. *Elife*, *7*. https://doi.org/10.7554/eLife.40037

Izzo, A., Kamieniarz, K., & Schneider, R. (2008). The histone H1 family: specific members, specific functions? *Biol Chem*, *389*(4), 333-343. https://doi.org/10.1515/bc.2008.037

Izzo, A., Kamieniarz-Gdula, K., Ramírez, F., Noureen, N., Kind, J., Manke, T., van Steensel, B., & Schneider, R. (2013). The genomic landscape of the somatic linker histone subtypes H1.1 to H1.5 in human cells. *Cell Rep*, *3*(6), 2142-2154. https://doi.org/10.1016/j.celrep.2013.05.003

Jaenisch, R., & Bird, A. (2003). Epigenetic regulation of gene expression: how the genome integrates intrinsic and environmental signals. *Nat Genet*, *33 Suppl*, 245-254. https://doi.org/10.1038/ng1089

Jarov, A., Williams, K. P., Ling, L. E., Koteliansky, V. E., Duband, J.-L., & Fournier-Thibault, C. (2003). A dual role for Sonic hedgehog in regulating adhesion and differentiation of neuroepithelial cells. *Developmental biology*, *261*(2), 520-536. https://doi.org/https://doi.org/10.1016/S0012-1606(03)00351-8

Kalluri, R., & Weinberg, R. A. (2009). The basics of epithelial-mesenchymal transition. *J Clin Invest*, *119*(6), 1420-1428. https://doi.org/10.1172/JCI39104

Karafiat, V., Dvorakova, M., Pajer, P., Cermak, V., & Dvorak, M. (2007). Melanocyte fate in neural crest is triggered by Myb proteins through activation of c-kit. *Cellular and Molecular Life Sciences*, *64*, 2975-2984.

Kasai, Y., Nambu, J. R., Lieberman, P. M., & Crews, S. T. (1992). Dorsal-ventral patterning in Drosophila: DNA binding of snail protein to the single-minded gene. *Proceedings of the National Academy of Sciences*, *89*(8), 3414-3418.

Katsuno, Y., Lamouille, S., & Derynck, R. (2013). TGF-β signaling and epithelial-mesenchymal transition in cancer progression. *Curr Opin Oncol*, *25*(1), 76-84. https://doi.org/10.1097/CCO.0b013e32835b6371

Keller, G. (2005). Embryonic stem cell differentiation: emergence of a new era in biology and medicine. *Genes & development*, *19*(10), 1129-1155.

Khanbabaei, H., Ebrahimi, S., García-Rodríguez, J. L., Ghasemi, Z., Pourghadamyari, H., Mohammadi, M., & Kristensen, L. S. (2022). Non-coding RNAs and epithelial mesenchymal transition in cancer: molecular mechanisms and clinical implications. *Journal of*

Experimental & Clinical Cancer Research, *41*(1), 278. https://doi.org/10.1186/s13046-022-02488-x

Kim, W. K., Kwon, Y., Jang, M., Park, M., Kim, J., Cho, S., Jang, D. G., Lee, W.-B., Jung, S. H., Choi, H. J., Min, B. S., Il Kim, T., Hong, S. P., Paik, Y.-K., & Kim, H. (2019). β-catenin activation down-regulates cell-cell junction-related genes and induces epithelial-to-mesenchymal transition in colorectal cancers. *Scientific Reports*, *9*(1), 18440. https://doi.org/10.1038/s41598-019-54890-9

Ko, U. H., Choi, J., Choung, J., Moon, S., & Shin, J. H. (2019). Physicochemically Tuned Myofibroblasts for Wound Healing Strategy. *Scientific Reports*, *9*(1), 16070. https://doi.org/10.1038/s41598-019-52523-9

Kohan, M., Muro, A. F., White, E. S., & Berkman, N. (2010). EDA-containing cellular fibronectin induces fibroblast differentiation through binding to alpha4beta7 integrin receptor and MAPK/Erk 1/2-dependent signaling. *Faseb j*, *24*(11), 4503-4512. https://doi.org/10.1096/fj.10-154435

Konishi, A., Shimizu, S., Hirota, J., Takao, T., Fan, Y., Matsuoka, Y., Zhang, L., Yoneda, Y., Fujii, Y., Skoultchi, A. I., & Tsujimoto, Y. (2003). Involvement of histone H1.2 in apoptosis induced by DNA double-strand breaks. *Cell*, *114*(6), 673-688. https://doi.org/10.1016/s0092-8674(03)00719-0

Kouzarides, T. (2007). Chromatin modifications and their function. *Cell*, *128*(4), 693-705. https://doi.org/10.1016/j.cell.2007.02.005

Kriz, W., Kaissling, B., & Le Hir, M. (2011). Epithelial-mesenchymal transition (EMT) in kidney fibrosis: fact or fantasy? *J Clin Invest*, *121*(2), 468-474. https://doi.org/10.1172/jci44595

Kume, T., Deng, K., & Hogan, B. L. (2000). Murine forkhead/winged helix genes Foxc1 (Mf1) and Foxc2 (Mfh1) are required for the early organogenesis of the kidney and urinary tract. *Development*, *127*(7), 1387-1395. https://doi.org/10.1242/dev.127.7.1387

Lai, S., Jia, J., Cao, X., Zhou, P. K., & Gao, S. (2021). Molecular and Cellular Functions of the Linker Histone H1.2. *Front Cell Dev Biol*, *9*, 773195. https://doi.org/10.3389/fcell.2021.773195

Lambert, A. W., & Weinberg, R. A. (2021). Linking EMT programmes to normal and neoplastic epithelial stem cells. *Nat Rev Cancer*, *21*(5), 325-338. https://doi.org/10.1038/s41568-021-00332-6

Lamouille, S., Xu, J., & Derynck, R. (2014). Molecular mechanisms of epithelial-mesenchymal transition. *Nat Rev Mol Cell Biol*, *15*(3), 178-196. https://doi.org/10.1038/nrm3758

Lamouille, S., Xu, J., & Derynck, R. (2014). Molecular mechanisms of epithelial–mesenchymal transition. *Nature reviews Molecular cell biology*, *15*(3), 178-196.

Larue, L., & Bellacosa, A. (2005). Epithelial-mesenchymal transition in development and cancer: role of phosphatidylinositol 3' kinase/AKT pathways. *Oncogene*, *24*(50), 7443-7454. https://doi.org/10.1038/sj.onc.1209091

Lee, H., Habas, R., & Abate-Shen, C. (2004). MSX1 cooperates with histone H1b for inhibition of transcription and myogenesis. *Science*, *304*(5677), 1675-1678. https://doi.org/10.1126/science.1098096

Lee, J.-H., Laronde, S., Collins, T. J., Shapovalova, Z., Tanasijevic, B., McNicol, J. D., Fiebig-Comyn, A., Benoit, Y. D., Lee, J. B., Mitchell, R. R., & Bhatia, M. (2017). Lineage-Specific Differentiation Is Influenced by State of Human Pluripotency. *Cell Reports*, *19*(1), 20-35. https://doi.org/10.1016/j.celrep.2017.03.036

Lei, W., Zhang, K., Pan, X., Hu, Y., Wang, D., Yuan, X., Shu, G., & Song, J. (2010). Histone deacetylase 1 is required for transforming growth factor-beta1-induced epithelial-mesenchymal transition. *Int J Biochem Cell Biol*, *42*(9), 1489-1497. https://doi.org/10.1016/j.biocel.2010.05.006

Lennox, R. W., & Cohen, L. H. (1983). The histone H1 complements of dividing and nondividing cells of the mouse. *Journal of Biological Chemistry*, *258*(1), 262-268. https://doi.org/https://doi.org/10.1016/S0021-9258(18)33251-4

Lever, M. A., Th'ng, J. P., Sun, X., & Hendzel, M. J. (2000). Rapid exchange of histone H1.1 on chromatin in living human cells. *Nature*, *408*(6814), 873-876. https://doi.org/10.1038/35048603

Li, C. W., Xia, W., Huo, L., Lim, S. O., Wu, Y., Hsu, J. L., Chao, C. H., Yamaguchi, H., Yang, N. K., Ding, Q., Wang, Y., Lai, Y. J., LaBaff, A. M., Wu, T. J., Lin, B. R., Yang, M. H., Hortobagyi, G. N., & Hung, M. C. (2012). Epithelial-mesenchymal transition induced by TNF-α requires NF-κB-mediated transcriptional upregulation of Twist1. *Cancer Res*, *72*(5), 1290-1300. https://doi.org/10.1158/0008-5472.Can-11-3123

Li, J. Y., Patterson, M., Mikkola, H. K., Lowry, W. E., & Kurdistani, S. K. (2012). Dynamic distribution of linker histone H1.5 in cellular differentiation. *PLoS Genet*, *8*(8), e1002879. https://doi.org/10.1371/journal.pgen.1002879

Li, X., Sun, B., Qian, H., Ma, J., Paolino, M., & Zhang, Z. (2022). A high-efficiency and versatile CRISPR/Cas9-mediated HDR-based biallelic editing system. *J Zhejiang Univ Sci B*, *23*(2), 141-152. https://doi.org/10.1631/jzus.B2100196

Liem Jr, K. F., Jessell, T. M., & Briscoe, J. (2000). Regulation of the neural patterning activity of sonic hedgehog by secreted BMP inhibitors expressed by notochord and somites. *Development*, *127*(22), 4855-4866.

Liem Jr, K. F., Tremml, G., Roelink, H., & Jessell, T. M. (1995). Dorsal differentiation of neural plate cells induced by BMP-mediated signals from epidermal ectoderm. *Cell*, *82*(6), 969-979.

Lin, Y. T., & Wu, K. J. (2020). Epigenetic regulation of epithelial-mesenchymal transition: focusing on hypoxia and TGF-β signaling. *J Biomed Sci*, *27*(1), 39. https://doi.org/10.1186/s12929-020-00632-3

Lindsley, R. C., Gill, J. G., Kyba, M., Murphy, T. L., & Murphy, K. M. (2006). Canonical Wnt signaling is required for development of embryonic stem

cell-derived mesoderm. *Development*, *133*(19), 3787-3796. https://doi.org/10.1242/dev.02551

Lindsley, R. C., Gill, J. G., Murphy, T. L., Langer, E. M., Cai, M., Mashayekhi, M., Wang, W., Niwa, N., Nerbonne, J. M., Kyba, M., & Murphy, K. M. (2008). Mesp1 coordinately regulates cardiovascular fate restriction and epithelial-mesenchymal transition in differentiating ESCs. *Cell Stem Cell*, *3*(1), 55-68. https://doi.org/10.1016/j.stem.2008.04.004

Linker, C., Lesbros, C., Gros, J., Burrus, L. W., Rawls, A., & Marcelle, C. (2005). beta-Catenin-dependent Wnt signalling controls the epithelial organisation of somites through the activation of paraxis. *Development*, *132*(17), 3895-3905. https://doi.org/10.1242/dev.01961

Liu, J., Xiao, Q., Xiao, J., Niu, C., Li, Y., Zhang, X., Zhou, Z., Shu, G., & Yin, G. (2022). Wnt/β-catenin signalling: function, biological mechanisms, and therapeutic opportunities. *Signal Transduction and Targeted Therapy*, *7*(1), 3. https://doi.org/10.1038/s41392-021-00762-6

Liu, P., Wakamiya, M., Shea, M. J., Albrecht, U., Behringer, R. R., & Bradley, A. (1999). Requirement for Wnt3 in vertebrate axis formation. *Nat Genet*, *22*(4), 361-365. https://doi.org/10.1038/11932

Lomelí, H., Starling, C., & Gridley, T. (2009). Epiblast-specific Snai1 deletion results in embryonic lethality due to multiple vascular defects. *BMC Res Notes*, *2*, 22. https://doi.org/10.1186/1756-0500-2-22

Losa, M., Risolino, M., Li, B., Hart, J., Quintana, L., Grishina, I., Yang, H., Choi, I. F., Lewicki, P., Khan, S., Aho, R., Feenstra, J., Vincent, C. T., Brown, A. M. C., Ferretti, E., Williams, T., & Selleri, L. (2018). Face morphogenesis is promoted by Pbx-dependent EMT via regulation of Snail1 during frontonasal prominence fusion. *Development*, *145*(5). https://doi.org/10.1242/dev.157628

Lu, X., Hamkalo, B., Parseghian, M. H., & Hansen, J. C. (2009). Chromatin condensing functions of the linker histone C-terminal domain are mediated by specific amino acid composition and intrinsic protein disorder. *Biochemistry*, *48*(1), 164-172. https://doi.org/10.1021/bi801636y

Lu, X., & Hansen, J. C. (2004). Identification of specific functional subdomains within the linker histone H10 C-terminal domain. *J Biol Chem*, *279*(10), 8701-8707. https://doi.org/10.1074/jbc.M311348200

Luger, K., Mäder, A. W., Richmond, R. K., Sargent, D. F., & Richmond, T. J. (1997). Crystal structure of the nucleosome core particle at 2.8 Å resolution. *Nature*, *389*(6648), 251-260. https://doi.org/10.1038/38444

Lv, M., Zhong, Z., Huang, M., Tian, Q., Jiang, R., & Chen, J. (2017). lncRNA H19 regulates epithelial-mesenchymal transition and metastasis of bladder cancer by miR-29b-3p as competing endogenous RNA. *Biochim Biophys Acta Mol Cell Res*, *1864*(10), 1887-1899. https://doi.org/10.1016/j.bbamcr.2017.08.001

Ma, C., Malessa, A., Boersma, A. J., Liu, K., & Herrmann, A. (2020). Supercharged Proteins and Polypeptides. *Advanced Materials*, *32*(20), 1905309. https://doi.org/https://doi.org/10.1002/adma.201905309

Mackey-Cushman, S., Gao, J., Holmes, D. A., Nunoya, J. i., Wang, R., Unutmaz, D., & su, L. (2011). FoxP3 Interacts with Linker Histone H1.5 to Modulate Gene Expression and Program Treg Cell Activity. *Genes and immunity*, *12*, 559-567. https://doi.org/10.1038/gene.2011.31

Madapura, P., & Rao, S. (2007). Chromatin remodeling during mammalian spermatogenesis: Role of testis specific histone variants and transition proteins. *Society of Reproduction and Fertility supplement*, *63*, 1-10.

Mahadevan, I. A., Kumar, S., & Rao, M. R. S. (2020). Linker histone variant H1t is closely associated with repressed repeat-element chromatin domains in pachytene spermatocytes. *Epigenetics Chromatin*, *13*(1), 9. https://doi.org/10.1186/s13072-020-00335-x

Mandemaker, I. K., van Cuijk, L., Janssens, R. C., Lans, H., Bezstarosti, K., Hoeijmakers, J. H., Demmers, J. A., Vermeulen, W., & Marteijn, J. A. (2017). DNA damage-induced histone H1 ubiquitylation is mediated by HUWE1 and stimulates the RNF8-RNF168 pathway. *Sci Rep*, *7*(1), 15353. https://doi.org/10.1038/s41598-017-15194-y

Marconi, G., Fonticoli, L., Thangavelu, S. R., Trubiani, O., & Diomede, F. (2021). Epithelial-Mesenchymal Transition (EMT): The Type-2 EMT in Wound Healing, Tissue Regeneration and Organ Fibrosis. *Cells*, *10*, 1587. https://doi.org/10.3390/cells10071587

Mariño-Ramírez, L., Kann, M. G., Shoemaker, B. A., & Landsman, D. (2005). Histone structure and nucleosome stability. *Expert Rev Proteomics*, *2*(5), 719-729. https://doi.org/10.1586/14789450.2.5.719

Massagué, J. (2012). TGFβ signalling in context. *Nat Rev Mol Cell Biol*, *13*(10), 616-630. https://doi.org/10.1038/nrm3434

Mathur, R., Wang, Q., Schupp, P. G., Nikolic, A., Hilz, S., Hong, C., Grishanina, N. R., Kwok, D., Stevers, N. O., Jin, Q., Youngblood, M. W., Stasiak, L. A., Hou, Y., Wang, J., Yamaguchi, T. N., Lafontaine, M., Shai, A., Smirnov, I. V., Solomon, D. A.,…Costello, J. F. (2024). Glioblastoma evolution and heterogeneity from a 3D whole-tumor perspective. *Cell*, *187*(2), 446-463.e416. https://doi.org/10.1016/j.cell.2023.12.013

Matsushima, H., Geng, S., Lu, R., Okamoto, T., Yao, Y., Mayuzumi, N., Kotol, P. F., Chojnacki, B. J., Miyazaki, T., & Gallo, R. L. (2013). Neutrophil differentiation into a unique hybrid population exhibiting dual phenotype and functionality of neutrophils and dendritic cells. *Blood, The Journal of the American Society of Hematology*, *121*(10), 1677-1689.

Mayor, R., Izquierdo-Bouldstridge, A., Millán-Ariño, L., Bustillos, A., Sampaio, C., Luque, N., & Jordan, A. (2015). Genome distribution of replication-independent histone H1 variants shows H1.0 associated with nucleolar domains and H1X associated with RNA polymerase II-enriched regions. *J Biol Chem*, *290*(12), 7474-7491. https://doi.org/10.1074/jbc.M114.617324

Medici, D., Hay, E. D., & Olsen, B. R. (2008). Snail and Slug promote epithelial-mesenchymal transition through beta-catenin-T-cell factor-4-dependent expression of transforming growth factor-beta3. *Mol Biol Cell*, *19*(11), 4875-4887. https://doi.org/10.1091/mbc.e08-05-0506

Medrzycki, M., Zhang, Y., Zhang, W., Cao, K., Pan, C., Lailler, N., McDonald, J. F., Bouhassira, E. E., & Fan, Y. (2014). Histone h1.3 suppresses h19 noncoding RNA expression and cell growth of ovarian cancer cells. *Cancer Res*, *74*(22), 6463-6473. https://doi.org/10.1158/0008-5472.Can-13-2922

Millán-Ariño, L., Islam, A. B., Izquierdo-Bouldstridge, A., Mayor, R., Terme, J. M., Luque, N., Sancho, M., López-Bigas, N., & Jordan, A. (2014). Mapping of six somatic linker histone H1 variants in human breast cancer cells uncovers specific features of H1.2. *Nucleic Acids Res*, *42*(7), 4474-4493. https://doi.org/10.1093/nar/gku079

Mills, C. (2012). M1 and M2 macrophages: oracles of health and disease. *Critical Reviews™ in Immunology*, *32*(6).

Mills, C. D. (2015). Anatomy of a Discovery: M1 and M2 Macrophages [Review]. *Frontiers in Immunology*, *6*. https://doi.org/10.3389/fimmu.2015.00212

Misteli, T. (2020). The Self-Organizing Genome: Principles of Genome Architecture and Function. *Cell*, *183*(1), 28-45. https://doi.org/10.1016/j.cell.2020.09.014

Na, Y. R., Seok, S. H., Kim, D. J., Han, J. H., Kim, T. H., Jung, H., Lee, B. H., & Park, J. H. (2009). Bone morphogenetic protein 7 induces mesenchymal-to-epithelial transition in melanoma cells, leading to inhibition of metastasis. *Cancer Sci*, *100*(11), 2218-2225. https://doi.org/10.1111/j.1349-7006.2009.01301.x

Nakaya, Y., Kuroda, S., Katagiri, Y. T., Kaibuchi, K., & Takahashi, Y. (2004). Mesenchymal-epithelial transition during somitic segmentation is regulated by differential roles of Cdc42 and Rac1. *Dev Cell*, *7*(3), 425-438. https://doi.org/10.1016/j.devcel.2004.08.003

Nakaya, Y., & Sheng, G. (2008). Epithelial to mesenchymal transition during gastrulation: an embryological view. *Development, growth & differentiation*, *50*(9), 755-766.

Nakaya, Y., & Sheng, G. (2013). EMT in developmental morphogenesis. *Cancer letters*, *341*(1), 9-15.

Nieto, M. A., Sargent, M. G., Wilkinson, D. G., & Cooke, J. (1994). Control of cell behavior during vertebrate development by Slug, a zinc finger gene. *Science*, *264*(5160), 835-839.

Nocera, G., & Jacob, C. (2020). Mechanisms of Schwann cell plasticity involved in peripheral nerve repair after injury. *Cell Mol Life Sci*, *77*(20), 3977-3989. https://doi.org/10.1007/s00018-020-03516-9

Noll, M. (1976). Differences and similarities in chromatin structure of neurospora crassa and higher eucaryotes. *Cell*, *8*(3), 349-355. https://doi.org/https://doi.org/10.1016/0092-8674(76)90146-X

Oko, R. J., Jando, V., Wagner, C. L., Kistler, W. S., & Hermo, L. S. (1996). Chromatin reorganization in rat spermatids during the disappearance of testis-specific histone, H1t, and the appearance of transition proteins TP1 and TP2. *Biol Reprod*, *54*(5), 1141-1157. https://doi.org/10.1095/biolreprod54.5.1141

Oltean, S., Febbo, P. G., & Garcia-Blanco, M. A. (2008). Dunning rat prostate adenocarcinomas and alternative splicing reporters: powerful tools to study epithelial plasticity in prostate tumors in vivo. *Clin Exp Metastasis*, *25*(6), 611-619. https://doi.org/10.1007/s10585-008-9186-y

Oltean, S., Sorg, B. S., Albrecht, T., Bonano, V. I., Brazas, R. M., Dewhirst, M. W., & Garcia-Blanco, M. A. (2006). Alternative inclusion of fibroblast growth factor receptor 2 exon IIIc in Dunning prostate tumors reveals unexpected epithelial mesenchymal plasticity. *Proc Natl Acad Sci U S A*, *103*(38), 14116-14121. https://doi.org/10.1073/pnas.0603090103

Otero, M., Plumb, D. A., Tsuchimochi, K., Dragomir, C. L., Hashimoto, K., Peng, H., Olivotto, E., Bevilacqua, M., Tan, L., Yang, Z., Zhan, Y., Oettgen, P., Li, Y., Marcu, K. B., & Goldring, M. B. (2012). E74-like factor 3 (ELF3) impacts on matrix metalloproteinase 13 (MMP13) transcriptional control in articular chondrocytes under proinflammatory stress. *J Biol Chem*, *287*(5), 3559-3572. https://doi.org/10.1074/jbc.M111.265744

Paksa, A., & Rajagopal, J. (2017). The epigenetic basis of cellular plasticity. *Curr Opin Cell Biol*, *49*, 116-122. https://doi.org/10.1016/j.ceb.2018.01.003

Pan, C., & Fan, Y. (2016). Role of H1 linker histones in mammalian development and stem cell differentiation. *Biochimica et Biophysica Acta (BBA) - Gene Regulatory Mechanisms*, *1859*(3), 496-509. https://doi.org/https://doi.org/10.1016/j.bbagrm.2015.12.002

Pang, Q. Y., Tan, T. Z., Sundararajan, V., Chiu, Y. C., Chee, E. Y. W., Chung, V. Y., Choolani, M. A., & Huang, R. Y. (2022). 3D genome organization in the epithelial-mesenchymal transition spectrum. *Genome Biol*, *23*(1), 121. https://doi.org/10.1186/s13059-022-02687-x

Park, S.-M., Gaur, A. B., Lengyel, E., & Peter, M. E. (2008). The miR-200 family determines the epithelial phenotype of cancer cells by targeting the E-cadherin repressors ZEB1 and ZEB2. *Genes & development*, *22*(7), 894-907.

Parseghian, M. H., & Hamkalo, B. A. (2001). A compendium of the histone H1 family of somatic subtypes: an elusive cast of characters and their characteristics. *Biochem Cell Biol*, *79*(3), 289-304.

Pavlič, A., Hauptman, N., Boštjančič, E., & Zidar, N. (2022). Long Non-Coding RNAs as Potential Regulators of EMT-Related Transcription Factors in Colorectal Cancer-A Systematic Review and Bioinformatics Analysis. *Cancers (Basel)*, *14*(9). https://doi.org/10.3390/cancers14092280

Pfefferle, A., Jacobs, B., Netskar, H., Ask, E. H., Lorenz, S., Clancy, T., Goodridge, J. P., Sohlberg, E., & Malmberg, K.-J. (2019). Intra-lineage Plasticity and Functional Reprogramming Maintain Natural Killer Cell Repertoire Diversity. *Cell Reports*, *29*(8), 2284-2294.e2284. https://doi.org/10.1016/j.celrep.2019.10.058

Pinson, K. I., Brennan, J., Monkley, S., Avery, B. J., & Skarnes, W. C. (2000). An LDL-receptor-related protein mediates Wnt signalling in mice. *Nature*, *407*(6803), 535-538. https://doi.org/10.1038/35035124

Pöpperl, H., Schmidt, C., Wilson, V., Hume, C. R., Dodd, J., Krumlauf, R., & Beddington, R. S. (1997). Misexpression of Cwnt8C in the mouse induces an ectopic embryonic axis and causes a truncation of the anterior neuroectoderm. *Development*, *124*(15), 2997-3005. https://doi.org/10.1242/dev.124.15.2997

Powell, D. W., Mifflin, R. C., Valentich, J. D., Crowe, S. E., Saada, J. I., & West, A. B. (1999). Myofibroblasts. I. Paracrine cells important in health and disease. *Am J Physiol*, *277*(1), C1-9. https://doi.org/10.1152/ajpcell.1999.277.1.C1

Qu, N., Luan, T., Liu, N., Kong, C., Xu, L., Yu, H., Kang, Y., & Han, Y. (2023). Hepatocyte nuclear factor 4 a (HNF4α): A perspective in cancer. *Biomedicine & Pharmacotherapy*, *169*, 115923. https://doi.org/https://doi.org/10.1016/j.biopha.2023.115923

Quina, A. S., Buschbeck, M., & Di Croce, L. (2006). Chromatin structure and epigenetics. *Biochemical Pharmacology*, *72*(11), 1563-1569. https://doi.org/https://doi.org/10.1016/j.bcp.2006.06.016

Rajabi, F., Smith, R., Liu-Bordes, W.-Y., Schertzer, M., Huet, S., & Londoño-Vallejo, A. (2024). DNA damage-induced PARP/ALC1 activation leads to Epithelial-to-Mesenchymal transition stimulating homologous recombination. *bioRxiv*, 2024.2001.2016.575847. https://doi.org/10.1101/2024.01.16.575847

Rajabi, H., & Kufe, D. (2017). MUC1-C oncoprotein integrates a program of EMT, epigenetic reprogramming and immune evasion in human carcinomas. *Biochimica et Biophysica Acta (BBA)-Reviews on Cancer*, *1868*(1), 117-122.

Ramadoss, S., Chen, X., & Wang, C. Y. (2012). Histone demethylase KDM6B promotes epithelial-mesenchymal transition. *J Biol Chem*, *287*(53), 44508-44517. https://doi.org/10.1074/jbc.M112.424903

Ramakrishnan, V., Finch, J. T., Graziano, V., Lee, P. L., & Sweet, R. M. (1993). Crystal structure of globular domain of histone H5 and its implications for nucleosome binding. *Nature*, *362*(6417), 219-223. https://doi.org/10.1038/362219a0

Reckzeh, K., & Cammenga, J. (2010). Molecular mechanisms underlying deregulation of C/EBPalpha in acute myeloid leukemia. *Int J Hematol*, *91*(4), 557-568. https://doi.org/10.1007/s12185-010-0573-1

Reske, J. J., Wilson, M. R., Holladay, J., Wegener, M., Adams, M., & Chandler, R. L. (2020). SWI/SNF inactivation in the endometrial epithelium leads to loss of epithelial integrity. *Human Molecular Genetics*, *29*(20), 3412-3430. https://doi.org/10.1093/hmg/ddaa227

Roque, A., Iloro, I., Ponte, I., Arrondo, J. L. R., & Suau, P. (2005). DNA-induced Secondary Structure of the Carboxyl-terminal Domain of Histone H1*. *Journal of Biological Chemistry*, *280*(37), 32141-32147. https://doi.org/https://doi.org/10.1074/jbc.M505636200

Rossant, J., Ciruna, B., & Partanen, J. (1997). FGF signaling in mouse gastrulation and anteroposterior patterning. *Cold Spring Harb Symp Quant Biol*, *62*, 127-133.

Saitoh, M. (2023). Transcriptional regulation of EMT transcription factors in cancer. *Semin Cancer Biol*, *97*, 21-29. https://doi.org/10.1016/j.semcancer.2023.10.001

Sancho, M., Diani, E., Beato, M., & Jordan, A. (2008). Depletion of human histone H1 variants uncovers specific roles in gene expression and cell growth. *PLoS Genet*, *4*(10), e1000227. https://doi.org/10.1371/journal.pgen.1000227

Sancho, M., Diani, E., Beato, M., Jordan, A.,. (2008). Depletion of Human Histone H1 Variants Uncovers Specific Roles in Gene Expression and Cell Growth. e1000227. *PLOS Genetics*, *4,*.

Sauka-Spengler, T., & Bronner-Fraser, M. (2008). A gene regulatory network orchestrates neural crest formation. *Nat Rev Mol Cell Biol*, *9*(7), 557-568. https://doi.org/10.1038/nrm2428

Scadden, David T. (2014). Nice Neighborhood: Emerging Concepts of the Stem Cell Niche. *Cell*, *157*(1), 41-50. https://doi.org/10.1016/j.cell.2014.02.013

Schmidt, C., Stoeckelhuber, M., McKinnell, I., Putz, R., Christ, B., & Patel, K. (2004). Wnt 6 regulates the epithelialisation process of the segmental plate mesoderm leading to somite formation. *Dev Biol*, *271*(1), 198-209. https://doi.org/10.1016/j.ydbio.2004.03.016

Schuettengruber, B., & Cavalli, G. (2009). Recruitment of polycomb group complexes and their role in the dynamic regulation of cell fate choice. *Development*, *136*(21), 3531-3542. https://doi.org/10.1242/dev.033902

Sedzinski, J., Hannezo, E., Tu, F., Biro, M., & Wallingford, J. B. (2016). Emergence of an Apical Epithelial Cell Surface In Vivo. *Developmental Cell*, *36*(1), 24-35. https://doi.org/https://doi.org/10.1016/j.devcel.2015.12.013

Semënov, M. V., Tamai, K., Brott, B. K., Kühl, M., Sokol, S., & He, X. (2001). Head inducer Dickkopf-1 is a ligand for Wnt coreceptor LRP6. *Curr Biol*, *11*(12), 951-961. https://doi.org/10.1016/s0960-9822(01)00290-1

Sengez, B., Aygun, I., Shehwana, H., Toyran, N., Avci, S., Konu, O., Stemmler, M., & Alotaibi, H. (2019). The Transcription Factor Elf3 Is Essential for a Successful Mesenchymal to Epithelial Transition. *8*, 858. https://doi.org/10.3390/cells8080858

Serna-Pujol, N., Salinas-Pena, M., Mugianesi, F., Le Dily, F., Marti-Renom, M. A., & Jordan, A. (2022). Coordinated changes in gene expression, H1 variant distribution and genome 3D conformation in response to H1 depletion. *Nucleic Acids Res*, *50*(7), 3892-3910. https://doi.org/10.1093/nar/gkac226

Serrano-Gomez, S. J., Maziveyi, M., & Alahari, S. K. (2016). Regulation of epithelial-mesenchymal transition through epigenetic and post-translational modifications. *Molecular Cancer*, *15*(1), 18. https://doi.org/10.1186/s12943-016-0502-x

Setlai, B. P., Hull, R., Reis, R. M., Agbor, C., Ambele, M. A., Mulaudzi, T. V., & Dlamini, Z. (2022). MicroRNA Interrelated Epithelial Mesenchymal Transition (EMT) in Glioblastoma. *Genes (Basel)*, *13*(2). https://doi.org/10.3390/genes13020244

Shah, S. B., Skromne, I., Hume, C. R., Kessler, D. S., Lee, K. J., Stern, C. D., & Dodd, J. (1997). Misexpression of chick Vg1 in the marginal zone induces primitive streak formation. *Development*, *124*(24), 5127-5138. https://doi.org/10.1242/dev.124.24.5127

Shen, S., & Clairambault, J. (2020). Cell plasticity in cancer cell populations. *F1000Research*, *9*, 635. https://doi.org/10.12688/f1000research.24803.1

Shetty, S. S., Sharma, M., Fonseca, F. P., Jayaram, P., Tanwar, A. S., Kabekkodu, S. P., Satyamoorthy, K., & Radhakrishnan, R. (2020). Signaling pathways promoting epithelial mesenchymal transition in oral submucous fibrosis and oral squamous cell carcinoma. *Japanese Dental Science Review*, *56*(1), 97-108. https://doi.org/https://doi.org/10.1016/j.jdsr.2020.07.002

Sica, A., & Mantovani, A. (2012). Macrophage plasticity and polarization: in vivo veritas. *The Journal of clinical investigation*, *122*(3), 787-795.

Skromne, I., & Stern, C. D. (2001). Interactions between Wnt and Vg1 signalling pathways initiate primitive streak formation in the chick embryo. *Development*, *128*(15), 2915-2927. https://doi.org/10.1242/dev.128.15.2915

Smigielski, L., Jagannath, V., Rössler, W., Walitza, S., & Grünblatt, E. (2020). Epigenetic mechanisms in schizophrenia and other psychotic disorders: a systematic review of empirical human findings. *Molecular Psychiatry*, *25*(8), 1718-1748. https://doi.org/10.1038/s41380-019-0601-3

Sokolova, V., Sarkar, S., & Tan, D. (2022). Histone Variants and Chromatin Structure, Update of Advances. *Computational and Structural Biotechnology Journal*, *21*. https://doi.org/10.1016/j.csbj.2022.12.002

Song, Y., Wang, R., Li, L.-W., Liu, X., Wang, Y.-F., Wang, Q.-X., & Zhang, Q. (2018). Long non-coding RNA HOTAIR mediates the switching of histone H3 lysine 27 acetylation to methylation to promote epithelial-to-mesenchymal transition in gastric cancer. *International Journal of Oncology*, *54*. https://doi.org/10.3892/ijo.2018.4625

Spatz, L. B., Jin, R. U., & Mills, J. C. (2021). Cellular plasticity at the nexus of development and disease. *Development*, *148*(3). https://doi.org/10.1242/dev.197392

Spender, L. C., O'Brien, D. I., Simpson, D., Dutt, D., Gregory, C. D., Allday, M. J., Clark, L. J., & Inman, G. J. (2009). TGF-β induces apoptosis in human B cells by transcriptional regulation of BIK and BCL-XL. *Cell Death & Differentiation*, *16*(4), 593-602. https://doi.org/10.1038/cdd.2008.183

Suzuki, T., Conant, A., Curow, C., Alexander, A., Ioffe, Y., & Unternaehrer, J. (2023). Role of epithelial-mesenchymal transition factor SNAI1 and its targets in ovarian cancer aggressiveness. *Journal of Cancer Metastasis and Treatment*, *9*, 25. https://doi.org/10.20517/2394-4722.2023.34

Takahashi, Y., Hiraoka, S., Kitajima, S., Inoue, T., Kanno, J., & Saga, Y. (2005). Differential contributions of Mesp1 and Mesp2 to the epithelialization and rostro-caudal patterning of somites. *Development*, *132*(4), 787-796. https://doi.org/10.1242/dev.01597

Takahashi, Y., Koizumi, K., Takagi, A., Kitajima, S., Inoue, T., Koseki, H., & Saga, Y. (2000). Mesp2 initiates somite segmentation through the Notch signalling pathway. *Nat Genet*, *25*(4), 390-396. https://doi.org/10.1038/78062

Takashima, A., & Yao, Y. (2015). Neutrophil plasticity: acquisition of phenotype and functionality of antigen-presenting cell. *Journal of Leucocyte Biology*, *98*(4), 489-496.

Takeichi, M. (1991). Cadherin cell adhesion receptors as a morphogenetic regulator. *Science*, *251*(5000), 1451-1455. https://doi.org/10.1126/science.2006419

Tanaka, H., Iguchi, N., Isotani, A., Kitamura, K., Toyama, Y., Matsuoka, Y., Onishi, M., Masai, K., Maekawa, M., Toshimori, K., Okabe, M., & Nishimune, Y. (2005). HANP1/H1T2, a novel histone H1-like protein involved in nuclear formation and sperm fertility. *Mol Cell Biol*, *25*(16), 7107-7119. https://doi.org/10.1128/mcb.25.16.7107-7119.2005

Tanaka, M., Hennebold, J. D., Macfarlane, J., & Adashi, E. Y. (2001). A mammalian oocyte-specific linker histone gene H1oo: homology with the genes for the oocyte-specific cleavage stage histone (cs-H1) of sea urchin and the B4/H1M histone of the frog. *Development*, *128*(5), 655-664. https://doi.org/10.1242/dev.128.5.655

Tatton-Brown, K., Loveday, C., Yost, S., Clarke, M., Ramsay, E., Zachariou, A., Elliott, A., Wylie, H., Ardissone, A., Rittinger, O., Stewart, F., Temple, I. K., Cole, T., Childhood Overgrowth, C., Mahamdallie, S., Seal, S., Ruark, E., & Rahman, N. (2017). Mutations in Epigenetic Regulation Genes Are a Major Cause of Overgrowth with Intellectual Disability. *Am J Hum Genet*, *100*(5), 725-736. https://doi.org/10.1016/j.ajhg.2017.03.010

Terme, J. M., Sesé, B., Millán-Ariño, L., Mayor, R., Belmonte, J. C. I., Barrero, M. J., & Jordan, A. (2011). Histone H1 variants are differentially expressed and incorporated into chromatin during differentiation and reprogramming to pluripotency. *J Biol Chem*, *286*(41), 35347-35357. https://doi.org/10.1074/jbc.M111.281923

Thiery, J. P. (2003). Epithelial–mesenchymal transitions in development and pathologies. *Current Opinion in Cell Biology*, *15*(6), 740-746. https://doi.org/https://doi.org/10.1016/j.ceb.2003.10.006

Thorslund, T., Ripplinger, A., Hoffmann, S., Wild, T., Uckelmann, M., Villumsen, B., Narita, T., Sixma, T. K., Choudhary, C., Bekker-Jensen, S., & Mailand, N. (2015). Histone H1 couples initiation and amplification of ubiquitin signalling after DNA damage. *Nature*, *527*(7578), 389-393. https://doi.org/10.1038/nature15401

Tie, Y., Tang, F., Peng, D., Zhang, Y., & Shi, H. (2022). TGF-beta signal transduction: biology, function and therapy for diseases. *Molecular Biomedicine*, *3*(1), 45. https://doi.org/10.1186/s43556-022-00109-9

Title, A. C., Hong, S.-J., Pires, N. D., Hasenöhrl, L., Godbersen, S., Stokar-Regenscheit, N., Bartel, D. P., & Stoffel, M. (2018). Genetic dissection of the miR-200–Zeb1 axis reveals its importance in tumor differentiation

and invasion. *Nature Communications*, *9*(1), 4671. https://doi.org/10.1038/s41467-018-07130-z

Tiwari, R., Manzar, N., & Ateeq, B. (2020). Dynamics of Cellular Plasticity in Prostate Cancer Progression [Review]. *Frontiers in Molecular Biosciences*, *7*. https://www.frontiersin.org/journals/molecular-biosciences/articles/10.3389/fmolb.2020.00130

Tominaga, K., & Suzuki, H. I. (2019). TGF-β Signaling in Cellular Senescence and Aging-Related Pathology. *Int J Mol Sci*, *20*(20). https://doi.org/10.3390/ijms20205002

Topczewska, J. M., Topczewski, J., Shostak, A., Kume, T., Solnica-Krezel, L., & Hogan, B. L. (2001). The winged helix transcription factor Foxc1a is essential for somitogenesis in zebrafish. *Genes Dev*, *15*(18), 2483-2493. https://doi.org/10.1101/gad.907401

Torres, C. M., Biran, A., Burney, M. J., Patel, H., Henser-Brownhill, T., Cohen, A. S., Li, Y., Ben-Hamo, R., Nye, E., Spencer-Dene, B., Chakravarty, P., Efroni, S., Matthews, N., Misteli, T., Meshorer, E., & Scaffidi, P. (2016). The linker histone H1.0 generates epigenetic and functional intratumor heterogeneity. *Science*, *353*(6307). https://doi.org/10.1126/science.aaf1644

Torres, M., Wang, J., Yannie, P. J., Ghosh, S., Segal, R. A., & Reynolds, A. M. (2019). Identifying important parameters in the inflammatory process with a mathematical model of immune cell influx and macrophage polarization. *PLoS Comput Biol*, *15*(7), e1007172. https://doi.org/10.1371/journal.pcbi.1007172

Tremblay, M. W., Green, M. V., Goldstein, B. M., Aldridge, A. I., Rosenfeld, J. A., Streff, H., Tan, W. D., Craigen, W., Bekheirnia, N., Al Tala, S., West, A. E., & Jiang, Y. H. (2022). Mutations of the histone linker H1-4 in neurodevelopmental disorders and functional characterization of neurons expressing C-terminus frameshift mutant H1.4. *Hum Mol Genet*, *31*(9), 1430-1442. https://doi.org/10.1093/hmg/ddab321

Tulsyan, S., Aftab, M., Sisodiya, S., Khan, A., Chikara, A., Tanwar, P., & Hussain, S. (2022). Molecular basis of epigenetic regulation in cancer diagnosis and treatment [Review]. *Frontiers in Genetics*, *13*. https://www.frontiersin.org/journals/genetics/articles/10.3389/fgene.2022.885635

van Genderen, C., Okamura, R. M., Farinas, I., Quo, R.-G., Parslow, T. G., Bruhn, L., & Grosschedl, R. (1994). Development of several organs that require inductive epithelial-mesenchymal interactions is impaired in LEF-1-deficient mice. *Genes & development*, *8*(22), 2691-2703.

van Roy, F., & Berx, G. (2008). The cell-cell adhesion molecule E-cadherin. *Cell Mol Life Sci*, *65*(23), 3756-3788. https://doi.org/10.1007/s00018-008-8281-1

Varlet, I., Collignon, J., & Robertson, E. J. (1997). nodal expression in the primitive endoderm is required for specification of the anterior axis during mouse gastrulation. *Development*, *124*(5), 1033-1044. https://doi.org/10.1242/dev.124.5.1033

Vicente-Dueñas, C., Cobaleda, C., Pérez-Losada, J., & Sánchez-García, I. (2010). The evolution of cancer modeling: the shadow of stem cells. *Dis Model Mech*, *3*(3-4), 149-155. https://doi.org/10.1242/dmm.002774

Vila, R., Ponte, I., Collado, M., Arrondo, J. L. R., Jiménez, M. A., Rico, M., & Suau, P. (2001). DNA-induced α-Helical Structure in the NH2-terminal Domain of Histone H1*. *Journal of Biological Chemistry*, *276*(49), 46429-46435. https://doi.org/https://doi.org/10.1074/jbc.M106952200

Villanueva, S., Glavic, A., Ruiz, P., & Mayor, R. (2002). Posteriorization by FGF, Wnt, and retinoic acid is required for neural crest induction. *Developmental biology*, *241*(2), 289-301.

Vincan, E., Brabletz, T., Faux, M. C., & Ramsay, R. G. (2007). A human three-dimensional cell line model allows the study of dynamic and reversible epithelial-mesenchymal and mesenchymal-epithelial transition that underpins colorectal carcinogenesis. *Cells Tissues Organs*, *185*(1-3), 20-28. https://doi.org/10.1159/000101299

Viola, A., Munari, F., Sánchez-Rodríguez, R., Scolaro, T., & Castegna, A. (2019). The Metabolic Signature of Macrophage Responses [Review]. *Frontiers in Immunology*, *10*. https://doi.org/10.3389/fimmu.2019.01462

von Gise, A., & Pu, W. T. (2012). Endocardial and epicardial epithelial to mesenchymal transitions in heart development and disease. *Circ Res*, *110*(12), 1628-1645. https://doi.org/10.1161/circresaha.111.259960

Wang, G., Sun, D., Li, W., & Xin, Y. (2021). CircRNA_100290 promotes GC cell proliferation and invasion via the miR-29b-3p/ITGA11 axis and is regulated by EIF4A3. *Cancer Cell Int*, *21*(1), 324. https://doi.org/10.1186/s12935-021-01964-2

Wang, P. H., Huang, B. S., Horng, H. C., Yeh, C. C., & Chen, Y. J. (2018). Wound healing. *J Chin Med Assoc*, *81*(2), 94-101. https://doi.org/10.1016/j.jcma.2017.11.002

Wang, Q.-S., Kong, P.-Z., Li, X.-Q., Yang, F., & Feng, Y.-M. (2015). FOXF2 deficiency promotes epithelial-mesenchymal transition and metastasis of basal-like breast cancer. *Breast Cancer Research*, *17*(1), 30. https://doi.org/10.1186/s13058-015-0531-1

Wang, X., Eichhorn, P. J. A., & Thiery, J. P. (2023). TGF-β, EMT, and resistance to anti-cancer treatment. *Seminars in Cancer Biology*, *97*, 1-11. https://doi.org/https://doi.org/10.1016/j.semcancer.2023.10.004

Warzecha, C. C., Sato, T. K., Nabet, B., Hogenesch, J. B., & Carstens, R. P. (2009). ESRP1 and ESRP2 are epithelial cell-type-specific regulators of FGFR2 splicing. *Mol Cell*, *33*(5), 591-601. https://doi.org/10.1016/j.molcel.2009.01.025

Whiteman, E. L., Liu, C. J., Fearon, E. R., & Margolis, B. (2008). The transcription factor snail represses Crumbs3 expression and disrupts apico-basal polarity complexes. *Oncogene*, *27*(27), 3875-3879. https://doi.org/10.1038/onc.2008.9

Wicker, M. N., & Wagner, K.-U. (2023). Cellular Plasticity in Mammary Gland Development and Breast Cancer. *Cancers*, *15*(23), 5605. https://www.mdpi.com/2072-6694/15/23/5605

Wiggan, O. N., Shaw, A. E., & Bamburg, J. R. (2006). Essential requirement for Rho family GTPase signaling in Pax3 induced mesenchymal–epithelial transition. *Cellular Signalling*, *18*(9), 1501-1514. https://doi.org/https://doi.org/10.1016/j.cellsig.2005.12.002

Wu, S., Du, Y., Beckford, J., & Alachkar, H. (2018). Upregulation of the EMT marker vimentin is associated with poor clinical outcome in acute myeloid leukemia. *Journal of Translational Medicine*, *16*(1), 170. https://doi.org/10.1186/s12967-018-1539-y

Xu, Q., & Tata, J. R. (1992). Characterization and developmental expression of Xenopus C/EBP gene. *Mechanisms of Development*, *38*(1), 69-81. https://doi.org/https://doi.org/10.1016/0925-4773(92)90039-M

Xu, R., Won, J. Y., Kim, C. H., Kim, D. E., & Yim, H. (2019). Roles of the Phosphorylation of Transcriptional Factors in Epithelial-Mesenchymal Transition. *J Oncol*, *2019*, 5810465. https://doi.org/10.1155/2019/5810465

Yan, W., Ma, L., Burns, K. H., & Matzuk, M. M. (2003). HILS1 is a spermatid-specific linker histone H1-like protein implicated in chromatin remodeling during mammalian spermiogenesis. *Proceedings of the National Academy of Sciences*, *100*(18), 10546-10551. https://doi.org/doi:10.1073/pnas.1837812100

Yang, C., Chen, H., Tan, G., Gao, W., Cheng, L., Jiang, X., Yu, L., & Tan, Y. (2013). FOXM1 promotes the epithelial to mesenchymal transition by stimulating the transcription of Slug in human breast cancer. *Cancer Lett*, *340*(1), 104-112. https://doi.org/10.1016/j.canlet.2013.07.004

Yang, J., Antin, P., Berx, G., Blanpain, C., Brabletz, T., Bronner, M., Campbell, K., Cano, A., Casanova, J., Christofori, G., Dedhar, S., Derynck, R., Ford, H. L., Fuxe, J., García de Herreros, A., Goodall, G. J., Hadjantonakis, A. K., Huang, R. Y. J., Kalcheim, C.,…Sheng, G. (2020). Guidelines and definitions for research on epithelial-mesenchymal transition. *Nat Rev Mol Cell Biol*, *21*(6), 341-352. https://doi.org/10.1038/s41580-020-0237-9

Yang, M. H., Wu, M. Z., Chiou, S. H., Chen, P. M., Chang, S. Y., Liu, C. J., Teng, S. C., & Wu, K. J. (2008). Direct regulation of TWIST by HIF-1alpha promotes metastasis. *Nat Cell Biol*, *10*(3), 295-305. https://doi.org/10.1038/ncb1691

Yates, C., Wells, A., & Turner, T. (2005). Luteinising hormone-releasing hormone analogue reverses the cell adhesion profile of EGFR overexpressing DU-145 human prostate carcinoma subline. *Br J Cancer*, *92*(2), 366-375. https://doi.org/10.1038/sj.bjc.6602350

Yates, C. C., Shepard, C. R., Stolz, D. B., & Wells, A. (2007). Co-culturing human prostate carcinoma cells with hepatocytes leads to increased expression of E-cadherin. *Br J Cancer*, *96*(8), 1246-1252. https://doi.org/10.1038/sj.bjc.6603700

Yee, D. S., Tang, Y., Li, X., Liu, Z., Guo, Y., Ghaffar, S., McQueen, P., Atreya, D., Xie, J., Simoneau, A. R., Hoang, B. H., & Zi, X. (2010). The Wnt inhibitory factor 1 restoration in prostate cancer cells was associated with reduced tumor growth, decreased capacity of cell migration and

invasion and a reversal of epithelial to mesenchymal transition. *Mol Cancer*, *9*, 162. https://doi.org/10.1186/1476-4598-9-162

Yu, F., Li, J., Chen, H., Fu, J., Ray, S., Huang, S., Zheng, H., & Ai, W. (2011). Kruppel-like factor 4 (KLF4) is required for maintenance of breast cancer stem cells and for cell migration and invasion. *Oncogene*, *30*(18), 2161-2172. https://doi.org/10.1038/onc.2010.591

Yu, Z., Mannik, J., Soto, A., Lin, K. K., & Andersen, B. (2009). The epidermal differentiation-associated Grainyhead gene Get1/Grhl3 also regulates urothelial differentiation. *EMBO J*, *28*(13), 1890-1903. https://doi.org/10.1038/emboj.2009.142

Zavadil, J., & Böttinger, E. P. (2005). TGF-beta and epithelial-to-mesenchymal transitions. *Oncogene*, *24*(37), 5764-5774. https://doi.org/10.1038/sj.onc.1208927

Zeisberg, M., Bottiglio, C., Kumar, N., Maeshima, Y., Strutz, F., Müller, G. A., & Kalluri, R. (2003). Bone morphogenic protein-7 inhibits progression of chronic renal fibrosis associated with two genetic mouse models. *Am J Physiol Renal Physiol*, *285*(6), F1060-1067. https://doi.org/10.1152/ajprenal.00191.2002

Zeisberg, M., Shah, A. A., & Kalluri, R. (2005). Bone morphogenic protein-7 induces mesenchymal to epithelial transition in adult renal fibroblasts and facilitates regeneration of injured kidney. *J Biol Chem*, *280*(9), 8094-8100. https://doi.org/10.1074/jbc.M413102200

Zhang, J., & Li, L. (2005). BMP signaling and stem cell regulation. *Dev Biol*, *284*(1), 1-11. https://doi.org/10.1016/j.ydbio.2005.05.009

Zhou, Z., Song, X., Chi, J., Gius, D. R., Huang, Y., Cristofanilli, M., & Wan, Y. (2020). Regulation of KLF4 by posttranslational modification circuitry in endocrine resistance. *Cellular Signalling*, *70*, 109574. https://doi.org/https://doi.org/10.1016/j.cellsig.2020.109574

8. APPENDIX

8.1. Appendix I.

Table 14. qPCR Primers and Probe Informations

Primer	Sequence	Probe
Cdh1 F	ATCCTCGCCCTGCTGATT	18
Cdh1 R	ACCACCGTTCTCCTCCGTA	18
Grhl3 F	AAGGAAGATGTCGAATGAACTTG	100
Grhl3 R	TCGTCCTCATTACTGTAGGGAAA	100
Elf3 F	ACCGAACCCTGACACACC	46
Elf3 R	AGCTGTACATGGCGTTGAAGT	46
Cebpα F	AAACAACGCAACGTGGAGA	47
Cebpα R	GCGGTCATTGTCACTGGTC	47
Klf4 F	CGGGAAGGGAGAAGACAC	62
Klf4 R	GAGTTCCTCACGCCAACG	62
Hnf4α F	AGCCTAAATGACAGGTCCTCT	73
Hnf4α R	TTAATCAGCTGGCCCCATT	73
Snai1 F	CTTGCTCCACAAGCACCA	71
Snai1 R	GAGGATGGGGAGGTAGCAG	71
Snai2 F	ATCCTTGGGGCGTGT AAG T	6
Snai2 R	TGAACCACTGTCATCCTTGG	6
Vim F	ACGTTTCCA AGCCTG ACCT	74
Vim R	AGCCACGCTTTCATACTGCT	74
Fn1 F	AGGTGGACCCCGCTAAAC	31
Fn1 R	TGCCGCAACTACTGTGATTC	31
Dnmt1_F	TGGCAAGCAAACCAGAGTCA	132
Dnmt 1_R	TTGCCTGAAGAGGTGGCTC	132
Dnmt3b_F	GTCGAAAAGCCAATGCAGGG	120
Dnmt3b _R	TTCACAGGTCTGGATGAGCG	120
Uhrf_F	TCAGAAGTCTCGGGGTGGT	14
Uhrf_R	CTGCCGGCTATGCTCACTT	14
Ddx17 F	GTGGAGGGTTTGGAGCAAGA	165
Ddx17 R	GTA ACCGCTCCCCAGGATTAC	165
h1b 142	CAAGGCTAAGAAGACCGGGG	142
1h1b 142	CCCGCAGTCTTCTTAGGCTT	142
1h1a 8	AGGTGGTGAAGGCCAAGAAG	8
h1a 8	ACTTTCGCCTTGGAAGCCTT	8
h1d	CGCGTCTAAAGCCGTAAAGC	117
h1d	CTTGGCTGCAACCTTCTTGG	117
H1C	CCAAGAAGGTGAAGGCTGCT	8
H1C 8	GGAAGCCTTAGCCTTGGGAG	8
h1f0	CCACCATGACCGAGAACTCC	149
h1f0	CGTGGACTTCTTGGAAGCCT	149
H1D-Human	GCTGCCAAGAGTCCAGCTAA	117
H1D-Human	TTGTAACCTTCGGCTTCCCC	117
H1C-Human	GCCCAAGAAAGCTGCCAAAA	135

H1C- Human	TAGGCTTGACAACCTTGGGC	135
Human H1E	GTCGGGTTCCTTCAAACTCA	60
Human H1E	GCTCCTGCTGGCTTCTTG	60
HIST1H1E-M-	AAGAAAGCGAAGAAGCCAGC	92
HIST1H1E-M	GTTGCCTTTGCCTTCTTCGG	92

Table 15. PCR Primers for gDNA and cDNA.

Primer	Sequence
KD-419	ATGCCCTCTGCTCAATAGGC
KD_420	GAACCTGCGTGCAATCCATC
KD_155	TCAGTTCATTCAGGGCACCGGACAG
SD-100	TCGTCCTCATTACTGTAGGGAAA
KD-396	CGCTCCTTGTCCTTCTGTTTGTT
KD_397	CGTCAAGAAGAAGGCCCGCAA
H1f1-F	AGCACAGCACTGCTCTATAAATACTCCGTGCAGG
H1f1-R	AACAAGTGTCAGGCTCTTTGAGTTATGTTGGTGGC
H1f2-F	ATCGGCGTACTGCCACTAGTTCCTGACTTCC
H1f2-R	TGGTGGCTCTGAAAAGAGCCTTTTGGATTGTTAGG
H1f3-F	AGGCAAAGCTGAAGATCCTTTCTCTGGCAACG
H1f3-R	TGCTCCTAAATGTACCCATAACAAAGTGCACAGAATTGATCTGC
H1f4-F	AGTCCTGGCCAGTCCCTCTGCTTCC
H1f4-R	AGAGCCTTTGGGTTGTTGGGCTTCTAAGCAG
H1f6-F	GATGCACCAATCACAGCGCGCCC
H1f6-R	ATAGGGACCCTAGGATTCTACTCTAGGGTTTCAACGACAGG
h1c 5'	GAAGTCAATGGGGTGCCCCG
h1c 5'	TTCTTTTTGGCAGGCGCCTTCT
h1b 5'	GCTATCACACTGGAAATATTGCG
h1b 5'	TCTTGTTAAGCTTGAAGGAACCA
h1a 5'	AGAGCTATTGTGTACTTGCATATC
h1a 5'	TAGAAGCAGCCTGAGCGACT
h1d 5'	CCAGTTGCTAAACTTCTGTTCCTTC
h1d 5'	GCCGCCTTCTTGTTGAGTTTGAA
h1f0 5'	AAATGTGCCGGCGCCCCAGC
h1f0 5'	GGCGCTTGATGGACAACTTGATCTG
h1c 5'	GAAGTCAATGGGGTGCCCCG
h1c 5'	TTCTTTTTGGCAGGCGCCTTCT
h1b 5'	GCTATCACACTGGAAATATTGCG
h1b 5'	TCTTGTTAAGCTTGAAGGAACCA

8.2. Ethics Approval

İZMİR BİYOTIP VE GENOM MERKEZİ
GİRİŞİMSEL OLMAYAN ARAŞTIRMALAR ETİK KURULU (İBG-GOEK)
KARARI

Toplantı Tarihi	: 26/05/2023	**Toplantı Günü**	: Cuma
Toplantı Sayısı	: 6	**Toplantı Saati**	: 10:30

Sayın Dr. Hani ALOTAİBİ,

2023-018 Protokol No'lu; sorumlusu olduğunuz "EMT ve MET'DE H1E'nin Fonksiyonel Katkısının İncelenmesi" başlıklı araştırmanın uygulanmasında etik açıdan sakınca olmadığına oy birliği ile karar verilmiştir.

Bilgilerinizi ve gereğini rica ederiz.

Prof. Dr. H. Alper BAĞRIYANIK **Başkan**	**Prof. Dr. Hilmi ORHAN** **Başkan Yardımcısı**
Prof. Dr. Sedef AKGÜNGÖR **Üye** (Katılmadı)	**Prof. Dr. Gülgün OKTAY** **Üye**
Dr. Serap ERKEK ÖZHAN **Üye** (Katılmadı)	**Prof. Dr. Şermin GENÇ** **Üye**
Doç. Dr. Canan Aslı YILDIRIM **Üye**	**Doç. Dr. Can KÜÇÜK** **Üye** (Katılmadı)
Dr. Öğr. Üyesi Yavuz OKTAY **Üye**	

8.3. Thesis Output

Part of this thesis was accepted to be presented as a poster at 14th EMBO Young Scientists' Forum under name of *"Generation of Rahman Syndrome Disease Model by CRISPR/Cas9 Genome Editing for EMT/MET Studies"*

